

---

# **POLYAMIC ACID COMPOSITES FOR MULTIIPLE SENSING APPLICATIONS IN COMPLEX SAMPLE MATRICES**

**BY**

**EUÒDIA HALLOUISE HESS**



A thesis submitted in partial fulfilment of the requirements for the degree of

**UNIVERSITY of the  
WESTERN CAPE**

Doctor Philosophiae in the Department of Chemistry, University of the

Western Cape.

Supervisors

**Professor Priscilla G.L. Baker**

**Professor Emmanuel I. Iwuoha**

**June 2013**

---

---

## ABSTRACT

Polyamic acid-polypyrrole (PAA/PPy) composite films were prepared and characterised for the use as conducting platforms in the design of biosensor systems. The thin films were synthesised by electrochemical method from a solution containing controlled molar ratio of chemically synthesised polyamic acid (PAA) and pyrrole monomer. Homogenous films were obtained incorporating PAA into electropolymerised polypyrrole (PPy) thin film. The concentration of PAA ( $1.37 \times 10^{-6}$  M) was kept fixed throughout the composite ratio analysis, whilst the concentration of PPy was varied from  $1.9 \times 10^{-3}$  M to  $9.9 \times 10^{-3}$  M. The PAA/PPy thin films were electrodeposited at a glassy carbon electrode (GCE) and characterised using Fourier Transform Infrared Spectroscopy (FTIR), Raman spectroscopy, Atomic Force microscopy (AFM), Scanning electron microscopy (SEM) and electrochemical (CV, SWV) techniques. The composition that best represented the homogenous incorporation of PAA into PPy matrix was observed at a PAA/PPy ratio of 1:  $4.13 \times 10^{-3}$ . This composite was observed to have two sets of coupled peaks with formal potential 99 mV and 567 mV respectively. The  $D_e$  determined from cyclic voltammetry using the anodic peak currents were found to be twice as high ( $5.82 \times 10^{-4}$  cm<sup>2</sup>/s) as the  $D_e$  calculated using the cathodic peak currents ( $2.60 \times 10^{-4}$  cm<sup>2</sup>/s), indicating that the composite favours anodic electron mobility. Surface morphology and spectroscopy data support the formation of a homogenous polymer blend at the synthesis ratio represented by composite 3. For the construction of a biosensor the spectroscopic and electrochemical properties of the enzyme, luciferase and the analytes i.e naphthalene and fluoranthene were evaluated. Fluorescence spectroscopy studies were carried out to characterize the enzyme's bioluminescence response in PBS at pH 7. Luciferase showed an absorption peak at 340 nm. The bioluminescence properties of the enzyme with the analytes were explored by fluorescence spectroscopy. The emission peak at 340 nm

---

gradually decreased as the concentration of each analyte was increased respectively. Electrochemical characterization and immobilisation of the enzyme; Photobacterium *Vibrio* fisheri luciferase, and its application as a biosensor for selected polycyclic aromatic hydrocarbons was investigated. The enzyme was electroactive in PBS (pH 7) with two reversible redox couples at  $E^{\circ'} = +110$  mV and  $E^{\circ'} = +730$  mV and was observed to have a diffusion coefficient of  $1.1 \times 10^{-12}$  cm<sup>2</sup>/s. The surface coverage was calculated to be  $1.50 \times 10^{-13}$  moles/cm<sup>2</sup> based on Brown-Anson model. The mass changes due to the addition of each analyte were measured by Electrochemical Quartz microbalance (EQCM). % Inhibition was calculated as an indicator of analyte interaction with the immobilised enzyme, in order to evaluate the sensitivity of the enzyme binding. Electrochemical impedance spectroscopy studies were done at a fixed potential of -730 mV over the frequency range 100 mHz to 1 kHz. The  $R_{ct}$  values increased for each analyte, naphthalene and fluoranthene as the concentrations of each analyte was increased. The system thus became less conductive as the amount of PAHs was introduced to the PAA/PPy/LUC biosensor.  $R_{ct}$  was identified as the parameter to most appropriately model the binding event between luciferase and the two analytes.

---

# KEYWORDS

Polyamic acid

Polypyrrole

Composites

Luciferase

Naphthalene

Fluoranthene

Biosensor

Incubation

Drop coating

Cyclic Voltammetry

Electrochemical Impedance spectroscopy

Electrochemical Quartz Microbalance

Fluorescence



---

# DECLARATION

I declare that “**Polyamic acid composites for multiple sensing applications in complex matrices**” is my own work, that it has not been submitted before for any degree or assessment in any other university, and that all the sources I have used or quoted have been indicated and acknowledged by means of complete references.

**Euodia H. Hess**

**June 2013**

Signature .....



UNIVERSITY of the  
WESTERN CAPE

Supervisors: **Prof. Priscilla G.L. Baker**

**Prof. Emmanuel I. Iwuoha**

---

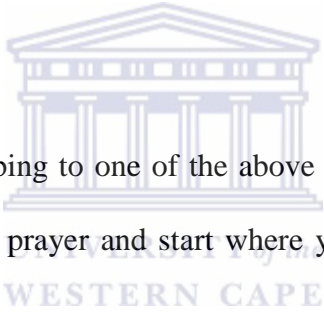
# DEDICATION

‘Don’t ever give up.

Don’t ever give in.

Don’t ever stop trying.

Don’t ever sell out.



And if you find yourself succumbing to one of the above for a brief moment, pick yourself up, brush yourself off, whisper a prayer and start where you left off. But never, ever, ever give up.’ -Richelle E. Goodrich.

This thesis is dedicated to everyone who never let me give up on myself;

To our Heavenly Father, for His glory, love and grace.

To my wonderful parents, John and Myrtle Hess who are personal source of encouragement and inspiration. You are the cause of my passionate pursuit to excellence in leadership.

My sisters, brother and niece; Donell, Anastasia, John-Carl and Jemca for their trust and encouragement.

---

My special and true friend Aldridge Wallenstein, for his consistent support, guidance and encouragement.

The Church (Rehoboth Covenant Ministries), for their persistent prayers and support.

My supervisor Prof P.G.L Baker, your support and belief in my work made it easier for me to pursue and finish my degree.



---

# ACKNOWLEDGEMENTS

In acknowledgement of God, our Creator

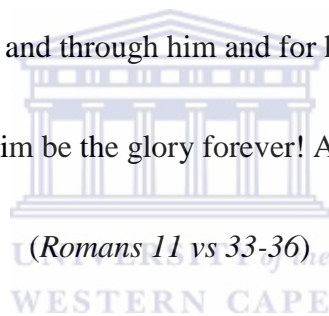
<sup>33</sup> “Oh, the depth of the riches of the wisdom and knowledge of God! How unsearchable his judgments, and his paths beyond tracing out!

<sup>34</sup> “Who has known the mind of the Lord? Or who has been his counselor?”

<sup>35</sup> “Who has ever given to God, that God should repay them?”

<sup>36</sup> “For from him and through him and for him are all things.

To him be the glory forever! Amen.



Every accomplishment in life is the result of corporate effort. Just as it takes a village to raise a child, it takes a dedicated team to author a book. I must submit that no one can claim full credit of any measure of success in any endeavour. Therefore, this work is a synergistic product of many minds. This is a collective contribution of many minds. This is a collective contribution of many mentors, lectures, supporters, family, friends and advisors. I am eternally grateful to the inspiration, passion, commitment and wisdom of many great men and women. I owe every measure of success to an array of contribution from so many minds, known and unknown. Here are just a few who laboured with me to make this work possible:



---

I would like to acknowledge the University of the Western Cape, Science Faculty, Department of Chemistry, SensorLab, South Africa, for giving me the opportunity to pursue my Doctoral degree at this University and for providing all the apparatus and instrumentation required for my research.

Supervisors: Professor Priscilla Baker and Professor Emmanuel Iwuoha, thank you very much for all your academic guidance, patience and always believing and giving shape to this work.

Chemistry Department staff: Professor Farouk Ameer (HOD), Mrs Wilhelma Jackson, all the Academic and Technical staff for your willingness to assist.

To my beloved parents, John and Myrtle Hess. Your investment in my life can never be quantified. Thank you for teaching me time-tested principles. To my sisters Donell and Anastasia, my brother John-Carl, niece Jemca, my best friend Aldridge, my extended family and friend's thank you for your advice, support and contribution to this work is a clear demonstration of your commitment to my development. Thank you for believing in me you're a great source of inspiration, and I am eternally indebted to your unwavering support that you continue to demonstrate.

SensorLab Research group colleagues: Your contribution to this project is highly valued and appreciated and thank you for making SensorLab such a conducive working environment.

Sponsorship: I would also like to thank the DAAD (TUCSIN) and Chemistry Department (National Research Foundation) for funding my studies and attendance of conferences.

---

## LIST OF PUBLICATIONS

Xolile Fuku, Faiza Iftikar, Euodia Hess, Emmanuel Iwuoha, Priscilla Baker; Cytochrome c biosensor for determination of trace levels of cyanide and arsenic compounds, *Analytica Chimica Acta*, 2012, 730, 49–59.

Naumih M. Noah, Marcells Omole, Samantha Stern, Siyi Zhang, Omowunmi A. Sadik  
Euodia H. Hess, Jasmina Martinovic, Priscilla G.L. Baker, Emmanuel I. Iwuoha, Conducting polyamic acid membranes for sensing and site-directed immobilization of proteins, *Analytical Biochemistry* 2012, 428, 54–63.



---

# TABLE OF CONTENTS

POLYAMIC ACID COMPOSITES FOR MULTIPLE SENSING APPLICATIONS IN COMPLEX SAMPLE MATRICES.....	1
ABSTRACT.....	i
KEYWORDS.....	iii
DECLARATION .....	iv
DEDICATION .....	v
ACKNOWLEDGEMENTS.....	vii
LIST OF PUBLICATIONS.....	ix
LIST OF FIGURES.....	xiii
LIST OF TABLES.....	xx
LIST OF ABBREVIATIONS .....	xxi
Chapter 1.....	1
General Introduction.....	1
1.1 Background .....	1
1.2 Problem statement .....	6
1.3 Rationale and motivation.....	7
1.4 Aim .....	8
1.5 Objectives.....	9
1.6 Thesis layout .....	10
Chapter 2.....	12
Literature Review .....	12
2.1 Introduction .....	12
2.2 Synthesis of conducting polymers .....	16
2.3 Conducting Polymers .....	20
2.4 Biosensors .....	33
2.5 Naphthalene.....	36
2.6 Fluoranthene.....	39
2.7 Luciferase .....	41
Chapter 3.....	47
3.1 Introduction .....	47
3.2 Reagents and materials .....	47
3.3 Methodology.....	51

3.3.1 PAA synthesis .....	51
3.3.2 Composite preparation .....	52
3.3.3 Biosensor preparation.....	53
3.3.4 Preparation and analysis of the PAHs.....	53
3.4 Measurements and Instrumentation.....	54
3.5 Electrochemical techniques .....	55
3.5.1 Cyclic voltammetry (CV).....	55
3.5.2 Square Wave Voltammetry (SWV).....	62
3.5.3 Electrochemical Impedance Spectroscopy (EIS) .....	63
3.5.4 Electrochemical Quartz Crystal Microbalance (EQCM) .....	67
3.5.5 Fourier Transform Infrared Spectroscopy.....	71
3.5.6 Raman Spectroscopy.....	71
3.5.7 Fluorescence spectroscopy.....	71
3.5.8 Scanning electron microscopy (SEM).....	72
3.5.9 Atomic Force Microscopy .....	72
Chapter 4.....	75
<i>Results and Discussion: Polymers and Polymer Composites Synthesis and Characterization .....</i>	<i>75</i>
4.1 Introduction .....	75
4.2 Reagents and materials .....	76
4.3 Synthesis and Characterization of PAA.....	78
4.3.1 Electrochemical synthesis and characterization of PAA .....	78
4.4 Synthesis and Characterization of PPy.....	84
4.4.1 Electrochemical synthesis and characterization PPy .....	84
4.5 Synthesis and Characterization of PAA/PPy Composites.....	87
4.5.1 Electrochemical synthesis and characterization PAA/PPy composites .....	87
4.6 Fourier Transform Infrared (FTIR) spectroscopy of PAA.....	98
4.7 Fourier Transform Infrared (FTIR) spectroscopy of PPy.....	99
4.8 FTIR Spectroscopy: Overlay of PAA/PPy composites.....	100
4.9 Raman Spectroscopy of polyamic acid (PAA) .....	102
4.10 Raman Spectroscopy of PPy.....	104
4.11 Raman Spectroscopy: Comparison of different PAA/PPy composites .....	105
4.12 Scanning electron microscopy (SEM) of polyamic acid .....	108
4.13 Scanning electron microscopy (SEM) PPy.....	110
4.14 Scanning electron microscopy: Different ratios of PAA/PPy composites.....	111

4.15 Atomic Force Microscopy (AFM) of PAA, PPy and PAA/PPy composites .....	114
Chapter 5:.....	122
<i>Part 1: Evaluation of Spectroscopic Properties and Electrochemical of Enzyme (Luciferase) and Analytes (Naphthalene and Fluoranthene)</i> .....	122
5.1 Introduction .....	122
5.2 Fluorescence Spectroscopy of Luciferase and Luciferase with analytes .....	123
5.2.1 Fluorescence Spectroscopy of Luciferase .....	123
5.2.2 Fluorescence spectroscopy of Luciferase with Naphthalene .....	126
5.2.3 Fluorescence spectroscopy of Luciferase with Fluoranthene.....	128
5.3 Electrochemical evaluation of the Enzyme; Luciferase and Analytes i.e. Naphthalene and Fluoranthene.....	132
5.3.1 Electrochemistry of GCE/Luciferase in 0.2 M PBS (pH 7).....	132
5.3.2 Electrochemistry of Naphthalene (1 mM) on bare GCE in 0.2 M PBS (pH 7) .....	137
5.3.3 Electrochemistry of GCE/Luciferase and Naphthalene (1 $\mu$ M) in 0.2 M PBS (pH 7).....	139
5.3.4 Electrochemistry of Fluoranthene on a bare GCE in 0.2 M PBS (pH 7).....	144
5.3.5 Electrochemistry of GCE/Luciferase with fluoranthene in 0.2 M PBS (pH 7) .....	147
5.4 Electrochemical Quartz Microbalance (EQCM) of Luciferase and analytes in 0.2 M PBS (pH 7) .....	153
5.4.1 EQCM of Luciferase and Naphthalene.....	153
5.4.2 EQCM analysis of Luciferase and Fluoranthene.....	162
<i>Part 2: Application of PAA/PPy as a Platform for Luciferase attachment for the Detection of PAHs.</i> .....	167
5.5 Evaluation of Electrochemical Impedance Spectroscopy and of the biosensor and Analytes (Naphthalene and Fluoranthene).....	167
5.5.1 Introduction.....	167
5.5.2 Electrochemical Impedance Spectroscopy of GCE/ PAA/PPy/Luciferase and Naphthalene in 0.2 M PBS (pH 7) .....	169
5.5.3 Electrochemical Impedance Spectroscopy of GCE/PAA/PPy/Luciferase and Fluoranthene .....	172
Chapter 6.....	175
<i>Conclusions and recommendations</i> .....	175
6.1 Conclusions .....	175
6.2 Recommendation and Future work:.....	179
References.....	180

---

## LIST OF FIGURES

<i>Figure 1 Bacterial luciferase</i> .....	5
<i>Figure 2 Electropolymerization of aniline</i> .....	18
<i>Figure 3 Electropolymerization of conducting polymers X=NH, S, O</i> .....	20
<i>Figure 4 Polyaniline base</i> .....	21
<i>Figure 5 (a) The reduced (leucoemeraldine) and the (b) oxidised pernigraniline forms of the emeraldine base</i> .....	22
<i>Figure 6 Reaction scheme for the preparation of polyamic acid</i> .....	27
<i>Figure 7 Molecular structure of naphthalene</i> .....	37
<i>Figure 8 Molecular structure of Fluoranthene</i> .....	40
<i>Figure 9 The arrangement of the luxCDABE open reading frames</i> .....	43
<i>Figure 10 The net chemical equation of the bacterial luciferase catalyzed reaction</i> .....	44
<i>Figure 11 Flow chart of research design</i> .....	44
<i>Figure 12 Polyamic acid prepared as a viscous liquid</i> .....	52
<i>Figure 13 A three electrode system electrochemical cell; WE = working electrode, RE = reference electrode and AE = auxiliary electrode</i> .....	56
<i>Figure 14 The important parameters in a cyclic voltammogram are the peak potentials (<math>E_{pc}</math>, <math>E_{pa}</math>) and peak currents (<math>I_{pc}</math>, <math>I_{pa}</math>) of the cathodic and anodic peaks, respectively</i> .....	59
<i>Figure 15 Diagram of a Square wave voltammogram</i> .....	62
<i>Figure 16 A bridge circuit for measurements of electrochemical impedance</i> .....	65
<i>Figure 17 Faradaic impedance spectra presented in the form of Nyquist plots, along with the electronic equivalent circuit of the electrified interface (Schlapfer, P. et. al. 1974)</i> .....	67
<i>Figure 18 Quartz crystal microbalance: (1) the quartz crystal; (2) the gold electrode; (3, 4) connecting metal wires; (5) the base</i> .....	68

---

<i>Figure 19 EQCM (bottom) and cyclic voltammetry (top) profiles at an ion exchanger-coated electrode in the presence of <math>6 \times 10^{-3} M Ru(NH_3)_6Cl_6</math>. (Wang, J et. al. 1996)</i> .....	70
<i>Figure 20 easyScan 2 AFM system: Computer, Cantilever with deflection measurement system scanning the sample</i> .....	73
<i>Figure 21 Cyclic Voltammogram of the electrochemical synthesis PAA in 0.2 M PBS at a scan rate of 50 mV/s</i> .....	79
<i>Figure 22 Cyclic Voltammogram (CV) of PAA film on a GCE in 0.2 M PBS (pH 7) at different scan rates; 50, 60, 70, 80, 90 and 100 mV/s</i> .....	81
<i>Figure 23 Square Wave Voltammograms of (a) oxidation (b) reduction of PAA in 0.2 M PBS (pH 7)</i> .....	83
<i>Figure 24 Cyclic Voltammograms of the synthesis PPy in 0.2 M PBS (pH 7) at a scan rate of 50 mV/s</i> .....	85
<i>Figure 25 Cyclic Voltammogram of PPy in 0.2 M PBS (pH 7) at scan rates 50, 60, 70, 80, 90 and 100 mV/s on GCE</i> .....	86
<i>Figure 26 Cyclic Voltammogram of an in-situ polymerization process PAA/PPy composite in 0.2 M PBS (pH 7) at a scan rate of 50 mV/s</i> .....	88
<i>Figure 27 Schematic representation of PAA/PPy and hydrogen bonding interaction (Iroh et al., 2002)</i> .....	90
<i>Figure 28 Bar charts of oxidation and reduction peaks of PAA/PPy composites prepared on GCE</i> .....	94
<i>Figure 29 Bar charts of the diffusion coefficients (<math>D_e</math>) of the oxidation and reduction peaks of PAA and the different ratios of PAA/PPy composites on GCE</i> .....	96
<i>Figure 30 FTIR spectra of polyamic acid film on GCE</i> .....	99
<i>Figure 31 FTIR spectra of PPy film on GCE</i> .....	100

---

---

<i>Figure 32 FTIR spectra of PAA/ PPy composites 1, 2, 3, 4 and 5 on GCE .....</i>	<i>101</i>
<i>Figure 33 Raman spectra of polyamic acid (PAA) film on SPCE .....</i>	<i>103</i>
<i>Figure 34 Raman spectra of polypyrrole PPy on SPCE.....</i>	<i>104</i>
<i>Figure 35 The change in Raman shift (<math>827\text{ cm}^{-1}</math> = amide band) for the PAA film and the composites 1 to 5 on SPCE.....</i>	<i>106</i>
<i>Figure 36 Raman Spectra of the composite 1, 2, 3, 4 and 5 on SPCE .....</i>	<i>107</i>
<i>Figure 37 SEM micrographs recorded for electrodeposited films on the screen printed carbon electrode (SPCE): (a) bare screen printed electrode (b) PAA film.....</i>	<i>109</i>
<i>Figure 38 SEM micrographs recorded for electrodeposited PPy film on the screen printed carbon electrode (SPCE).....</i>	<i>110</i>
<i>Figure 39 SEM micrographs recorded for electrodeposited PAA/PPy films on the SPCE (a) Composite 1; (b) Composite 2; (c) Composite 3; (d) Composite 4 and (e) Composite 5.....</i>	<i>114</i>
<i>Figure 40 AFM image of polyamic acid (PAA) film on screen printed carbon electrode (SPCE).....</i>	<i>115</i>
<i>Figure 41 AFM image of polypyrrole (PPy) on screen printed carbon electrode (SPCE)...</i>	<i>115</i>
<i>Figure 42 AFM image of Composite 1 on screen printed carbon electrode (SPCE).....</i>	<i>116</i>
<i>Figure 43 AFM image of Composite 2 on screen printed carbon electrode (SPCE).....</i>	<i>117</i>
<i>Figure 44 AFM image of Composite 3 on screen printed carbon electrode (SPCE).....</i>	<i>117</i>
<i>Figure 45 AFM image of Composite 4 on screen printed carbon electrode (SPCE).....</i>	<i>118</i>
<i>Figure 46 AFM image of Composite 5 on screen printed carbon electrode (SPCE).....</i>	<i>118</i>
<i>Figure 47 XY plot of <math>R_a</math> as a function of electropolymerised thin film composition, where 0 = PAA, 1 = composite 1; 2 = composite 2; 3 = composite 3; 4 = composite 4 and 5 = composite 5 (the composites 1 to 5 as previously defined); 6 = PPy .....</i>	<i>119</i>

---



---

<i>Figure 48 Chemical reactions involved in the oxidation of luciferin via a dioxetanone to excited state oxyluciferins. These reactions are catalysed by luciferase and are the basis for light emission in the firefly luciferase.</i>	124
<i>Figure 49 Fluorescence spectra of the enzyme; luciferase in a 0.2 M PBS (pH 7) solution.</i>	125
<i>Figure 50 Fluorescence spectra of the enzyme; luciferase with increasing concentrations (<math>6.7 \times 10^{-4}</math> to <math>6.6 \times 10^{-3}</math> <math>\mu\text{M}</math>) of naphthalene in 0.2 M PBS (pH 7)</i>	126
<i>Figure 51 Calibration curve of the Intensity vs concentration of the enzyme; luciferase with increasing concentrations of naphthalene</i>	127
<i>Figure 52 The linear range of the Intensity vs concentration calibration curve of the enzyme; luciferase with increasing concentrations of naphthalene</i>	128
<i>Figure 53 Fluorescence spectra of the enzyme; luciferase with increasing concentrations of fluoranthene (decrease in bioluminescence)</i>	129
<i>Figure 54 Calibration curve of the Intensity vs concentration of the enzyme; luciferase with increasing concentrations of fluoranthene</i>	130
<i>Figure 55 The linear range of the Intensity vs concentration calibration curve of the enzyme; luciferase with increasing concentrations of fluoranthene</i>	131
<i>Figure 56 Cyclic voltammogram of a bare GCE in 0.2 M PBS (pH 7) at a scan rate of 100 mV/s</i>	133
<i>Figure 57 Cyclic voltammogram of luciferase on a bare GCE in 0.2 M PBS (pH 7) at different scan rates; 25, 40, 50, 60, 70, 80, 90 and 100 mV/s</i>	135
<i>Figure 58 <math>I_p</math> vs <math>\sqrt{v}</math> calibration curves of luciferase on GCE in 0.2 M PBS (pH 7)</i>	136
<i>Figure 59 Cyclic voltammogram of different concentrations (<math>5 \times 10^{-3}</math> to <math>3.4 \times 10^{-2}</math> mM) of naphthalene at a bare GCE electrode in 0.2 M PBS (pH 7)</i>	138

---

---

<i>Figure 60 Calibration curve of <math>I_p</math> vs concentration of naphthalene at a bare GCE electrode in 0.2 M PBS (pH 7).....</i>	<i>139</i>
<i>Figure 61 Cyclic voltammogram of GCE/luciferase with different concentrations of naphthalene in 0.2 M PBS (pH7).....</i>	<i>140</i>
<i>Figure 62 Square wave voltammogram of GCE/luciferase with <math>5.5 \times 10^{-3} \mu\text{M}</math> naphthalene in 0.2 M PBS (pH 7), showing the cathodic peak at -730 mV decreased .....</i>	<i>141</i>
<i>Figure 63 <math>I_p</math> vs concentration calibration curve of GCE/luciferase with increasing concentrations of naphthalene in 0.2 M PBS (pH 7).....</i>	<i>142</i>
<i>Figure 64 The linear range of the <math>I_p</math> vs concentration calibration curve of the GCE/luciferase with increasing concentration of naphthalene in 0.2 M PBS (pH 7).....</i>	<i>143</i>
<i>Figure 65 Cyclic voltammogram of different concentrations (<math>5 \times 10^{-3}</math> to <math>5.5 \times 10^{-3}</math> mM) fluoranthene in 0.2 M PBS (pH 7).....</i>	<i>145</i>
<i>Figure 66 Calibration curve of different concentrations of fluoranthene at a bare GCE in 0.2 M PBS (pH 7).....</i>	<i>146</i>
<i>Figure 67 Cyclic Voltammetry of GCE/luciferase with different concentrations of fluoranthene from <math>5 \times 10^{-4}</math> to <math>5.5 \times 10^{-3}</math> in 0.2 M PBS .....</i>	<i>148</i>
<i>Figure 68 Square wave voltammetry of GCE/luciferase with fluoranthene in 0.2 M PBS (pH 7).....</i>	<i>149</i>
<i>Figure 69 Calibration curve of GCE/Luciferase with different concentrations of fluoranthene in 0.2 M PBS (pH 7).....</i>	<i>150</i>
<i>Figure 70 Linear range of the calibration curve of GCE/Luciferase with different concentrations of fluoranthene in 0.2 M PBS pH 7.....</i>	<i>151</i>
<i>Figure 71 <math>\Delta\text{mass}</math> vs potential profile obtained at Au/LUC coated quartz crystal in 0.2 M PBS (pH 7) at a scan rate of 100 mV.....</i>	<i>156</i>

---

---

<i>Figure 72 <math>\Delta</math>mass vs. potential profiles obtained at an Au/LUC coated quartz microbalance using concentrations of <math>9.99 \times 10^{-11}</math> M to <math>9.99 \times 10^{-10}</math> <math>\mu</math>M of naphthalene in 0.2 M PBS (pH 7) (the concentration profiles up to <math>6.99 \times 10^{-10}</math> <math>\mu</math>M were not included in figure) .....</i>	<i>158</i>
<i>Figure 73 Concentration-dependent <math>\Delta</math>m of the Au/LUC sensor with naphthalene plotted calibration curve.....</i>	<i>159</i>
<i>Figure 74 Time-dependent resonant frequency profiles at different concentrations of naphthalene in 0.2 M PBS (pH 7).....</i>	<i>160</i>
<i>Figure 75 Concentration-dependent inhibitions of the Au/LUC QCM- sensor with naphthalene concentrations from <math>5 \times 10^{-9}</math> to <math>3.5 \times 10^{-9}</math> <math>\mu</math>M.....</i>	<i>161</i>
<i>Figure 76 <math>\Delta</math>mass vs. potential profiles obtained at an Au/LUC coated quartz microbalance using concentrations of <math>9.99 \times 10^{-11}</math> M to <math>9.99 \times 10^{-10}</math> <math>\mu</math>M of fluoranthene in 0.2 M PBS (pH 7) (the concentration profiles up to <math>6.99 \times 10^{-10}</math> <math>\mu</math>M were not included in figure) .....</i>	<i>163</i>
<i>Figure 77 Concentration-dependent <math>\Delta</math>m of the Au/LUC sensor with fluoranthene plotted calibration curve.....</i>	<i>164</i>
<i>Figure 78 Time-dependent resonant frequency profiles at different concentrations of fluoranthene in 0.2 M PBS (pH 7) .....</i>	<i>165</i>
<i>Figure 79 Concentration-dependent inhibitions of the Au/LUC QCM- sensor with fluoranthene concentrations from <math>3 \times 10^{-9}</math> to <math>3.25 \times 10^{-9}</math> <math>\mu</math>M .....</i>	<i>166</i>
<i>Figure 80 Randle's Circuit used to fit EIS data .....</i>	<i>168</i>
<i>Figure 81 <math>R_{ct}</math> vs Concentration calibration plot of the GCE/PAA/PPy/LUC biosensor with different concentrations of naphthalene in 0.2 M PBS (pH 7) .....</i>	<i>170</i>
<i>Figure 82 Linear range of the <math>R_{ct}</math> vs Concentration calibration curve of the GCE/PAA/PPy/LUC biosensor with naphthalene additions .....</i>	<i>171</i>
<i>Figure 83 The <math>R_{ct}</math> vs Concentration calibration curve of the GCE/PAA/PPy/LUC biosensor with increasing concentration of fluoranthene in 0.2 M PBS (pH 7) .....</i>	<i>173</i>

---

---

*Figure 84 Linear range of the Rct vs Concentration calibration curve of the  
GCE/PAA/PPy/LUC biosensor with fluoranthene additions in 0.2 M PBS (pH 7).....174*



---

## LIST OF TABLES

<i>Table 1 Electrical and mechanical properties of polypyrrole, polyaniline and polyacetylene.</i>	15
<i>Table 2 Electron affinity of common aromatic dianhydrides.</i>	29
<i>Table 3 Methods of analysing naphthalene.</i>	38
<i>Table 4 Diagnostic tests for the electrochemical reversibility of a redox couple, carried out by cyclic voltammetry.</i>	60
<i>Table 5 Operating modes with the type of cantilever</i>	73
<i>Table 6 Electrochemical parameters of PAA, PPy and their composites.</i>	91
<i>Table 7 The analytical response of the biosensor to analytes.</i>	152



---

## LIST OF ABBREVIATIONS

PAA	Polyamic Acid
PPy	Polypyrrole
PANI	Polyaniline
PI	Polyimide
PBS	Phosphate-Buffer Solution
ICP	Intrinsically conducting polymer
LUC	Luciferase
BL	Bacterial luminescence
FFL	Firefly luminescence
DMAc	N,N'-dimethylacetamide
THF	Tetrahydrofuran
ACN	Acetonitrile
NMP	1-methyl-2-pyrrolidone
DMSO	dimethyl sulfoxide
ODA	4,4'-oxydianiline
Triethylamine	TEA

---

PMDA	pyromellitic dianhydride or 1,2,3,4,5- benzenetetracarboxylic acid
Methanol	MeOH
Polycyclic hydrocarbons	PAHs
CV	Cyclic Voltammetry
SWV	Square Wave Voltammetry
EIS	Electrochemical Impedance Spectroscopy
EQCM	Electrochemical Quartz Microbalance
QCM	Quartz crystal microbalance
AFM	Atomic Force Microscopy
FTIR	Fourier Transform Infrared
SEM	Scanning Electron Microscopy
$D_e$	Diffusion Coefficient
$I_{p_a}$	Anodic peak current
$I_{p_c}$	Cathodic peak current
$E^{0'}$	Formal potential
$E_{p_a}$	Anodic peak potential
$E_{p_c}$	Cathodic peak potential
$R_{ct}$	Charge transfer resistance

---

---

$\Delta E_p$	Difference in peak potentials
GCE	Glassy Carbon Electrode
SPCE	Screen printed carbon electrode
$\Delta m$	Change in mass
$\Delta f$	Change in frequency





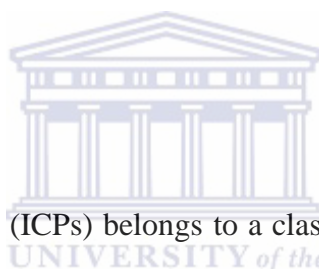
---

# Chapter 1

## General Introduction

*This chapter gives a brief background on conducting polymers, polycyclic hydrocarbons, biosensors, luciferase, problem statement, project's rationale and motivation, aim and specific objectives and also the thesis outline.*

### 1.1 Background



Intrinsically conducting polymers (ICPs) belongs to a class of organic materials with unique electronic properties i.e. electric conductivity up to  $10^4$  S/cm for doped polyacetylene (H. Shirakava et. al.; 1977), electrochromism, and electroactivity. Conjugated  $\pi$  electrons in the backbone of their macromolecules are responsible for these properties. The most studied conducting polymers are polypyrrole (PPy), polythiophene, polyfuran and other heterocyclic ICPs, polyaniline (PANI) and polyacetylene. Because of their high electrical properties, ICPs are investigated for application in electronics, microelectronics, optoelectronics (T.A. Scotheim et. al., 1998). Corrosion protection (J.O. Iroh et. al.; 1999), solid-state charge storage devices (T.F. Otero et. al.; 1999), electromagnetic screens (A. Kaynak et. al.; 1996) and antistatic coatings (R.S. Kohlman et. al.; 1998), gas separation coatings (A.G. Kozlov et. al.; 1998) are among the most promising applications of the ICPs. Poor mechanical properties, environmental sensitivity, moderate stability of electrical properties with temperature considerably limit the industrial pertinence of ICPs. Heterocyclic ICPs which can

---

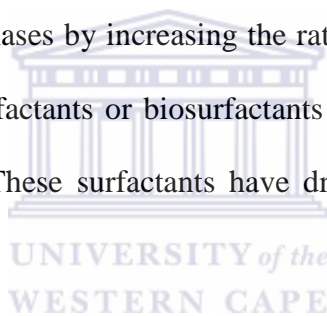
be prepared either chemically or electrochemically, have high environmental stability and a high electric conductivity (up to 400 – 1000 S/cm). Most commercially produced composites use a polymer matrix material often called a resin solution. There are many different polymers available depending upon the starting raw ingredients. The most common are known as polyester, vinyl ester, epoxy, phenolic, polyimide, polyamide, polypropylene, polyether ether ketone, to name a few.

Composites can be defined as materials that consist of two or more chemically and physically different phases separated by a distinct interface. The different systems are combined to achieve a system with more useful structural or functional properties which cannot be attained by any of the constituent alone. The difference between blends and composites is that the two main constituents in the composites remain identifiable while these may not be recognizable in blends. Composites are combinations of materials differing in composition, where the individual constituents retain their separate identities. These separate constituents act together to give the necessary mechanical strength or stiffness to the composite (Josmin P. Jose et al.; 2012). Composites in structural applications have the following characteristics; they consist of two or more physically distinct and mechanically separable materials, they are made by mixing the separate materials in such a way as to achieve controlled and uniform dispersion of the constituents, they have superior mechanical properties and in some cases uniquely different from the properties of their constituents (Mayer C. et al., 1998).

Polycyclic aromatic hydrocarbons (PAHs) belong to a group of organic compounds containing two or more fused benzene rings. PAHs may exhibit mutagenic and carcinogenic effects and is becoming an environmental concern. They tend to be found in soils, aerosols, water, animals and plants (Henner et al., 1996). They get released into the environment

---

through the disposal of coal tar and other coal processing wastes, petroleum sludge, asphalt, creosote, and other wood preservative wastes, chemical waste and soot (Laha et al., 1991). When the PAHs and their degradation products get into the soil it not only pollutes the soil but it endangers human health as well as aquatic ecosystems by directly affecting soil biota or after runoff or percolation, water or groundwater biota (Gu M. et al., 2001). The detection of PAHs toxicity in the environment is restricted due to its low solubility and sorption to solid surfaces and its hydrophobic nature results in the partitioning onto soil matrix, limiting their bioavailability. *In-situ* detection of the toxicity of PAHs in contaminated soil has not been successfully conducted because of the absence of appropriate biosensing cells as well as tools and techniques. Zang et al reported on the fact that surfactants can enhance the rate of mass transfer from solid and sorbed phases by increasing the rate of dissolution and desorption of PAHs. Microbially produced surfactants or biosurfactants offer the advantage of being less toxic and more biodegradable. These surfactants have drawbacks such as time and space consumption and high costs.



Biosensors have major advantages over chemical or physical analyses with regard to specificity, sensitivity, and portability. A biosensor is an analytical device that combines a biological sensing element with a transducer to produce a signal which is proportional to the analyte concentration. Biosensors are used in clinical, food and environmental areas due to the advantage of fast detection speed, high selectivity and sensitivity. Enzymes were historically the first biological recognition elements included in biosensors and continue to be the basis for major number of publications reported for biosensors in general as well as biosensors for environmental applications. The advantages of enzyme biosensors include a stable source of material, the ability to modify the catalytic properties of substrate specificity by means of genetic engineering, and the catalytic amplification of the biosensor response by

---

modulation of the enzyme activity with respect to the target analyte. Recombinant bioluminescent bacterial strains that use specific promoters fused to the bioluminescence genes have recently been applied in environmental monitoring (Heitzer et al., 1994). The advantages of using these recombinant bioluminescence bacteria as biosensing cells include rapid responses, low cost, and improved reproducibility. *Mytilus galloprovincialis* may be used as PAHs pollution bioindicator due to its ability to filter the water and accumulate these toxicants (Frenzilli G. et al., 2004). Bioluminescent organisms comprise a diverse set of species that are widely distributed, inhabiting terrestrial, freshwater and marine ecosystems. Bioluminescent bacteria as bio-indicators have been used since the 1950s. There are varieties of applications range using bioluminescent bacteria for the assessment of environmental toxic compounds (Steinberg et al., 1995). They are promising tools for the detection of bioavailable heavy metals as the bioluminescence bacteria can be specifically modified to respond to toxic concentrations of heavy metals such as Cd, As, Sb, Cr, Cu, Hg, Zn and Pb (Kahru et al., 2008). Scheerer et al., has demonstrated the conditions for bioluminescence of *Vibrio fischeri*. Bacterial bioluminescence (BL) measures cellular metabolism and is a reliable sensor for measuring the presence of toxic chemicals in aquatic samples (Leitgib et al., 2007). For the presence of carcinogens, drugs, mutagenic, pollutant with binding affinities for DNA, DNA electrochemical biosensors can be used (Lucarelli F et al., 2002).

Bacterial luciferase is an enzyme that catalyses light emission of bacterial bioluminescence. The DNA sequences coding the proteins in the luminescent system are termed the *lux* genes. Bacterial luciferase is a heterodimer, composed of two different polypeptides, designated alpha and beta (of molecular mass 40 kDa and 37 kDa, respectively, and encoded by the *luxA* and *luxB* genes, respectively. The active site is located within the subunit (Figure 1).

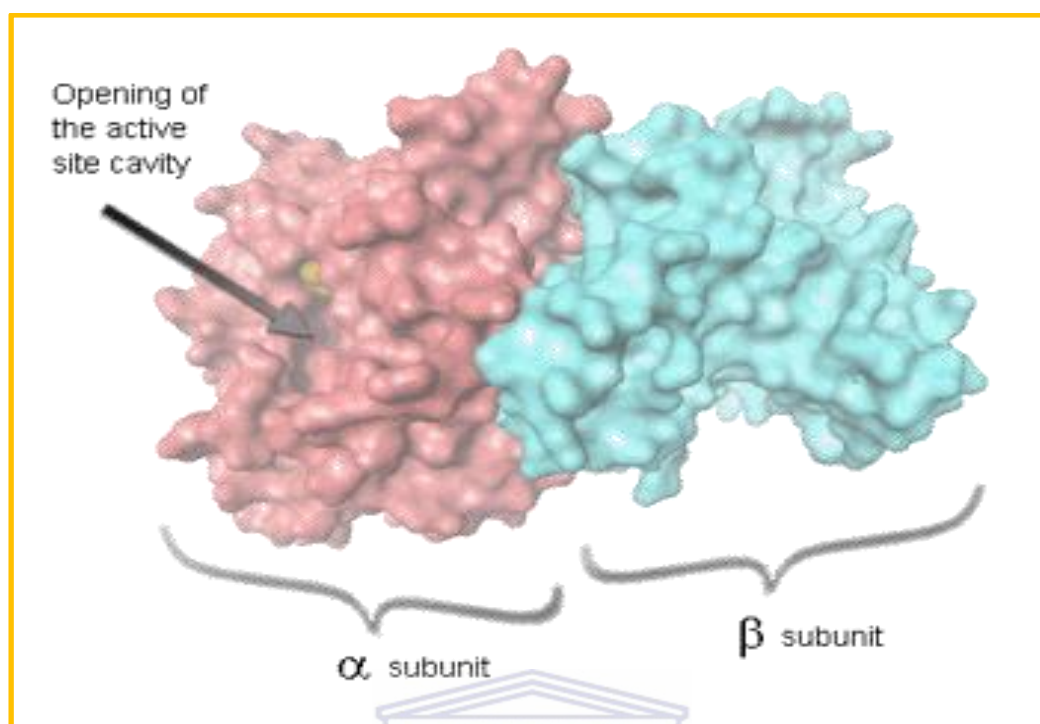


**Figure 1** Bacterial luciferase.

This research work focuses on advances, directions and strategies in the development of a simple, cheap and sensitive electrochemical nanobiosensor for the determination of the polycyclic aromatic hydrocarbons, naphthalene and fluoranthene. It entails the use of electrochemical methods such as cyclic voltammetry (CV), Square wave voltammetry (SWV) and Electrochemical quartz microbalance (EQCM); spectroscopic methods such as Fourier transform infrared (FTIR), Raman and fluorescence spectroscopy as well as the morphological techniques such as scanning electron microscopy (SEM) and Atomic force microscopy (AFM). The electrochemical techniques are important for the characterization of the electroactive species, the study of the electrochemical reactions and direct electron transfer of enzymes at the electrode surfaces as well as in the detection of analytes by incorporation of biological recognition elements such as enzymes. Spectroscopic techniques are highly valuable for the determination of the conducting states of the polymers by

---

monitoring the changes in their absorption bands. The morphological techniques are highly applicable for the characterization of materials and for the estimation of their sizes. Special attention has been given to the synthesis of nanostructured PAA/PPy composites by the electrochemical method (using polyamic acid and polypyrrole) to be used as mediators in the luciferase biosensor; the development of luciferase biosensor and its application for binding determination of the polycyclic aromatic hydrocarbons. Luciferase was the desirable model molecule for this study because of its commercial availability, moderate cost; it's known documented structure and its direct electron transfer when in solution and when immobilized on electrode surfaces. The detection principle used was based on the inhibition of the activity of the enzyme luciferase by the polycyclic hydrocarbons.

## 1.2 Problem statement



The occurrence of phenols as industrial pollutants in surface waters is quite common due to the release of by-products in the petrochemical industry, production of plastics and dyes and pulp industry. These anthropogenic pathways far outweighs the natural formation pathways i.e. biodegradation of various sources of organic waste. Phenolic derivatives are toxic for living organisms because they penetrate through natural membranes causing a broad spectrum of toxic effects. Among the compounds of interest are polycyclic aromatic hydrocarbons e.g. naphthalene and fluoranthene. Presently instrumental methods of analysis involving chromatographic (TLC, GC, HPLC), spectroscopic (UV-Vis, IR, MS) or coupled techniques (GC-MS) are heavily relied upon for environmental analysis. These instrumental techniques are usually expensive, not easily amenable to on site applications, require extensive pre-treatment stages before

---

analyte quantification and they fail to indicate whether the compounds are accessible for assimilation by living organisms. There is a need to monitor different types of PAHs and their levels (compositional proportion) in the environment. Certain world organizations concerning the pollutants found in water and soil such as PAHs has set guidelines. In drinking water, the world health organization (WHO) has recommended concentration of lower than 15 ng/L for each PAH and 700 ng/L for benzo(a)pyrene (WHO, *Guidelines of drinking-water Quality* Geneva, 1998. vol. 1, 2nd edition) . It has been recommended that drinking water samples can contain around 8 PAHs; the concentration level should be under 200 ng/L (Kabzinski et al., 2002). According to Kabzinski et al. the concentration of PAHs in surface water range from 0.1 – 830 ng/L and should not exceed that limit. Several methods for the analysis and determination of PAHs have been reported. These methods include immunoassay (Woodward K.L.A, 1984), gas chromatography (Colmsjo A., A.H.N, 1998) and high performance liquid chromatography (HPLC) using UV-vis absorbance (Ferrer R. et al., 1997; Andrade E. et al., 2000) and capillary electrophoresis (CE) equipped with laser-induced fluorescence (Szolar, O.H.J. et al., 1996). These methods are known to manifest underlying disadvantages such as complicated pre-treatment, high costs, and time consuming processes.

### 1.3 Rationale and motivation

It has been shown that electrochemical methods are inexpensive, simple, and effective, and are less time consuming (Geffard, O., et. al., 2003; Cai, Z.-Q., et. al., 2008). Thus, the fabrication of a biosensor sensor based on PAA/PPy and luciferase presents a novel, simple, and cheap, less time consuming, electrode fouling free and environmentally friendly method of detecting the highly carcinogenic PAHs. However to optimise the

---

enzyme kinetics for analyte molecules that are not their natural substrate, we need to ensure efficient electrocatalysis by improving the electron shuttling capacity of the platform. An approach that augers well for this purpose is the combination of different polymer systems in order to harness their individual catalytic advantages to produce novel materials with superior performance, chemical stability and response times. We have explored the feasibility of combining polyamic acid electrochemistry typified by COOH and NH<sub>3</sub> electrochemistry in a one pot synthesis approach with polypyrrole to incorporate its chemical stability into the overall performance of the composite polymer matrices, thus produced. The success of the novel polymer complexes as transducer platforms has been demonstrated using luciferase as the biosensing element in the analytical determination of naphthalene and flouranthene.



#### **1.4 Aim**

The project will investigate the electrocatalytic behaviour of the PAA/PPy composites and the interaction between luciferase from *Vibrio Fisheri* and PAHs i.e. naphthalene and fluoranthene.



---

## 1.5 Objectives

- i. To synthesize nanostructured PAA/PPy polymer composites in-situ
- ii. To characterize the synthesized nanostructured PAA/PPy films by Cyclic voltammetry (CV), Scanning electron microscopy (SEM), Atomic force microscopy (AFM), Fourier transform infrared (FTIR) and Raman Spectroscopy;
- iii. Evaluate the interaction between the luciferase and the analytes; naphthalene and fluoranthene by Cyclic Voltammetry, Fluorescence Spectroscopy and Electrochemical quartz microbalance;
- iv. To develop an electrochemical biosensor by immobilising the enzyme; luciferase onto the surface of glassy carbon electrode (GCE) modified with nanostructured PAA/PPy film;
- v. To characterize the developed luciferase/PAA/PPy biosensor by Electrochemical impedance spectroscopy and to optimize the biosensor parameters such as sensitivity, stability and limit of detection;

---

## 1.6 Thesis layout

Chapter 2 presents reviews the recent developments in the use of conducting polymers and nanostructured conducting polymers as materials for biosensor construction, as well as the features and applications of biosensors. Various synthetic routes for nanostructured polyaniline materials and their improved features over the conventional polyaniline are discussed. The chapter also highlights the enzyme kinetics in relation to their inhibition principles and on the health effects and environmental occurrence of naphthalene and fluoranthene as well as the analytical techniques used for their detection.

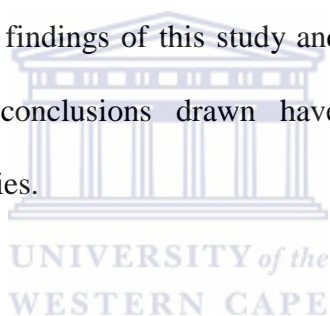
Chapter 3 describes the various analytical techniques employed, detailed research methodology and general experimental procedures for the electrochemical synthesis of nanostructured conducting polymer composites, biosensor construction, characterization and application of the developed biosensor for the determination of PAHs.

Chapter 4 presents the results for the synthesis and characterization of the PAA/PPy electrochemically synthesized composites. The results for the electrochemical characterization of the PAA/PPy film are presented. The structural characterizations of PAA/PPy films were investigated by Fourier transform infrared (FTIR) and Raman spectroscopy and the results are presented in this chapter. In addition, the results obtained from the morphological characterization of PAA/PPy by scanning electron microscopy (SEM) and Atomic force microscopy to estimate their sizes and line roughness are presented. The features of the nanostructured materials were investigated in relation to their application as biosensor materials.

---

Chapter 5 presents the results for the characterization of the electrochemical and spectroscopic evaluation of the enzyme (luciferase) and analytes (naphthalene and fluoranthene). The inhibition/binding of luciferase and analytes were investigated by cyclic voltammetry and fluorescence spectroscopy as well as with electrochemical quartz microbalance and the results discussed in this chapter. In addition the results obtained for the luciferase biosensor as well as those for its optimization for the detection of PAHs. The direct electron transfer of luciferase immobilized on nanostructured PAA/PPy film as well as the biosensor parameters was characterized by electrochemical impedance spectroscopic technique.

Chapter 6 summarizes the major findings of this study and the conclusions drawn from the results of the research. The conclusions drawn have been used to formulate the recommendations for further studies.



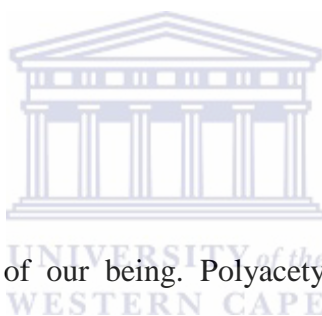
---

# Chapter 2

## Literature Review

*The main focus of this chapter is a review of conducting polymers (CP) i.e polyaniline, polypyrrole, polyamic acid, polyimide, etc., synthesis of CP, a review on biosensors and the occurrence and method of detection of PAHs i.e. naphthalene and fluoranthene and lastly a review on bacterial luciferase.*

### 2.1 Introduction



Polymers form an integral part of our being. Polyacetylene, polypyrrole, polythiophene, polyaniline etc, with their conjugate structures have been investigated and reviewed in view of various applications. These applications include batteries, electrochromic devices, corrosion protection and microelectronic devices. The chemical behaviour of the conducting polymers is due to their intrinsic redox properties and high electronic conductivity. Conducting polymers are also studied for their catalytic behaviour towards electrochemical reactions (K.R. Prasad et al., 2002). Features like poor mechanical properties, environmental sensitivity, and moderate stability of electrical properties with temperature (Table 1) significantly limit the industrial applicability of ICPs. Research interest in electroactive polymers started in 1977, when Heeger, MacDiarmid, Shirakawa and their co-workers demonstrated that the conductivity of polyacetylene (PAC) can be increased by several orders of magnitude by treatment with appropriate oxidizing or reducing agents, the so-called

---

'dopants' (Shirakawa et al., 1977). These scientists were awarded the Nobel Prize in chemistry in 2000 for the discovery and development of the so-called 'conducting polymers' (<http://nobelprize.org/chemistry/laureates/2000>). This has generated renewed interest of the scientific community towards the study and discovery of new conducting polymeric systems. Since the mid-1970s, research into conducting polymers has supported the industrial development of conducting polymer products and provided the fundamental understanding of the chemistry, physics and material science of these polymers (Wallace et al., 2009). Research on polypyrrole dates back to the 1960s, but little was understood then about the polymer at the time and this discovery was essentially lost (Gerhard M et al., 2002). Polyacetylene was the first inherently conductive polymer to be recognized. Even though it is a non-cyclic polyene, polyacetylene is still one of the most studied polymers in this field; it has significant limitations, such as, difficulty with processing and high instability in air. Unlike polyacetylene, polyphenylenes, cyclic polyenes, are known to be thermally stable as a result of their aromaticity. These polymers are conducting due to an extended conjugation along the polymer backbone (Guimard M. et al., 2007, Harsanyi G et al., 1996). Their structure contains a one-dimensional organic backbone based on the alternation of single and double bonded  $sp^2$  hybridized atoms which give the polymer with metal like semi-conductive properties. These enable  $\pi$ -molecular orbitals to be formed for electronic conduction. In the neutral (undoped) state these polymers can only be semiconducting. The neutral polymer is converted into an ionic complex consisting of a polymeric cation or anion and a counter-ion which is the reduced form of the oxidizing agent or the oxidized form of the reducing agent, respectively (Bredas N. et al. 2007). The oxidation or reduction of  $\pi$ -electronic systems in conducting polymers is referred to as *p*- or *n*-type doping. This doping can be effected chemically or electrochemically. In order to maintain electro-neutrality, doping requires incorporation of a counter-ion. The doped and undoped states have different electronic,

---

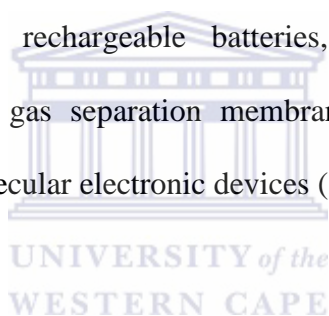
optical, physical, chemical and electrochemical aspects. Therefore, reversible interchange between the redox states in conducting polymers gives rise to the changes in its properties including polymer conformation, doping level, conductivity and colour. Electrons of  $\pi$ -character can be easily removed or added to form a polymeric ion without much disruption of the sigma-bonds which are primarily responsible for holding the polymer together. Unsaturated  $\pi$ -bonded polymers also have small ionization potentials and large electron affinities. The electronic conductivity, a measure of electrical conduction and thus a measure of the ability of a material to pass a current, appears when the material is doped. A variety of factors including polaron length, the conjugation length and overall chain length and by the charge transfer to adjacent molecules affects the conductivity in conducting polymers. Studies have demonstrated that planar conformation of the alternating double-bond system, which maximizes sideways overlap between the molecular orbitals, is critical for conductivity (Guimard, N. et al., 2007). This  $\pi$ -bonded system is further described in terms of electronic wave-functions that are delocalized over the entire chain. This delocalization allows charge mobility along the polymer backbone and between adjacent chains, but delocalization is limited by both disorder and Coulombic interactions between electrons and holes. Generally, materials with conductivities less than  $10^{-8}$  S/cm are considered insulators, while those between  $10^{-8}$  and  $10^3$  S/cm are semiconductors and those with conductivities greater than  $10^3$  S/cm are considered conductors. The mechanism of conduction in conducting polymers is very complex because such materials exhibit conductivity across a range of about fifteen orders of magnitude and many involve different mechanisms within different regimes (Gerard M et al., 2002). Conducting polymers show enhanced electrical conductivity by several orders of magnitude of doping. The concept of polarons and bipolarons has been used to explain the electronic phenomena in these systems (Bredas J. et al. 1985).

**Table 1** Electrical and mechanical properties of polypyrrole, polyaniline and polyacetylene.

Conducting Polymer	Maximum Electrical conductivity, S/cm	Thermal stability of films, K	Mechanical properties:
Polypyrrole	10 <sup>-5</sup> -1000 (A.F. Diaz et al., 1979, S. Rane et al., 1999)	523 (S. Rane et al., 1999)	Breaking stress (films), 4.1-12.1 MPa (P. Murray et al., 1997)
Polyaniline	10 <sup>-8</sup> -400 (T.A. Scotheim et al., 1998)	453 in air, 673 in N <sub>2</sub> (S.S. Hardaker, et al., 1999)	Tensile strength, MPa, 0.5-3.3 (G.R. Valenciano et al., 2000) reported for PANI/Poly(ethylene) composed films
Polyacetylene	10 <sup>-9</sup> -10 <sup>4</sup> (H. Shirakava et al., 1977)	693 in N <sub>2</sub> (S. Wang et al., 1999)	Tensile strength (in bulk), MPa 100 (E.T. Kang et al., 1997)

---

Conductive filler materials such as carbon black, graphite fibres, or metal particles were used for preparation of composite materials. Scientists from many disciplines are now combining expertise to study organic solids that exhibit remarkable conducting properties. Organic compounds which effectively transport charge are divided into three groups; organometallic species (Debuigne A et al. 2009, Gligorich, K. et al. 2009, Moreda-Piñeiro, J et al. 2009, Nakai, H. et al. 2010), charge transfer complexes (ion radical salts) (Casar, Z. et al. 2009, Kobayashi, Y et al. 2010, Demolliens, A. et al. 2010) and conjugated organic polymers (Gerard M et al., 2002, Snook, G. et al 2011, Adhikari, B. et al. 2004, Kumar D. 1998). Polymers as electric insulators are being discarded as they are now taking charge as conductors with a range of novel applications. They have a wide range of potential applications in areas such as rechargeable batteries, light emitting diodes (LED), electrochromic display devices, gas separation membranes, electromagnetic interference (EMI) shielding, sensors and molecular electronic devices (Kumar, D. et al., 1998).



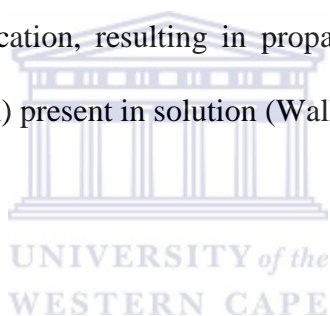
## **2.2 Synthesis of conducting polymers**

Two different techniques are mainly used in preparation of conducting polymers: chemical synthesis and electrochemical synthesis. Chemical polymerization is carried out in either aqueous solution or vapour phase by the presence of an oxidant. PPy in powder form precipitates either in solution or onto surfaces in contact with vapour media. PPy obtained by chemical method is usually non-soluble (T.A. Scothorn et al., 1998) and cannot be used for preparation of nanocomposites. Chemical synthesis is known to permit the scale-up of the polymers, which is not possible with electrochemical synthesis. Electrochemical polymerization is the preferred general method for preparing CPs because of its relatively straightforward synthetic procedure, simplicity and reproducibility. Generally,



---

electrochemical polymerization can be carried out galvanostatically (a constant current applied), potentiostatically (a constant potential applied) or by potential cycling or sweeping methods. The thickness of the film can be controlled by varying either the potential or current with time. Potentiodynamic techniques are preferred because of the homogenous film produced and strong adherence of the film to the electrode surface (Trivedi, D. C., 1996). The mechanism of electrochemical polymerization of CPs, using PANI as an example is shown in Figure 2. Formation of the radical cation of aniline by oxidation on the electrode surface is considered to be the rate determining step. This is followed by coupling of radicals, mainly *N*- and para-forms, and elimination of two protons. The dimer (oligomer) formed undergoes oxidation on the electrode surface along with aniline. The radical cation of the oligomer couples with an aniline radical cation, resulting in propagation of the chain. The formed polymer is doped by the acid (HA) present in solution (Wallace et al., 2003).



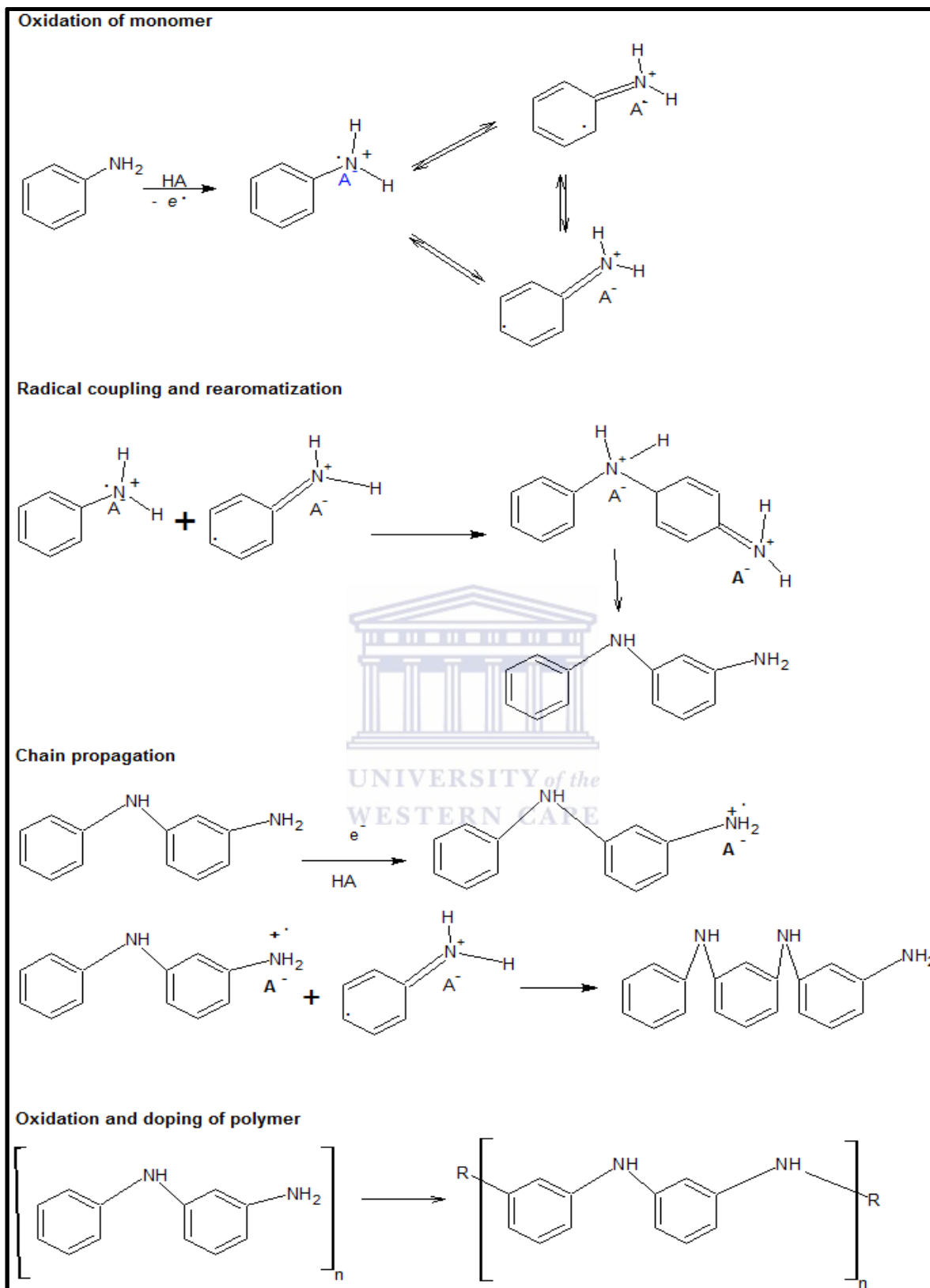


**Figure 2** Electropolymerization of aniline.

---

Electrochemical oxidative polymerization of PPy was primarily carried out by Diaz et al. (A.F. Diaz et al., 1971) in aqueous solution of pyrrole using sulfuric acid as an electrolyte. Diaz et al. have obtained PPy in an insoluble powder form. Tourillon et al. in (T.A. Scotheim, 1983) studied the electrochemical polymerization of heterocyclic ICPs. Electrochemical polymerization of pyrrole (Figure 3) involves the formation of radical cation followed by the formation of dimer and deprotonation followed by formation of trimer and the next radical-cation, etc. As the result of this process, a coating consisting of ICP as a freestanding flexible film is formed on a surface of a working electrode. The electrochemical method described by Tourillon et al. has some disadvantages. Two mechanisms are mostly responsible for the imperfections of resulting polymer molecules: formation of side chains and termination by oxidation of dissolved oxygen. The electrochemical method has the advantage of that the doping of the polymer occurs simultaneously with the film formation. Doping is the formation of a complex between the polymer and the counterion where both components are connected electrostatically. During doping, cation-radicals (polarons) and dications (bipolarons) are formed in ICP backbone. The electrical conductivity of doped PPy is due to polarons and bipolarons. Important variables to be considered during electrochemical polymerization are deposition time and temperature, nature of solvent, pH of solvent, electrolyte, electrode materials, and deposition charge. Each of these parameters has an effect on film morphology the thickness and topography, mechanics, and conductivity, which are properties that directly impact the effectiveness of the material for biosensor applications. All CPs can be synthesized chemically, but electrochemical synthesis is limited to those systems in which the monomer can be oxidized in the presence of a potential to form reactive radical ion intermediates for polymerization. Polypyrrole, polythiophene and polyaniline are of the conducting polymers that can be synthesized both chemically and electrochemically. Several novel conducting polymers with modified monomers are only open to chemical

polymerization. Electrochemical synthesis has been used to prepare homogeneous and self-doped films (Guimard et al., 2007).

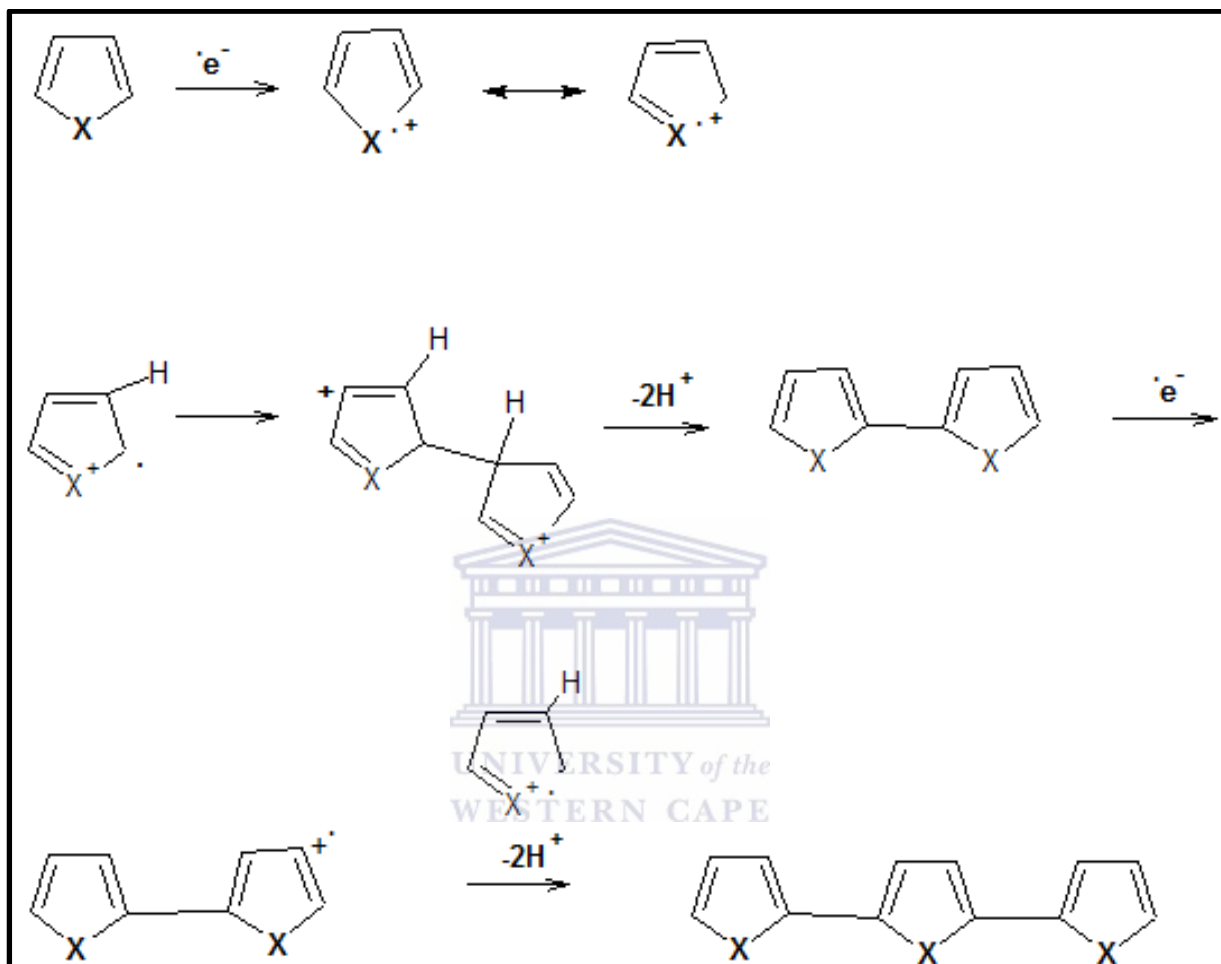


**Figure 3** Electropolymerization of conducting polymers X=NH, S, O.

### 2.3 Conducting Polymers

Polyaniline (PANI) has been known for over one hundred years in its 'aniline black' form, and undesirable black deposit formed on the anode during electrolysis involving aniline. Due to its simple synthesis it is the most promising polymer with controllable electrical

---

conductivity, and good environmental stability. PANI is a phenylene-base polymer having a chemically flexible  $-NH-$  group in the polymer chain edged on either side by a phenylene ring. The protonation and deprotonation and various other physico-chemical properties of PANI can be traced to the presence of the  $-NH-$  group. There are three different oxidation states of PANI, namely leucoemeraldine, emeraldine, and pernigraniline; in which only polyemeraldine is electrically conductive.

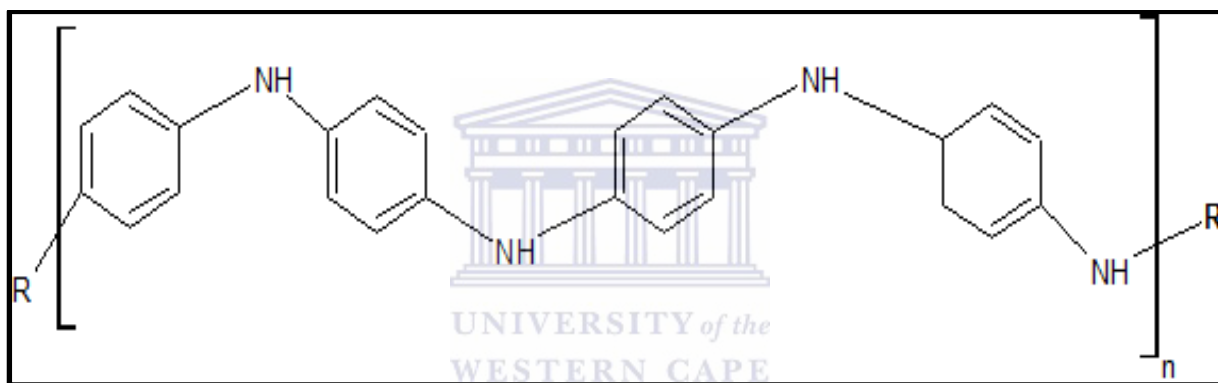
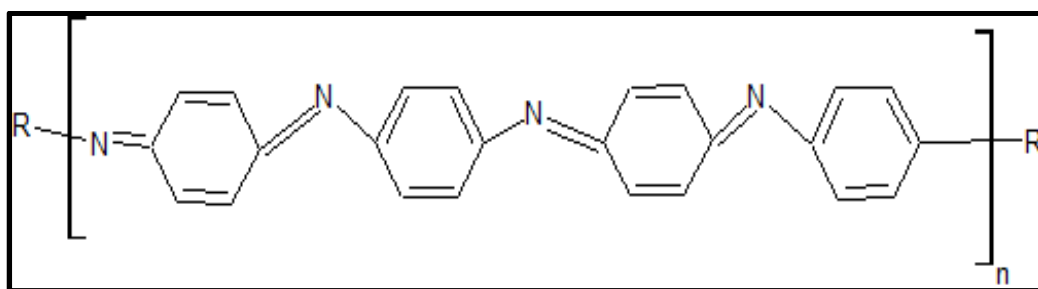
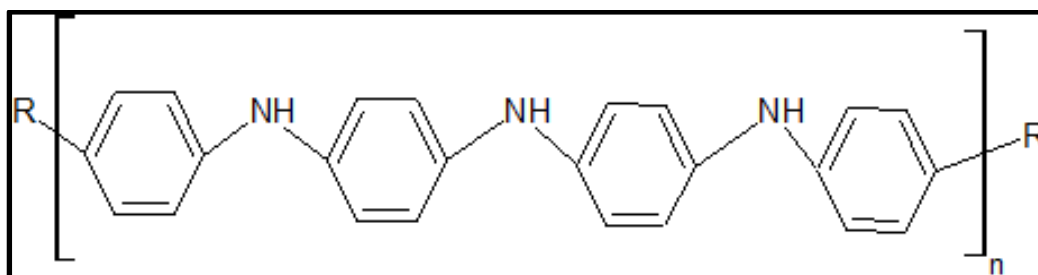


**Figure 4** Polyaniline base.

The terms “leucoemeraldine”, “emeraldine” and “pernigraniline” refer to the different oxidation states of the polyaniline. The base form of polyaniline consists of alternating reduced and oxidized repeated units. The presence of both the reduced and oxidised form is referred to as the emeraldine base. The leucoemeraldine is the reduced state and the pernigraniline is the oxidised state of polyaniline.

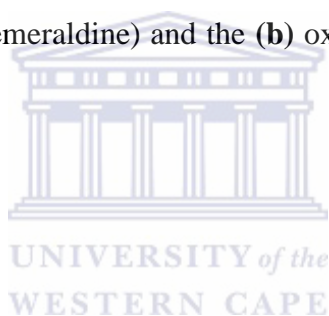


(a)



(b)

**Figure 5** (a) The reduced (leucoemeraldine) and the (b) oxidised pernigraniline forms of the emeraldine base.



Polyaniline can be prepared by either chemical or electrochemical oxidation of aniline under acidic conditions. The electrochemical method of polymerization is preferred because of its better-ordered polymers and thin films. In electrochemical techniques the best films are reported to be produced that employ the three electrode system in a cell, that is, working, counter and reference electrodes. The imine nitrogen atoms can be protonated in whole or in part to give the corresponding salts. The degree of protonation of the polymeric base will depend on its oxidation state and on the pH of the aqueous acid. This protonated form of polyaniline is electronically conducting and the magnitude of increase in its conductivity is a function of the level of protonation. Conducting polyaniline polymers, for example poly (2,5 dimethoxyaniline) (PDMA) and poly (ortho-methoxyaniline) (POMA), are capable of incorporating different functionalities in their matrix during or after polymerisation. These

---

conducting polymers have conjugated  $\pi$ -electron backbones, which display unusual properties such as low-energy optical transitions, low ionisation potentials and high electron affinities. Therefore these polymers can be oxidised or reduced more readily and more reversibly than conventional polymers. A lot of interest has been focused on enhancing the properties of these materials by changing their surface properties. The change in surface properties is commonly achieved by surrounding a conductive polymer by another material, usually a bulky dopant. This forces the polymer backbone to the inside of the molecule forming different nanostructures including nanotubes and nanomicelles. M.J. Klink et al. incorporated phenanthrene sulfonic acid (PSA) and anthracene sulfonic acid (ASA) into the polyaniline (PANI), poly (2,5 dimethoxyaniline) [PDMA] and poly (ortho-methoxyaniline) [POMA] backbones (Klink et al., 2012). An amperometric biosensor has been developed, incorporating the electroactive polymer, polyaniline (PANI), which undergoes redox cycling, and can couple electrons directly from the enzyme active site, to the electrode surface (Killard et al., 1999). The determination of  $H_2O_2$  and other organic peroxides is of practical importance in clinical, environmental, industrial and many other fields. The current  $H_2O_2$  assay techniques based on volumetric, colorimetric and chemiluminescence analysis are complex, time consuming, and are prone to interferences. Polyaniline based peroxide sensors are easily fabricated and combine the exquisite selectivity of horseradish peroxidase (HRP) with the excellent PANI stability to produce sensors with high sensitivity. Also the simultaneous electrodeposition of the polymer together with the biomolecule incorporation allows for the control of the spatial distribution of the immobilized protein, control of film thickness and enzyme activity and can be manipulated to produce sensors with excellent performance (Mathebe N, et al. 1995). Anthracene sulfonic acid doped polyaniline nanomaterials has been prepared through the chemical oxidative polymerisation process. Ammonium peroxydisulfate (APS) was employed as an oxidant. The polyaniline (PANI)

---

materials exhibited nanofibrillar morphology with diameter sizes less than 300 nm. The nanofibrillar PANI was used as amperometric biosensors for H<sub>2</sub>O<sub>2</sub> and erythromycin (Michira I, et al. 2007). Uniform composite films of nanostructured polyaniline (PANI) (e.g. nanotubes or nanorods with 60–80 nm in diameter) were successfully fabricated by blending with water-soluble poly(vinyl alcohol) (PVA) as a matrix. The PANI nanostructures were synthesized by a template-free method in the presence of b-naphthalene sulfonic acid (b-NSA) as a dopant (Zhang Z, et al., 2002).

Pyrrole is a heterocyclic aromatic organic compound, a five-membered ring with the formula C<sub>4</sub>H<sub>4</sub>NH. Polypyrrole (PPy) can be prepared by oxidizing pyrrole using different techniques, electrochemical polymerization and chemical polymerization. Electrochemical polymerization makes it easier to determine the polymer structure and components in a controllable manner for diverse purposes. Advantages of PPy include environmental stability, good redox properties and the ability to give high electrical conductivities. Polypyrrole (PPy) is frequently used in electrocatalytic and affinity sensors and biosensors based on its unique electrical, optical, and thermal properties. As a result of its good intrinsic properties, polypyrrole has proven promising for several applications including batteries, supercapacitors, electrochemical biosensors, conductive textiles and fabrics, mechanical actuators, electromagnetic interference shielding, anti-static coatings and drug delivery systems. The intrinsic properties of polypyrrole are highly dependent on electropolymerization conditions. In order to further enlarge the application of PPy in sensors, much effort has been carried out in recent years to fabricate functionalized PPy derivatives through either modification of the pyrrole monomer's structure or the preparation of block and graft copolymers. Hua Dong et al. prepared a carboxyl-functionalized PPy derivative film, poly(pyrrole-*N*-propanoic acid), by electrochemical polymerization.

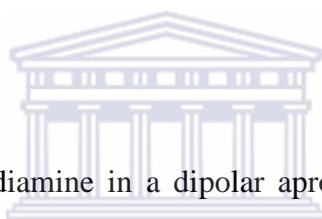


---

Polypyrrole offers tremendous technological potential such as fabrication of molecular electronic devices, electrodes for solid-state batteries, solid electrolytes for capacitors, electromagnetic interference shielding materials, and sensors. Electrochemical polymerization on a metal electrode or ITO glass results in good quality film, while chemical polymerization yields fine conducting powders. Polypyrrole polymerized either electrochemically or chemically is known to be insoluble and infusible due to the strong inter- and intra-molecular interactions and crosslinking's. The poor processibility of polypyrrole has limited its applications (Lee J et al., 1995). By employing chemical synthesis routes the polypyrrole is mainly produced in the bulk solution and the transfer of the polypyrrole to a suitable electrode surface is limited. Polypyrrole is insoluble in most common solvents and adherence of polypyrrole to the electrode surface during sensor preparation, is also problematic in the absence of suitable dopants that improves its properties. These disadvantages however may be avoided, if electrochemical polymerization is applied. Thickness and morphology of the film are easily controlled by type of solvent, electrolyte concentration and type of electrode material, current density, applied potential, polymerization time and temperature. The optimization of these parameters in order to obtain nanostructured and reasonably stable PPy in air and in aqueous media opens the way for entrapment and/or doping of polypyrrole by various biomaterials such as small organic molecules, DNA, proteins and even living cells. PPy may also be synthesized in the overoxidized state and entrapped molecules may be removed to produce molecularly imprinted polymer electrodes. Electropolymerization also allows the deposition of films independent of the electrochemical cell geometry and this is particularly useful in the design of micro fluidic systems. Surfactants are used as polymer additives in order to control the morphology and when implicitly incorporated into the conducting polymer backbone, it serves to improve the conductivity, stability, solubility in organic solvents and processability.

---

Surfactants affect the preparation of conducting polymers in three ways, i.e., (i) the micelles control the distribution of reactants between the micellar and the aqueous phase and thus exerts some control over the polymerization pathway (ii) anionic surfactants may act as counter ions for the polymer polycations and (iii) the hydrophobic tail of the surfactant may adsorb on the polymer formed at the electrode surface and thus becomes part of the resulting material, influencing its chemical properties. on a platinum disk electrode to form stable thin films with good electrochemical activity, improved conductivity and visibly different colors on the oxidized state as opposed to the neutral state 1, 2-naphthaquinone sulfonic acid doped polypyrrole (PPyNQSA) through potentiodynamic electropolymerization from aqueous solution, at low pH was prepared (Akinyeye R et al., 2007).



Addition of a dianhydride to a diamine in a dipolar aprotic solvent such as DMAc or 1-methyl-2-pyrrolidone (NMP) at ambient temperatures leads to the formation of the intermediate polyamic acid due to the nucleophilic attack of the amino group on the carbonyl carbon of the anhydride group. Polar aprotic solvents form strongly hydrogen bonded complexes with the free carboxyl at ambient conditions. If the polymerization reaction is carried out in ether or hydrocarbon solvents, considerable differences in equilibrium constant are observed depending upon the amine's basicity and the dianhydride's electrophilicity. Polyamic acid formation is exothermic and the equilibrium is favoured at lower temperatures. The equilibrium however is shifted so far to the right at ambient that further lowering of the temperature usually does not show any detectable effect on the reaction. The monomer concentration is another important factor affecting the reaction equilibrium. As the forward reaction is bimolecular and the reverse reaction is unimolecular, increasing the monomer concentration favours high molecular weight products. For very dilute solutions this feature

becomes especially important and leads to decreased molecular weight of the polyamic acid  
(Chapter 1 POLYIMIDES: chemistry & structure-property relationships).

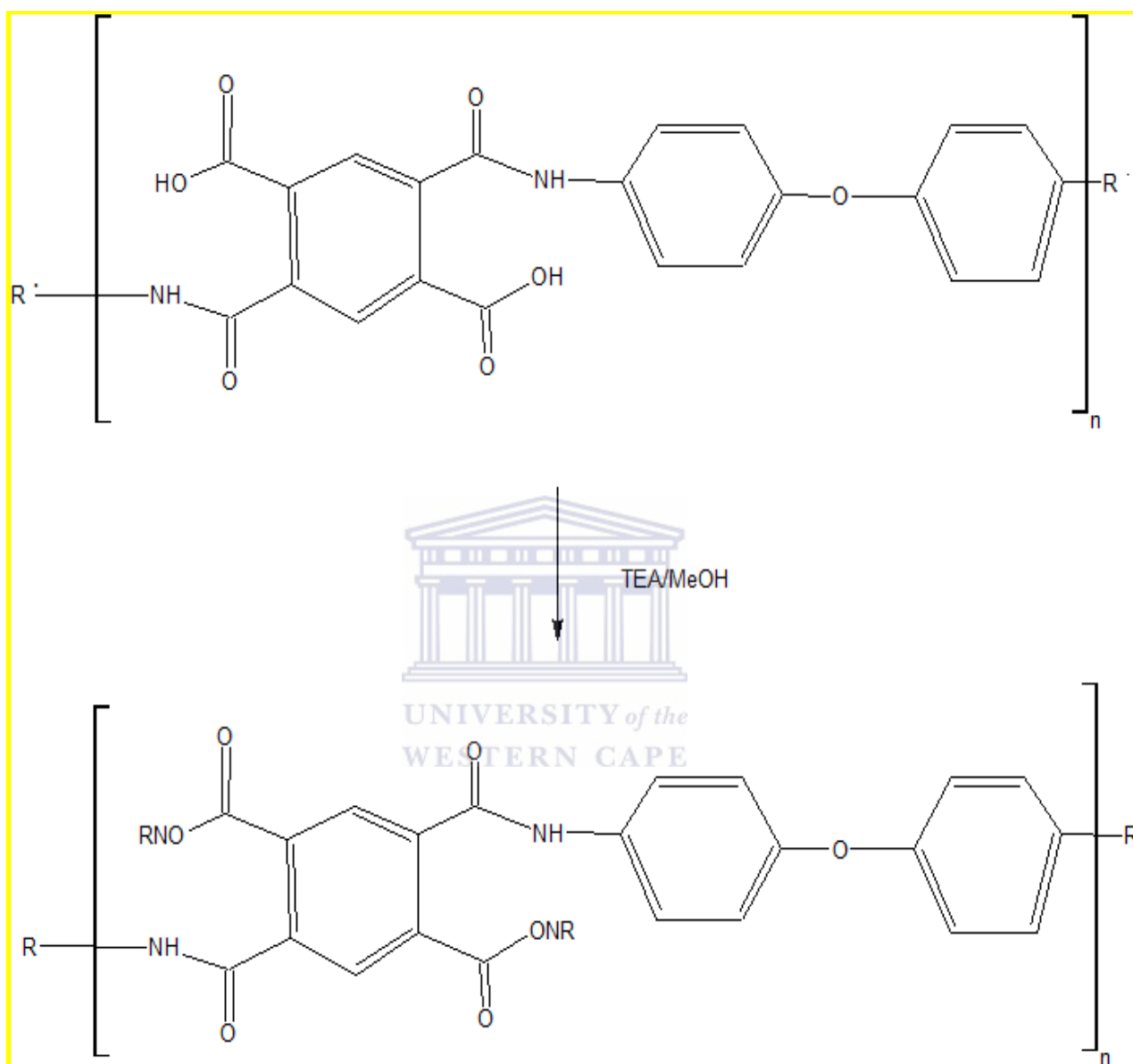
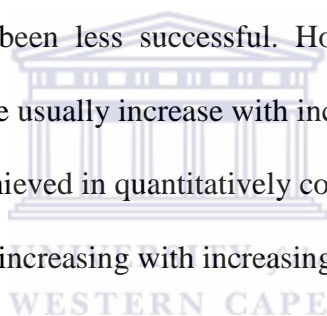


**Figure 6** Reaction scheme for the preparation of polyamic acid.

The mechanism of polyamic acid formation involves a nucleophilic substitution reaction at the carbonyl carbon atom of the dianhydride with a diamine. The reaction is expected to depend upon the electrophilicity of the carbonyl groups of the dianhydride and the nucleophilicity of the amino nitrogen atom of the diamine. Electrophilicity of the dianhydride

---

is usually gauged in terms of electron affinity ( $E_a$ ) of the molecule measured by polarographic measurement techniques. PMDA that has the highest  $E_a$ , of the common aromatic diamines also usually demonstrates the highest reactivity when reacted with different diamines. For dianhydrides with bridged bisphthalic anhydride structure, electrophilicity is strongly influenced by the bridging group. In comparison to BPDA, which lacks a bridging group, the electron-withdrawing groups such as  $\text{SO}_2$  and  $\text{C}=\text{O}$  increases the  $E_a$  value substantially whereas electron donating groups such as ethers decrease the  $E_a$  value. Due to this difference in reactivity, while ether-containing dianhydrides are not readily affected by atmospheric moisture, PMDA and BTDA have to be handled in strictly moisture free environments at all times. Attempts at correlating the reactivity of the aromatic diamines with their nucleophilicity have been less successful. However, the reaction rates of the diamines with a given dianhydride usually increase with increasing ionization potential. Also, considerable success has been achieved in quantitatively correlating the diamine basicity with reactivity, with the rate constants increasing with increasing value of  $\text{pK}_a$ .



---

**Table 2** Electron affinity of common aromatic dianhydrides.

Name	Electron Affinity (eV)
Pyromellitic dianhydride (PMDA)	1.90
3,3',4,4'-Diphenylsulfone tetracarboxylic dianhydride (DSDA)	1.57
3,3',4,4'-Benzophenonetetracarboxylic dianhydride (BTDA)	1.55
Biphenyl-tetracarboxylic acid dianhydride (BPDA)	1.38
4,4' oxydiphthalic anhydride (ODPA)	1.30
Hydroquinone diphthalic anhydride (HQDA)	1.19
4,4'-Bisphenol A dianhydride (BPADA)	1.12

Polyimides (PI's) are usually synthesized in two steps. The final product is often prepared by thermal solid-state imidization of a two- or one-dimensional shape of the polyimide precursor polyamic acid (PAA). Synthesis of PI involves reacting a dianhydride and a diamine at ambient conditions in a dipolar aprotic solvent such as N,N-dimethylacetamide (DMAc) or N-methylpyrrolidinone (NMP) to yield the corresponding polyamic acid, which is then cyclized into the final polyimide. This process was pioneered by workers at Dupont in 1950's, involving a soluble polymer precursor and is it continues to be the primary route by which

---

most polyimides are made today (Takekoshi, T., 1996). Poly-(4,4'-oxydiphenylene) pyromellite imide (PI) is one of the suitable materials. It is commercially available, and manufactured for various applications because of its high thermal stability and chemical durability. However, this polymer is not processable. Therefore, the products, including membranes, can be molded only from its prepolymer - polyamic acid (PAA), which is then transformed into insoluble polyimide by thermal dehydration at 300 – 400° C. This thermal treatment has its disadvantages, especially in the case of porous membranes because the pores tend to collapse at high temperatures. To avoid this problem, soluble polyimides are frequently used, although insoluble polyimides are much more promising in view of chemical durability (Bessonov, M.I. et. al., 1987). Synthesis of Kapton™ polyimide, utilizes the monomer pyromellitic dianhydride (PMDA) and 4,4'-oxydianiline (ODA). This process involves several elementary reactions and the course of these reactions can be immensely affected by a large number of factors that include reaction conditions and even the mode of monomer addition. The success of the overall reaction to yield high molecular weight polymers is critically dependent on seemingly refined details (Chapter 1 POLYIMIDES: chemistry & structure-property relationships –literature review).

PAA is usually prepared from organic precursors such as described by Daniel Andreescu et al. It is synthesized in organic medium from 4,4'-oxydianiline (ODA) and 1,2,4,5-benzenetetracarboxylic acid (PMDA) precursors. Since the type of solvent used for the preparation and deposition of the PAA film plays a critical role in obtaining homogeneous surface coverage and controlling polymer thickness and polymerization degree, they Andreescu et al. studied several solvents for the synthesis and characterization of the PAA. PAA can be prepared as a viscous liquid or a powder, depending on the solvent used, and the resulting polymers were soluble either in aqueous or in organic solvent medium. When THF was used as solvent, the resulting PAA was a viscous liquid. When acetonitrile (ACN) was

---

used as solvent, another PAA derivative was obtained in a powdered form from the same ODA and PMDA (Andreescu D et al. 2005). Electrochemical synthesis of PAA films can be carried out under galvanostatic conditions. The amount of polymer film electrodeposited onto an electrode surface is dependent on the composition of the growth medium (solvent, supporting electrolyte, surfactant) and other deposition conditions such as the deposition time and current density (Chen, Y. et al., 1999). By varying these parameters it is possible to control the deposition process. Daniel Andreescu et al. studied the effect of these parameters on PAA film formation by performing electrochemical synthesis in both aqueous and organic solvent at different current densities and deposition times. They electrodeposited PAA (powder) film from organic medium, N,N-dimethylacetamide( DMAc), onto a RVC electrode at a current density of  $1.0 \text{ mA/cm}^2$ . The chronopotentiometric responses indicated the occurrence of a steady-state electrodeposition process. The process was slightly affected when the PAA (liquid) film was prepared from an aqueous solution, PBS. For the same current density, for example,  $1.0 \text{ mA/cm}^2$ , the electrodeposition equilibrium potential was  $0.92 \text{ V}$  in PBS compared to  $1.4 \text{ V}$  when DMAc was used as solvent. It was concluded that the organic solvents stabilize the cations. The electrode potential increases with increasing applied current. This behaviour suggested that the process obeyed Faraday's law of electrolysis. Silver (Ag) and gold (Au) nanoparticles was then also incorporated into polyamic acid (PAA) film. This method utilized the unique reactivity of PAA by preventing the cyclization of the reactive soluble intermediate into polyimides at low temperature to design polymer-assisted nanostructured materials (Andreescu D et al., 2005). Polyamic acids (PAAs) containing benzothiazole (BT) and benzoxazole (BO) pendent groups (PAA-BT and PAA-BO, respectively) possesses electroactivity. The addition of  $\text{H}_2\text{O}_2$  chemically oxidized the intrinsic carboxylic acid groups of PAA to form peroxy acid groups, and the peroxy acid further oxidized the electroactive sites of BT and BO to form N-oxides. The N-oxides could

---

be reverted to their original form by electrochemical reduction, thus increasing the electrochemical reductive current. Based on this mechanism, enzyme-free hydrogen peroxide ( $H_2O_2$ ) biosensors were prepared by modifying gold electrodes with the PAA derivatives (PAA-BT/Au and PAA-BO/Au, respectively) (Hua M et al., 2011). By manipulating the delocalized  $\pi$  electron system of PAA, a conducting polymer, it can be used for chemical and electrocatalytic applications. PAA provides a means of generating nano-composites containing monodispersed metal particles while retaining its physical and chemical properties. It is versatile in both organic and inorganic solvents because of its chemical resistance. The carbonyl and amide functionalities in polyamic acids act as anchors resulting in the fabrication of flexible nanostructured polyamic acid-silica (PSG) films. The reduction of Cr (VI) to Cr (III) using PAA was carried out in both the solution phase and at solid gold electrodes (Omole M. et al. 2011). Electrically conducting polymers and their composites attract a lot of attention because of their high charge storage ability. The composite of polypyrrole (PPy) and polyimide (PI) possesses better charge storage properties than pure PPy. The electrochemical properties of a polypyrrole-polyimide composite makes it a prospective material in polymer based charge storage devices, that is, rechargeable batteries and supercapacitors (Levin K et al., 2011). If we can keep PAA from converting to the imide form then we have a stable polymeric matrix. This is what we hope to achieve by encapsulating the PAA into another semiconducting polymer network without PAA converting to PI.



---

## 2.4 Biosensors

The recognition abilities of biological organisms for foreign substances are unparalleled. Scientists have developed new chemical analysis tools known as biosensors. They are defined as analytical devices incorporating a biological recognition element (enzyme, antibody, whole-cell, DNA, receptor or microorganisms) (Sadik and Wallace, 1993), which is integrated within a physicochemical signal transducer or transducing micro system. The signal transducing element (electrode, optical detector, piezo crystal etc.) converts the biochemical response into electric and optic signals which are amplified, measured and decoded by an appropriate electronic unit. A biosensor can produce either individual or successive digital electronic signals that are equivalent to the concentration of a single analyte or a group of analytes being monitored. Many parameters have been used to characterize a biosensor. Some are commonly used to evaluate the functional properties and quality of the sensor, such as sensitivity, stability and response time; while other parameters are related to the application rather than to the sensor functional properties. Piezoelectric biosensors and optical biosensors based on the phenomenon of surface plasmon resonance are both evanescent wave techniques. This utilises a property shown of gold and other materials; specifically that a thin layer of gold on a high refractive index glass surface can absorb laser light, producing electron waves (surface plasmons) on the gold surface. This occurs only at a specific angle and wavelength of incident light and is highly dependent on the surface of the gold, such that binding of a target analyte to a receptor on the gold surface produces a measurable signal. Other optical biosensors are mainly based on changes in absorbance or fluorescence of an appropriate indicator compound. Piezoelectric sensors utilise crystals which undergo a phase transformation when an electrical current is applied to them. An alternating current (A.C.) produces a standing wave in the crystal at a characteristic

---

frequency. This frequency is highly dependent on the surface properties of the crystal, such that if a crystal is coated with a biological recognition element the binding of a (large) target analyte to a receptor will produce a change in the resonant frequency, which gives a binding signal. Electrochemical biosensors are normally based on enzymatic catalysis of a reaction that produces ions. The sensor substrate contains three electrodes, a reference electrode, an active electrode and a sink electrode. A counter electrode may also be present as an ion source. The target analyte is involved in the reaction that takes place on the active electrode surface, and the ions produced create a potential which is subtracted from that of the reference electrode to give a signal.

Polymeric structures have been developed for biochemical sensing, environmental monitoring, and microelectronic applications. Omowunmi A. Sadik et al. has explored the feasibility of designing advanced conducting polymeric materials for sensing and remediation applications. These include the synthesis of (i) polyamic acid–silver nanoparticle composite membranes, (ii) polyoxydianiline films, and (iii) electrochemical deposition of gold nanoparticle films onto functionalized conducting polymer substrate. One of their approaches utilizes the unique reactivity of polyamic acid (PAA) by preventing the cyclization of the reactive soluble intermediate into polyimides at low temperature to design polymer-assisted nanostructured materials. The ability to prevent the cyclization process has enabled them to design of a new class of electrode materials (Sadik O et al., 2010). Novel materials are needed to improve the mechanical and biochemical stability of the sensor while improving the immobilization scheme to achieve bio-stability and spatial control of biomolecules. An ideal electrode material for the construction of biosensors must possess the following characteristics i.e (i) biocompatibility with the biological element, (ii) absence of diffusion barriers, (iii) stability with changes in temperature, pH, ionic strength, and/or macro-environment, (iv) sufficient sensitivity and selectivity for the analyte of interest, and (v) ease

---

of mass production. Moreover, the ideal material either should possess the necessary functional groups needed for the attachment of biomolecules or can be easily functionalized. In addition, an ideal electrode material must be characterized by good conductivity to ensure rapid electron transfer. A biosensor platform based on polyamic acid (PAA) has been reported for oriented immobilization of biomolecules. PAA, a functionalized conducting polymer substrate that provides electrochemical detection and control of biospecific binding, was used to covalently attach biomolecules, resulting in a significant improvement in the detection sensitivity. The biosensor sensing elements comprised of a layer of PAA antibody (or antigen) composite self-assembled onto gold (Au) electrode via N-hydroxysuccinimide (NHS) and 1-ethyl-3-(3-dimethylaminopropyl) carbodiimide (EDC) linking (Noah N et al., 2012). From literature, it is evident that PAA is a promising polymer matrix for various sensor applications. The carboxyl and amine functionalities have been employed in the design and fabrication of derivatised polymer platforms for applications. The challenge of course is to prevent imidization since this restricts the functionality of the carboxyl and amine moieties. A second challenge is to improve the chemical stability of the PAA, usually achieved by blending with other polymers such as polypyrrole on conductive matrices with graphene. The aim of this work is to produce stable PAA/Ppy composites and construct feasible biosensors for the detection of polycyclic hydrocarbons.

---

## 2.5 Naphthalene

Naphthalene is a toxic air pollutant generally found in ambient and indoor air due to emissions from the chemical and primary metals industries, biomass burning, gasoline and oil combustion, tobacco smoking, the use of mothballs, fumigants and deodorizers, and many other sources. Naphthalene is commonly used as an intermediate in the production of phthalic anhydride (66,000 metric tons in the U.S. in 2000), surfactants (27,000 tons) and pesticides (14,000 tons) (Preuss, R. et al., 2003). It is also found in many other environments, e.g., 40% of National Priority List (Superfund) sites contain naphthalene in soils. Naphthalene is also named tar camphor, naphthene, naphthalin, naphthaline, mothballs, mothflakes and white tar; trade names include albocarbon, dezodorator, mighty 150, and mighty RD1. Naphthalene is a special compound in terms of its properties and chemical structure. Naphthalene is a flammable white solid with the formula  $C_{10}H_8$  and the structure of two fused benzene rings, with melting and boiling points of 80.5 and 218 °C, respectively. Its odour is distinctive but not unpleasant, and its odour threshold is about 440  $\mu\text{g m}^{-3}$ . Due to its vapour pressure of 0.087 mmHg at 25 °C it is classified as a semi-volatile organic compound (SVOC), which is just below the 0.1 mmHg cut-off often used to define volatile organic compounds (VOCs). At room temperatures naphthalene sublimates rapidly. Naphthalene due to its bicyclic aromatic structure is also a polycyclic aromatic hydrocarbon (PAH), and it is the most volatile member of this group. In environmental studies examining VOCs, SVOCs and PAHs; naphthalene has been a target compound. While known as a common and widespread air contaminant, naphthalene received rather little attention prior to the finding of its carcinogenicity in rats in 2000. The general public is vulnerable to naphthalene mainly through inhalation of ambient and indoor air, followed by dietary and non-dietary ingestion. One estimate of the average intake rate for inhalation is 19  $\mu\text{g day}^{-1}$ , and 0.002 to 4.0  $\mu\text{g day}^{-1}$  for ingestion of water.

---

Exposure to naphthalene has been linked to a number of hostile health effects. The major non-cancer endpoints are hyperplasia and metaplasia in respiratory and olfactory epithelium and the cancer endpoint of concern are nasal tumors (Jia C et al., 2010).

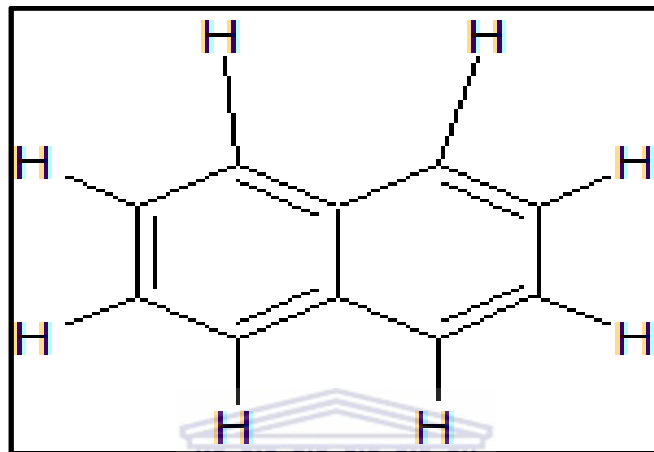


**Figure 7** Molecular structure of naphthalene.

Polycyclic aromatic hydrocarbons can be detected by Fluorescence spectroscopy which is 10 to 100 times more sensitive than UV-vis spectroscopy which is also another method used for the detection of PAHs. Gas-liquid chromatography is extensively used to determine the naphthalene content in mixtures.

**Table 3** Methods of analysing naphthalene.

Sample matrix	Assay procedure	Limit of detection
Air	GC/FID	1–10 µg/sample; 4 µg/sample
	HPLC/UV	0.6–13 µg/sample
	GC/FID	0.3–0.5 µg/sample
Drinking, ground and surface water	GC/MS	0.04 µg/L
Drinking water and raw source water	GC/PID	0.01-0.05 µg/L
Drinking water	HPLC/UV/FD	2.20 µg/L
Wastewater municipal and industrial	HPLC/UV or GC/FID	1.8 µg/L

Abbreviations: GC, gas chromatography, FID, flame ionization detection, HPLC, high performance liquid chromatography, UV, ultra violet detection, MS, mass spectroscopy, PID, photoionization detection, FD, fluorescence detection

---

Following dermal exposure to diapers or other clothing stored with naphthalene mothballs or playing in a room used to store naphthalene mothballs, children aged 1.5-36 months have developed hemolytic anemia (Shah et al., 1995). A 68-year-old woman developed aplastic anemia following inhalation and possibly dermal exposure to naphthalene and paradichlorobenze, which she placed into containers with stored clothing several hours a day for three weeks while working for a clothing resale business. With poor ventilation and no air conditioning during hot weather, this contributed to high vapor concentrations of naphthalene and paradichlorobenzene (Harden et al., 1978). Atlantic croaker fish (*Micropogonias undulatus*) exposed to naphthalene at either 0.5 or 1.0 ppm daily during sexual maturation demonstrated reduced rates of sexual maturity and arrested or reduced egg development. Reduced egg growth was associated with the decreased gonadal steroid levels in plasma (Thomas et al., 1995).



## 2.6 Fluoranthene

Fluoranthene, also known as 1,2-benzacenaphthene, benzo(j,k)fluorene, idryl, 1,2-(1,8-naphthalenediyl)benzene, or 1,2-(1,8-naphthylene)benzene, is a polycyclic aromatic hydrocarbon (PAH). Chemical formula of fluoranthene is  $C_{16}H_{10}$  and it has a molecular weight of 202.26 g/mol. Fluoranthene exists as pale yellow needles or plates; it has a boiling point of 375 °C, it has a melting point of 111 °C and it has a density of 1.252. Fluoranthene is soluble in alcohol, ether, benzene, and acetic acid and basically insoluble in water. The vapour pressure of Fluoranthene is  $1.91 \times 10^{-3}$  mmHg at 25°C. It can be produced by the pyrolysis of organic raw materials such as coal and petroleum at high temperatures; it is also known to occur naturally as a product of plant biosynthesis. It is a constituent of coal tar and

---

petroleum-derived asphalt. Fluoranthene is a common environmental pollutant that has been found in products of incomplete combustion of fossil fuels, main stream cigarette smoke, and in char-broiled foods. It has been recognized in surface, drinking, and waste water, in lake sediments, and in ambient air. It has been ranked number one of PAHs on Environmental protection agencies, (EPA's) priority pollutant list. There are no commercial productions or use of this compound (International Agency for Research on Cancer, 1983). Following dermal exposure fluoranthene can be absorbed through the skin (Storer, J.S et al., 1990) and, by analogy to structurally-related PAHs, would be expected to be absorbed from the gastrointestinal tract and lungs (U.S. Environmental Protection Agency, 1988).

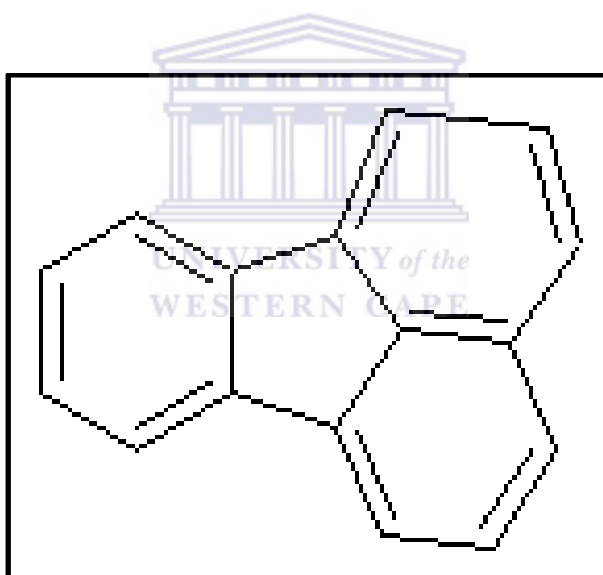


**Figure 8** Molecular structure of Fluoranthene.

Laser-induced fluorescence spectroscopy (LIFS) is a fast and reliable method for the online detection of contaminations with polycyclic aromatic hydrocarbons (PAHs) and oil in groundwater and soils (Baumann T et al., 2000). PAHs constitute a large and diverse class of organic compounds and are generally described as molecules which consist of three or more fused aromatic rings in various structural configurations. The biodegradation of PAHs by



---

microorganisms has been the subject of many excellent reviews and the biodegradation of PAHs composed of three rings is well documented (Robert A et al., 2000). Fluoranthene metabolites resulting from degradation by a *Mycobacterium* species has been reported. Kelley and Cerniglia showed that in mineral medium supplemented with organic nutrients, *Mycobacterium* sp. strain PYR-1 was capable of degrading greater than 95% of added fluoranthene within 24 h (Kelley, I. et al., 1991). HPLC method can be used for simultaneous determination of polyaromatic hydrocarbons (PAHs). Fluorescence and UV detection in combination with a HPLC system allows for limits of detection below 1 µg/L for all PAH (Rapid analysis of 17 polycyclic aromatic hydrocarbons with UV- and FL-detection according to DIN EN 17993:2002).

## 2.7 Luciferase



Scientists have always been interested in bioluminescent organisms, with their inherent beauty and ease of detection. Bioluminescence is chemiluminescence that requires an enzyme (luciferase). Bioluminescent organisms consist of a diverse set of species that are widely distributed, inhabiting terrestrial, freshwater and marine ecosystems. The biological significance of bioluminescence in the case of insects often focused on the effects of light emission as an attractant in mating. The clarification of luciferase genes regulation permitted the discovery of intercellular communication among bacteria, which then led to an improved understanding of bacterial pathogenesis and the associations of microorganisms in the environment. With the advent of molecular biology, it has been possible to construct bioluminescent bacteria that are naturally dark by insertion of lux genes. Initial studies in the elucidation of the bacterial bioluminescence mechanism suggested that a series of steps

---

would be involved in the bioluminescence. It was proposed that one molecule of reduced flavin mononucleotide (FMNH<sub>2</sub>) was utilized to reduce the luciferase. These conclusions were then modified, when it was found that its two reduced flavin molecules instead of one flavin mononucleotide to be involved. During bioluminescence one molecule of FMNH<sub>2</sub> combined with oxygen to form highly reactive organic peroxide while the other combined with an aldehyde molecule to form an aldehyde-FMNH<sub>2</sub> compound. These reactions account for the energetics. The blue-green light emission of bioluminescence, such as that produced by the bacteria *Photobacterium phosphoreum* and *Vibrio harvey*, arises from the reaction of molecular oxygen with FMNH<sub>2</sub> and a long-chain aldehyde to give FMN, water and a corresponding fatty acid. The luciferase enzyme catalyses a mixed function oxidation of the long-chain aldehyde and FMNH<sub>2</sub>. The reaction is highly specific for FMNH<sub>2</sub>, which is protected against autooxidation once bound to the enzyme. The bioluminescent reaction is as follows (da Silva Nunes-Halldorson et al., 2003):



Bioluminescence proteins use molecular oxygen to oxidize their substrates to a product molecule in its electronically excited state. To get an excited-state product, all bioluminescence reactions must be strongly exoergonic. The energy released from the oxidation of D-luciferin catalysed by firefly luciferase is about 10 times greater than that obtained from the hydrolysis of ATP. There are more than 30 different chemically unrelated bioluminescence systems in nature, found in organisms ranging from bacteria and fungi to fireflies and fishes, showing emissions ranging from blue-violet to red (Shimomura, 2006). The bacterial luciferase (*lux*) a widely employed bioluminescence protein, obtained from the marine luminous bacteria *Vibrio fischeri* and *Vibrio harvey*, catalyses a two-step reaction: the

---

reduced flavin bound to bacterial luciferase reacts with oxygen to form an intermediate peroxide, which then reacts with the bacterial luciferin (a long-chain aliphatic aldehyde like decanal or dodecanal) yielding the luciferase-bound excited hydroxyflavin, which is responsible for light emission (Figure 10). The individuality of bacterial luciferase is the possibility of constructing self-luminescent engineered organisms through the introduction of the whole *luxCDABE* (Figure 9) gene cassette, encoding for both luciferase and the enzymes able to synthesize its BL substrate. The engineered cells expressing other luciferases always require the addition of the proper luciferin to emit light (Roda et al., 2009).

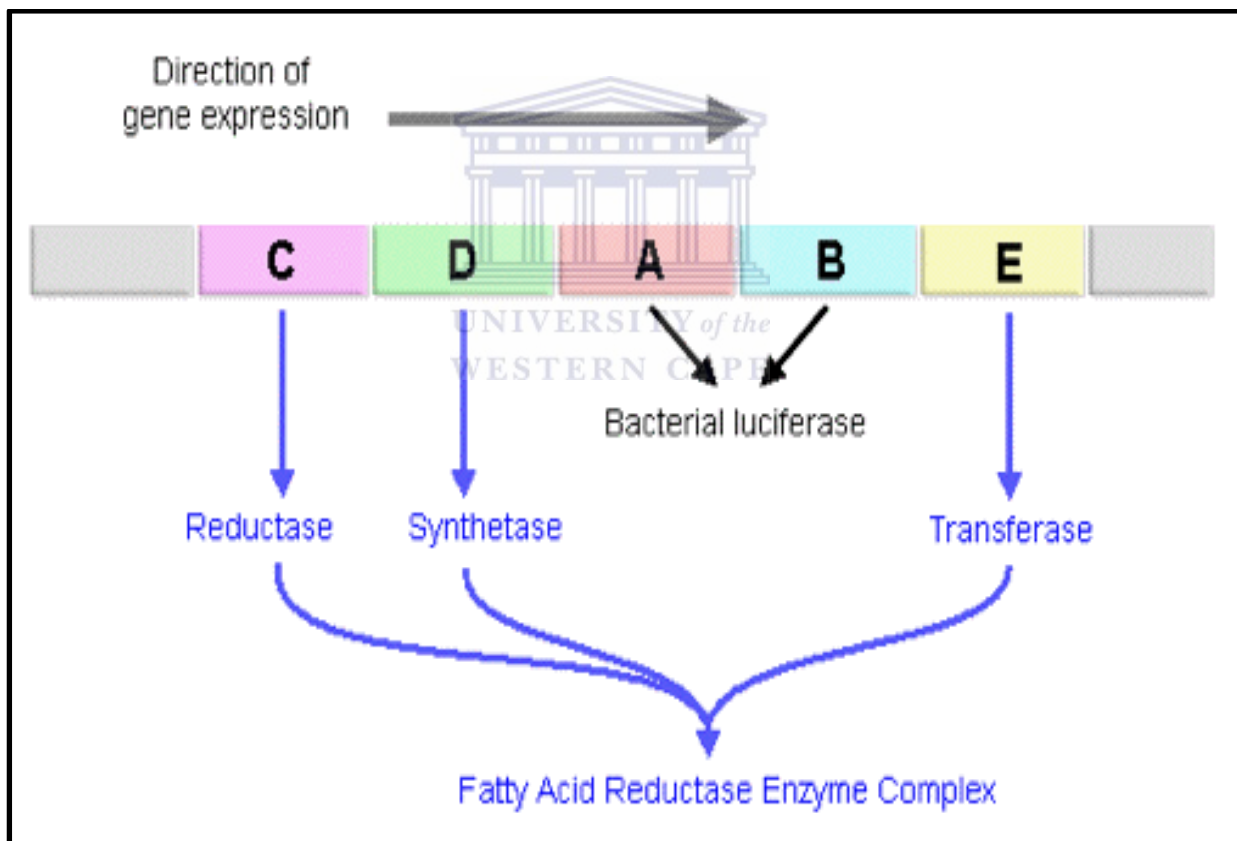


**Figure 9** The arrangement of the *luxCDABE* open reading frames.

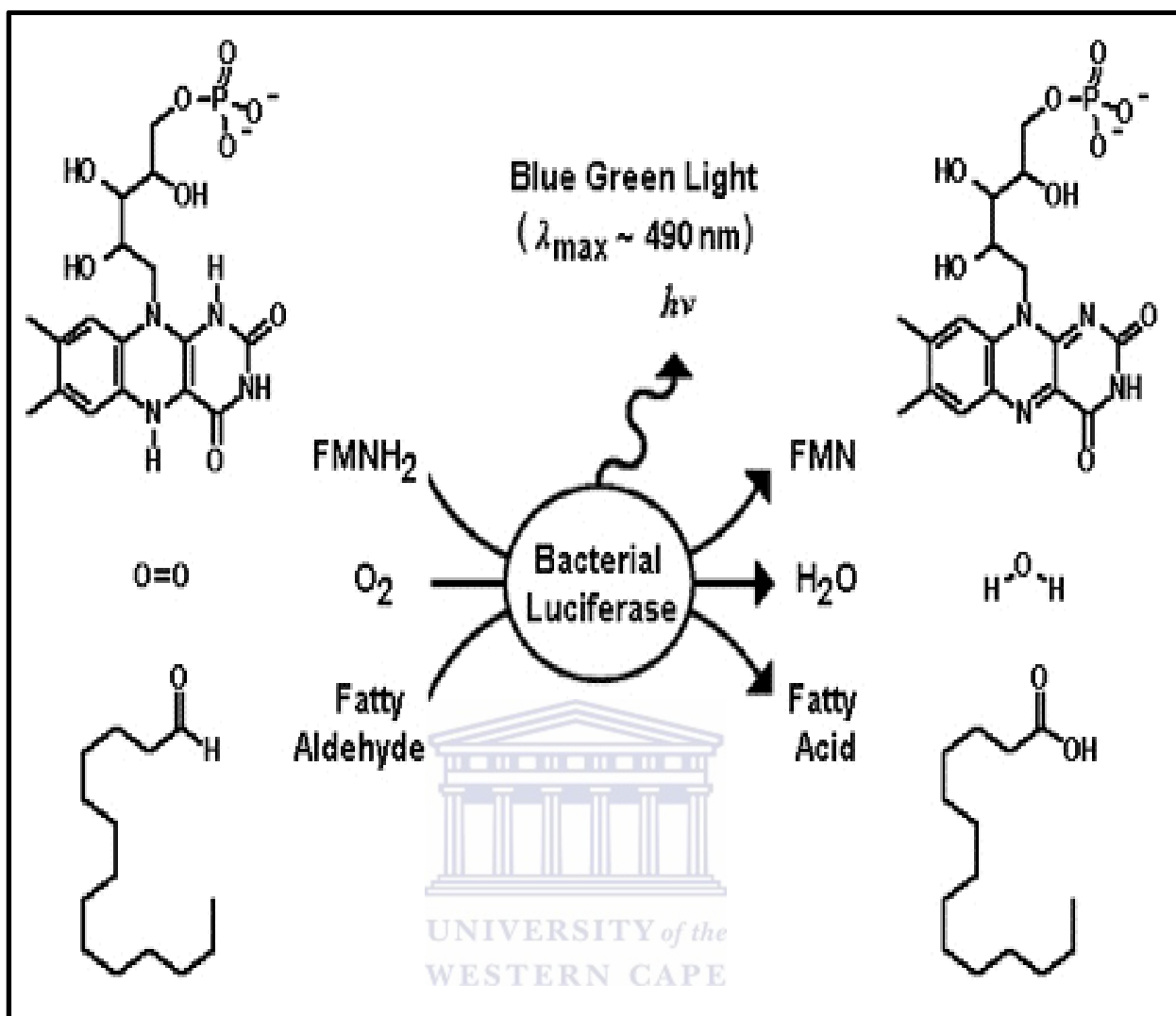


**Figure 10** The net chemical equation of the bacterial luciferase catalyzed reaction.

Among the analytical methods used for environmental monitoring, microbial and cellular biosensors play a crucial role. Microbial biosensors have several advantages in ecotoxicity testing. They respond rapidly to toxic compounds and indicate the bioavailability of compounds in a way that chemical analysis can't do. The use of the luciferase genes *lux* (from the marine bacterium *Vibrio fischeri*) and *luc* (from the firefly *Photinus pyralis*) are used as biomarkers. These genes have been selected because there is a correlation between light output and the metabolic activity of the cell, so bioluminescence is a very rapid indicator of a healthy cell. The genes encoding bioluminescence have been engineered into a range of

---

microbes. Measurement of bioluminescence in response to exposure to samples can be used to assess the existence of a wide range of pollutants. Light itself is easy to measure in real time and offers itself well to automation, allowing the rapid processing of multiple samples. A variety of whole-cell-based bioluminescent biosensors have been constructed which respond to a wide range of pollutants while simultaneously assessing bioavailability in environmental samples. A series of algal and cyanobacterial PSII-based whole-cell and tissue biosensors have been developed for detection of a class of herbicides which inhibit photosynthetic electron transport. Herbicides are then detected by testing inhibition reaction, inhibition of 2,6-dichlorophenol indophenol photoreduction or change in chlorophyll fluorescence, which can be correlated with the pollutant concentration (Shao C et. al., 2002). Fibre optic biosensors are devices involving immobilised biological active material on the end of a single optic fibre or a fibre bundle. Luminescent enzyme systems associated with optical transducers are considered to be highly selective and ultrasensitive biosensors. Monitoring of light emission occurring during bioluminescence reactions offers strong advantages when considering its analytical potential in terms of sensitivity, dynamic range and detection limit. A novel fibre optic biosensor was developed whereby the membrane-bound biocatalyst was placed in close contact with the tip of the fibre bundle. The light emitted at the membrane during the bioluminescent process was transmitted into a photomultiplier tube allowing the quantification of adenosine triphosphate (ATP) or reduced nicotinamide adenine dinucleotide (NADH) (Blum L et al., 1991).

The bioluminescence reactions of luciferase have been widely used for various biochemical analyses due to their high sensitivity. Among the various types of luciferases, firefly luciferase (FFL) has been used as a model system of biological reactions because of the high quantum yield of the luminescence reaction (Ignowski, J.M. et. al., 2004; Eckenhoff, R.G.et.

---

al., 2001). FFL luminescence reaction has been reported to be inhibited by small hydrophobic drugs such as inhalation anaesthetics, and it has been utilized to study the action mechanisms of these drugs on the protein functions. FFL is unstable and rapidly loses its activity in an aqueous solution without stabilizing agents such as dithiothreitol and glycerol. These stabilizing agents have the risk, by binding to the FFL, to interfere with the clear understanding of the inhibition mechanism of the target drugs. Bacterial luciferase (BL), which is also a luminescent enzyme, has a higher stability than FFL in aqueous solution. The reaction mechanism of the BL was studied in detail by Hastings group (Hastings J et al 1963). Small hydrophobic drugs can be considered to bind to the BL in competition with the hydrophobic substrate alkyl aldehyde. The BL system is a potential model system to study the action mechanisms of hydrophobic drugs on proteins. There is however some underlying problems as to use the BL reaction as the model system, and needs to be solved before putting this model system into practice. Under aerobic conditions, the FMNH<sub>2</sub> is rapidly oxidized to FMN by dissolved oxygen before it binds to BL and hence the effective light emission is not obtained unless regenerating of the FMNH<sub>2</sub> from FMN. In biological systems, FMNH<sub>2</sub> is regenerated by the enzymatic catalysis of flavin reductase by coupling the oxidation of nicotinamide adenine dinucleotide (NADH). In artificial systems, FMNH<sub>2</sub> can be regenerated by chemical reducing agents such as sodium dithionite and sodium borohydride, by employing this method it is difficult to control the reduction of FMN to obtain the continuous and constant intensity of the BL luminescence (Yamasaki S et al 2009).

---

# Chapter 3

## Materials and Methodology

*This chapter describes the various analytical techniques employed, a detailed research methodology and general experimental procedures for the electrochemical synthesis of nanostructured conducting polymer composites, biosensor construction, characterization and application of the developed biosensor for the determination of selected polycyclic hydrocarbons.*

### 3.1 Introduction



This chapter consists of the following:

- Materials: Information on all the materials used.
- Research design: A general overview of all the sequential steps taken.
- Methodology: A more detailed presentation of the instrumental techniques and experimental parameters.

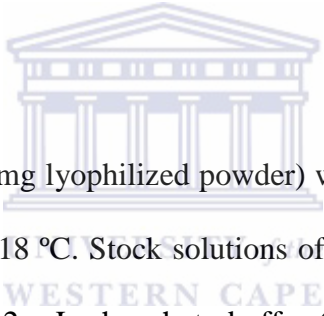
### 3.2 Reagents and materials

The reagents 4,4'-oxydianiline (97%) (ODA), 1,2,4,5-benzenetetracarboxylic acid (96%) (PMDA), tetrahydrofuran (99.9%) (THF), methanol (99.9%) (MeOH), triethylamine (99%) (TEA), acetonitrile (99%) (ACN), pyrrole (98%) was vacuum distilled and stored frozen under nitrogen, disodium hydrogen phosphate, potassium dihydrogen phosphate,

---

Naphthalene (99.7%) and Fluoranthene (98%) were all obtained from Sigma-Aldrich, South Africa. All chemicals were of analytical reagent grade and were used without further purification. Deionized (ultra-pure) water with a resistivity of 18.2 MΩcm was purified by a Milli-QTM system (Millipore) and was used as reagent water for aqueous solution preparation.

Phosphate buffer solution of 0.2 M and pH 7 was prepared by dissolving 17.79 g of disodium hydrogen phosphate and 15.60 g of potassium dihydrogen phosphate separately in 500 mL deionized water, then mixing the salt solutions according to Henderson-Hasselbalch equation to obtain the required pH values. The phosphate buffer solution (PBS) was refrigerated at 4° C.



Photobacterium f luciferase (100 mg lyophilized powder) was obtained from Sigma-Aldrich, South Africa and refrigerated at -18 °C. Stock solutions of Photobacterium f luciferase were prepared by dissolving 20 mg in 2 mL phosphate buffer (pH 7.01) in eppendorf vials. The stocks were refrigerated at -18° C and fresh enzyme solutions prepared prior to experiments.

Analytical grade Argon gas was purchased from Afrox Company, South Africa. Alumina polishing pads and powder (0.05, 0.3 and 1.0 μM) were obtained from Buehler, Illinois, USA.



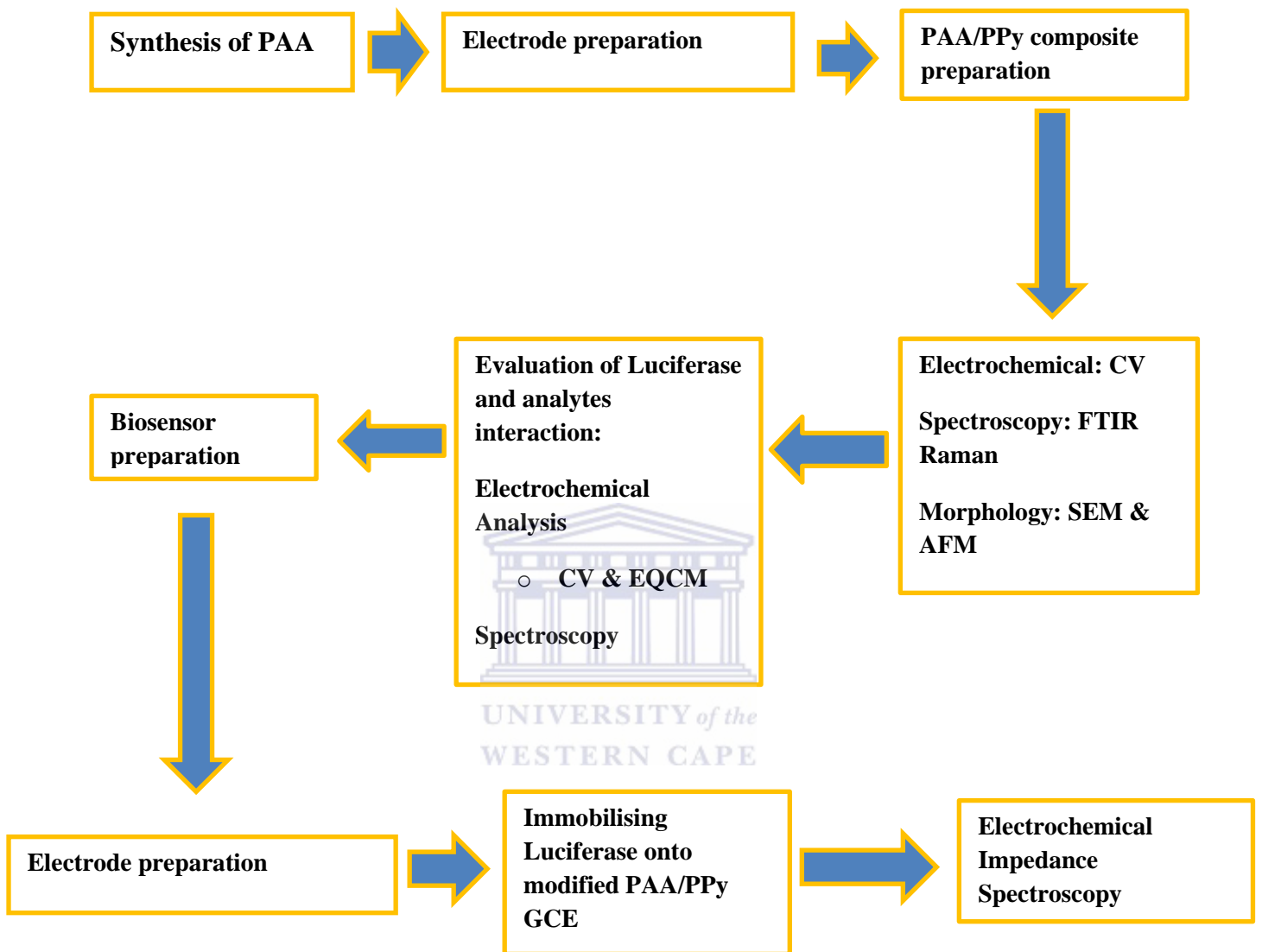


**Figure 11** Flow chart of research design.

- 
1. Chemical synthesis of polyamic acid
  2. Electrode preparation: cleaning GCE by polishing with pads and alumina powder (0.05, 0.3 and 1.0  $\mu\text{M}$ ) which was obtained from Buehler, Illinois, USA, followed by sonication of electrodes in ethanol and water this was done prior to electrochemical measurements.
  3. Different ratios of the PAA/PPy were synthesized via in situ polymerization processes.
  4. Electrochemical measurements: Voltammetric methods such as cyclic voltammetry (CV), square wave voltammetry (SWV) were used at different stages to obtain relevant data towards the characterization of the new composites. Spectroscopy measurements were done with FTIR and Raman spectroscopy. Morphology measurements were carried out using scanning electron microscopy (SEM) and Atomic force microscopy (AFM).
  5. Solution phase evaluation of luciferase with each analyte: Electrochemical (CV, SWV, EQCM) techniques and Fluorescence spectroscopy.
  6. Biosensor preparation: Incubating PAA/PPy modified GCE in a luciferase solution for 4 hours. The modified electrode was rinsed with PB (pH 7) to remove excess enzyme. The electrode was then ready for use.
  7. Biosensor evaluation with EIS: Measurement of response to naphthalene and fluoranthene, stability, linearity, sensitivity and detection limit.

---

## 3.3 Methodology

### 3.3.1 PAA synthesis

The PAA liquid was prepared according to Ref. (Andreescu et al, 2005). The synthesis of the PAA liquid was carried out in organic medium from 4,4'-oxydianiline (ODA) and 1,2,4,5-benzenetetracarboxylic acid (PMDA) precursors. The preparation procedure involved the following steps: 2.4 g (0.01 mol) of ODA plus 42 mL of THF were stirred in a 0.5 L round-bottom flask. PMDA powder (2.1812 g, 0.01 mol) was added to the solution over 1 hr. MeOH (35 mL) containing 0.02 mol (2.787 mL) of TEA was added. The solution was stirred for 24 hours, which resulted in a dark yellow viscous solution of PAA. The resulting PAA liquid content was 9.8%. This viscous PAA liquid (Figure 12) was soluble in phosphate-buffered saline (PBS) pH 7. When ACN was used as solvent, another PAA derivative was obtained in a powdered form from the same ODA and PMDA. To prepare this PAA, 2.0024 g (0.01 mol) of ODA plus 157 mL of ACN were stirred till solvation. Then, 50 mL of ACN containing 2.1812 g of PMDA (0.01 mol) was added dropwise over 1 h and the solution was stirred for over 24 h. The resulting precipitates were filtered under suction and finally The PAA solid dried at room temperature. The amount of PAA obtained was 2.170 g. The PAA solid was only soluble in organic media eg. N,N'-dimethylacetamide (DMAc), dimethyl sulfoxide (DMSO) or dimethylformamide (DMF) and was not used further because of solubility interferences when preparing composites.



**Figure 12** Polyamic acid prepared as a viscous liquid.

### 3.3.2 Composite preparation

The PAA/PPy was synthesized via in situ polymerization processes. The concentration of polyamic acid solution ( $1.37 \times 10^{-6}$  M) was kept fixed throughout the composite ratio process. The concentration of PPy was varied from  $1.9 \times 10^{-3}$  to  $9.09 \times 10^{-3}$  M. The ratios were as follows: 1: $1.34 \times 10^3$  (Composite one); 1: $2.81 \times 10^3$  (Composite two); 1: $4.13 \times 10^3$  (Composite three); 1: $5.41 \times 10^3$  (Composite four); 1: $6.64 \times 10^3$  (Composite five). The PAA/PPy ratios were mixed in 5 mL of 0.2 M PBS aqueous solution. The solutions were stirred for a minute and degassed before experiments. The GCE were cleaned by mechanical polishing of electrodes with polishing pads and powder (0.05, 0.3 and 1.0 micron) which was obtained from Buehler, Illinois, USA. The GCE were then sonicated with ethanol and with distilled water afterwards. The PAA/PPy composites were electropolymerized onto, working electrodes, glassy carbon electrodes (GCE) (diameter 3.0 mm) and a platinum wire (diameter 1.0 mm) and a

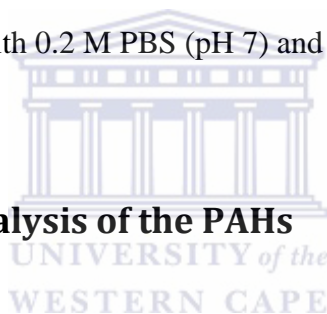
---

silver/silver chloride (3 M NaCl type) electrodes (Bioanalytical Systems Ltd., UK) were used as counter electrode and reference electrode, respectively.

### 3.3.3 Biosensor preparation

Onto a cleaned polished and sonicated GCE electrode,  $1:4.13 \times 10^3$  (Composite three) as prepared earlier was electropolymerized onto GCE. The functionalised electrode was rinsed with 0.2 M PBS and left to dry for 3-5 minutes. After drying, the functionalised electrode was incubated in 2 mL of the luciferase stock solution for 4 hours in the fridge at a temperature of 4 °C. The biosensor was rinsed with 0.2 M PBS (pH 7) and was ready for use.

### 3.3.4 Preparation and analysis of the PAHs



Most PAHs are insoluble in water hence a suitable organic solvent is necessary to completely dissolve them. The choice of solvents is determined by several factors, including conductance, solubility of electrolyte and electroactive substance and the reactivity with electrolytic products. In Fry and Britton's handy review of solvents and electrolytes, acetonitrile, ethanol, methanol, and methylene chloride are recommended as good oxidative (anodic) electrochemical solvents, while dimethylformamide (DMF) and dimethyl sulfoxide (DMSO) are suggested for reductive (cathodic) electrochemistry. Acetonitrile was chosen as a suitable solvent since it was found that the PAHs dissolved in it and ACN has been reported to have relatively high dielectric constant, it is also non-toxic and it portrays good electrochemical properties. Since, acetonitrile is a non-aqueous electrolyte, a suitable supporting electrolyte was necessary to enhance conductivity, minimize double-layer and

---

migration currents. Most PAHs are found in waste water hence the need to introduce water in the acetonitrile. In this work, water was introduced in to the acetonitrile by preparing a solution of acetonitrile and water in the ratio 80:20 (acetonitrile: water). This mixture of acetonitrile and water was used as the solvent in all sensor applications and will thus be referred to as acetonitrile. 1 mM of standard solutions of naphthalene and fluoranthene were prepared as follows: 0.022 g and 0.025 g of naphthalene and fluoranthene were dissolved each in about 15 cm<sup>3</sup> of acetonitrile (to achieve solubility), respectively, and later made up to 25cm<sup>3</sup> solutions in distilled water with continuous stirring for about 30 min. From these stock solutions, 1 μM stock solutions were made. From these 1 μM stock solutions 2 μL aliquots were drawn and added to the cell and used for assessment of biosensor behaviour.

### 3.4 Measurements and Instrumentation



Voltammetric experiments were recorded with BASi 100B electrochemical work station (LG Fayette) using a conventional three-electrode system. For the electropolymerization of polyamic acid and polypyrrole composites, the working electrodes used was glassy carbon electrodes (GCE) with a diameter of 3.0 mm and while a platinum mesh or wire (diameter 1.0 mm) and a silver/silver chloride (3 M NaCl type) electrode (Bioanalytical Systems Ltd., UK) were used as counter electrode and reference electrodes, respectively. The modified screen printed carbon electrode (SPCE's) with a diameter of 3.0 mm, was used for scanning electron microscopy (SEM) studies. SEM images were taken with a Hitachi S3000N Scanning electron microscope. An acceleration voltage of 20 kV was employed at various magnifications. Surface morphology of the modified SPCE was studied with Atomic force spectroscopy (AFM), NanoSurf model, tapping mode with silicon tip using spring constant of 1-5 N/m and resonance frequency of 60-100 kHz. To study the structural changes within

---

composites Raman and Fourier transform infrared (FTIR) spectroscopy was employed. The cleaning method involved mechanical polishing of GCE using alumina powder of size 1, 0.3 and 0.05 micron (Buehler, IL, USA) respectively followed by sonication in ethanol and water. Spectroscopic and electrochemical techniques were used to study the interaction of the enzyme and the analytes. Fluorescence spectra of liquid samples were recorded using Horiba NanoLog™ 3-22- TRIAX (USA), with double grating excitation and emission monochromators at a slit width of 5 nm. EQCM measurements of luciferase and the analytes were recorded using Nova 1.9.Ink Autolab. Electrochemical impedance spectroscopy of the biosensor was measured with a Voltalab instrument (Radiometer Analytical, France).

## 3.5 Electrochemical techniques



### 3.5.1 Cyclic voltammetry (CV)

The basic components of a modern electroanalytical system for voltammetric measurements are a potentiostat, a computer, and the electrochemical cell. The potentiostat plays the role of applying accurate and controlled potential and monitoring the current produced. In the computer-controlled instruments, the properties of the modulation and the waveform are under software control and can be specified by the operator. The most commonly used waveforms are linear scan, differential pulse, and square wave. The electrochemical cell, where the electrochemical measurements are carried out, consists of a working (indicator) electrode, a reference electrode, and usually a counter (auxiliary) electrode. The electrode provides the interface across which charge can be transferred. The reaction or transfers of interest takes place at the working electrode, whenever we refer to the electrode, we always mean the working electrode. The reduction or oxidation of a substance at the surface of a

---

working electrode, at the appropriate applied potential, results in the mass transport of new material to the electrode surface and the generation of current.



**Figure 13** A three electrode system electrochemical cell; WE = working electrode, RE = reference electrode and AE = auxiliary electrode.

**Working electrode** – this is the electrode at which the redox of the analyte or the electrochemical phenomena being investigated takes place. The commonly used materials for working electrodes include platinum, gold, glassy carbon and boron-doped diamond

**Reference electrode** – this is the electrode whose potential is known and is constant. Its potential is taken as the reference, against which the potentials of the other electrodes are measured. The most commonly used reference electrodes for aqueous solutions are the saturated calomel electrode (SCE) and silver/silver chloride electrode (Ag/AgCl);



---

*Auxiliary electrode* – it serves as a sink for electrons so that current can be passed from the external circuit through the cell. Reactions occurring at the auxiliary electrode surface are unimportant as long as it continues to conduct current well. To maintain the observed current, this electrode will often oxidize or reduce the solvent or bulk electrolyte though the reactions occur over short periods of time and rarely produce any appreciable changes in bulk concentrations. Most often the auxiliary electrode consists of a metallic foil or thin platinum wire, although gold and sometimes graphite have also been used.

The cyclic voltammetry (CV) and square wave voltammetry (SWV) measurements were performed using a potentiostat BAS 100B/W electrochemical analyzer from Bioanalytical Systems, Inc. (West Lafayette, IN) with a conventional three-electrode system consisting of glassy carbon electrode (1.6 mm diameter, 3.0 mm diameter) as the working electrode, platinum wire as the auxiliary electrode, and Ag/AgCl (saturated 3 M NaCl) as the reference electrode. Prior to experiments, the bare glassy carbon electrodes were polished with aqueous slurries of 1.0, 0.3 and 0.05  $\mu\text{m}$  alumina powder, rinsing with distilled water after polishing with each grade of alumina. The polished electrode was then sonicated in absolute ethanol and distilled water. The auxiliary electrode was cleaned by burning in a flame for several minutes and the Ag/AgCl electrode was cleaned by rinsing with distilled water. All potentials were quoted with respect to Ag/AgCl. The potentiostat was computer-controlled therefore the experimental modes were selected from the software and specified during its operation. Phosphate buffer solution (0.2 M PBS, pH 7) was used as the supporting electrolyte. All experimental solutions were purged with high-purity argon gas for 10 min and blanketed with argon atmosphere during measurements. The experiments were carried out at controlled room temperature of 22 °C.

---

The common characteristics of all voltammetric techniques is that they involve the application of a potential ( $E$ ) to an electrode and the monitoring of the resulting current ( $I$ ) flowing through the electrochemical cell. In many cases, the applied potential is varied or the current is monitored over a period of time ( $t$ ). Thus all voltammetric techniques can be described as some function of  $E$ ,  $I$ , and  $t$ . They are considered as active techniques (as opposed to passive techniques such as potentiometry) because the applied potential forces a change in the concentration of an electroactive species at the electrode surface by electrochemically reducing or oxidizing it. Cyclic voltammetry (CV) is a widely used electroanalytical technique. It has wide applications in the study of redox processes, electrochemical properties of analytes in solution, and for understanding reaction intermediates (Bard & Faulkner, 2001). In CV, the electrode potential is ramped linearly at a scan rate of  $v$ . The resultant trace of current against potential is termed as a voltammogram. During cyclic voltammetry measurement, the potential is ramped from an initial potential,  $E_i$  to a more negative potential but, at the end of its linear sweep, the direction of the potential scan is reversed, usually stopping at the initial potential  $E_i$  (or it may commence an additional cycle) (Monk, 2001). The potential is usually measured between the reference electrode and the working electrode and the current is measured between the working electrode and the auxiliary electrode, also known as the counter electrode. This data is then plotted as current versus potential as shown in Figure 14. The forward scan produces a current peak for any analytes that can be reduced (or oxidized depending on the initial scan direction) through the range of the potential scanned. The current increases as the potential reaches the reduction potential of the analyte, but then decreases as the concentration of the analyte is depleted close to the electrode surface. If the redox couple is reversible, then reversing the applied potential makes it reach a potential that re-oxidizes the product formed in the first reduction reaction, thus producing a current of reverse polarity from the forward scan. The oxidation

---

peak usually has the same shape as that of the reduction peak. As a result, the information about the redox potential and the electrochemical reaction rates of compounds can be obtained. For instance, if the electronic transfer at the surface is fast and the current is limited by the diffusion of species to the electrode surface, then the current peak will be proportional to the square root of the scan rate.

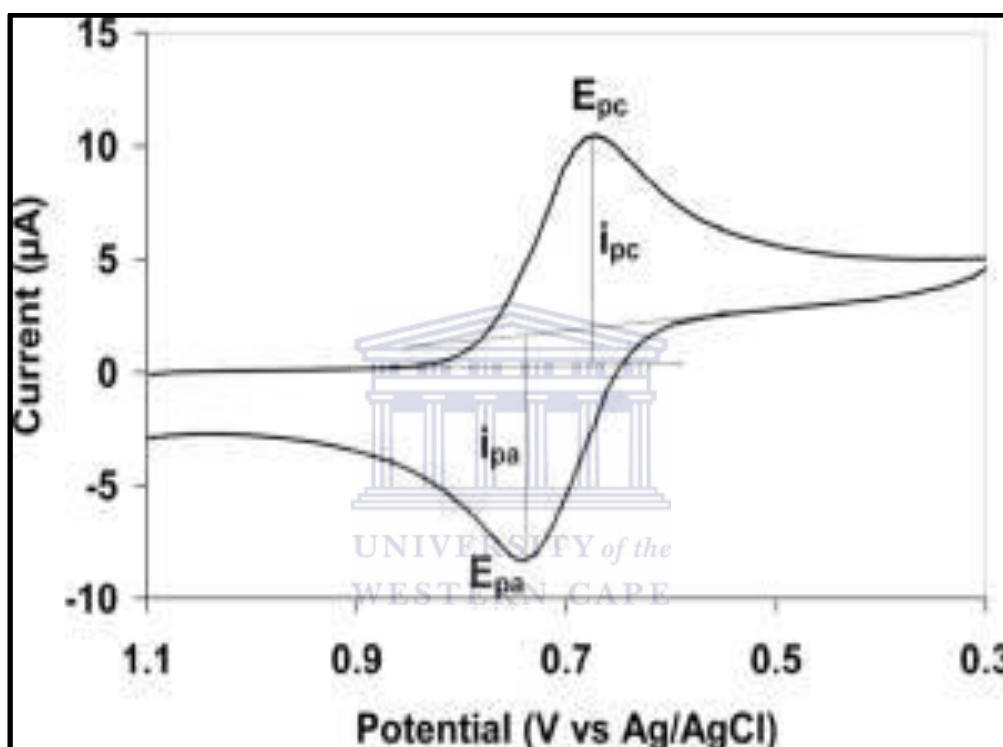


**Figure 14** The important parameters in a cyclic voltammogram are the peak potentials ( $E_{pc}$ ,  $E_{pa}$ ) and peak currents ( $i_{pc}$ ,  $i_{pa}$ ) of the cathodic and anodic peaks, respectively.

If the electron transfer process is fast compared with other processes (such as diffusion), the reaction is said to be electrochemically reversible, and the peak separation is:

$$\Delta E_p = |E_{pa} - E_{pc}| = 2.303 RT / nF$$

**Equation 3.1**

Thus, for a reversible redox reaction at 25 °C with  $n$  electrons  $\Delta E_p$  should be  $0.0592/nV$  or about 60 mV for one electron. In practice this value is difficult to attain because of such factors as cell resistance. Irreversibility due to a slow electron transfer rate results in  $\Delta E_p > 0.0592/n V$ , greater, say, than 70 mV for a one-electron reaction. The diagnostic tests for electro-reversibility are listed in Table 4.

**Table 4** Diagnostic tests for the electrochemical reversibility of a redox couple, carried out by cyclic voltammetry.

1.	$ I_{pa} / I_{pc}  = 1$
2.	The peak potentials, $E_{pc}$ and $E_{pa}$ , are independent of the scan rate $v$
3.	The formal potential ( $E^{\circ'}$ ) is positioned midway between $E_{pc}$ and $E_{pa}$ , so $E^{\circ'} = (E_{pa} + E_{pc}) / 2$
4.	$I_p$ is proportional to $\sqrt{v}$
5.	The separation between $E_{pc}$ and $E_{pa}$ is $0.0592/n V$ for an $n$ -electron couple (i.e. $\Delta E_p =  E_{pa} - E_{pc}  = 0.0592/n V$ )

For a reversible reaction, the concentration is related to peak current by the Randles–Sevcik expression (at 25 °C) (Monk, 2001; Bard & Faulkner, 2001):

$$I_p = 2.686 \times 10^5 n^{3/2} A C_0 D^{1/2} v^{1/2}$$

**Equation 3.2**

---

Where  $I_p$  is the peak current in amperes,  $n$  is the number of electrons transferred,  $A$  is the electrode area ( $\text{cm}^2$ ),  $D$  is the diffusion coefficient ( $\text{cm}^2 \text{s}^{-1}$ ),  $c_0$  is the concentration in  $\text{mol cm}^{-3}$ , and  $v$  is the scan rate in  $\text{V s}^{-1}$ .

For a surface thin layer adsorption or strong adsorption:

$$I_p = (n^2 F^2 / 4RT) v A \Gamma_0$$

**Equation 3.3**

Cyclic voltammetry is carried out in quiescent solution to ensure diffusion control. A three-electrode arrangement is used. The utility of cyclic voltammetry is highly dependent of the analyte being studied. The analyte has to be redox active within the experimental potential window. It is also highly desirable for the analyte to display a reversible wave. A reversible wave is displayed when an analyte is reduced or oxidized on a forward scan and is then re-oxidized or re-reduced in a predictable way on the return scan as shown in Figure 14. Electrochemical reactions sometimes show non-reversible or quasi-reversible waves with deviation from the above reversibility behaviours. For quasi-reversible systems for instance, the peak separation ( $\Delta E_p$ ) is greater than  $59 \text{ mV} / n$  and increases with increasing  $v$ ; the peak current  $I_p$  increases with  $\sqrt{v}$  but is not proportional to it and the cathodic peak potential shifts negatively with increasing  $v$ . In this study, CV was employed for the in-situ synthesis of the composites and to investigate the redox processes and the electrochemical properties of the biosensor and analytes in solution.

---

### 3.5.2 Square Wave Voltammetry (SWV)

Figure 15 is typical square wave voltammogram showing the forward ( $i_f$ ), reverse ( $i_r$ ) and net ( $i_{net}$ ) currents is shown below:

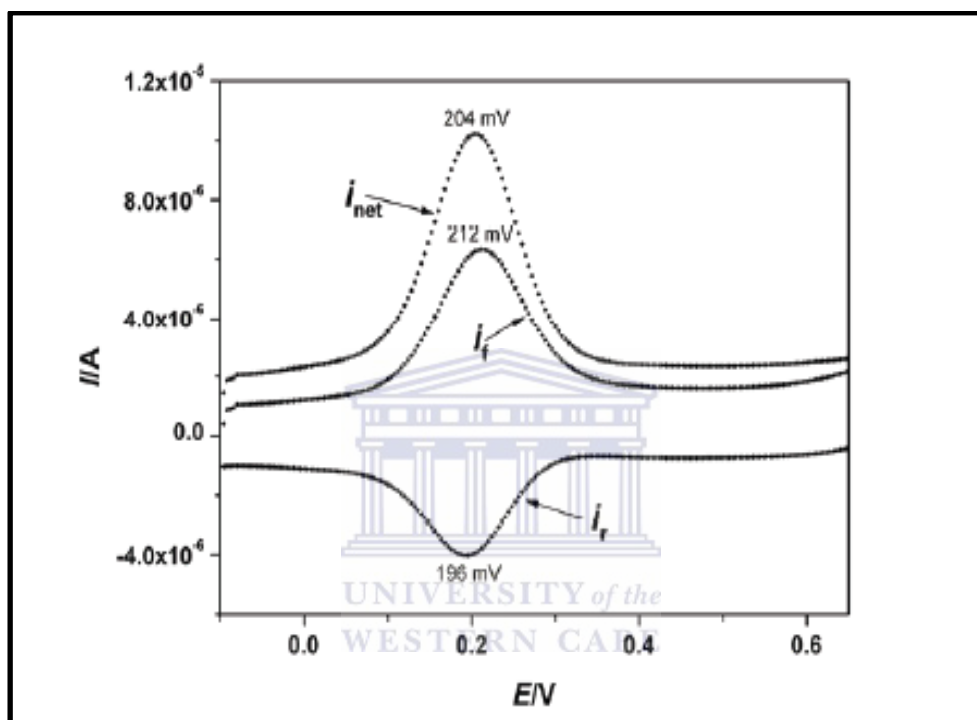


**Figure 15** Diagram of a Square wave voltammogram

Though SWV was pioneered by Barker (Barker GC, 1952), it was the work of Osteryoung and co-workers (Osteryoung, J, et al., 1986) that brought it to limelight. It has a slightly better sensitivity than DPV and can be used to study electrochemical processes at fast scan rates. The potential waveform above consists of a square wave superimposed on a staircase. The current at the end of the forward pulse,  $i_f$ , and the current at the end of the reverse pulse,  $i_r$ , are both registered as a function of the staircase potential, which is midway between the potentials corresponding to the forward and backward potential steps. The difference,  $i_{net}$ , ( $i_f$ -

$i_r$ ) is larger than each individual component in the region of the peak that is centred on the half-wave potential because  $i_f$  and  $i_r$  have opposite signs. This difference, effectively cancels the capacitive currents and thus higher scan rates are possible without background current interferences. This makes SWV a useful tool in kinetic study. SWV is characterised by four parameters: square wave period,  $\tau$ , pulse width,  $t_p = \tau / 2$ , step height,  $\Delta E_s$  and pulse height,  $\Delta E_{sw}$ . The pulse width is related to the square wave frequency,  $f = 1/(2t_p)$  and as the staircase step at the beginning of each cycle is  $\Delta E_s$  it means that the effective scan rate is  $v = \Delta E_s / 2t_p = f\Delta E_s$ . Peak Current is given by

$$\Delta i_p = (nFAD^{1/2} C / \pi^{1/2} t_p^{1/2}) \Delta \psi_p$$

**Equation 3.4**



Experimentally,  $\Delta E_s$  is usually kept constant while the frequency is varied.

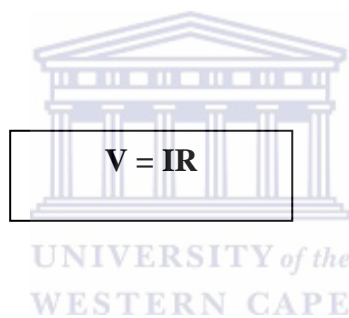
### 3.5.3 Electrochemical Impedance Spectroscopy (EIS)

Macdonald, in his review (Macdonald, D.D., 2006), traced the foundation of electrochemical impedance spectroscopy (EIS) back to a scientist called Oliver Heaviside. Heaviside was the first person to define the term impedance. Electrochemical impedance spectroscopy is an excellent, non-destructive, accurate and rapid in situ technique for examining processes occurring at electrode surfaces. A small amplitude ac (sinusoidal) excitation signal (potential or current), covering a wide range of frequencies, is applied to the system under investigation and the response (current or voltage or another signal of interest) is measured. This is in contrast to the ‘usual’ spectroscopic techniques where interactions of electromagnetic waves

---

and materials are measured. The measurement of impedance is only valid when the system is linear – thus the need for the small amplitude of the excitation signals in EIS. The measurement should be carried out without significantly disturbing the properties being measured. Due to the wide range of frequencies used, the complex sequence of coupled processes such as, electron transfer, mass transport, chemical reaction, etc. can often be separated and investigated with a single measurement. It is routinely used in electrode kinetics and mechanism investigations, and in the characterization of batteries, fuel cells, and corrosion phenomena (Macdonald, D.D, 1990). It is also widely applied in the characterization of semiconductors, organic films and very recently biosensors. The application of EIS in biosensor is relatively new (Pejic, B. et. al., 2006). A brief theory:

From Ohm's law



**Equation 3.5**

Resistance is independent of frequency. AC current (Figure 16) and voltage through a resistor are in phase with each other. Suppose we apply a sinusoidal potential excitation. The response to this potential is an AC current signal containing the excitation frequency and its harmonics which is not in the same phase with the AC voltage. The resultant resistance in this case is called Impedance.



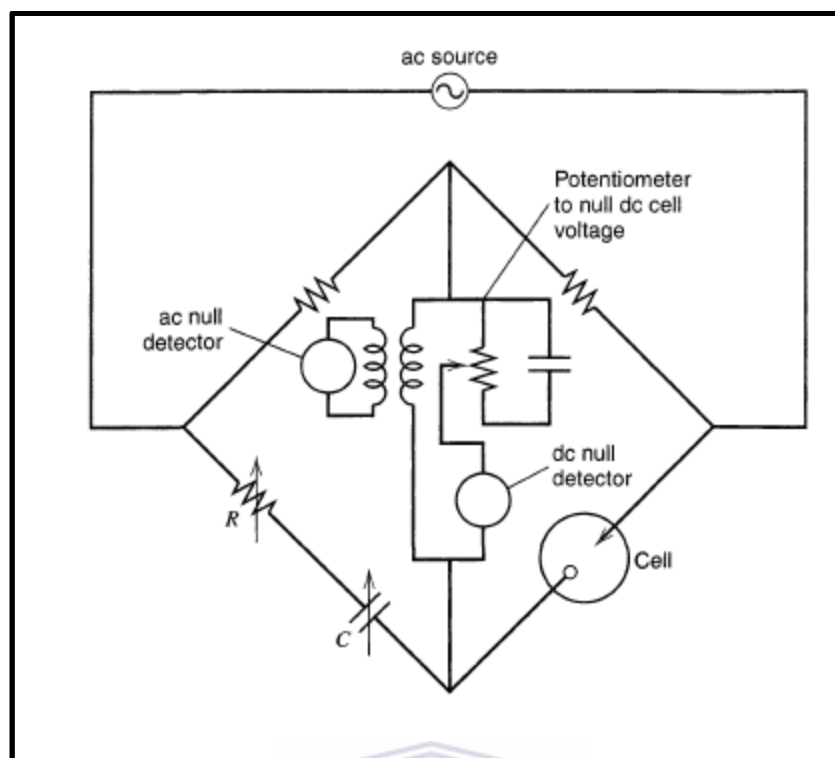


**Figure 16** A bridge circuit for measurements of electrochemical impedance

Impedance is the totally complex resistance encountered when a current flows through a circuit made of combinations of resistors, capacitors, or inductors. Electrochemical transformations occurring at the electrode–solution interface can be modeled using components of the electronic equivalent circuitry that correspond to the experimental impedance spectra. Particularly useful to model interfacial phenomena is the Randles and Ershler electronic equivalent-circuit model. This includes the double-layer capacitance  $C_d$ , the ohmic resistance of the electrolyte solution  $R_s$ , the electron transfer resistance  $R_p$ , and the Warburg impedance  $W$  resulting from the diffusion of ions from the bulk solution to the electrode surface. The impedance of the interface, derived by application of Ohm’s law, consists of two parts, a real number  $Z'$  and an imaginary one,  $Z''$ :

---

$$Z(\omega) = R_s + R_p (1 + \omega^2 R_p^2 C_d^2) - j\omega R_p^2 C_d (1 + \omega^2 R_p^2 C_d^2) = Z' + jZ''$$

where  $j = \sqrt{-1}$

**Equation 3.6**

Impedance spectroscopy involves the use of a small-amplitude perturbing sinusoidal voltage signal to the electrochemical cell and measuring the current response. The resulting faradaic impedance spectrum, known as a Nyquist plot, corresponds to the dependence of the imaginary number on the real number, and contains extensive information about the electrified interface and the electron transfer reaction. Nyquist plots commonly include a semicircle region lying on the axis followed by a straight line. The semicircle portion (observed at higher frequencies) relates to the electron-transfer-limited process, while the straight line (characteristic of the low-frequency range) signifies the diffusion-limited process. Such spectra can be used for extracting the electron transfer kinetics and diffusional characteristics. At very fast electron transfer processes the impedance spectrum includes only the linear part, while at very slow electron transfer processes are characterized by a large semicircular region. The diameter of the semicircle equals the electron transfer resistance. The intercepts of the semicircle with the  $Z'$  axis correspond to those of Resistance ( $R_s$ ). This technique has been found extremely useful for transduction of bioaffinity events in connection to modern electrical immunosensors and DNA biosensors (Buch, R.M et. al., 1989). Such transduction of bioaffinity events relies on the increased insulation of the electrode surface in respect to redox probes (e.g., ferrocyanide), present in the solution, on binding of large biomolecules (e.g., capture of an antigen that retards the electron transfer). Figure 17 Faradaic impedance spectra presented in the form of Nyquist plots, along with the electronic equivalent circuit of the electrified interface (Schlapfer, P. et. al. 1974).

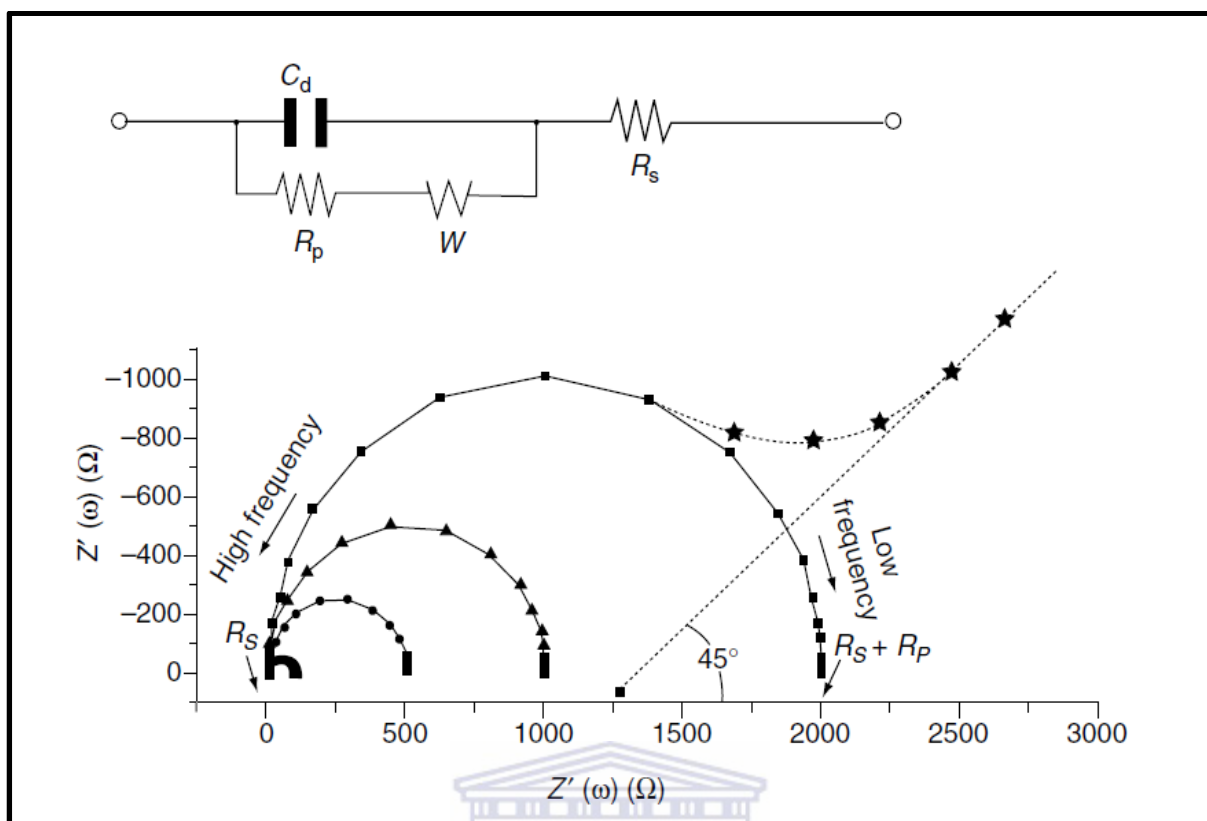
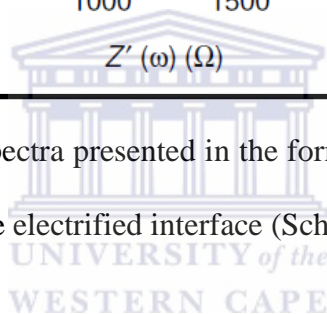


**Figure 17** Faradaic impedance spectra presented in the form of Nyquist plots, along with the electronic equivalent circuit of the electrified interface (Schlapfer, P. et. al. 1974)



### 3.5.4 Electrochemical Quartz Crystal Microbalance (EQCM)

The mass changes of the enzyme, luciferase due to the addition of each analyte were measured by Electrochemical Quartz microbalance (EQCM) from the N series Autolab potentiostat/galvanostat instrument, PGSTAT128N. EQCM provides the means to perform Electrochemical Quartz Crystal Microbalance measurements. The EQCM module measures a mass change per unit area by measuring the change in resonant frequency of a quartz crystal. Quartz crystals belong to a group of materials displaying the so-called piezoelectric effect. The microbalance is based on a quartz crystal wafer, which is sandwiched between two electrodes, used to induce an electric field (Figure 18). Such a field produces a mechanical

---

oscillation in the bulk of the wafer. Surface reactions, involving minor mass changes, can cause perturbation of the resonant frequency of the crystal oscillator. The frequency change ( $\Delta f$ ) relates to the mass change ( $\Delta m$ ) according to the Sauerbrey equation:

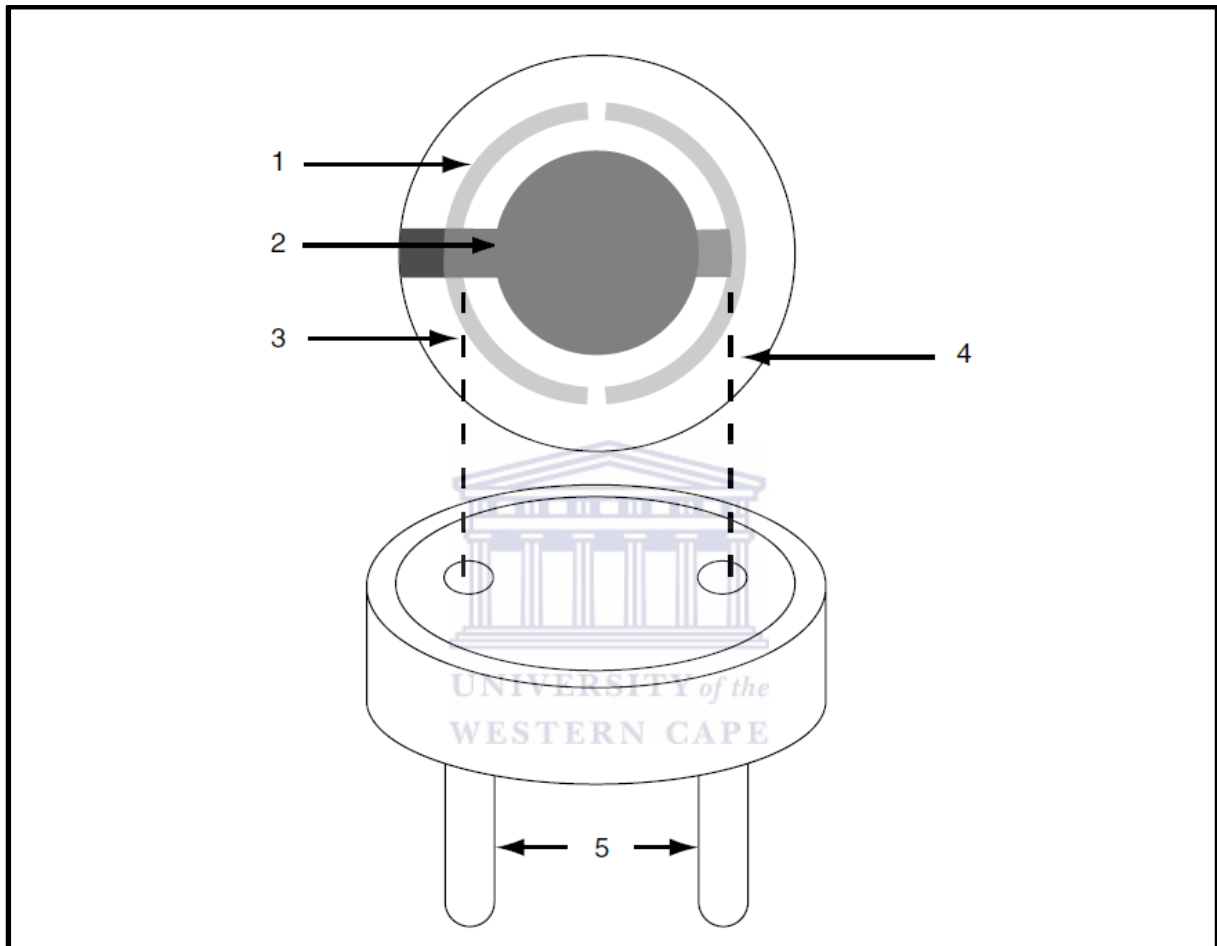


**Figure 18** Quartz crystal microbalance: (1) the quartz crystal; (2) the gold electrode; (3, 4) connecting metal wires; (5) the base

$$\Delta f = -\frac{2f_0^2}{A\sqrt{\rho_q\mu_q}} \cdot \Delta m$$

**Equation 3.7**

---

Where  $\Delta f$  is the change in frequency, in Hz,  $f_0$  is the nominal resonant frequency of the crystal (6 MHz),  $\Delta m$  is the change in mass, in  $\text{g}/\text{cm}^2$ ,  $A$  is the area of the crystal in  $\text{cm}^2$ ,  $\rho_q$  is the density of quartz, in  $\text{g}/\text{cm}^3$  and  $\mu_q$  is the shear modulus of quartz, in  $\text{g}/\text{cm}\cdot\text{s}^2$ . For a 6 MHz crystal, the same equation can be reduced to:

$$-\Delta f = \Delta m \cdot C_f$$

**Equation 3.8**

Where  $C_f$  is  $0.0815 \text{ Hz}/\text{ng}/\text{cm}^2$ .

The Sauerbrey equation forms the basis for the excellent mass sensitivity of the EQCM. In-situ mass changes of  $1 \text{ ng}/\text{cm}^2$  can thus be detected. The EQCM is very useful for probing processes that occur uniformly across the surface. Numerous surface reactions have thus been investigated, including deposition or dissolution of surface layers and various uptake processes. Such changes can be probed using various controlled-potential or controlled-current experiments. In these experiments, one of the electrodes (on the wafer) contacts the solution and serves as the working electrode in the electrochemical cell, to allow simultaneous frequency and current measurements. Figure 19 displays the frequency (mass) vs. potential profiles, and the corresponding cyclic voltammograms, during the uptake of a multiply charged complex ion at an ion exchanger coated electrode. Application of the Sauerbrey equation to the study of polymeric films in solutions requires adherence to the rigid-film approximation (i.e., behavior of elastic, solvent-free thin layer). In the absence of molecular specificity EQCM cannot be used for molecule-level characterization of surfaces. Electrochemical quartz crystal microbalance devices also hold promise for the task of affinity-based chemical sensing, as they allow simultaneous measurements of both the mass

---

and current. The combination of EQCM with scanning electrochemical microscopy has also been reported recently for studying the dissolution and etching of various thin films (85). The development of multichannel quartz crystal microbalance (86), based on arrays of resonators, should further enhance the scope and power of EQCM.

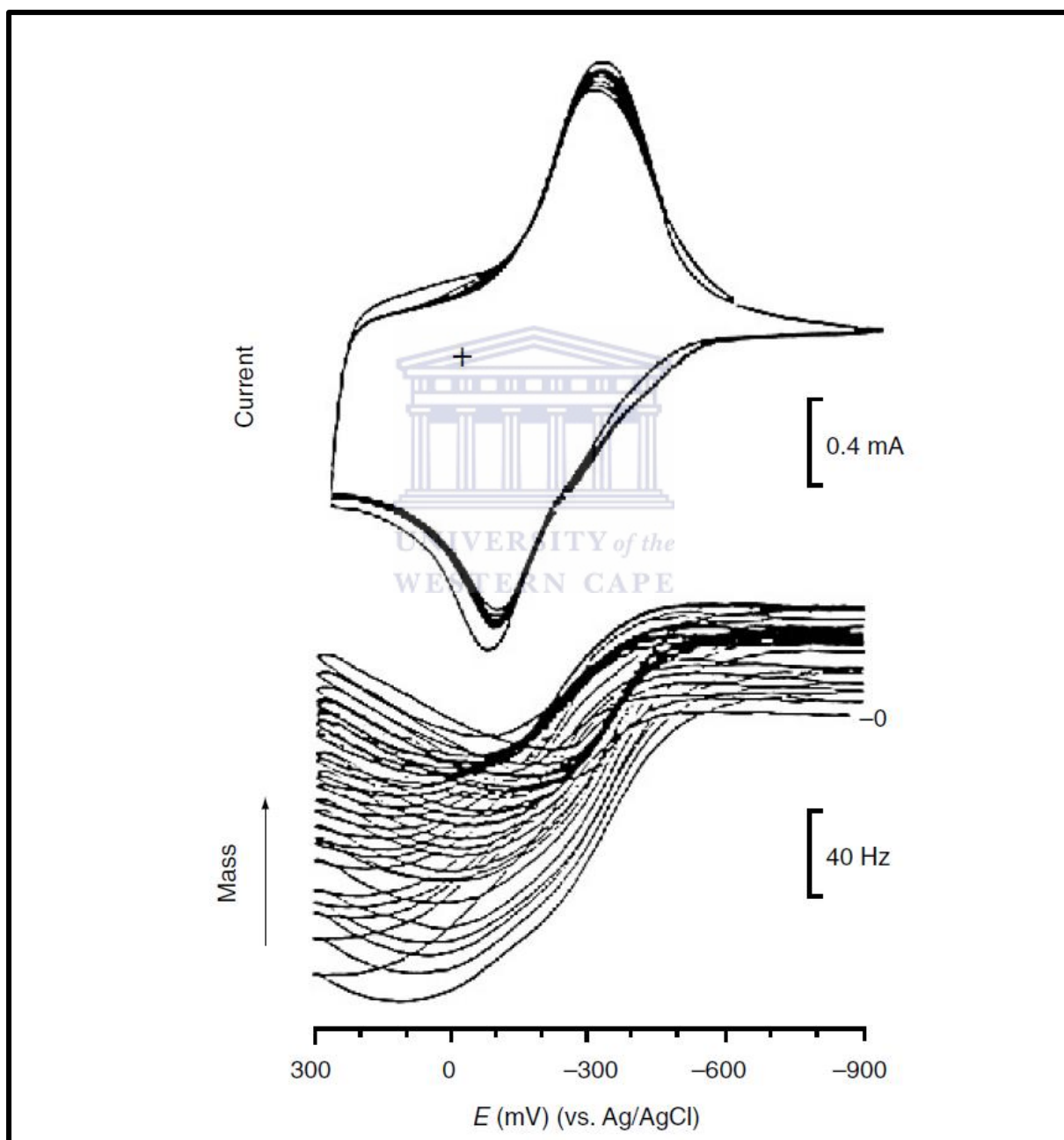


**Figure 19** EQCM (bottom) and cyclic voltammetry (top) profiles at an ion exchanger-coated electrode in the presence of  $6 \times 10^{-3}$  M  $\text{Ru}(\text{NH}_3)_6\text{Cl}_6$ . (Wang, J et. al. 1996)

---

### 3.5.5 Fourier Transform Infrared Spectroscopy

The FTIR spectra were recorded on a PerkinElmer Spectrum 100, FT-IR spectrometer. The specimens were prepared by first electrodepositing polyamic acid/polypyrrole composites on the glassy carbon electrode (GCE) surface. The spectra of the specimen were recorded in the region 400 - 4000  $\text{cm}^{-1}$ . The spectra obtained were used to identify the various functional groups in polyamic acid, polypyrrole and the composites.

### 3.5.6 Raman Spectroscopy

Raman measurements were carried out with Raman spectrometer (LabRam HR by Jobin-Yvon Horiba scientific Explora, France with a 1200 lines  $\text{mm}^{-1}$  grating) coupled to a microscope (Model BX41, Olympus). The excitation of Raman scattering was operated with a laser at a wavelength of 532 nm. The laser beam was focused on the sample by means of an x100 microscope objective.

### 3.5.7 Fluorescence spectroscopy

The fluorescence spectra were recorded on Fluorescence spectra of liquid samples were recorded using Horiba NanoLog™ 3-22-TRIAX (USA), with double grating excitation and emission monochromators at a slit width of 5 nm. Fluorescence is a type of electromagnetic spectroscopy which analyzes fluorescence from a sample. Fluorescence spectroscopy involves using a beam of light, usually ultraviolet light, that excites the electrons in molecules of certain compounds and causes them to emit light; typically, visible light. A complementary technique is absorption spectroscopy. The luciferase dissolved in 0.2 M PBS pH 7 was placed

---

in 4 cm<sup>3</sup> quartz cuvettes and their Fluorescence spectra recorded. The obtained spectra were then used to characterize the absorption bands of the active sites of luciferase as well as the binding events of luciferase with naphthalene and fluoranthene.

### **3.5.8 Scanning electron microscopy (SEM)**

Scanning electron microscopy was used to characterize the morphology of PAA/PPy composites. The images were acquired using either a Gemini LEO 1525 Model or a Hitachi X-650 analyzer employing the secondary electron (SE) mode with interchangeable accelerating voltages of 25 kV. Screen-printed carbon electrodes were used for electrodeposition of samples for SEM analysis. After electrodeposition of samples, the electrodes were rinsed with deionized water and left to dry at room temperature for about 30 min. The same samples were subjected to further analysis by EDX to determine their percentage atomic compositions.

### **3.5.9 Atomic Force Microscopy**

The Nanosurf easyScan 2 AFM is an atomic force microscope system that can make nanometer scale resolution measurements of topography and several other properties of a sample. The main parts of the basic system are the easyScan 2 AFM scan head, the AFM Sample stage, the easyScan 2 Controller with AFM Basic module, and the easyScan 2 software.



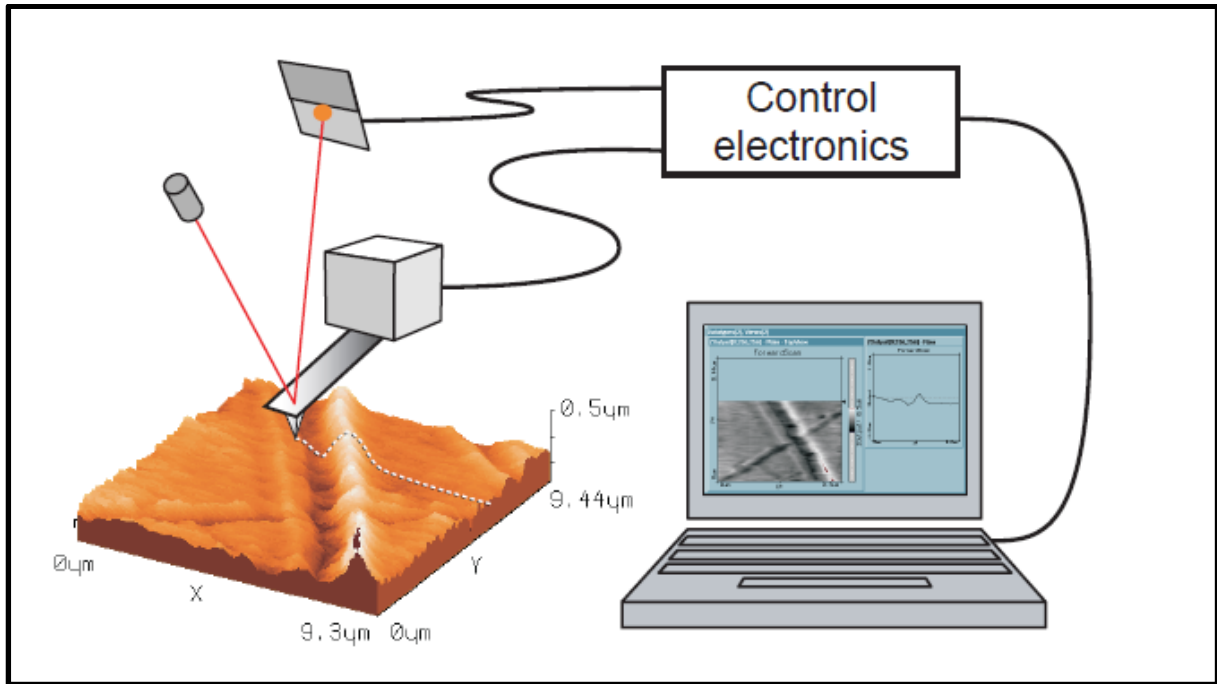
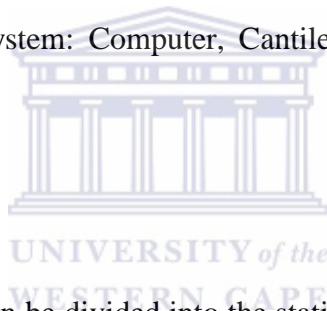


**Figure 20** easyScan 2 AFM system: Computer, Cantilever with deflection measurement system scanning the sample



There are different modes and can be divided into the static operating modes that control the Z-position control using the cantilever deflection, the dynamic operating modes that control the Z-position using the vibration amplitude.

**Table 5** Operating modes with the type of cantilever

Operating mode	Type of cantilever
Static force	Contact
Dynamic force	Non-contact
Phase contrast	Non-contact

---

In the Static Force mode, the ‘static’ deflection of the cantilever is used as the error signal for the Z-position Controller. The Set point in Newton is calculated by multiplying the deflection with the spring constant of the selected cantilever. In order to minimize tip/sample wear, the force set point should be made as small as possible. In some cases, even a negative set point (i.e. an adhesive force) may work, but when the tip momentarily loses contact with the sample due to some disturbance, the Z-Controller will always fully retract the cantilever from the sample. In the Dynamic Force mode, changes in the dynamic behaviour of the cantilever are detected by measuring changes in its vibration amplitude when it is excited with a sinusoidal signal with a frequency close to the cantilever’s free resonance frequency. The set point is the percentage of the vibration amplitude when the cantilever was far away from the surface. To minimize tip/sample wear, the set point should be made as large as possible. The Phase Contrast mode is an extension of the Dynamic Force mode. In addition to the vibration amplitude, the phase shift between the cantilever vibration and a reference signal is measured. This phase shift changes when the resonance characteristic of the cantilever changes due to changes in the tip-sample interaction. Thus, the Phase contrast mode can be used to produce material contrast when there is a significant difference in the tip sample interaction of these materials (AFM Theory, Nanosurf easyScan 2 User manual;pg 70-72).

These techniques have been used to study the voltammetry, morphology and spectroscopy of all the PAA/PPy composites synthesised in-situ.

---

# Chapter 4

## *Results and Discussion: Polymers and Polymer Composites Synthesis and Characterization*

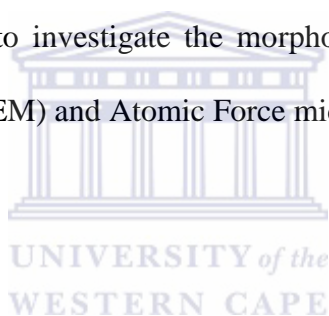
### 4.1 Introduction

A drawback in the usage of conducting polymers is that they have low mechanical properties; preparation of composites with conducting polymer fillers is one of the ways to solve this problem. The most effective way to improve the mechanical properties and environmental stability of ICPs is to prepare composites with a chemically inert and a mechanically stable matrix. For commercial development PPy is said to be the best candidate. To its disadvantage polypyrrole's mechanical properties and thermostability are low. To improve the mechanical properties and thermal stability is to prepare composites comprised of intrinsically conducting polymers. Polyimides (PI) are considered to be attractive candidates as a matrix for formation composites with ICPs filler because of its excellent thermal stability and excellent mechanical properties and environmental stability. Conducting polymer-polyimide composites has exclusively high temperature stability, good mechanical properties, and high chemical stability (Su, T. M. et. al., 1997). Langmuire-Blodgett films containing conducting polymers have been reported (Brynda, M.M. et. al., 1996). Conducting Ag-PI films prepared by the electrochemical method have shown that the electric conductivity in the range from semiconductor to metallic silver and were suggested for flexible electrical circuits applications (Levine, K.L et. al., 1999). The same applications such as electromagnetic

---

screens and antistatic coatings were suggested for PPy/PI composites (Tieke B. et al., 1990; Levin, K.L. et. al., 1993; Selampinar, U. et. al., 1997), active elements in rechargeable batteries (Lu, W. et. al., 1999), and gas separation membranes (Brynda, M.M et. al., 1996). They show enhanced temperature and environmental stability (Levin, K.L. et. al., 2000).

This chapter presents results and discussion on the electrochemical synthesis and characterization of polyamic acid, polypyrrole and their composites. Cyclic Voltammetry (CV) and square wave voltammetry (SWV) was performed to evaluate the electrochemistry of the individual polymers and their composites, Fourier Transform Infrared spectroscopy (FTIR) and Raman spectroscopy to understand the structure and structural changes of PAA, PPy and PAA/PPy composites, to investigate the morphology and morphological changes Scanning electron microscope (SEM) and Atomic Force microscopy (AFM) was employed.



## 4.2 Reagents and materials

The reagents 4,4'-oxydianiline (ODA), 1,2,4,5-benzenetetracarboxylic acid (PMDA), tetrahydrofuran (THF), methanol (MeOH), triethylamine (TEA), acetonitrile (ACN), pyrrole (98%) was vacuum distilled and stored frozen under nitrogen., disodium hydrogen phosphate, potassium dihydrogen phosphate, were all obtained from Sigma-Aldrich, South Africa. All chemicals were of analytical reagent grade and were used without further purification. Deionized water (18.2 MΩcm) purified by a Milli-QTM system (Millipore) was used as reagent water for aqueous solution preparation. Phosphate buffer solution of 0.2 M was prepared by dissolving 17.79 g of disodium hydrogen phosphate and 15.60 g of potassium dihydrogen phosphate separately in 500 mL deionized water, then mixing the salt solutions

---

according to Henderson-Hasselbalch equation to obtain the required pH 7 value. The phosphate buffer solution (PBS) was refrigerated at 4 °C. Analytical grade Argon gas was purchased from Afrox Company, South Africa. Alumina polishing pads and powder (0.05, 0.3 and 1.0 μM) were obtained from Buehler, Illinois, USA.

Voltammetric experiments were recorded with BASi 100B electrochemical work station (LG Fayette) using the conventional three-electrode system. For the electropolymerization of polyamic acid, polypyrrole and PAA/PPy composites, the working electrode used was glassy carbon (GCE) (diameter 3.0 mm) electrodes while a platinum mesh or wire and a silver/silver chloride (3 M NaCl type) electrode (Bioanalytical Systems Ltd., UK) were used as counter electrode and reference electrode, respectively. Alumina micro-polish (1.0, 0.3 and 0.05 μM alumina slurries) and polishing pads (Buehler, IL, USA) were used for polishing the electrode. The modified SPCEs screen printed carbon (SPCE) (diameter 3.0 mm), were used for scanning electron microscopy (SEM) and Atomic Force microscopy studies. SEM images were taken with a Hitachi S3000N scanning electron microscope. An acceleration voltage of 20 kV was employed at various magnifications. Surface morphology of the modified SPCE was studied with atomic force spectroscopy (AFM) tapping mode NanoSurf model with silicon tip using spring constant of 1-5 N/m and resonance frequency of 60-100 kHz. To study the structural changes within composites Raman measurements were carried out with Raman spectrometer (LabRam HR by Jobin-Yvon Horiba scientific Explora, France with a 1200 lines mm<sup>-1</sup> grating) coupled to a microscope (Model BX41, Olympus) and Fourier Transform Infrared (FTIR) on a PerkinElmer Spectrum 100, FT-IR spectrometer was employed.

---

## 4.3 Synthesis and Characterization of PAA

### 4.3.1 Electrochemical synthesis and characterization of PAA

Cyclic voltammetry is often used to characterize conducting polymer films, for studying the reversibility of electron transfer because the oxidation and reduction can be monitored in the form of a current-potential diagram. The electrochemical polymerization of PAA film on glassy carbon electrode (GCE) surfaces was achieved by cycling the potential repeatedly between -400 and +600 mV at a scan rate of 50 mV/s. The cyclic voltammogram for the electrodeposition of PAA film on the glassy carbon electrode (GCE) surfaces are shown in Figure 21. All potential values are recorded *vs.* Ag/AgCl reference electrode.



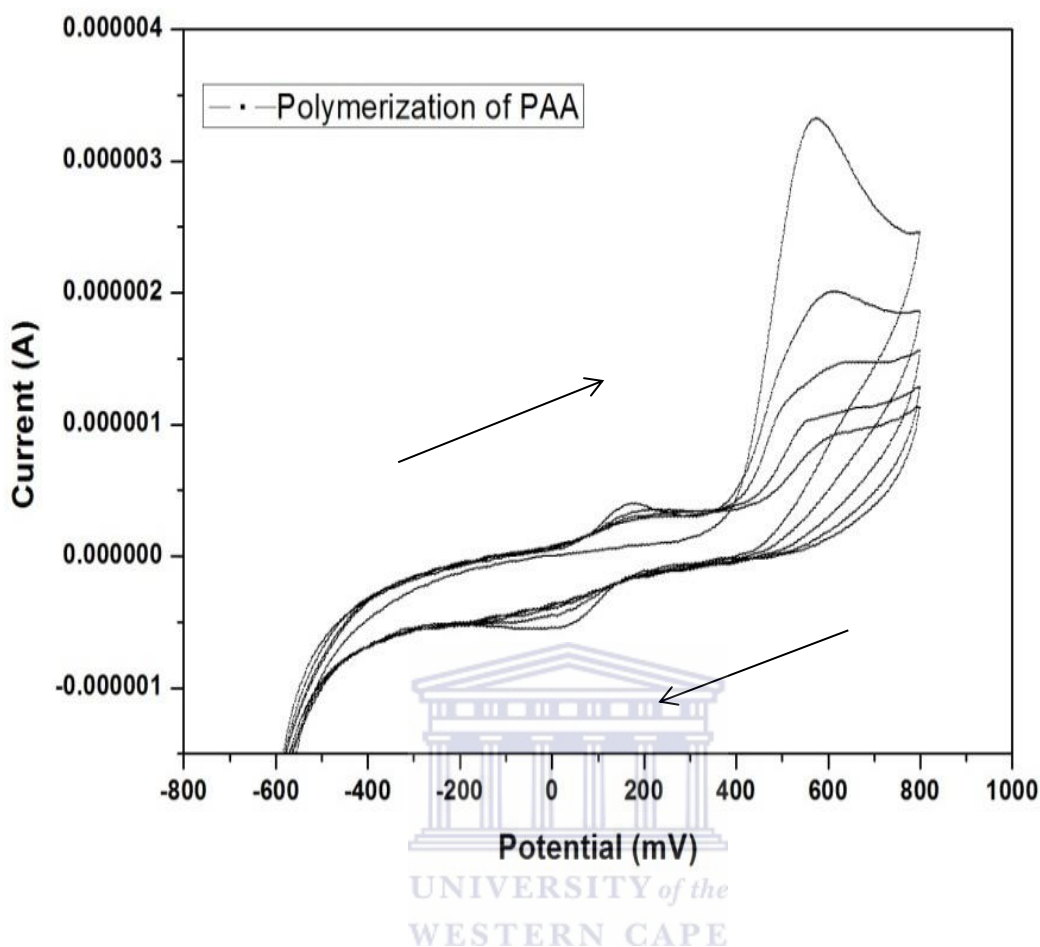


**Figure 21** Cyclic Voltammogram of the electrochemical synthesis PAA in 0.2 M PBS at a scan rate of 50 mV/s.

The electrodeposited PAA film was further subjected to characterization by CV in 0.2 M PBS (pH 7) at different scan rates of 50 mV/s, 60 mV/s, 70 mV/s, 80 mV/s, 90 mV/s and 100 mV/s, the CV of PAA/GCE are shown in Figure 22. As the potential was scanned from -1000 mV to 1000 mV, two quasi-reversible oxidation redox couples were observed at 190 mV and 516 mV respectively. From the CV data, PAA film was considered to be a multicomponent system (Bard and Faulkner). Multicomponent systems are the consecutive reduction of two substances eg. O and O' in one potential scan experiment. The first oxidation peak (Epa1) was due to the one electron removal from the nitrogen atoms at the tetraphenyl-1,2-

---

phenylenediamine structure in each repeating unit to yield one stable delocalised radical cation, poly(amine-amide)<sup>+</sup> and the second oxidation peak (Epa2) is due to one stable quinoid type dication poly(amine-amide)<sup>2+</sup> (Eq 4.1) respectively (Liou et al., 2006). The reverse scan from 1000 mV to -1000 mV showed two reduction couples (Epc1 and Epc2) at -125 mV (vs. Ag/AgCl) and -654 mV (vs. Ag/AgCl) respectively.



The first redox couple (Epa1 and Epc1) will be referred to as E<sup>0</sup>1, and the second redox couple (Epa2 and Epc2) will be referred to as E<sup>0</sup>2 throughout the discussions. Based on the results from CV the PAA film was considered to be electroactive and to be conductive at both couples (E<sup>0</sup>1 and E<sup>0</sup>2) because the CV showed a current (A) increase as the scan rates were increased, and also from the calibration plots of current (A) vs. scan rate (mV/s) that current was directly proportional to the scan rate with correlation coefficients (R<sup>2</sup>) of ±0.99. These results confirm that the PAA film was indeed successfully attached onto the glassy carbon electrode (GCE) surface. From the calibration plot of anodic/cathodic peak current versus square root of scan rate, the electron diffusion coefficient (D<sub>e</sub>), which is a measure of how fast charge can be transported through the polymer layer, was calculated using Randle Sevcik equation (Eq. 4.2).

$$i_p = (2.68 \times 10^5)(n)^{3/2}(A)(C)(\sqrt{v}) \quad \text{Equation 4.2}$$



The  $D_e$  was found to be  $7.10 \times 10^{-6} \text{ cm}^2/\text{s}$  for  $E^0_1$  and  $9.11 \times 10^{-6} \text{ cm}^2/\text{s}$  for  $E^0_2$  in good agreement with other  $D_e$  for PAA (N. Noah et al., 2012). The  $D_e$  were in range of some other conducting polymers PANI (Iwouha E.I et al., 1997) and poly(*p*-phenylene vinylene) (Vyas R. et al., 2010). Formal potentials ( $E^0$ ), linear regressions, diffusion coefficients ( $D_e$ ) and are listed in Table 6.

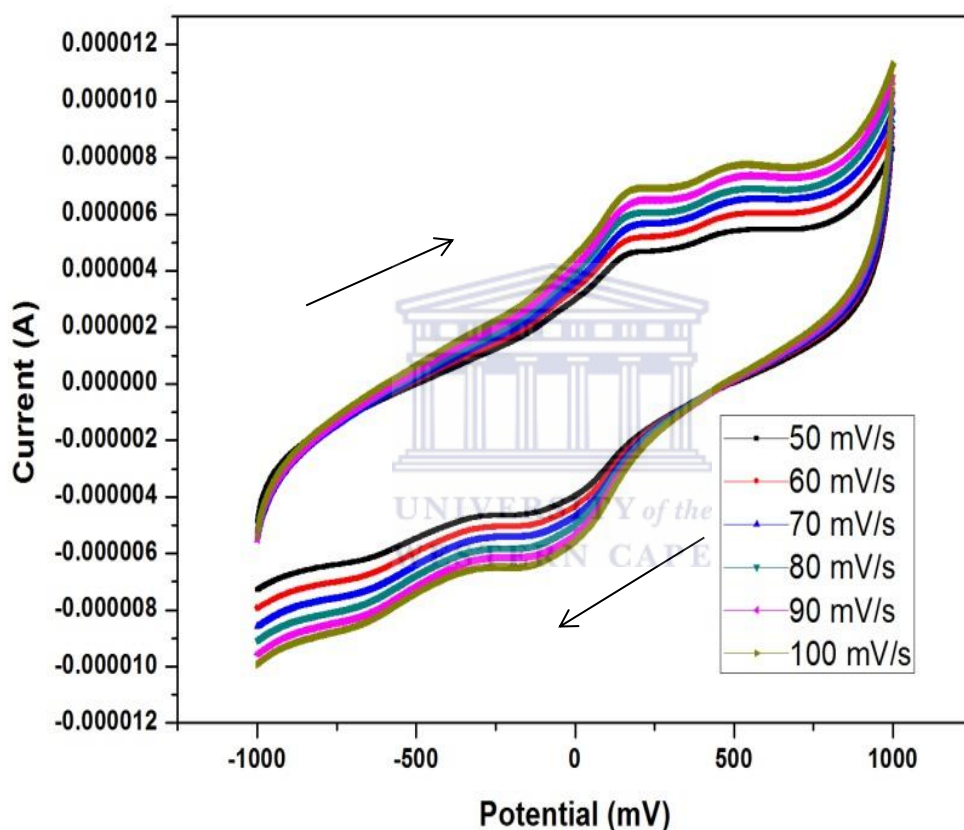


**Figure 22** Cyclic Voltammogram (CV) of PAA film on a GCE in 0.2 M PBS (pH 7) at different scan rates; 50, 60, 70, 80, 90 and 100 mV/s.

---

To verify the different peaks observed in CV, Ouster young square wave voltammetry (OSWV) a complimentary technique to CV was done. An oxidation sweep from -1000 mV to 1000 mV (Figure 23 a) was run to observe the oxidation peaks. In CV only peaks (ii) and (iii) was observed, but OSWV showed that there was a slight peak (i) at about -500 mV (vs. Ag/AgCl). On reverse scan, the reduction sweep from 1000 mV to -1000 mV (Figure 23 b) peaks (ii') and (iii') were observed. OSWV was also used to get the formal potentials ( $E^0$ ) and compare them to that of the  $E^0$  calculated from CV of the different redox couples (Table 6).



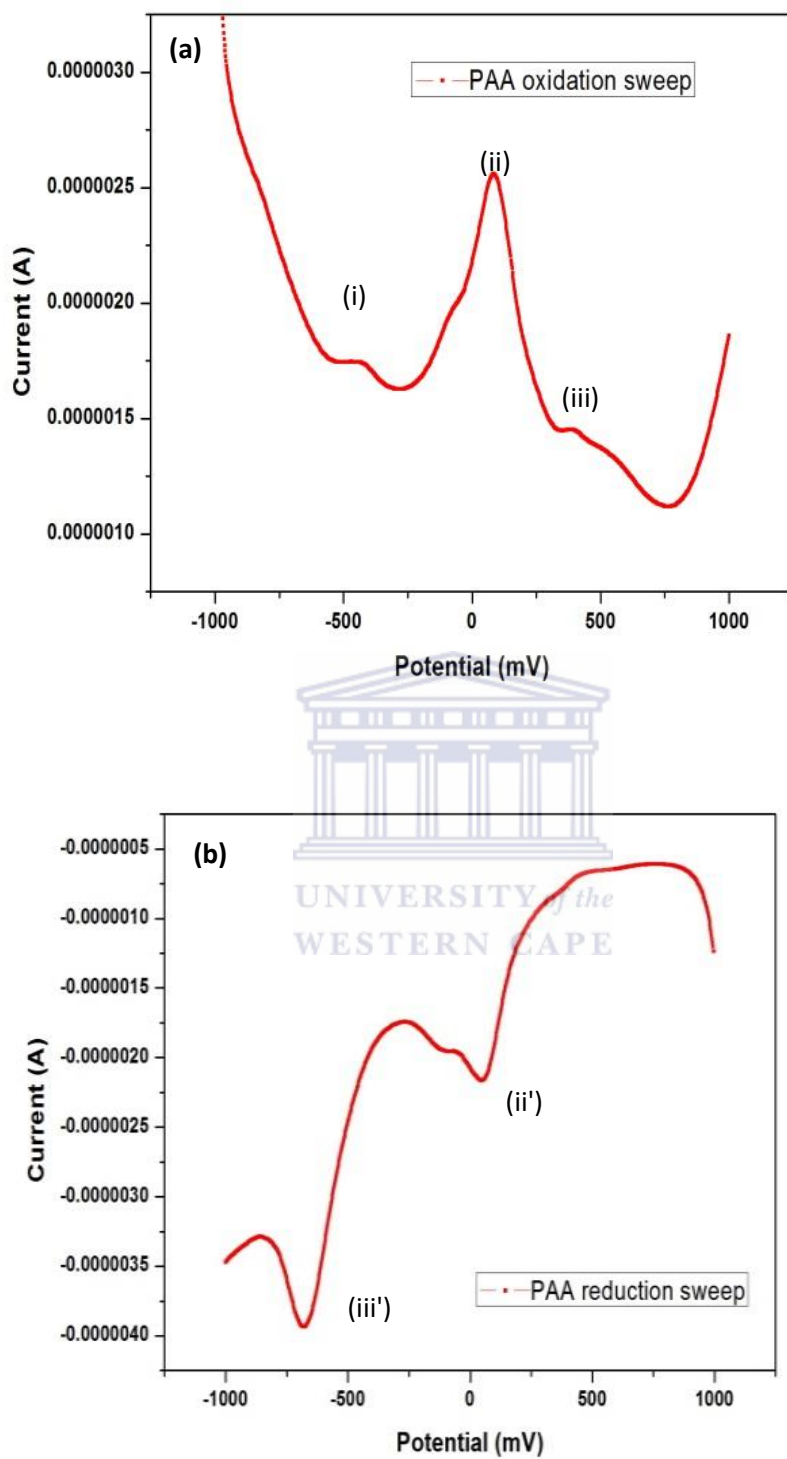


**Figure 23** Square Wave Voltammograms of (a) oxidation (b) reduction of PAA in 0.2 M PBS (pH 7).

---

## 4.4 Synthesis and Characterization of PPy

### 4.4.1 Electrochemical synthesis and characterization PPy

PPy was electrochemically synthesised from the monomer pyrrole in a 0.2 M PBS (pH 7) solution (Figure 24). Cyclic voltammetry was used to evaluate the film of PPy at the GCE. The oxidation or reduction of polypyrrole involves two simultaneous processes: (i) the transfer of electrons either from or to polypyrrole and (ii) the diffusion of the counterion, or in some cases the diffusion of the cation into or out of the polypyrrole film to maintain charge neutrality. The oxidation or reduction of polypyrrole requires two simultaneous processes: (i) the transfer of electrons either from or to polypyrrole and (ii) the diffusion of the counterion, or in some cases the diffusion of the cation into or out of the polypyrrole film to maintain charge neutrality. The redox mechanism of polypyrrole is described by one-electron transfer step;



Where PPy is the neutral species and PPy<sup>+</sup> is the radical cationic species or polaron (one positive charge localized over three to four monomer units). The polaron can further be oxidized;



Where PPy<sup>++</sup> is the dicationic species or bipolaron (two positive charges localized over three to four monomer units).

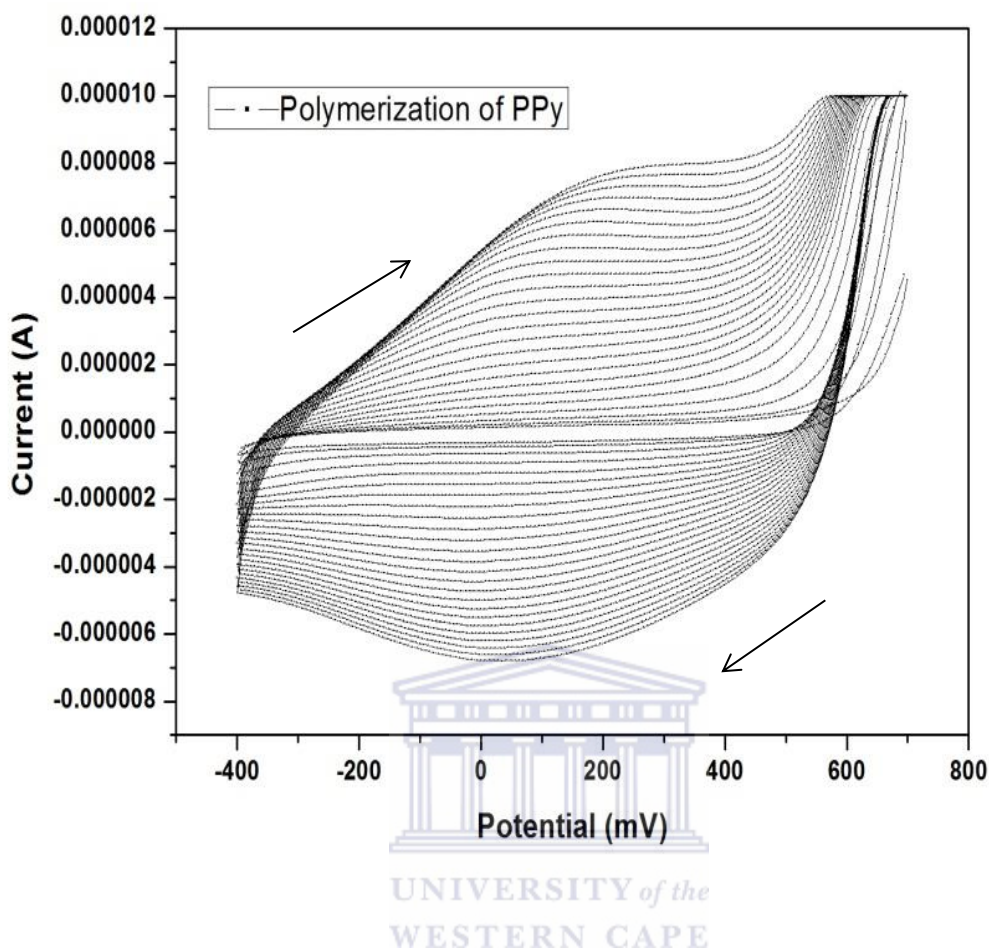
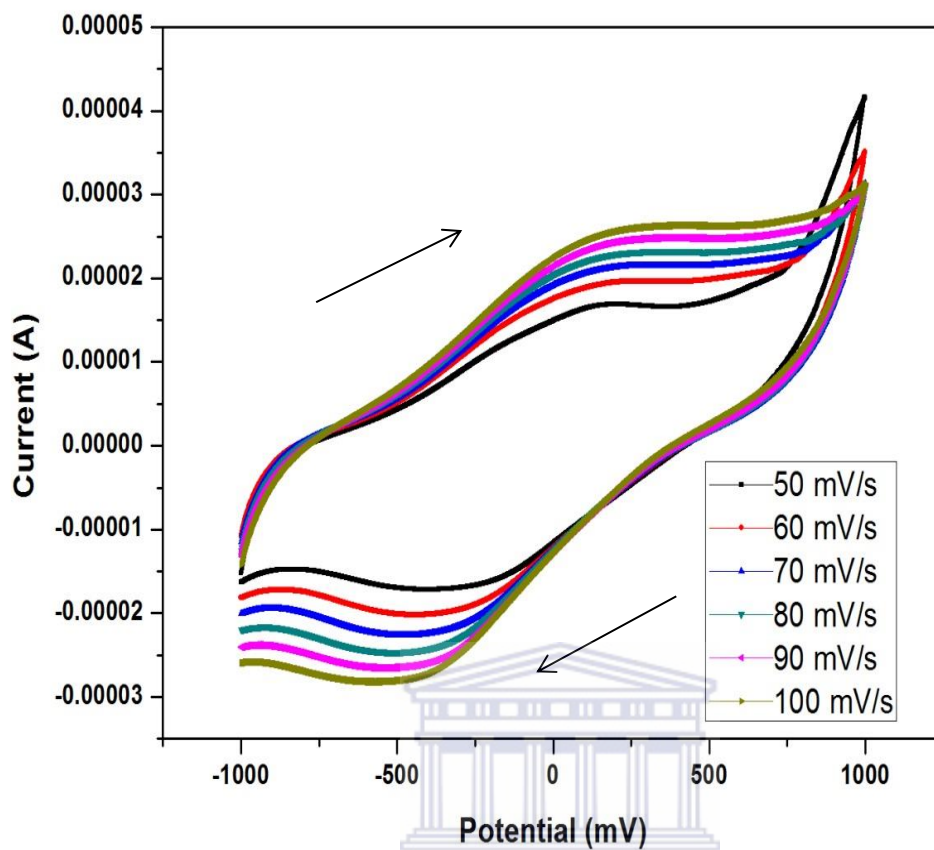


**Figure 24** Cyclic Voltammograms of the synthesis PPy in 0.2 M PBS (pH 7) at a scan rate of 50 mV/s.

On the forward scan from -1000 mV to 1000 mV, one oxidation peak at 192 mV was observed it was due to the neutral species PPy being oxidised to  $\text{PPy}^+$  (Equation 4.3). On the reverse scan a reduction peak at -480 mV was observed it was due to the cationic species,  $\text{PPy}^+$  being reduced back to PPy. The multiscan voltammograms of the PPy-modified GC electrode in 0.2 M PBS (pH 7) was recorded (Figure 25). Both peak potentials and corresponding peak currents varied, which showed that the polymer PPy was indeed electroactive and that diffusion of electrons was taking place.



UNIVERSITY of the  
WESTERN CAPE

**Figure 25** Cyclic Voltammogram of PPy in 0.2 M PBS (pH 7) at scan rates 50, 60, 70, 80, 90 and 100 mV/s on GCE.

---

## 4.5 Synthesis and Characterization of PAA/PPy Composites

### 4.5.1 Electrochemical synthesis and characterization PAA/PPy composites

The PAA/PPy composites were synthesized via in-situ polymerization processes. The concentration of polyamic acid solution ( $1.37 \times 10^{-6}$  M) was kept fixed throughout the composite ratio process. The concentration of pyrrole was varied from  $1.9 \times 10^{-3}$  to  $9.09 \times 10^{-3}$  M. The ratios were as follows: 1: $1.34 \times 10^3$ ; 1: $2.81 \times 10^3$ ; 1: $4.13 \times 10^3$ ; 1: $5.41 \times 10^3$ ; 1: $6.64 \times 10^3$ . The individual PAA/PPy ratios were added and mixed with 5mL of 0.2 M PBS (pH7) aqueous solution. The solutions were stirred for a minute and degassed before experiments. The electrochemical polymerization of PAA/PPy composites on glassy carbon electrode surfaces was achieved by cycling the potential repeatedly between -400 and 0.6 mV at a scan rate of 50 mV/s. An example of the in-situ electrochemical synthesis of PAA/PPy film onto glassy carbon electrode (GCE) surface is shown in Figure 26.

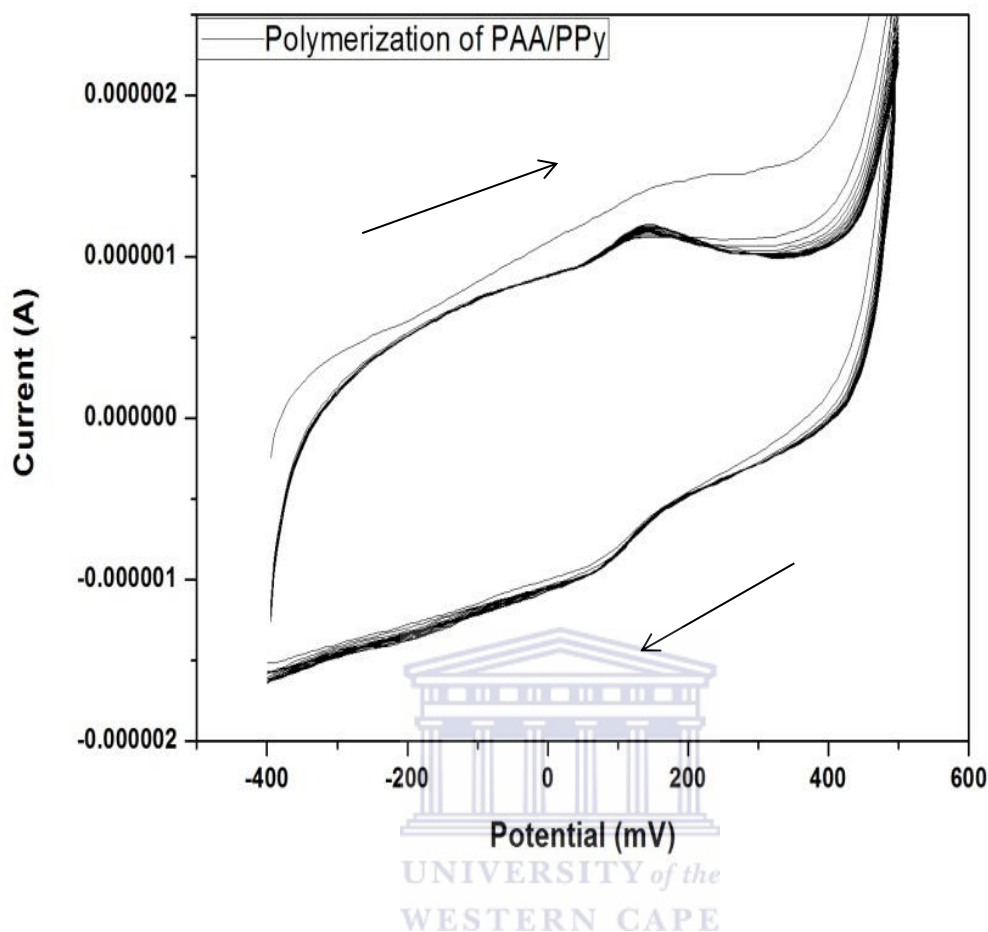


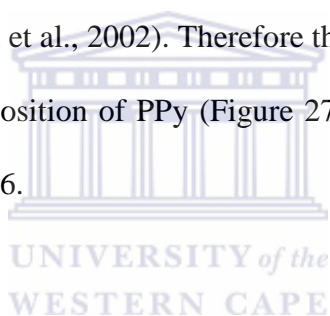
**Figure 26** Cyclic Voltammogram of an in-situ polymerization process PAA/PPy composite in 0.2 M PBS (pH 7) at a scan rate of 50 mV/s.

The *in-situ* electrochemical synthesis of PAA/PPy composites onto the glassy carbon electrodes was studied at different concentrations of PPy, under potentiodynamic conditions. The different composite films obtained were characterized by different shapes and slopes of the cyclic voltammograms as a function of different scan rates. The data from each individual CV plots of the different composites have been extracted and is summarised in Table 6, thus the individual cyclic voltammograms of each composite are not shown as well as their calibration curves. The prime variables which determine the films formation of polyamic and polypyrrole from electrochemistry aspect are the oxidation and reduction potentials,  $D_e$  and



---

the linearity of the calibration plots of the composites. The PAA concentration was kept constant throughout the different composites preparation. Comparisons to the freestanding PAA film parameters and the different composites were made. The different composite matrices are characterized by different shapes of the peaks and values of the oxidation and reduction potentials as well as the  $D_e$ . For the electrochemical polymerization of the freestanding PAA film on GCE (PAA/GCE) the capacitance is small as to when the PPy is added, the capacitance in the electrochemical polymerization CV of PAA/PPy on GCE is much larger. The current (I)–potential (E) curve for PPy deposition into PAA matrix (Figure 26) shows the occurrence of a steady state electrodeposition controlled by the diffusion of PPy. The changes in slope of I–E curves are due to increased rate of deposition of PPy into the PAA matrix on the GCE (Iroh et al., 2002). Therefore the permeability of the PAA film to ion flux increases during the deposition of PPy (Figure 27). The linear regressions of these slopes are also tabulated in Table 6.



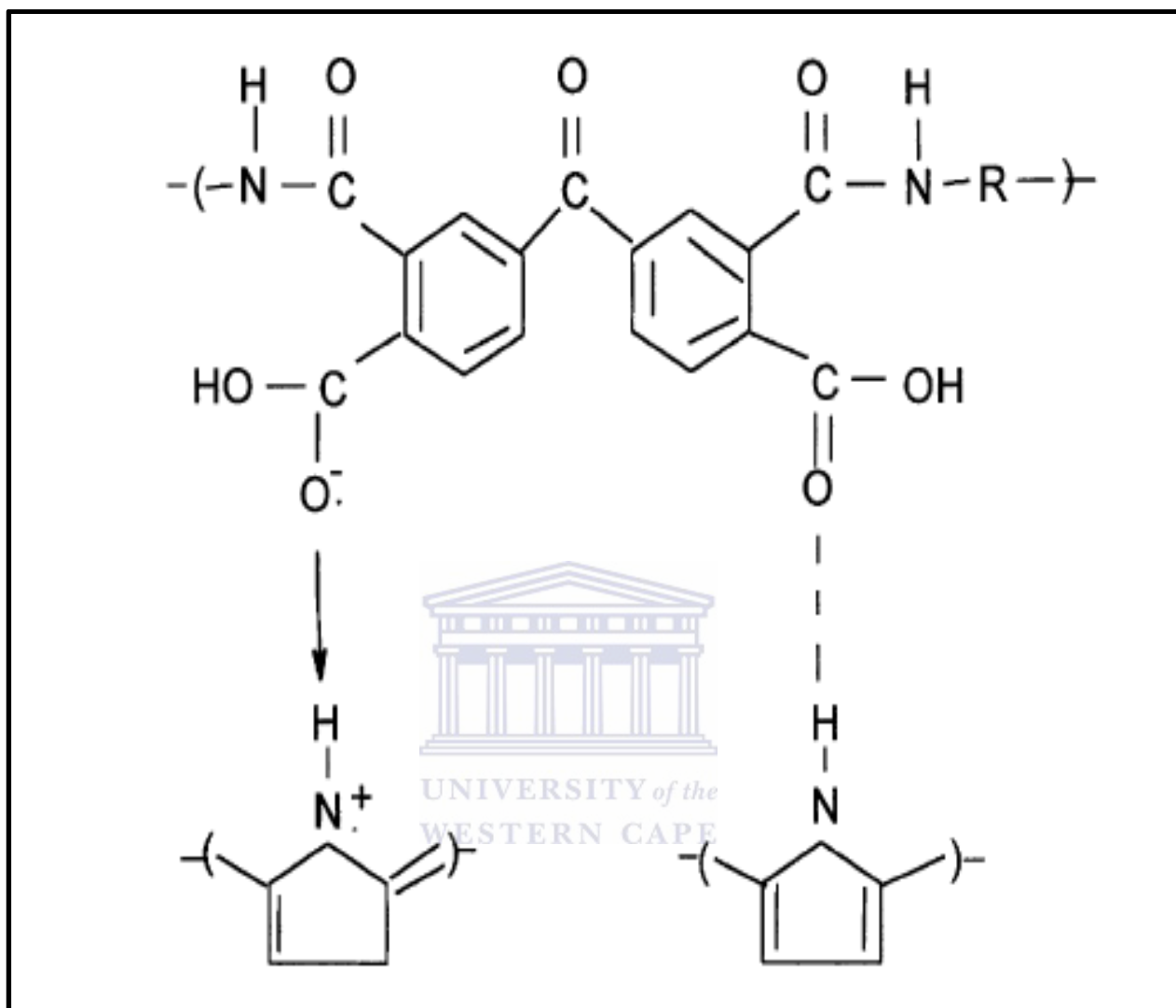


**Figure 27** Schematic representation of PAA/PPy and hydrogen bonding interaction (Iroh et al., 2002).

**Table 6** Electrochemical parameters of PAA, PPy and their composites.

Material	No of <i>e</i>	$D_e$ ( $\text{cm}^2/\text{s}$ )	$R^2$	$E^{0'}$ ( $E^{01}$ ) (mV)	$E^{0'}$ ( $E^{02}$ ) (mV)	$E_{pa1}$ (mV)	$E_{pa2}$ (mV)	$E_{pc1}$ (mV)	$E_{pc2}$ (mV)
PAA	1	$E^{01}: 7.1 \times 10^{-6}$ ; $E^{02}: 9.1 \times 10^{-6}$	$\pm 0.99$	158	585	190	516	-125	-654
PPy	1	$E_{pa}: 4.7 \times 10^{-14}$ ; $E_{pc}: 2.6 \times 10^{-14}$	$\pm 0.99$	334	-	192	-	-476	-
Comp 1	1	$E^{01}: 5.1 \times 10^{-4}$ ; $E^{02}: 9.9 \times 10^{-4}$	$\pm 0.99$	85	599	142	474	27	-723
Comp 2	1	$E^{01}: 4.9 \times 10^{-4}$ ; $E^{02}: 9.9 \times 10^{-4}$	0.99	91	573	162	493	20	-652
Comp 3	1	$E^{01}: 4.2 \times 10^{-4}$ ; $E^{02}: 3.3 \times 10^{-4}$	$\pm 0.99$	99	567	116	448	81	-686
Comp 4	1	$E^{01}: 5.4 \times 10^{-4}$ ; $E^{02}: 6.7 \times 10^{-4}$	$\pm 0.99$	80	500	113	374	46	-627
Comp 5	1	$E^{01}: 3.9 \times 10^{-4}$ ; $E^{02}: 1.4 \times 10^{-4}$	$\pm 0.99$	142	596	220	506	64	-686

PAA, polyamic acid; PPy, polypyrrole; the composite ratios are as follows [PAA (M): Py (M)]; Comp 1 = 1:1.34 $\times 10^3$ ; Comp 2 = 1:2.81 $\times 10^3$ ; Comp 3 = 1:4.13 $\times 10^3$ ; Comp 4 = 1:5.41 $\times 10^3$ ; Comp 5 = 1:6.64 $\times 10^3$ ;  $D_e$  = diffusion coefficient;  $R^2$  = linear regression coefficients;  $E^{01}$  = redox couple one;  $E^{02}$  = redox couple 2;  $E^{0'}$  = Formal potential;  $E_{pa}$  = anodic peak potential;  $E_{pc}$  = cathodic peak potential.

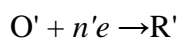
---

From the data obtained from cyclic voltammograms of the different ratios of PAA/PPy composites it is evident that as the amount of PPy increases the peak potentials ( $E_{pa}$  and  $E_{pc}$ ) shift to more positive values. The lowest redox current (Figure 28) was observed for Ep2 for composite 3. After that point as the PPy concentrations was further increased the oxidation potential decreased, this then affected the system's catalytic properties as a result the energy for catalysis was lowered.

The CV of PAA discussed in section 4.3.1, discussed PAA on GCE as a quasi-reversible multicomponent system with redox couples  $E^{01}$  (mV) and  $E^{02}$  mV. For multicomponent systems we consider that the reactions



and



With  $n = n'$ ; Concentration of  $O = O'$  and  $D_e$  of  $O = O'$

The second oxidation peak potential ( $E_{pa2}$ ) was observed to be slower than the first oxidation peak potential ( $E_{pa1}$ ), and was considered to be the rate determining step. The  $D_e$  of the PAA film on GCE is in the range of  $10^{-6}$  cm<sup>2</sup>/s.

The electrochemistry of PPy showed one oxidation peak potential and one cathodic peak potential. The neutral specie, PPy is oxidised to PPy<sup>+</sup> and it is reduced back to PPy. From the peak separation, it is an irreversible system. The  $D_e$  of  $E^{01}$  was in the range of  $10^{-14}$  cm<sup>2</sup>/s.

First observation from these electrochemical parameters showed that the peak potentials shifted to more positive values with respect to freestanding PAA film. The trend in oxidation as well as reduction peak potentials is displayed in Figure 28. The second redox couple  $E^{02}$

---

of the original PAA was observed to be present in every composite verifying the presence of PAA in each composite. The first redox couple  $E^{01}$  present in all composites, was a unique couple identified in the composites only and not in PAA or PPy individually. The homogeneous mixing of PAA and PPy during electrochemical synthesis, shifted the  $E^{01}$  of the PPy (334 mV) and  $E^{01}$  of PAA (158 mV) to a new  $E^{01}$  at 99 mV for composite 3. The average  $E^{01}$  for the composites 1 – 5 was observed to be 99.4 mV. This peak at  $E^{01} = 99$  mV (Standard deviation = 24, 85;  $n = 5$ ) confirms that a change in structure accompanies the interaction between PAA and PPy resulting in the unique composites represented in this dissertation. For further analytical evaluation only composite 3 was used in this work. However in related work the other composites was used for the detection of domoic acid which was able to detect domoic acid in real freshwater samples at a level of  $1.37 \times 10^{-5}$  M confirmed by SWV and UV/Vis spectroscopy. The second observation from the electrochemical parameters calculated, the  $D_e$  of the composites are in between the values of PAA and PPy, with  $D_e$  in the range of  $10^{-4}$  cm<sup>2</sup>/s. The comparison of the  $D_e$  of PAA and different composites are showed in Figure 29. Surface coverage of the PAA, PPy and their composite films produced were in the range of monolayer coverage of the electrode surface from  $10^{-13}$  to  $10^{-14}$  mol/cm<sup>2</sup>. The surface coverage was calculated from the Brown-Anson equation from of the  $I$  vs scan rate CV responses of the thin films. This was confirmation that rather than the PAA forming layers on the PPy or vice versa, a uniform monolayer of composites was formed.

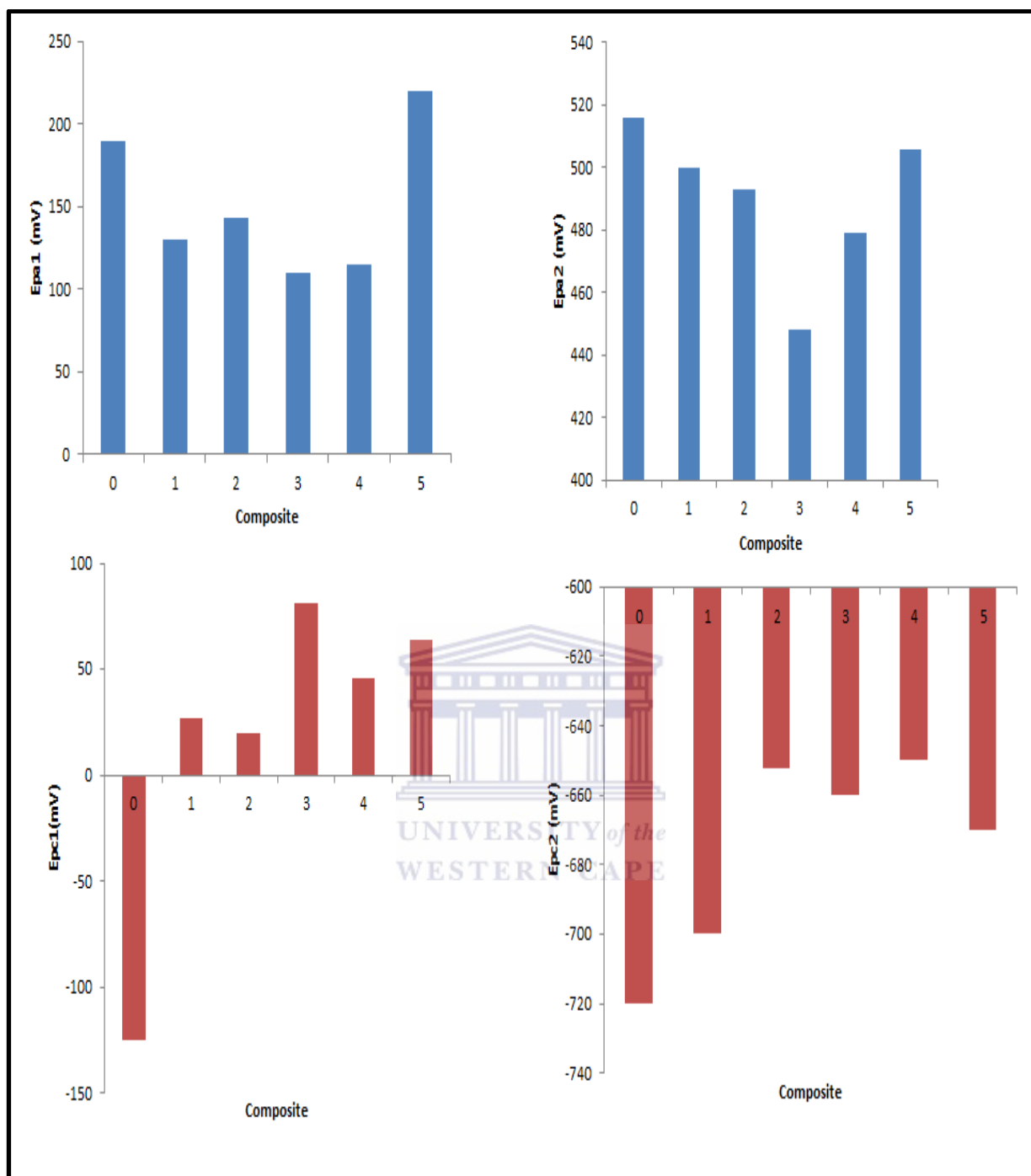


**Figure 28** Bar charts of oxidation and reduction peaks of PAA/PPy composites prepared on GCE.

0 = pure PAA film; 1 = composite 1; 2 = composite 2; 3 = composite 3; 4 = composite 4; and 5 = composite 5

---

As PPy was introduced into PAA matrix an initial increase in  $D_e$  was observed (composite 1 and 2). However a significant drop in  $D_e$  (Figure 29) was observed at composite 3. Uniform incorporation of the PAA into PPy matrix is supported by morphology data. From the  $D_e$  it was observed that the first oxidation reaction was catalytically faster than the second oxidation reaction which suggests that an electrochemical reaction is followed by a chemical reaction. At low concentrations of PPy (composite 1, 2 and 3) a consistent increase in diffusion coefficient was observed.

Bar charts showing the distribution of peak potentials for  $E_{pa_1}/E_{pc_1}$  and  $E_{pa_2}/E_{pc_2}$  are shown in Figure 28. The oxidative peak potential for the first couple, which presents the uniqueness of the composites, was observed to vary between 125 mV and 220 mV. The reduction peak potentials, representing the slower electron transfer in this couple, were distributed between 25 mV and 90 mV as a function of PPy incorporation. The second couple representing PAA incorporation was observed to be more or less equal in terms of oxidative and reductive electron shifting with  $E_{pa_2}$  spread between 500 mV and 510 mV, and  $E_{pc_2}$  spread between -670 and -700 mV.

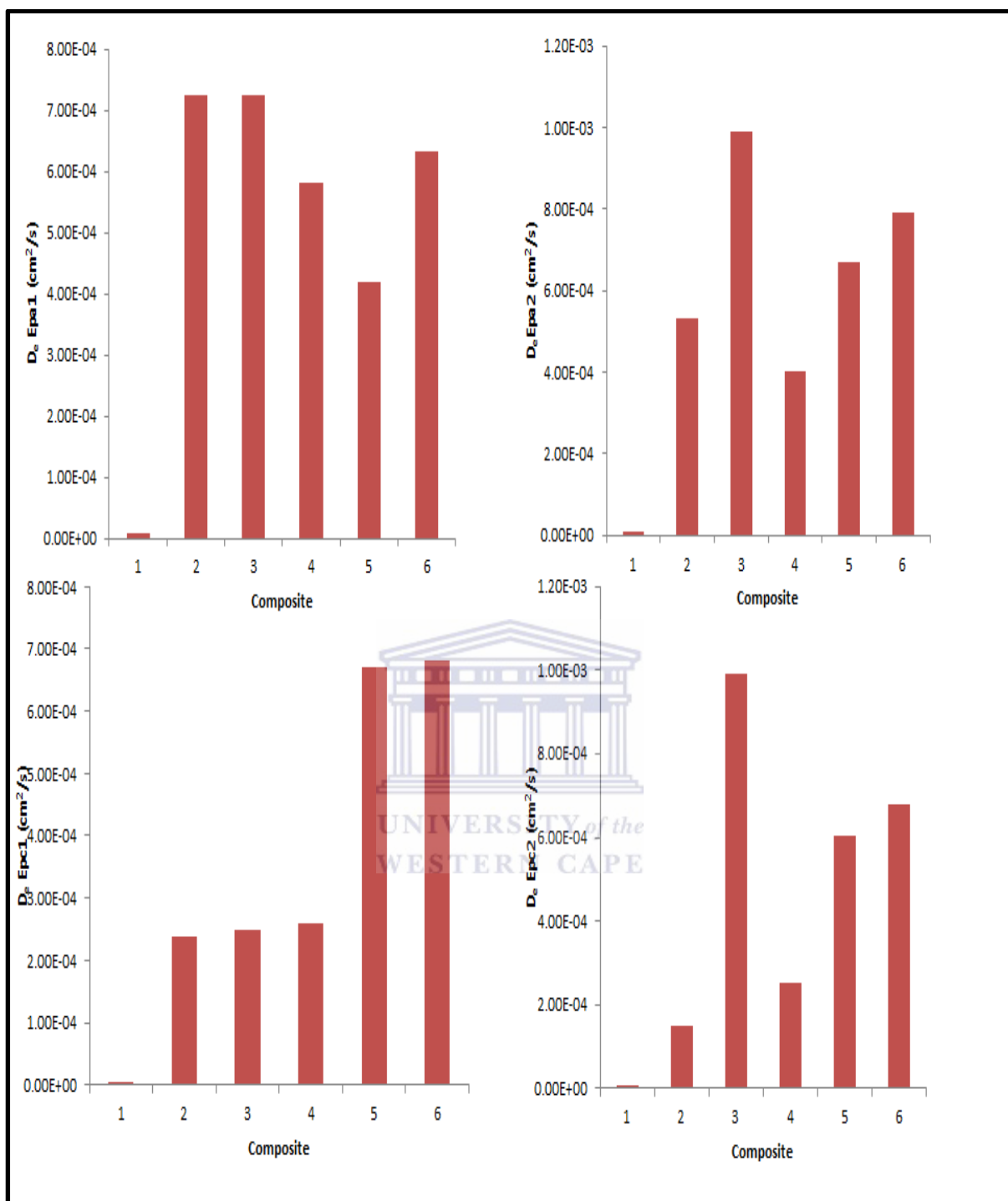


**Figure 29** Bar charts of the diffusion coefficients ( $D_e$ ) of the oxidation and reduction peaks of PAA and the different ratios of PAA/PPy composites on GCE.

Diffusion Coefficients ( $D_e$ ) of the anodic peak potentials ( $E_{pa1}$  &  $E_{pa2}$ ) and cathodic peak potential ( $E_{pc1}$  &  $E_{pc2}$ ); 1 = pure PAA; 2 = comp 1; 3 = composite 2; 4 = compo 3; 5 = comp 4; 6 = comp 5.



---

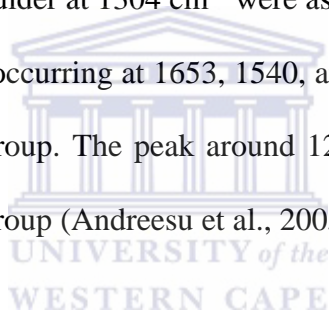
The  $D_e$  for the oxidative peaks (Figure 29) of the unique couple ( $E_{pa_1}$ ) representing the novel composites was consistent in the range from  $6 \times 10^{-4} \text{ cm}^2/\text{s}$  and  $7 \times 10^{-4} \text{ cm}^2/\text{s}$  (standard deviation  $1.22 \times 10^{-4}$ ;  $n = 5$ ). However depending on the ratio of PPy; the  $D_e$  of the PAA couple  $E_{pa_2}/E_{pc_2}$  may dominate.



---

## 4.6 Fourier Transform Infrared (FTIR) spectroscopy of PAA

In infrared spectroscopy, IR radiation is passed through a sample and the infrared radiation is then absorbed by the sample and some of it is passed through (transmitted). The spectrum then represents the molecular absorption and transmission, creating a molecular fingerprint of the sample. FTIR spectroscopy has been used extensively for characterization of conducting polymers in order to depict their conducting states. The FTIR spectra for PAA films were recorded in the range of 0 and 4500  $\text{cm}^{-1}$  (Figure 30) following the electrochemical polymerization and drying of PAA film in 0.2 M PBS (pH 7) on GCE. The absorption bands that occur at 1717  $\text{cm}^{-1}$  and a shoulder at 1304  $\text{cm}^{-1}$  were assigned to the vibrational modes of carboxylic acid, while the bands occurring at 1653, 1540, and 1410  $\text{cm}^{-1}$  were assigned to the vibrational mode of the amide group. The peak around 1225  $\text{cm}^{-1}$  that is associated with a stretching vibration of the ether group (Andreesu et al., 2005).



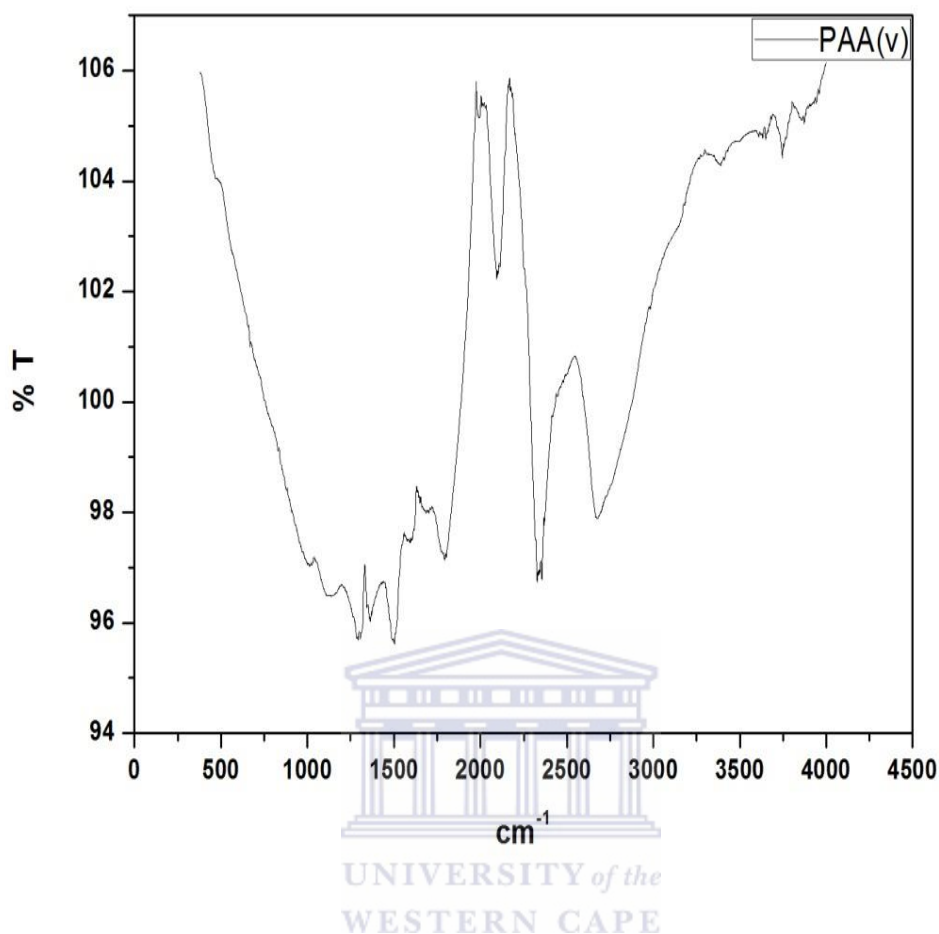


**Figure 30** FTIR spectra of polyamic acid film on GCE.

#### **4.7 Fourier Transform Infrared (FTIR) spectroscopy of PPy**

FTIR analysis of the PPy film (Figure 31) showed a band at around  $3400\text{ cm}^{-1}$  that was assigned to the N–H stretching mode. The heterocyclic aromatic ring C–C conjugation band was at  $1600\text{--}1300\text{ cm}^{-1}$ . The bands around  $1200\text{--}1000\text{ cm}^{-1}$  was assigned to the C–N stretching vibration modes. These results accounts for the presence of the PPy ring after electrochemical polymerization.

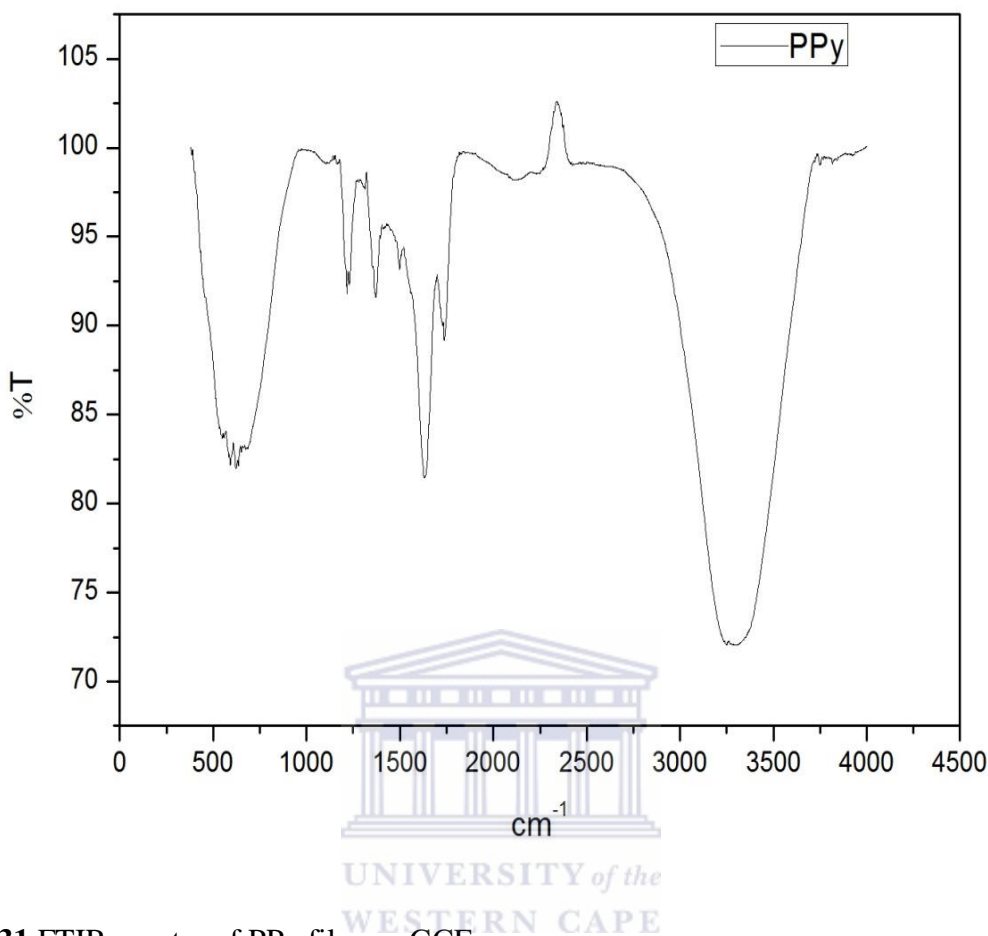


**Figure 31** FTIR spectra of PPy film on GCE.

#### **4.8 FTIR Spectroscopy: Overlay of PAA/PPy composites**

The IR spectra of the PAA/PPy composites are shown in Figure 32. The amide %T bands intensify from pure PAA film to composite 3 as a function of PPy concentration. Composite 4 and 5 however shows a decrease in %T which indicates a densification of the material. The characteristic IR peaks for PPy are nearly screened by the stronger PAA vibrations. The N-H stretching observed for the pure PPy is still visible, and the band intensity becomes stronger with increase concentration of PPy. The bands at 1653, 1540, and 1410  $\text{cm}^{-1}$  due to amide

---

ring increases when the amount of PPy increases indicating some changes in PAA spectrum. The C–H vibrations in the phenyl ring of PAA occur at (1100–1300)  $\text{cm}^{-1}$  and they are distorted possibly because of the interaction with PPy and cation-radical formation (Iroh et al., 2002). The FTIR confirms that the functionalities of both PAA and PPy are present confirming an interaction between the two polymers. The carboxylic and amide moieties from PAA are present in all the composites, confirmation that PAA is still present in the composites as PPy is incorporated into the PAA film.

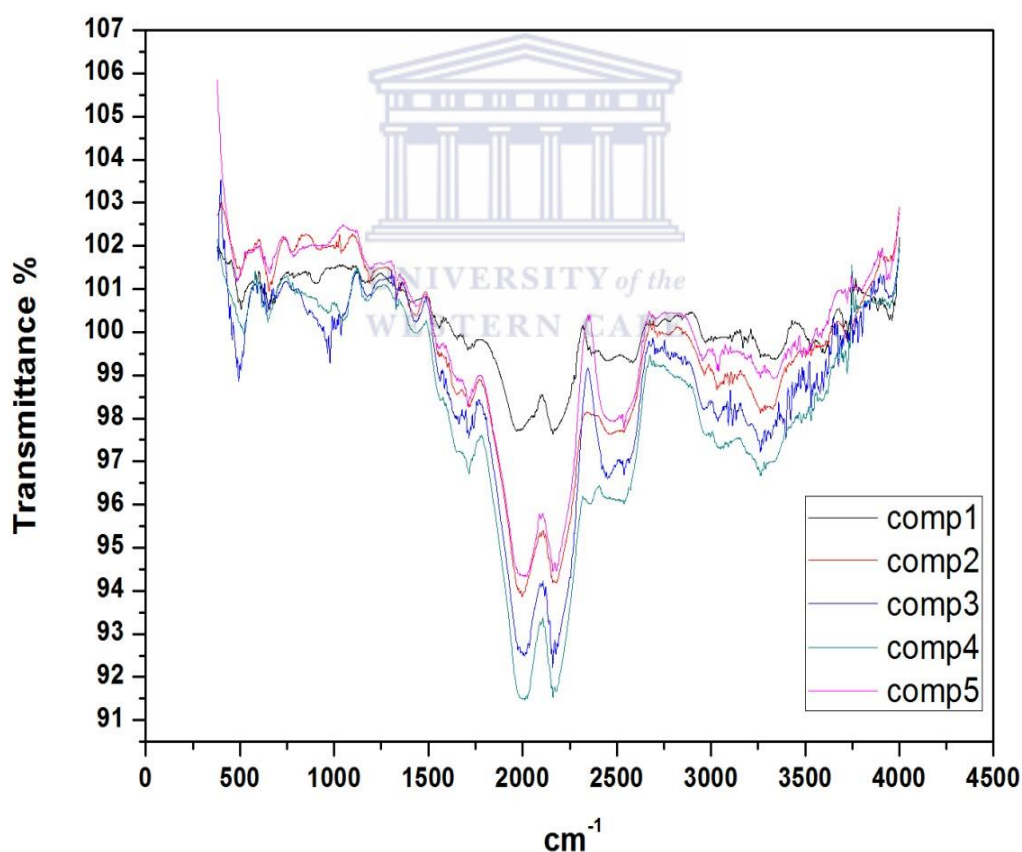


**Figure 32** FTIR spectra of PAA/ PPy composites 1, 2, 3, 4 and 5 on GCE.

---

## 4.9 Raman Spectroscopy of polyamic acid (PAA)

Raman spectroscopy is used to observe vibrational, rotational, and other low-frequency modes in a system, and the Raman effect occurs when light impinges upon a molecule and interacts with the electron cloud and the bonds of that molecule. The vibration is Raman active if it causes a change in polarisability. A change in the molecular polarization potential or amount of deformation of the electron cloud with respect to the vibrational coordinate is required for a molecule to exhibit a Raman effect. The amount of the polarizability change will determine the Raman scattering intensity. The pattern of shifted frequencies is determined by the rotational and vibrational states of the sample, in this case shift from the amide band of PAA film as a result of adding PPy. This dependence on the polarizability differs from Infrared spectroscopy where the interaction between the molecule and light is determined by the dipole moment; this contrasting feature allows analyzing transitions that might not be IR active via Raman spectroscopy. It's also important as the vibrational information is specific to the chemical bonds and symmetry of molecules. Therefore, it will provide a fingerprint by which the PAA molecule can be identified. The fingerprint region of organic molecules is usually in the (wavenumber) range 500–2000  $\text{cm}^{-1}$ . The characteristic bands of PAA film on SPCE (Figure 33) are as follows: 881  $\text{cm}^{-1}$ , amide I; 1247  $\text{cm}^{-1}$ , amide III; 1330  $\text{cm}^{-1}$ , symmetric stretching of carboxylic acid; 1565  $\text{cm}^{-1}$ , amide II; 1606  $\text{cm}^{-1}$ , ring vibration of carboxylic acid; 1662  $\text{cm}^{-1}$ , amide I; 1724  $\text{cm}^{-1}$ , C=O of carboxylic acid (Han Yu et al 2002). The assignments of the Raman bands are similar to those proposed by Tsai et al and Ishida et. al. for PMDA/ODA model compounds and by Varsanyi and Young et. al. for PMDA/ODA polyamic acid and polyimide. The band near 1623  $\text{cm}^{-1}$  was attributed to the tangential ring stretching mode of the  $\text{C}_6\text{H}_2$  ring while those near 1691 and 941  $\text{cm}^{-1}$  were assigned to the C 4 stretching and OH out-of-plane bending modes of the acid groups,

---

respectively. Bands near  $1577$  and  $1341\text{ cm}^{-1}$  were attributed to modes of the amide groups while the band near  $1180\text{ cm}^{-1}$  was assigned to the C-X stretching mode of the  $\text{C}_6\text{H}_{14}$  ring (W. H. Tsai et al 1992).

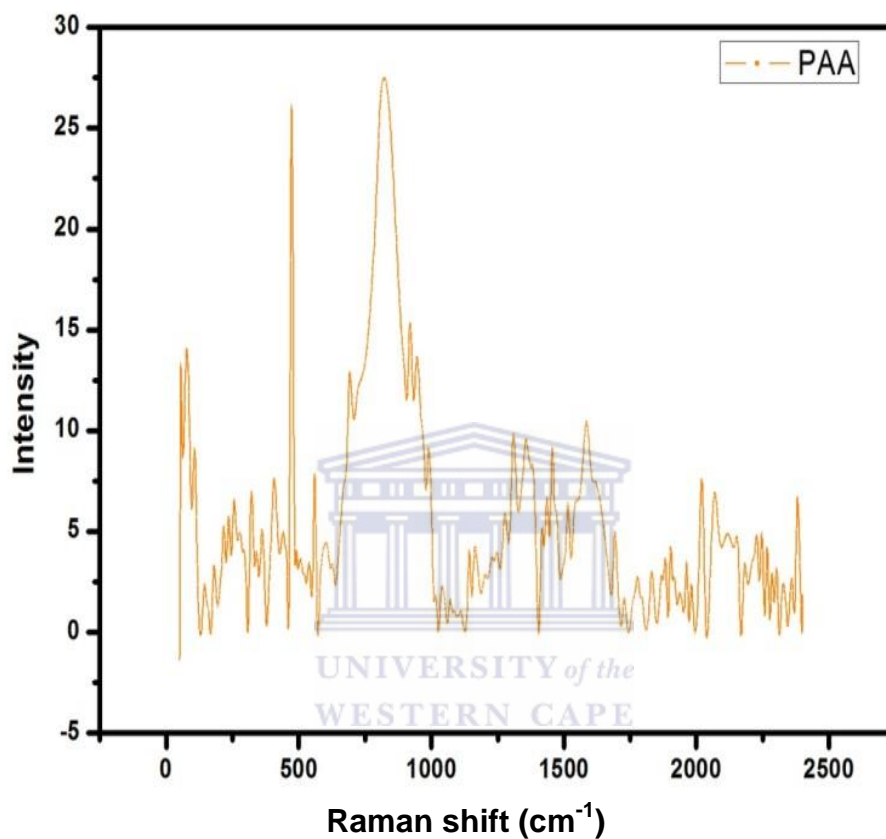


**Figure 33** Raman spectra of polyamic acid (PAA) film on SPCE.

---

## 4.10 Raman Spectroscopy of PPy

The Raman spectra of PPy (Figure 34) showed bands at 1556 and 1037  $\text{cm}^{-1}$ , was assigned as a symmetric stretching vibration of C = C and the CH in-plane deformation in the PPy (Chan S. Choi et. al., 1989). The Raman technique gave specific information, in particular, it allowed to follow accurately the doping level of the film through two bands, one corresponding to the continuous transition between the C = C and C – C intercycles vibration stretching.

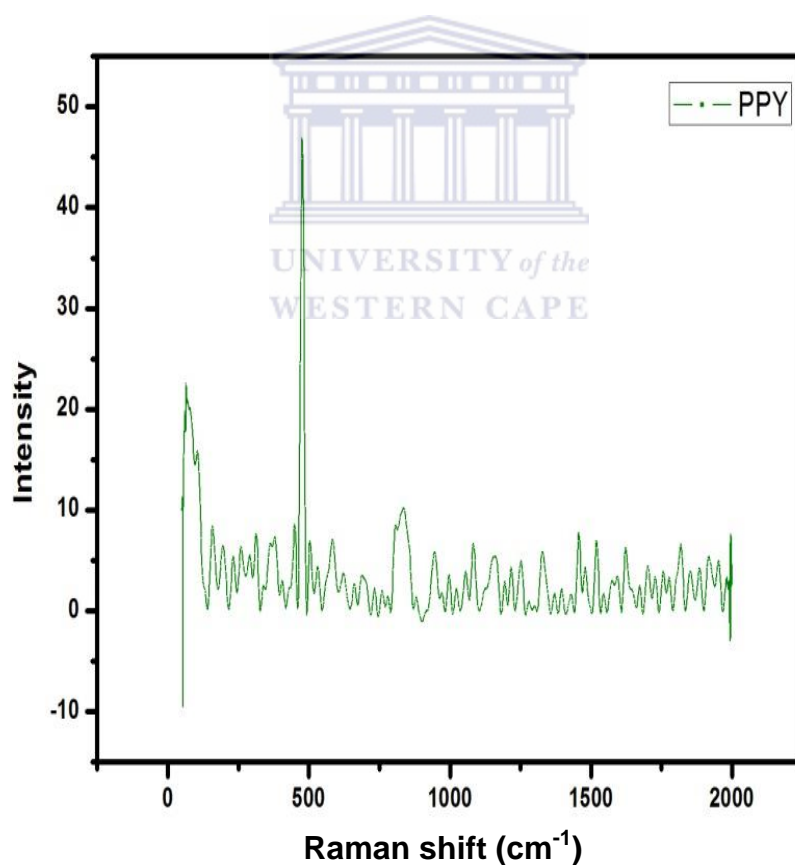


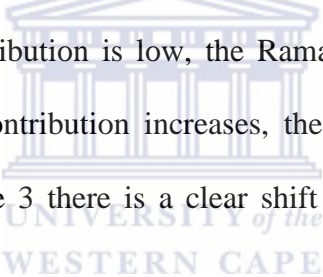
**Figure 34** Raman spectra of polypyrrole PPy on SPCE.



---

## 4.11 Raman Spectroscopy: Comparison of different PAA/PPy composites

The Raman spectrum obtained for PAA/PPy composites (Figure 36) shows the presence of characteristic absorption  $881\text{ cm}^{-1}$ , amide I;  $1247\text{ cm}^{-1}$ , amide III;  $1330\text{ cm}^{-1}$ , symmetric stretching of carboxylic acid;  $1565\text{ cm}^{-1}$ , amide II;  $1606\text{ cm}^{-1}$ , ring vibration of carboxylic acid;  $1662\text{ cm}^{-1}$ , amide I;  $1724\text{ cm}^{-1}$ , C = O of carboxylic acid as seen in pure PAA Raman spectrum (Han Yu et al 2002) respectively. The intensity of these bands increases, showing how PPy affects the Raman of pure PAA film on SPCE. At composite 3 from the Raman shift  $\text{cm}^{-1}$  vs composite calibration plot (Figure 35) it is evident that neither the PAA nor the PPy is dominating. When the PPy contribution is low, the Raman shift of amide bands from the PAA is small but as the PPy contribution increases, the Raman shift of the amide band increases. Therefore at composite 3 there is a clear shift from the original amide band of PAA.



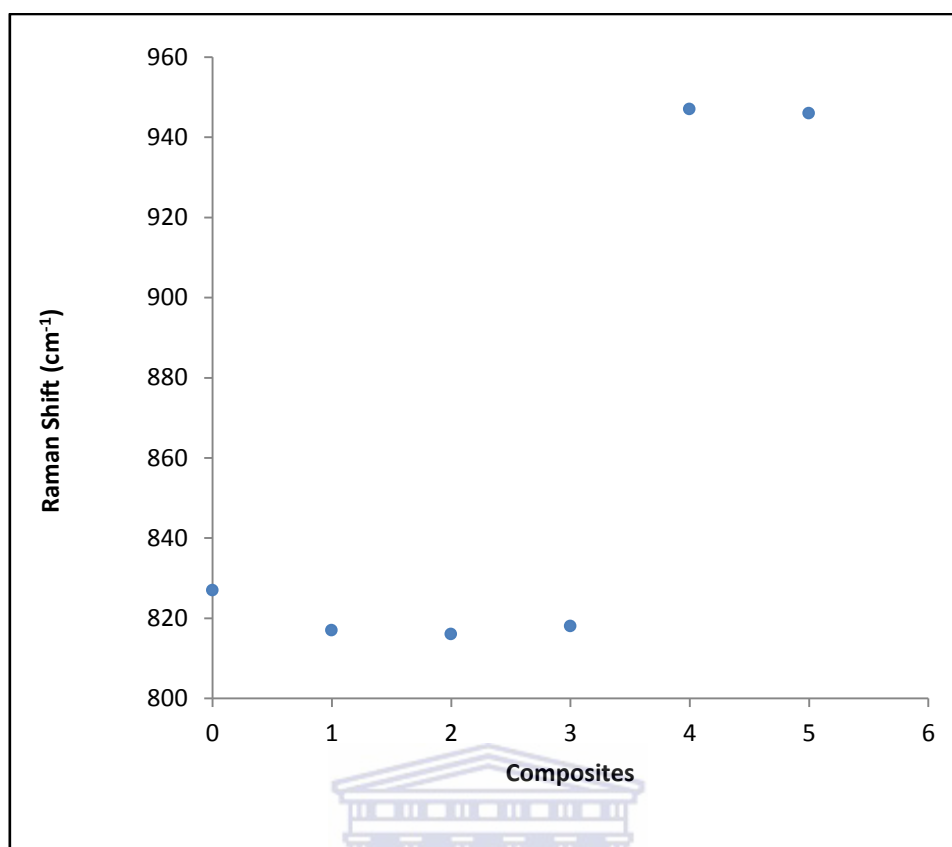


**Figure 35** The change in Raman shift ( $827\text{ cm}^{-1}$  = amide band) for the PAA film and the composites 1 to 5 on SPCE.

0 = pure PAA film; 1 = composite 1; 2 = composite 2; 3 = composite 3; 4 = composite 4; and 5 = composite 5

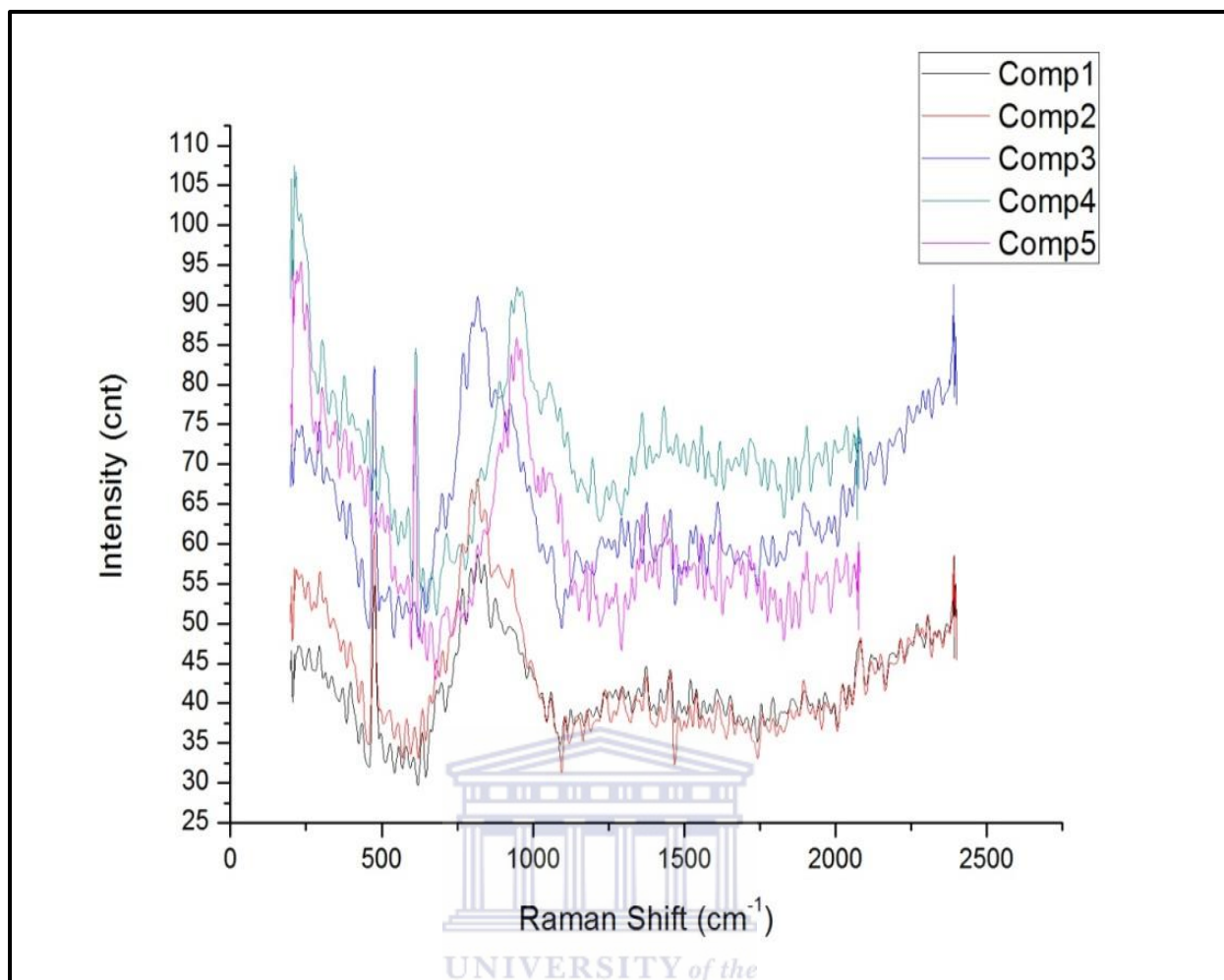
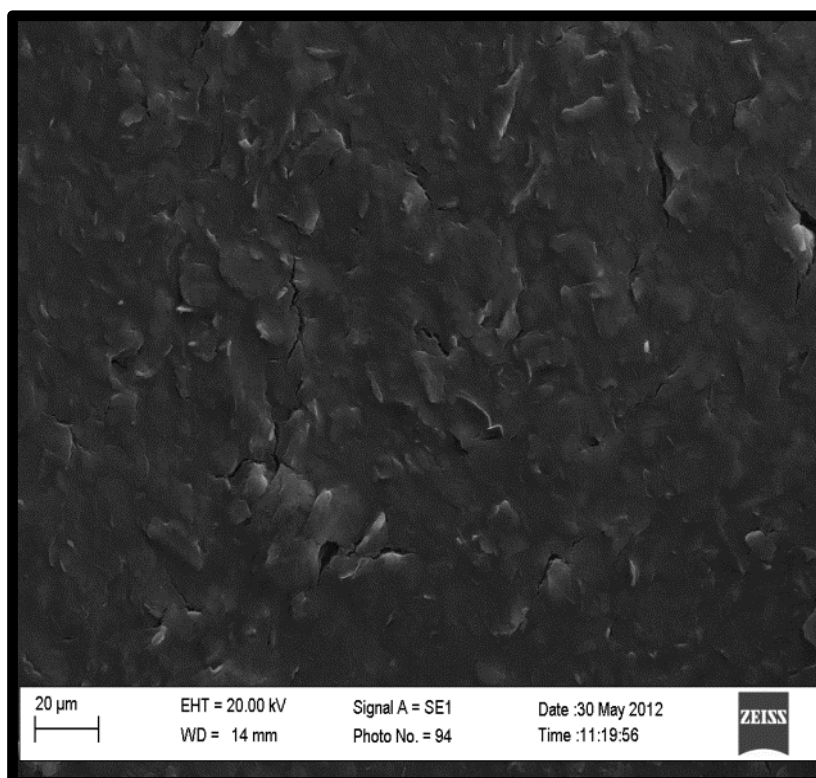
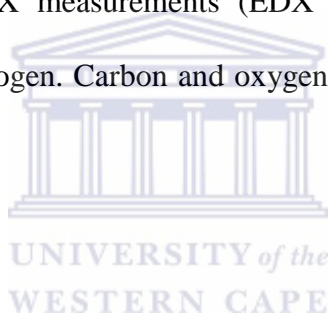


**Figure 36** Raman Spectra of the composite 1, 2, 3, 4 and 5 on SPCE.

---

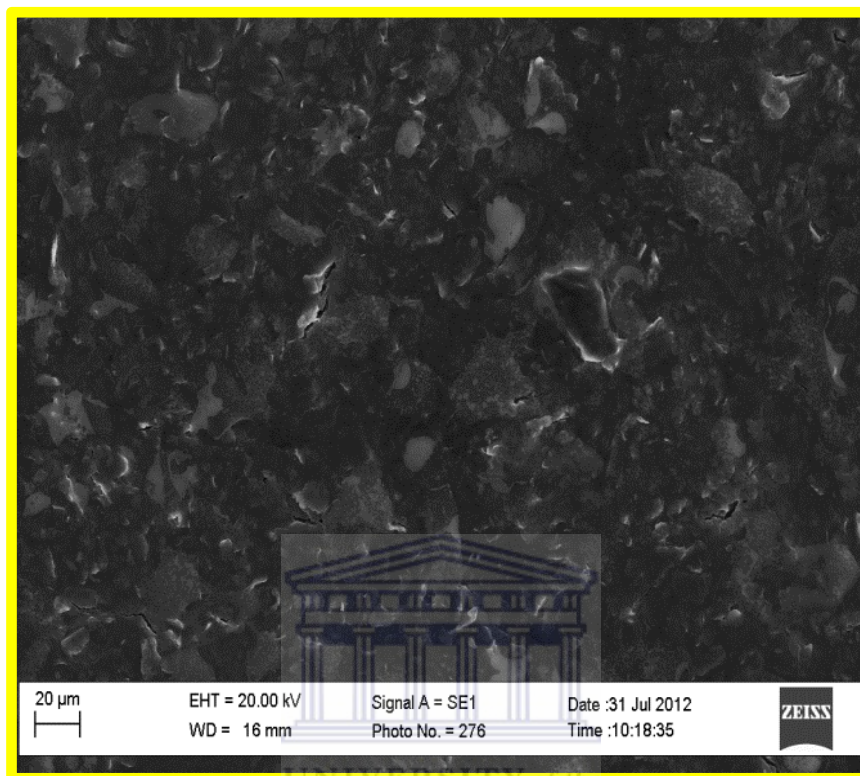
## 4.12 Scanning electron microscopy (SEM) of polyamic acid

Scanning electron microscopy (SEM) produces images of a sample by scanning it with a focused beam of electrons, which produces information about the sample's surface topography and composition. SEM was performed for a bare SPCE and for pure PAA films to determine the differences in morphology of the PAA film and the bare. SEM analysis was carried out on the PAA film that was electrodeposited onto a screen printed carbon electrode after drying for an hour at room temperature. The surface of the bare carbon SPCE was covered with a uniform PAA layer, containing few amorphous PAA clusters. For the electrodeposited PAA film, EDX measurements (EDX graph not shown) showed trace amounts carbon, oxygen and nitrogen. Carbon and oxygen as principle elements in the PAA layer (Andreesu et al., 2005).



---

(a)



(b)

**Figure 37** SEM micrographs recorded for electrodeposited films on the screen printed carbon electrode (SPCE): (a) bare screen printed electrode (b) PAA film.

---

### 4.13 Scanning electron microscopy (SEM) PPy

The surface morphology of the PPy film was characterized by scanning electron microscopy (SEM). Morphology plays an important role in determining conductivity and mechanical properties of the materials because electrical conductivity is related to surface morphology. The bulk polymer tends to aggregate in large particles in the form of large globules. This is probably due to an increased inter-chain interaction compared to its stabilized particles in which the polymeric surfactant chains act as a limiting factor for such an interaction.

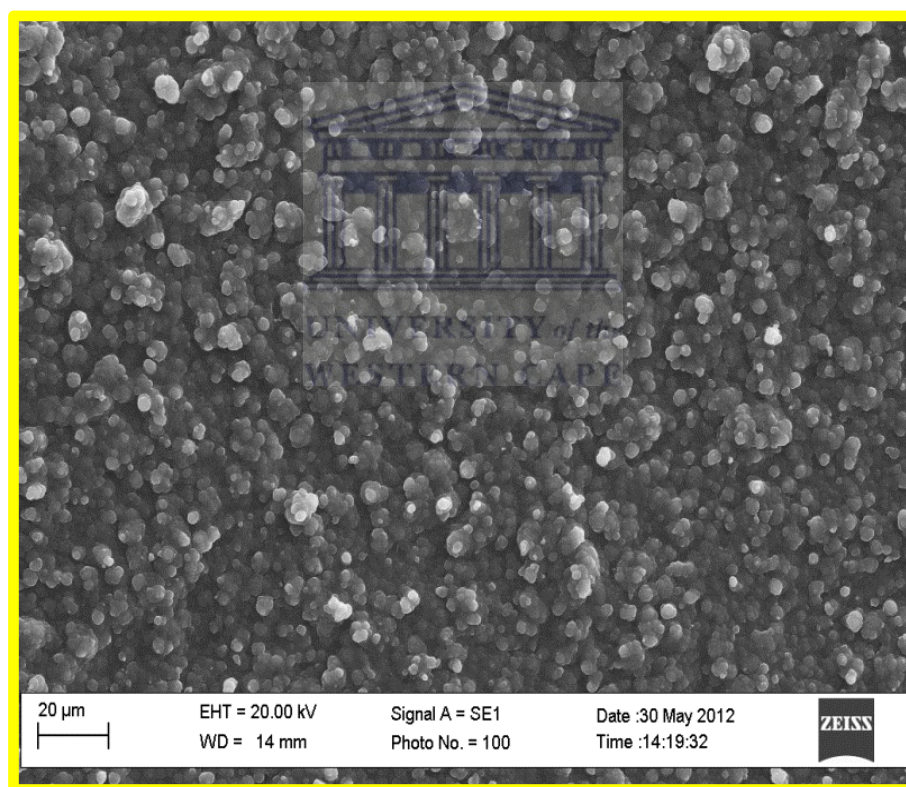
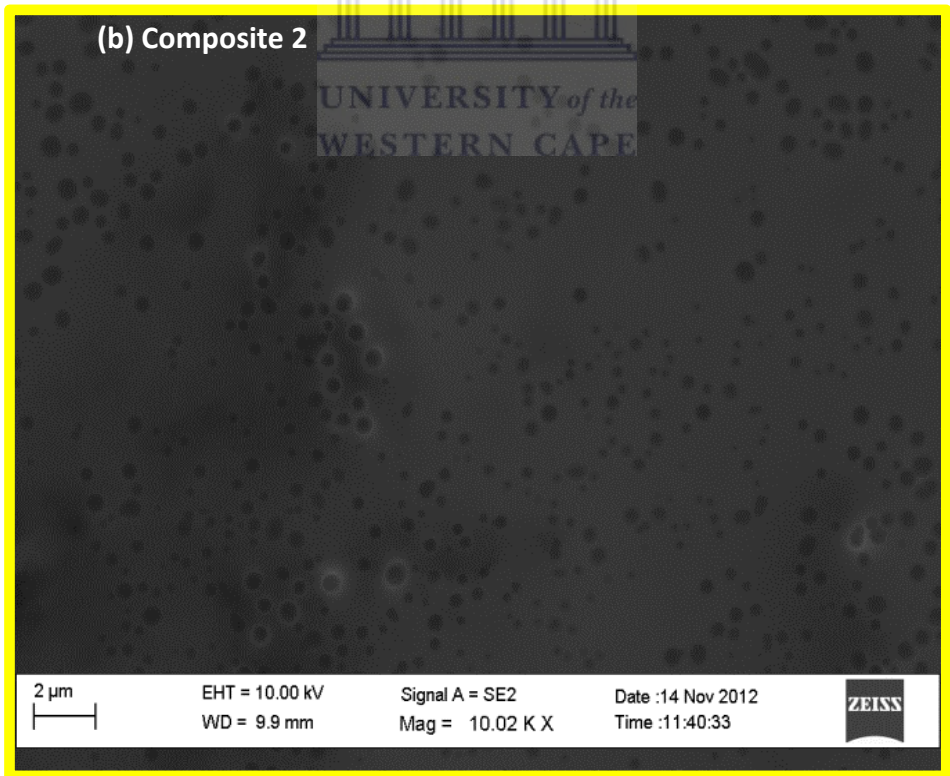
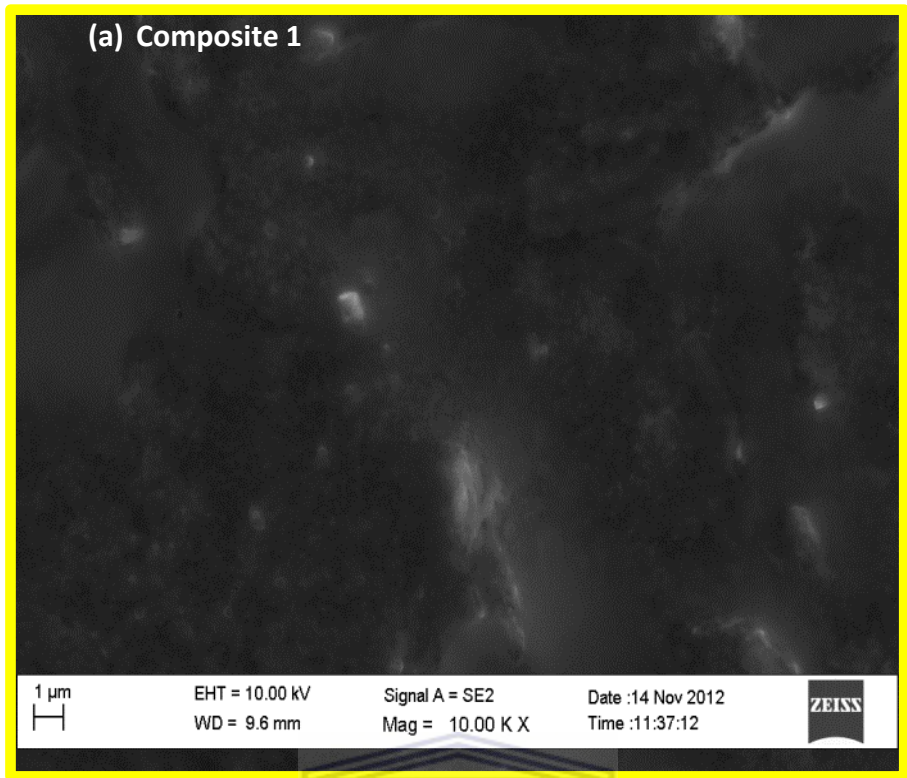


**Figure 38** SEM micrographs recorded for electrodeposited PPy film on the screen printed carbon electrode (SPCE).

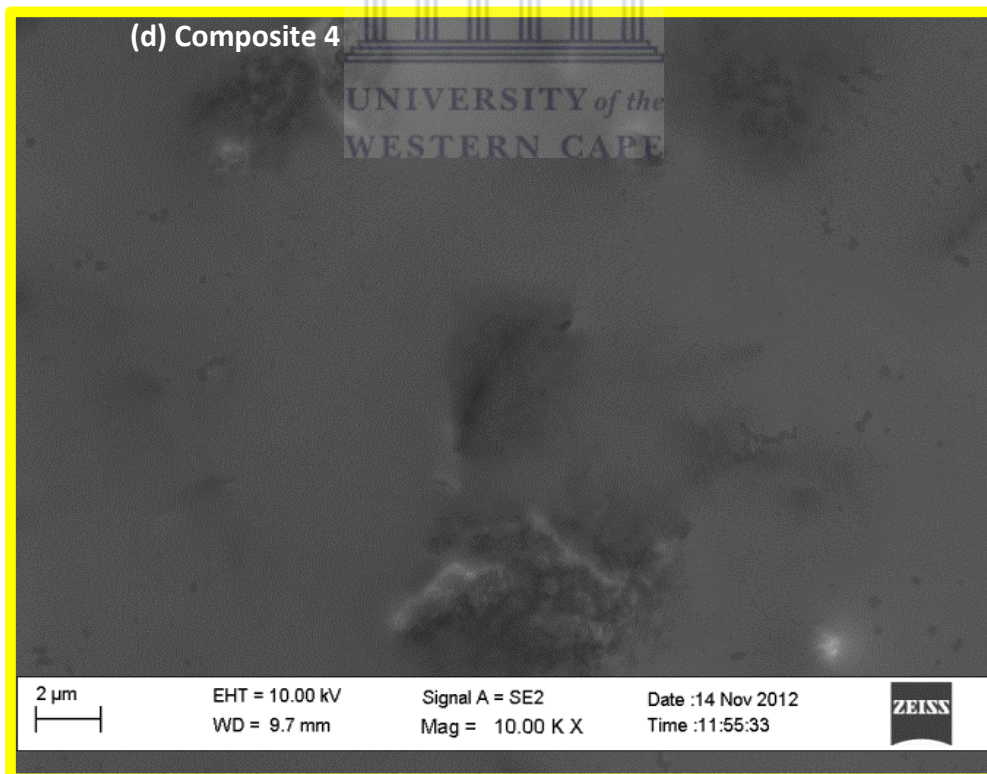
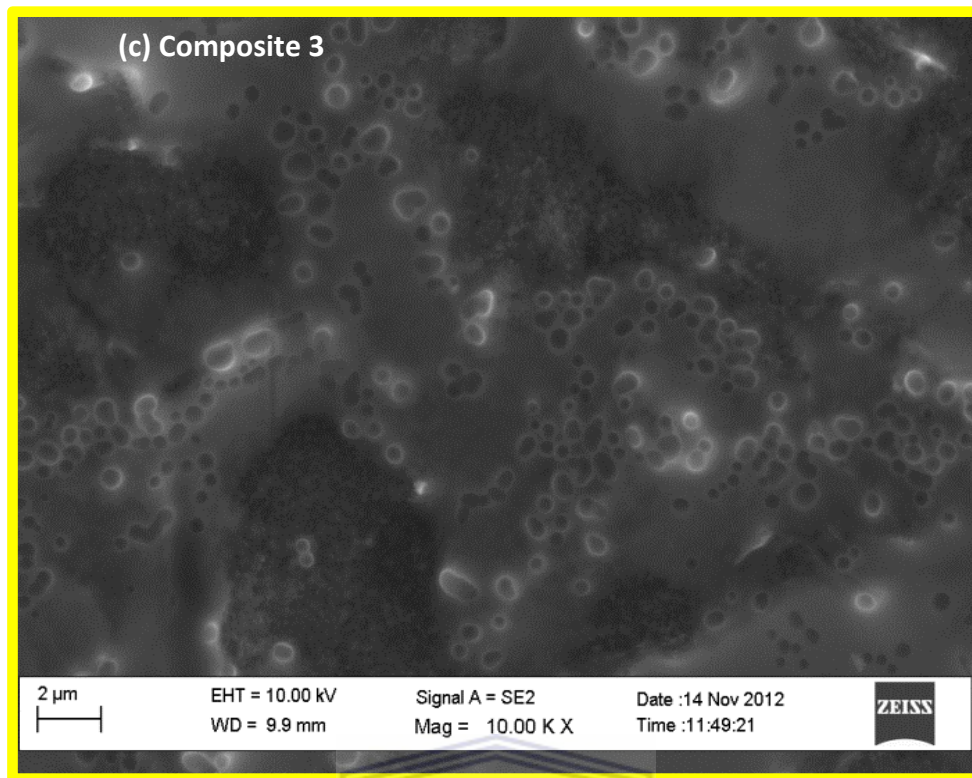
---

#### **4.14 Scanning electron microscopy: Different ratios of PAA/PPy composites**

The surfaces of the PAA/PPy composites have structures that incorporate both PAA and PPy (Figure 39 (a), (b), (c), (d) and (e)). The structure of the composite surfaces differs significantly from the rough structure (amorphorous) of the PAA film. As the concentration of PPy increases the film becomes a more smooth and porous (Iroh et al., 2002). The pores range from 350 to 550 nm filled with the filaments of a conducting polymer impregnated with the rough PAA matrix as shown on the microphotograph of PAA/PPy composite. It is believed that the PPy filaments are formed and anchored along the PAA matrix. This is confirmed by the EDX analysis as it still provides evidence of O<sub>2</sub> (from the carboxylic moiety) that comes from PAA, as PPy does not have oxygen moieties. This is important as it proves that the PPy film does not form a blanket layer on top of the PAA film and that a composite is formed rather than then two polymers forming layers on top of each other. This is best described in composite three as it clearly shows the best morphology of the two polymers combined. As the PPy concentration increases the PAA just becomes flooded with PPy and the rough porous structures are not evident anymore.







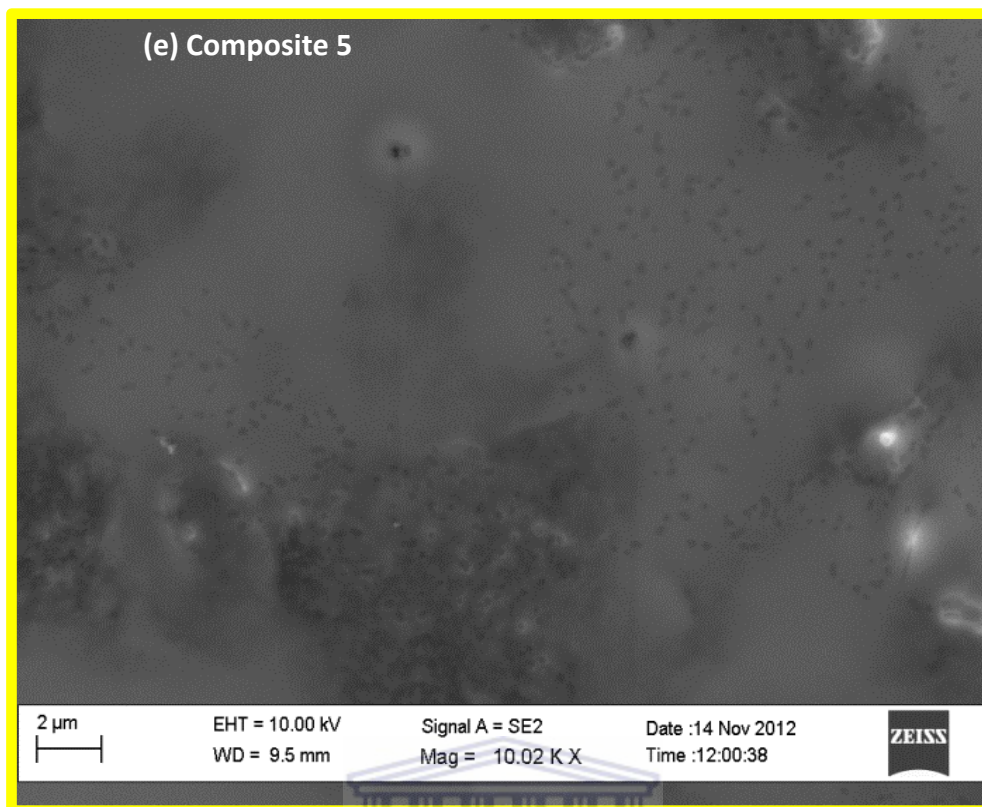


**Figure 39** SEM micrographs recorded for electrodeposited PAA/PPy films on the SPCE (a) Composite 1; (b) Composite 2; (c) Composite 3; (d) Composite 4 and (e) Composite 5.

UNIVERSITY of the  
WESTERN CAPE

#### **4.15 Atomic Force Microscopy (AFM) of PAA, PPy and PAA/PPy composites**

Atomic force microscopy (AFM) is a very high-resolution type of scanning probe microscopy, and can do imaging of almost any type of surface, including polymers, ceramics, composites, glass, and biological samples. AFM was used for surface morphology and roughness estimates of the polymers PAA, PPy (Figure 40 and 41) and the PAA/PPy composites (Figure 42 to 46) prepared.

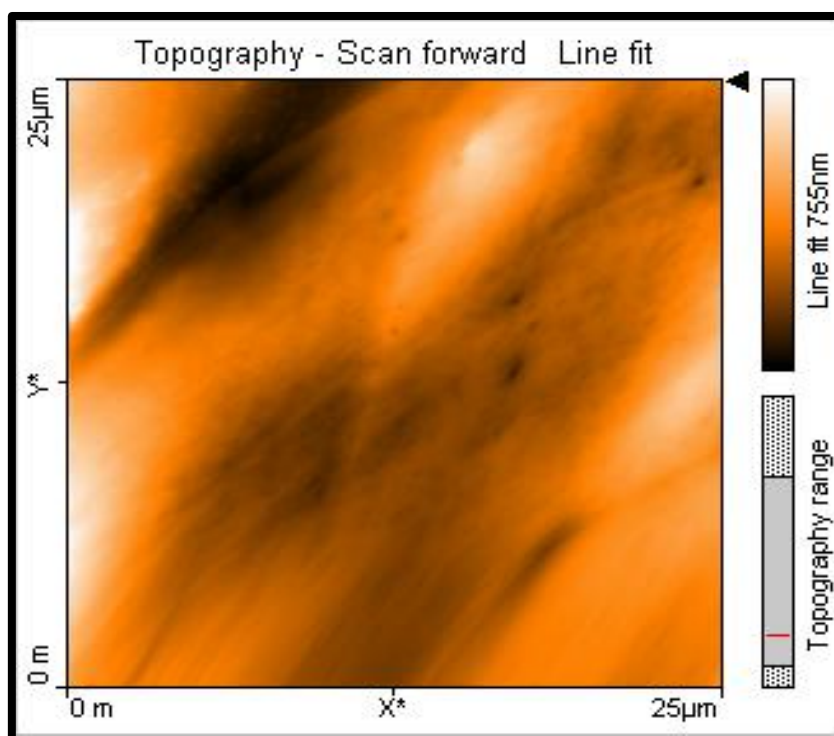


**Figure 40** AFM image of polyamic acid (PAA) film on screen printed carbon electrode (SPCE).

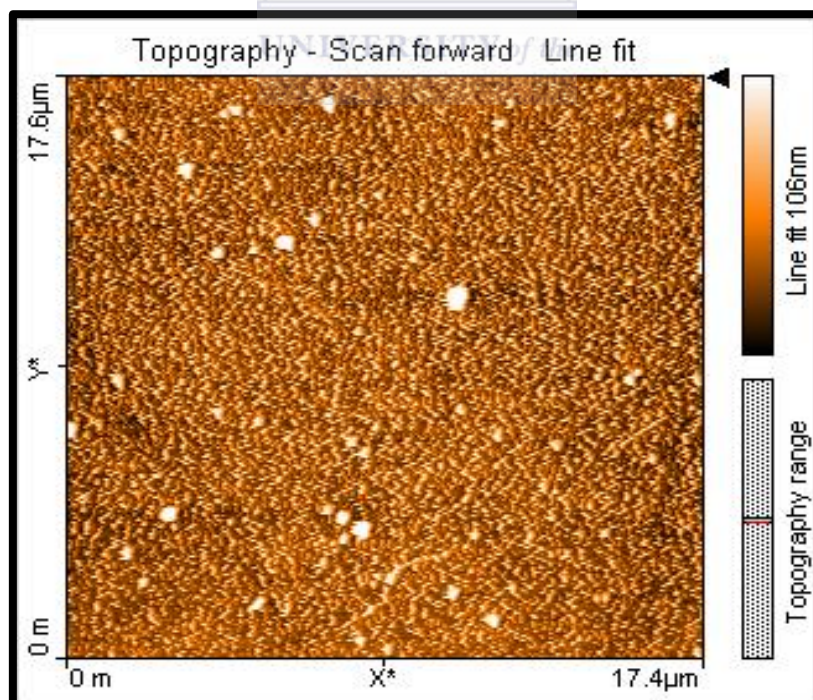


**Figure 41** AFM image of polypyrrole (PPy) on screen printed carbon electrode (SPCE).

---

The surface features of the PAA sample was observed to have a height distribution of 0-755 nm (Figure 40) whereas the PPy sample showed a height distribution of 0-106 nm (Figure 41). This height distribution is in good agreement with the observed surface features of the polymers from 20.00 kV SEM, where it was evident that the surface features of the PAA film was on a larger scale than that of the PPy. Polypyrrole (PPy) was observed to have a finer granular structure whereas PAA displayed comparatively larger scale like features.

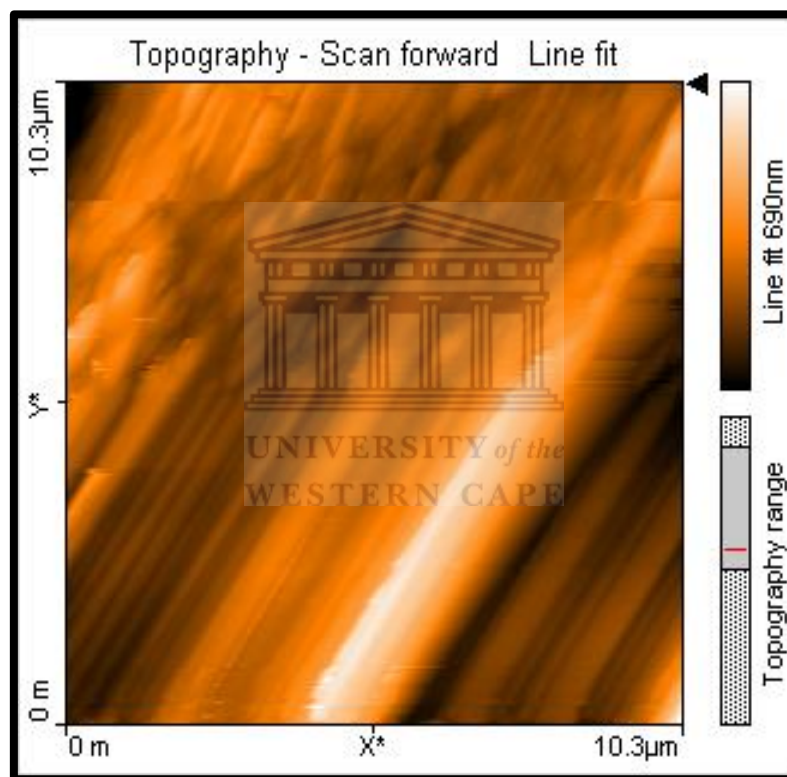


**Figure 42** AFM image of Composite 1 on screen printed carbon electrode (SPCE).

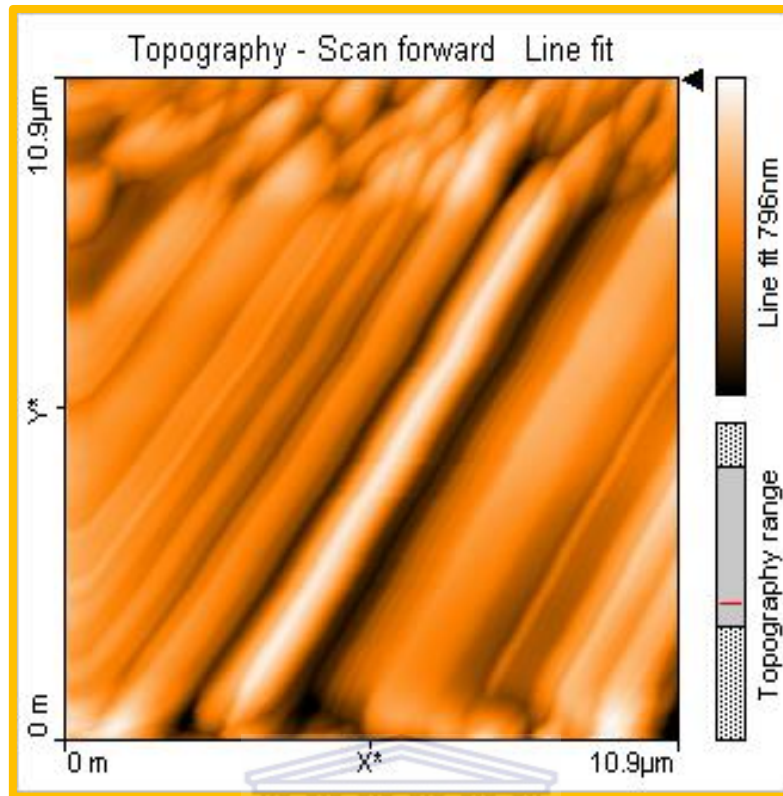


**Figure 43** AFM image of Composite 2 on screen printed carbon electrode (SPCE).

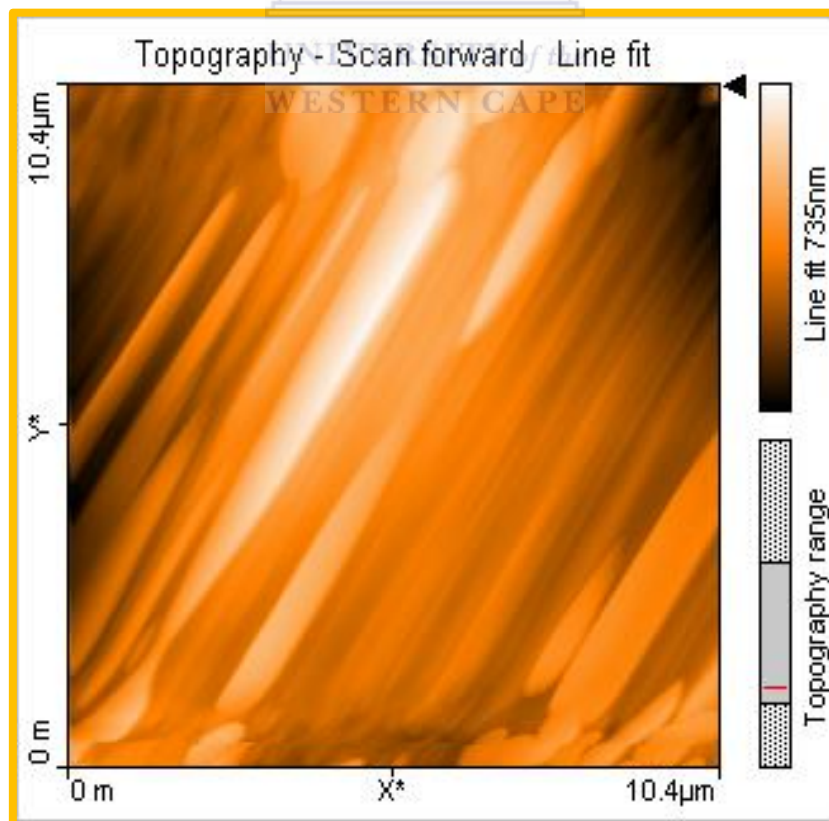


**Figure 44** AFM image of Composite 3 on screen printed carbon electrode (SPCE).

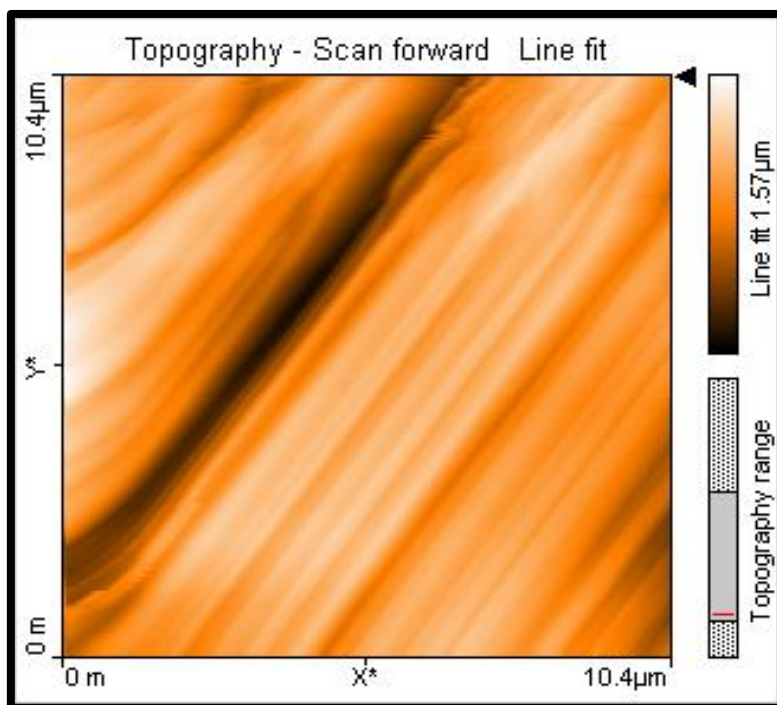


**Figure 45** AFM image of Composite 4 on screen printed carbon electrode (SPCE).

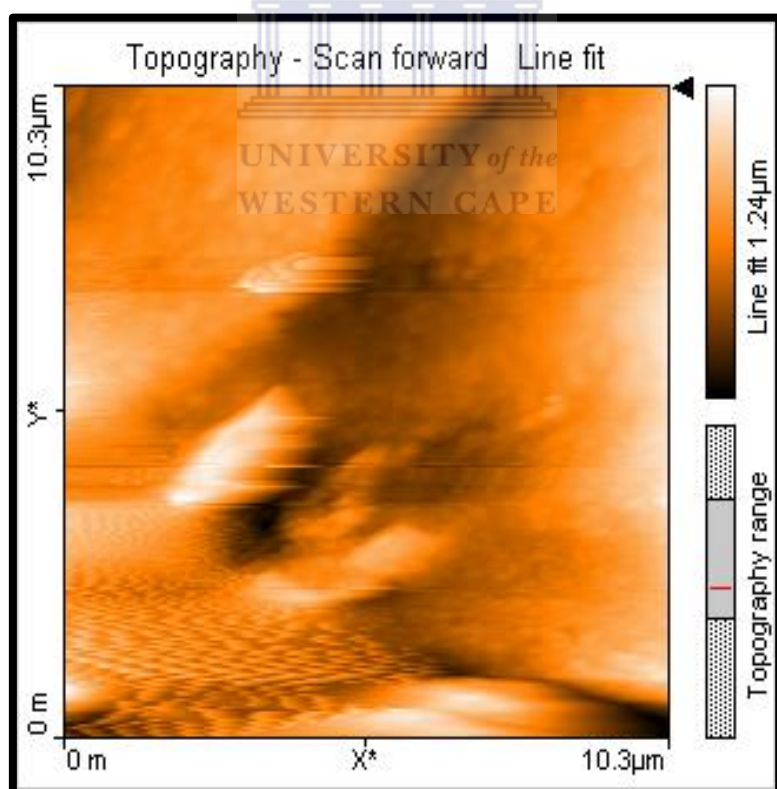


**Figure 46** AFM image of Composite 5 on screen printed carbon electrode (SPCE).

---

The presence of the PPy in the composite breaks up the large scale like appearance of the pure PAA film and introduces a controlled laminar surface morphology as a function of PPy concentration. This is most clearly defined in composite 2 and 3 (Figure 43 and 44) where individual needle-like surface features can be clearly distinguished. At higher PPy concentrations these features become less distinct and eventually blend into a smoothed surface appearance.

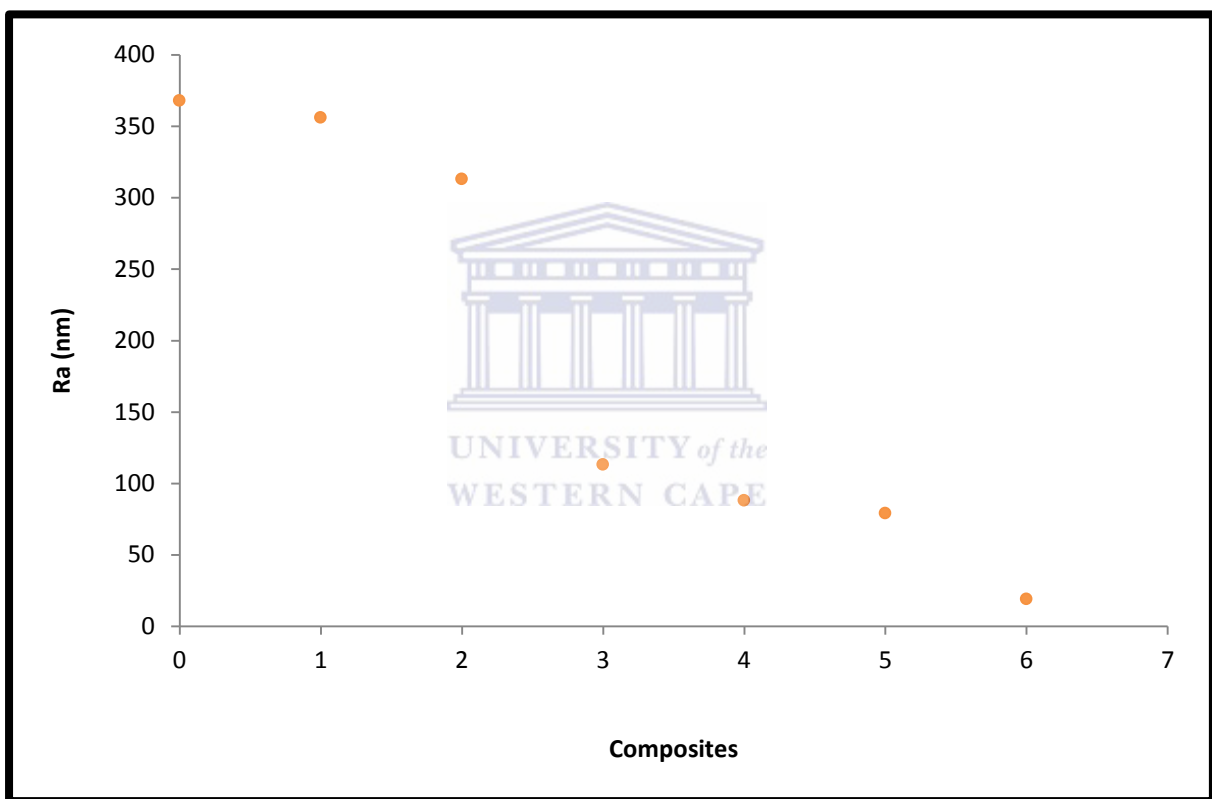


**Figure 47** XY plot of Ra as a function of electropolymerised thin film composition, where 0 = PAA, 1 = composite 1; 2 = composite 2; 3 = composite 3; 4 = composite 4 and 5 = composite 5 (the composites 1 to 5 as previously defined); 6 = PPy.

---

The line roughness (Ra) (Figure 47) values showed a clear distribution of roughness associated with pure PAA and PPy respectively and a decreasing trend upon inclusion of PPy into the PAA matrix. The samples most distinctly associated with equal contribution from the pure polymers appear to be composites 2 and 3. It is clear from AFM and SEM micrographs that the PAA provides a template for highly ordered arrangement of polypyrrole formation at these ratios during electrochemical synthesis, resulting in unique nanorod formation, yielding a highly reactive surface area. This trend in Ra is supported by electrocatalysis as evidenced in CV measurements and  $D_e$  calculations.

The viscous liquid PAA was chemically synthesised from the monomers ODA and PMDA. Homogeneity played crucial role in composite preparation, thus the viscous PAA was used for composite preparation with PPy. A series of new polyamic acid and polypyrrole (PAA/PPy) composites was electrochemically synthesised *in-situ* and characterized in 0.2 M phosphate buffer solutions at pH of 7. A total of five PAA/PPy composites were prepared. Electrochemical characterization proved that PAA/PPy composites was formed as a new peak was observed, that was not in observed in the individual polymers (PAA and PPy) characterization.  $E^{02}$  of PAA was still present in all composites, confirming PAA existence in composites. Peak potentials and  $D_e$  were evaluated using the parameters from CV; composite 3 were proved to have the best electrochemical properties out of the five composites prepared. From FTIR the amide %T bands intensified from pure PAA film to composite 3 as a function of PPy concentration. Composite 4 and 5 however showed a decrease in %T which indicates a densification of the material. The Raman spectrum obtained for PAA/PPy composites shows the presence of characteristic amide and carboxylic absorption bands. The intensity of these bands increased, which was an indication of how PPy affects the Raman of pure PAA film on SPCE. At composite 3 from the Raman shift  $\text{cm}^{-1}$  vs composite calibration plot it is evident that neither the PAA nor the PPy is dominating. Therefore at composite 3



---

there is a clear shift from the original amide band of PAA. From SEM images it was observed that the surfaces of the PAA/PPy composites have structures that incorporate both PAA and PPy. The structure of the composite surfaces differs significantly from the rough structure (amorphorous) of the PAA film and the PPy filaments are formed and anchored along the PAA matrix. This is confirmed by the EDX analysis as it still provides evidence of O<sub>2</sub> (from the carboxylic moiety) that comes from PAA, as PPy does not have oxygen moieties. This is best described in composite three as it clearly shows the best morphology of the two polymers combined. The line roughness (Ra) values obtained from AFM showed a clear distribution of roughness associated with pure PAA and PPy respectively and a decreasing trend upon inclusion of PPy into the PAA matrix.



---

## Chapter 5:

### ***Part 1: Evaluation of Spectroscopic Properties and Electrochemical of Enzyme (Luciferase) and Analytes (Naphthalene and Fluoranthene)***

#### **5.1 Introduction**

This chapter presents the result of the interaction between the enzyme luciferase and analytes (naphthalene and fluoranthene) in preparation for the construction of a biosensor. Electrochemical characterization and immobilisation of the enzyme; *Photobacterium Vibrio fisheri* luciferase, and its application for a biosensor for the polycyclic aromatic hydrocarbons is described in this chapter. Fluorescence spectroscopy, cyclic voltammetry (CV), and electrochemical quartz microbalance (EQCM) studies were carried out to characterize the enzyme's response to each analyte in 0.2 M PBS at pH 7. To study the interaction of the enzyme with each analyte Fluorescence spectroscopy was used, also to see how the bioluminescence properties of the enzyme changes with the addition of each analyte. A diluted solution of the enzyme in 0.2 M PBS pH7 was put into a 3 mL cuvette. Luciferase showed an emission peak at 340 nm. Fluorescence measurements were done after adding 2  $\mu$ L aliquots of analytes into enzyme solution and shaking the mixture for few seconds. The emission peak at 340 nm gradually decreased as the concentrations of each analyte were increased. The luciferase biosensor was prepared by drop coating 10  $\mu$ L of luciferase solution onto a bare GCE surface (GCE/LUC) and left to immobilize for 24 hours. The enzyme was electroactive in 0.2 M PBS pH 7 with two quasi-reversible redox couples at  $E^{o'}$  = +110 mV and  $E^{o'}$  = +730 mV (vs. Ag/AgCl); has diffusion coefficient of  $1.1 \times 10^{-12}$  cm<sup>2</sup>/s and has a surface coverage of  $1.50 \times 10^{-13}$  moles/cm<sup>2</sup>. The mass changes due to the addition of

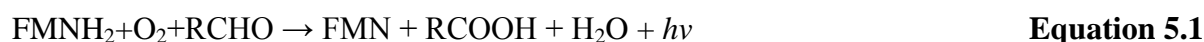
---

each analyte were measured by Electrochemical Quartz microbalance (EQCM) from the N series Autolab potentiostat/galvanostat instrument, PGSTAT128N.

## 5.2 Fluorescence Spectroscopy of Luciferase and Luciferase with analytes

### 5.2.1 Fluorescence Spectroscopy of Luciferase

Firefly bioluminescence arises from the oxidation of a substrate (luciferin), by an enzyme, a luciferase that results in the formation of the product (an oxyluciferin,) in an electronically excited singlet state. Relaxation of the oxyluciferin to the corresponding ground state is accompanied by the emission of light (Ren A. M. et. al., 2005). According to Baldwin et al the bacterial luciferase uses the oxygen in a flavin monooxygenase reaction in which the molecular oxygen has been activated by a reaction with reduced flavin mononucleotide (FMNH<sub>2</sub>), reacts with an aldehyde to yield carboxylic acid, oxidized flavin (FMN), and blue-green light in the following reaction (Baldwin T.O et. al., 1995):



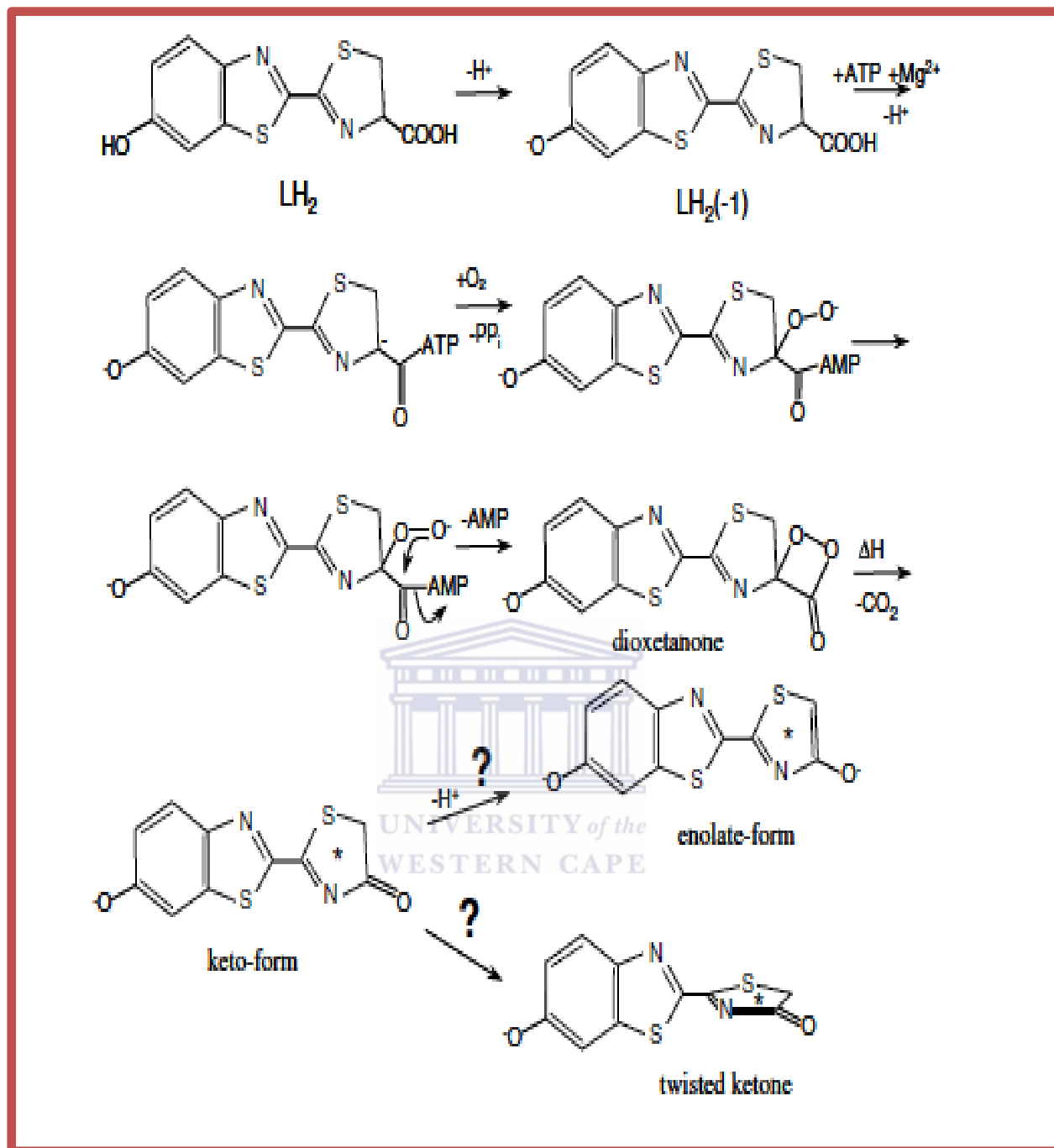


**Figure 48** Chemical reactions involved in the oxidation of luciferin via a dioxetanone to excited state oxyluciferins. These reactions are catalysed by luciferase and are the basis for light emission in the firefly luciferase (Baldwin T.O et. al., 1995).

---

An emission peak at around 340 nm was observed for luciferase in PBS pH 7, which agrees well with literature where the emittance for luciferase in aqueous media should occur (Figure 49). The reaction mechanism of the bacterial luciferase luminescence has been studied in detail by the Hastings group.

Where FMNH<sub>2</sub> and FMN are the reduced and oxidized forms of the flavin mononucleotide, respectively, C<sub>n</sub>CHO is the alkylaldehyde and C<sub>n</sub>COOH is the corresponding fatty acid. The BL system requires FMNH<sub>2</sub> for the light emission reaction. The FMNH<sub>2</sub> is easily oxidized to FMN by dissolved O<sub>2</sub>. To promote a continuous luminescence reaction FMNH<sub>2</sub> should be regenerated from FMN.

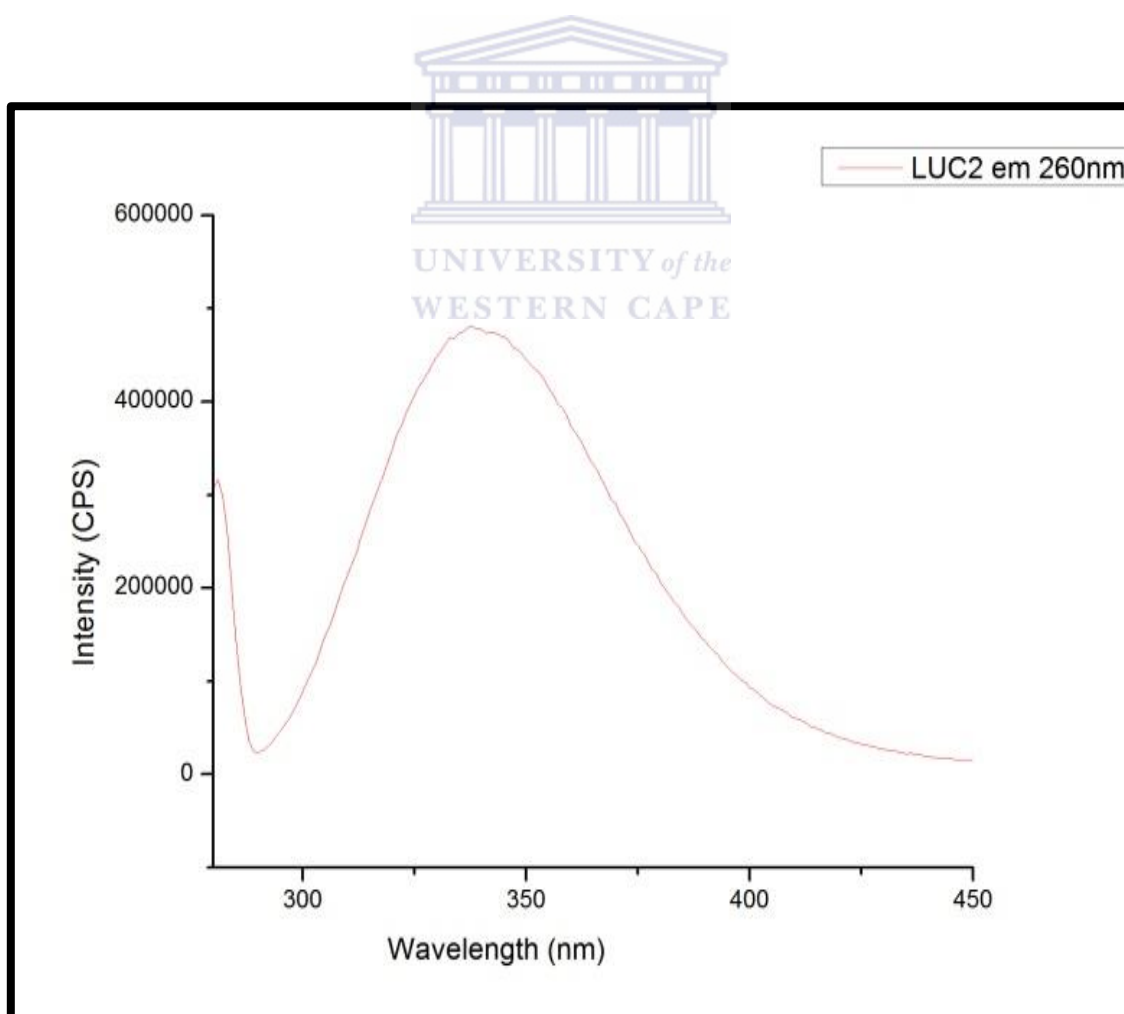


**Figure 49** Fluorescence spectra of the enzyme; luciferase in a 0.2 M PBS (pH 7) solution.

---

## 5.2.2 Fluorescence spectroscopy of Luciferase with Naphthalene

To examine the applicability of the developed luciferase luminescence system for a study of the effects of hydrophobic molecules such as naphthalene and fluoranthene on the enzymatic function of luciferase, aliquots of naphthalene was added and the corresponding change in the luciferase luminescence intensity was measured. As shown in Figure 50, the luciferase luminescence was shown to decrease (in aqueous media) in the presence of naphthalene. The decrease in the luciferase luminescence intensity was associated with the binding of naphthalene with the luciferase.

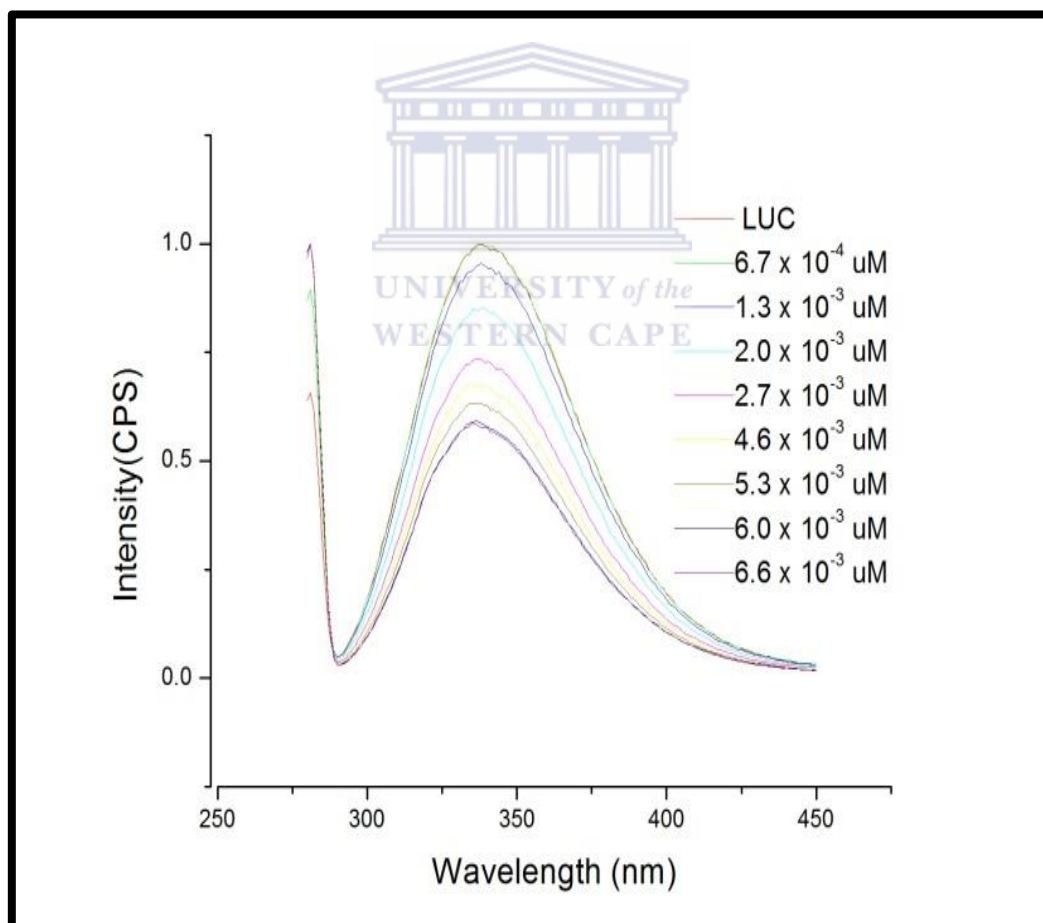


**Figure 50** Fluorescence spectra of the enzyme; luciferase with increasing concentrations ( $6.7 \times 10^{-4}$  to  $6.6 \times 10^{-3}$   $\mu$ M) of naphthalene in 0.2 M PBS (pH 7).

---

Figure 51 shows the calibration curve of intensity vs. concentration of naphthalene. From the linear region of the calibration curve (Figure 52) a sensitivity of 80  $\mu\text{M}$  was observed, and a limit of detection (LOD)  $6.6 \times 10^{-1} \mu\text{M}$ .

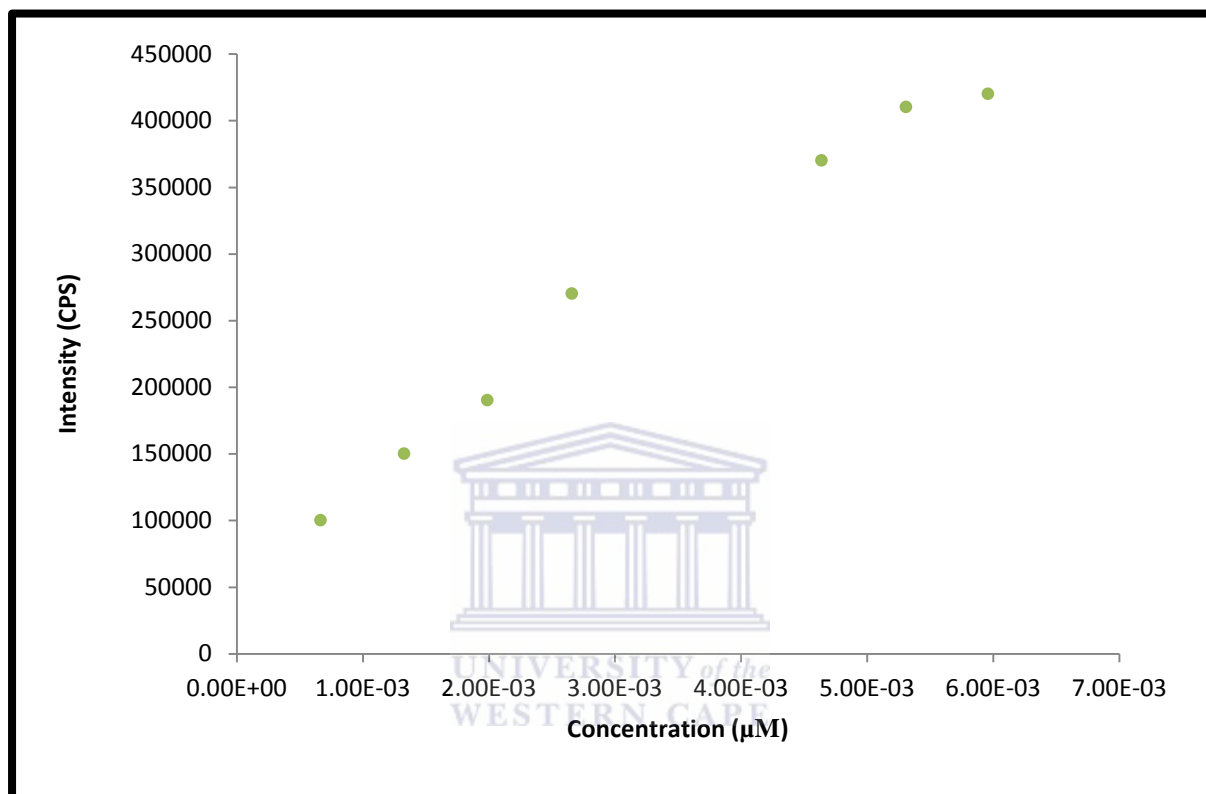


**Figure 51** Calibration curve of the Intensity vs. concentration of the enzyme; luciferase with increasing concentrations of naphthalene.

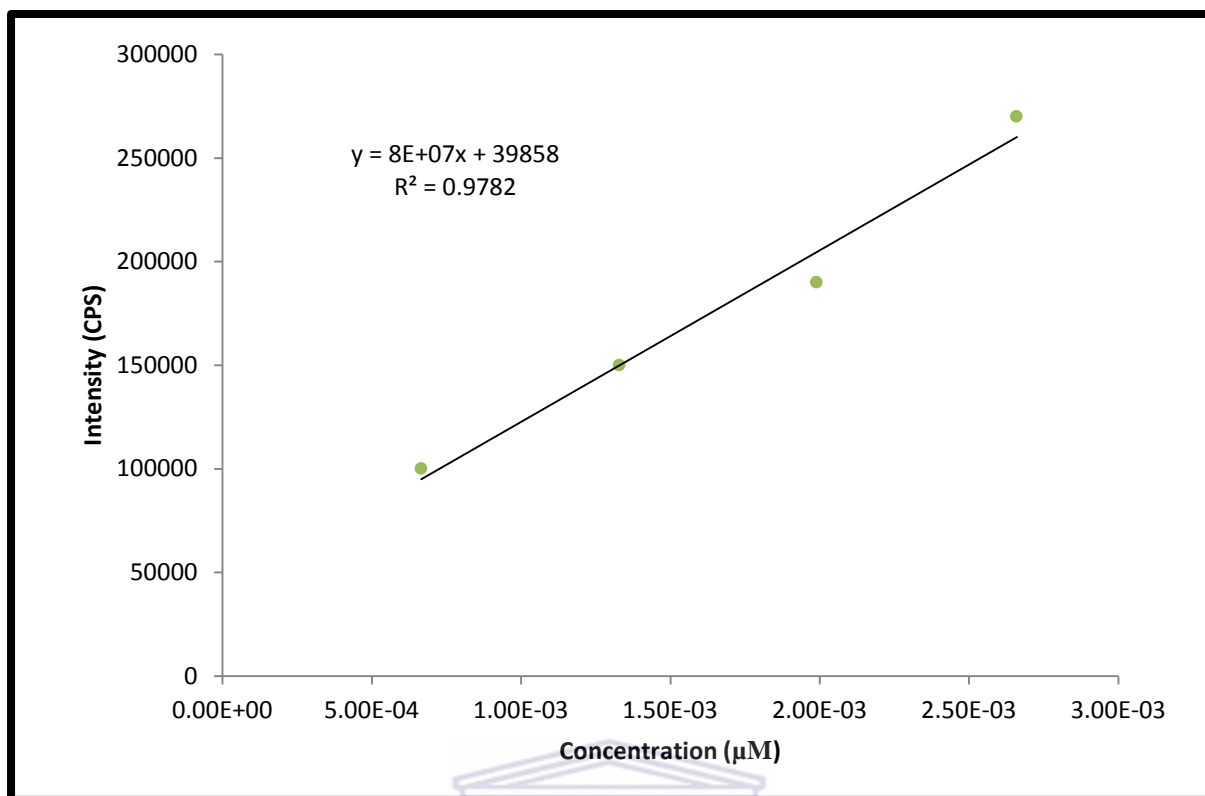
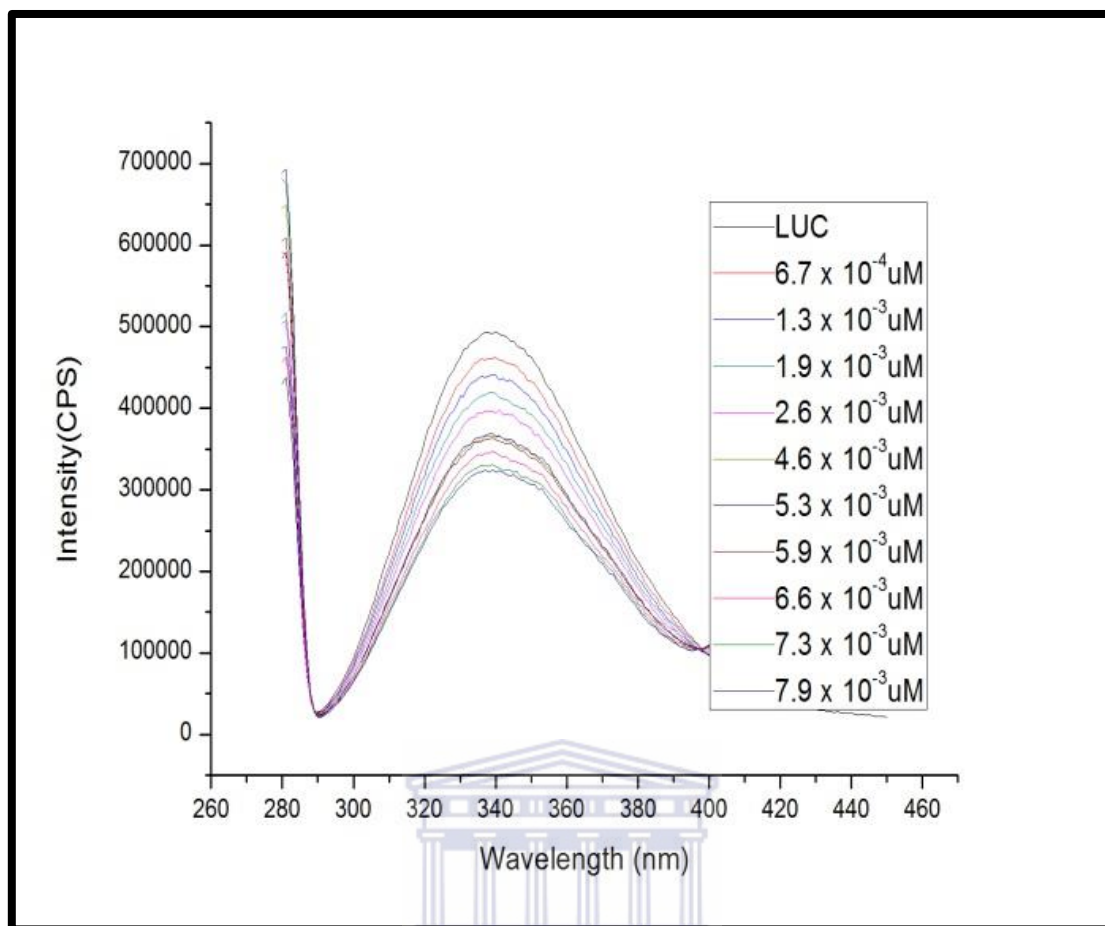


**Figure 52** The linear range of the Intensity vs. concentration calibration curve of the enzyme; luciferase with increasing concentrations of naphthalene.

### 5.2.3 Fluorescence spectroscopy of Luciferase with Fluoranthene

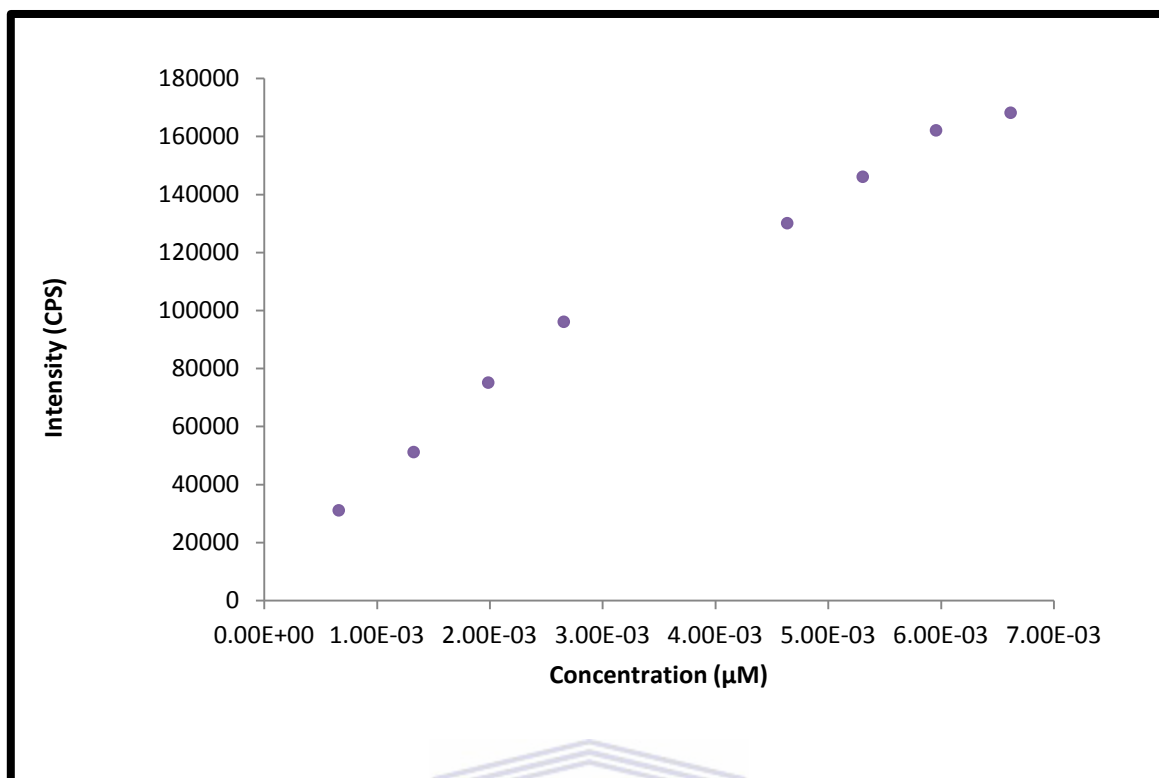
Aliquots of fluoranthene were added into the luciferase 0.2 M PBS (pH 7) solution system, and the corresponding change in the luciferase luminescence intensity was measured. As shown in Figure 53, the luminescence intensity gradually decreased with the addition of fluoranthene. The decrease in the luciferase luminescence intensity was caused by binding of fluoranthene with the luciferase.



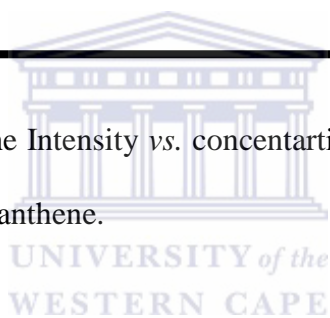


**Figure 53** Fluorescence spectra of the enzyme; luciferase with increasing concentrations of fluoranthene (decrease in bioluminescence).

Intensity vs. concentration profiles was drawn up for fluoranthene (Figure 54), and from the linear region of the calibration curve (Figure 55) a sensitivity of 30  $\mu\text{M}$  was observed, and a limit of detection (LOD) of  $2.67 \times 10^{-7} \mu\text{M}$  was calculated.



**Figure 54** Calibration curve of the Intensity vs. concentration of the enzyme; luciferase with increasing concentrations of fluoranthene.



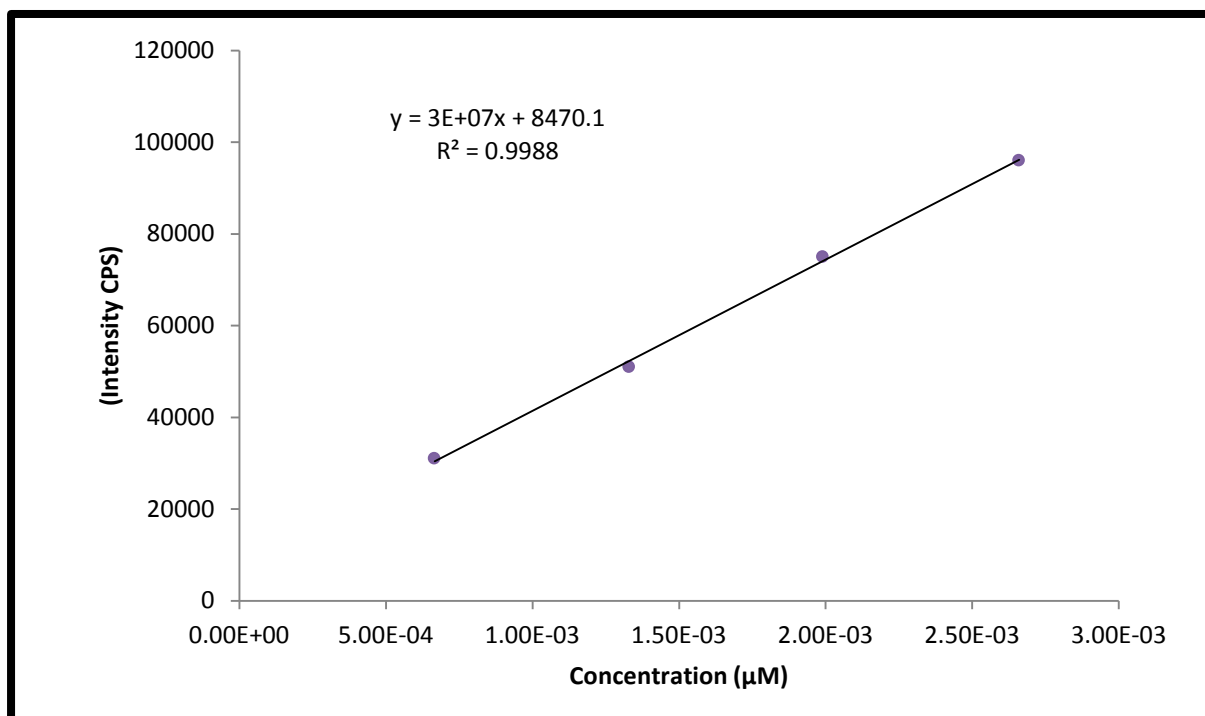
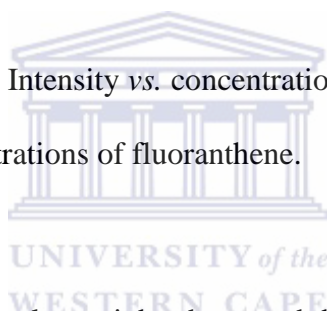


**Figure 55** The linear range of the Intensity vs. concentration calibration curve of the enzyme; luciferase with increasing concentrations of fluoranthene.



Fluoranthene has a higher molecular-weight than naphthalene therefore in solution with luciferase it would accumulate more to a certain level towards luciferase than naphthalene and exhibit more toxicity. Naphthalene has a lower partition coefficient than fluoranthene and its water solubility increases, thus hampering the intercalation of it to luciferase and subsequently reduces toxic effect of naphthalene.

---

## **5.3 Electrochemical evaluation of the Enzyme; Luciferase and Analytes i.e. Naphthalene and Fluoranthene**

### **5.3.1 Electrochemistry of GCE/Luciferase in 0.2 M PBS (pH 7)**

The bioluminescence reactions of various luciferase species have been widely used for a wide range of biochemical analyses because of their high sensitivity. Among the various types of luciferases, firefly luciferase has been most frequently used as a model system of biological reactions because of its high luminescence reaction efficiency. Firefly luciferase is unstable and rapidly loses its activity in aqueous solution. Bacterial luciferase has a higher solubility and stability in aqueous solution compared to firefly luciferase. Bacterial luciferase luminescence has been used to develop a model system to analyze the inhibition mechanisms of hydrophobic drugs on protein functions (Yoji K. et. al., 2012). A bare GCE in 0.2 M PBS (pH 7) was recorded (Figure 56) to ensure no peaks occurred in the areas of interest.

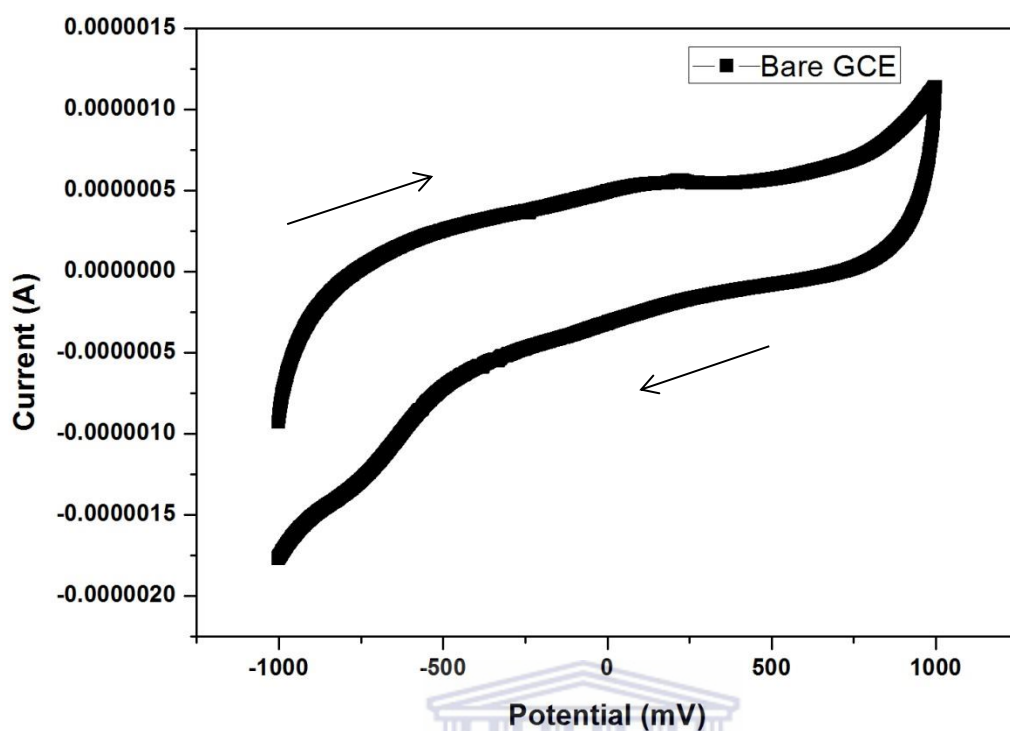
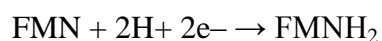


**Figure 56** Cyclic voltammogram of a bare GCE in 0.2 M PBS (pH 7) at a scan rate of 100 mV/s.

The enzyme, luciferase was electroactive in 0.2 M PBS (pH7), as two oxidation peaks ( $E_{pa1,2}$ ) and two reduction peaks ( $E_{pc1,2}$ ) was observed for the enzyme (Figure 57). The bare electrode (Figure 56) showed no peak as expected of the bare electrode in the buffer solution. The formal potentials ( $E^{0'}$ ) of these two redox couples was calculated from CV  $\{[E_{pa} + E_{pc}]/2\}$ ,  $E^{0'} = +110$  mV and  $E^{0'} = +730$  mV (as represented in table 7). From the  $I_{pc}$  vs  $\sqrt{v}$  calibration plot (Figure 58) the diffusion coefficient ( $D_e$ ) was calculated to be  $1.1 \times 10^{-12}$   $\text{cm}^2/\text{s}$  from Randle Sevcik equation. Using Brown-Anson equation the surface coverage was calculated to be  $1.50 \times 10^{-13}$  moles/ $\text{cm}^2$ , which is in the monolayer region. The  $k_s$  values were calculated using the following equation  $k_s(E_p) = 2.18 [D \alpha n F v / RT]^{1/2}$ , where  $k_s$  is the electron transfer rate constant, the sweep rate  $v$ ,  $D$  is the diffusion coefficient,  $F$  the Faraday's

---

constant,  $\alpha$  is the charge transfer coefficient,  $R$  is the gas constant ( $8.314 \text{ J K}^{-1} \text{ mol}^{-1}$ ) and  $T$  is the temperature and was calculated to be  $7.1 \times 10^{-5} \text{ cm/s}$  for CV. The  $D_e$  values was calculated from the  $E_{pc_2}$  (-730 mV) slope as the interaction between the analytes and enzymes occurs at this peak potential. The Flavin mononucleotide (FMN) maybe electrochemically reduced to  $\text{FMNH}_2$ , which is one of the substrates of the BL luminescence reaction. The peak observed at -730 mV was due to the reduced flavin mononucleotide,  $\text{FMNH}_2$  as reported by Yoji Kawanami et al., 2012. The  $\text{FMNH}_2$  was regenerated by the electrochemical reduction of FMN by using the following scheme:



**Equation 5.2**

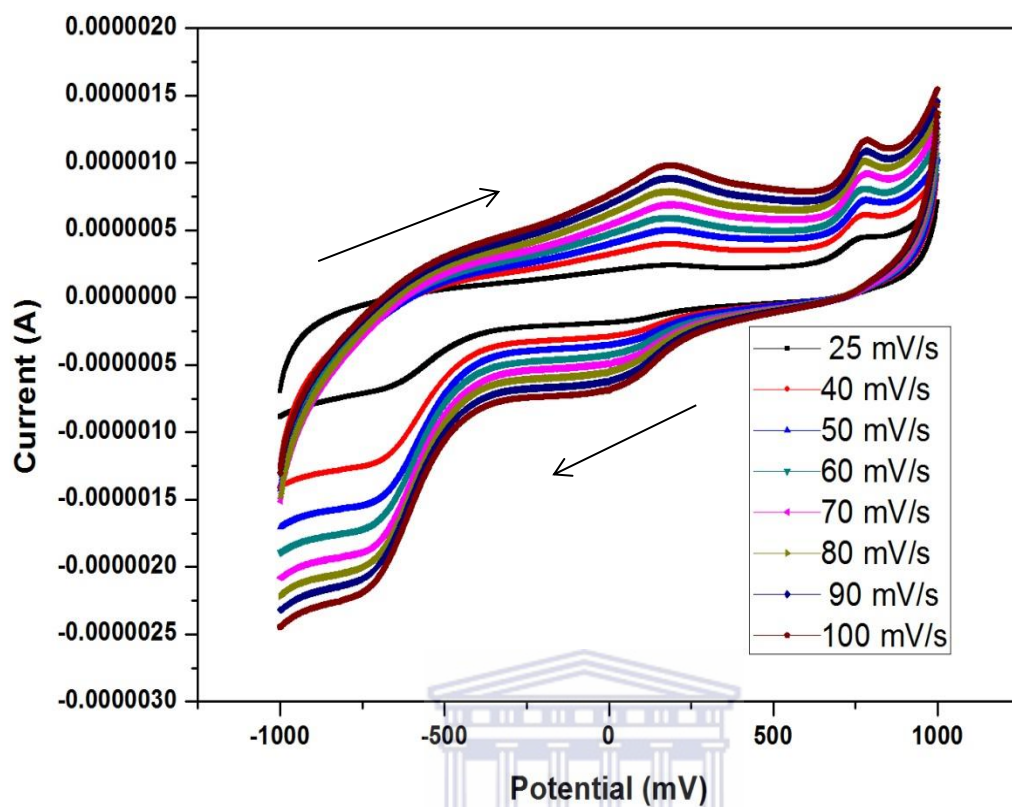


**Figure 57** Cyclic voltammogram of luciferase on a bare GCE in 0.2 M PBS (pH 7) at different scan rates; 25, 40, 50, 60, 70, 80, 90 and 100 mV/s.

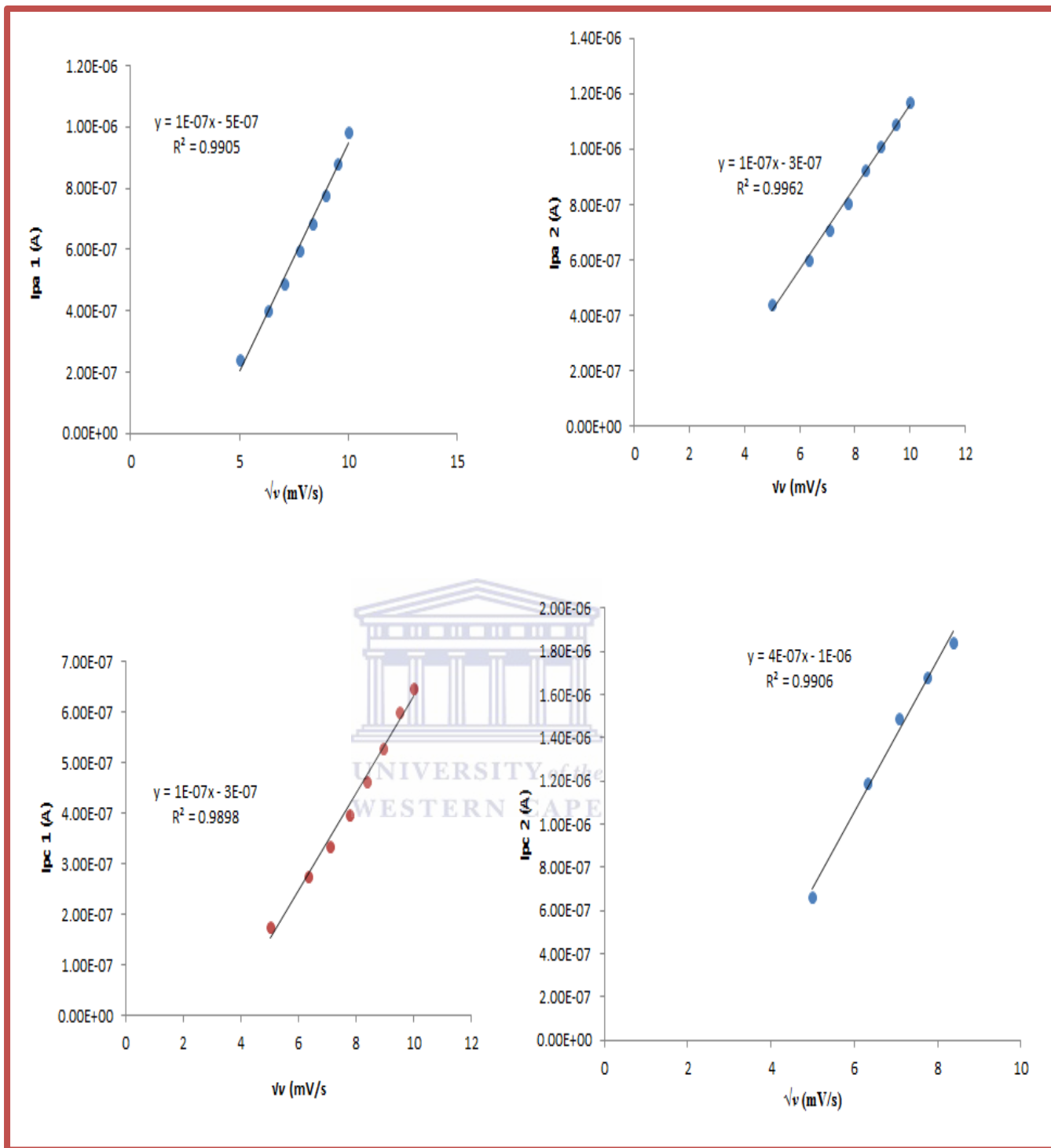


**Figure 58**  $I_p$  vs  $\sqrt{v}$  calibration curves of luciferase on GCE in 0.2 M PBS (pH 7).



---

### 5.3.2 Electrochemistry of Naphthalene (1 mM) on bare GCE in 0.2 M PBS (pH 7)

An experiment on the electrochemical behaviour of naphthalene was investigated using a bare GCE in 0.2 M PBS (pH 7) as the electrolyte. The following discussion is based on the cyclic voltammetric response to a stock solution of naphthalene which had a concentration of 1 mM, and was made up in a mixture of acetonitrile/water (85:15) solution. A cathodic peak ( $E_{pc}$ ) around -630 mV (*vs.* Ag/AgCl) was observed for naphthalene. The electrochemical process observed at the bare GCE was only for the reduction of naphthalene. This irreversible behaviour suggested that naphthalene was reduced.



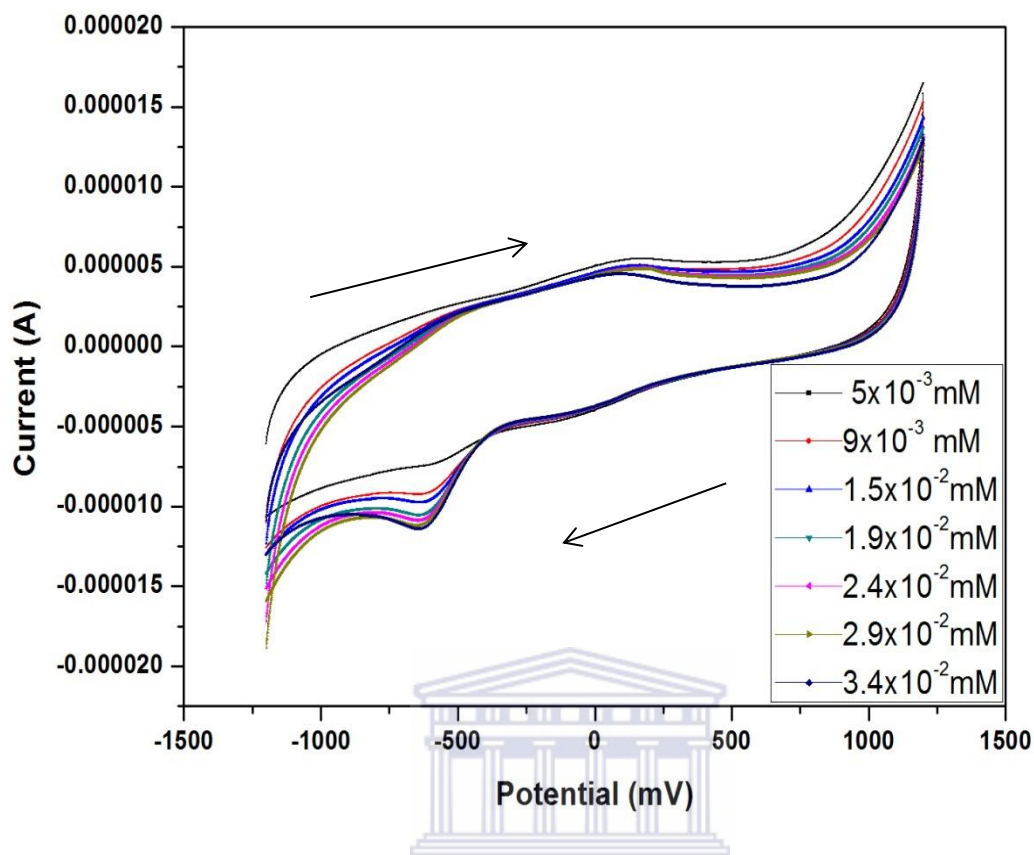


**Figure 59** Cyclic voltammogram of different concentrations ( $5 \times 10^{-3}$  to  $3.4 \times 10^{-2}$  mM) of naphthalene at a bare GCE electrode in 0.2 M PBS (pH 7).

From the calibration curve of  $I_p$  vs concentration (Figure 60) the bare GCE had a sensitivity of  $1 \times 10^{-4}$  mM towards the detection of naphthalene.

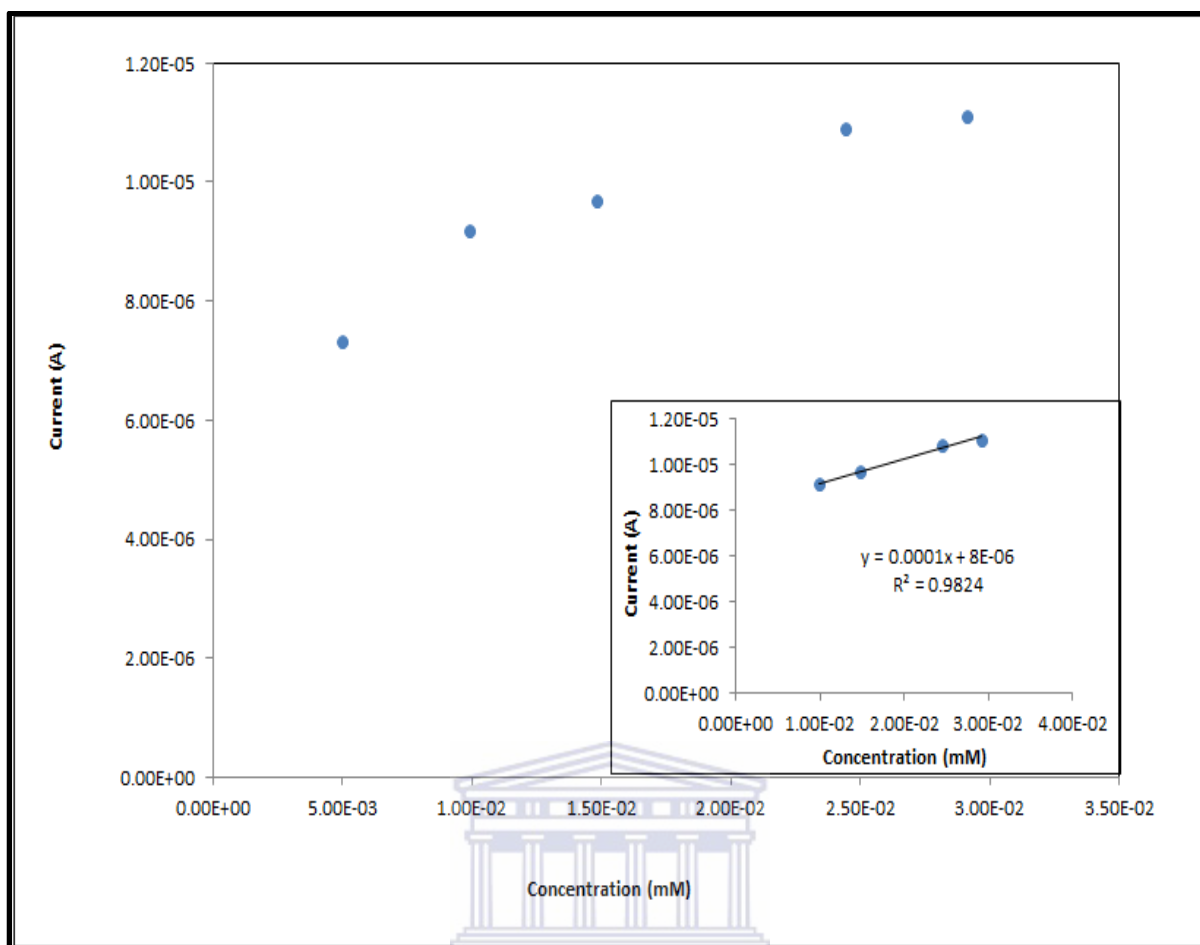


**Figure 60** Calibration curve of  $I_p$  vs concentration of naphthalene at a bare GCE electrode in 0.2 M PBS (pH 7).

### 5.3.3 Electrochemistry of GCE/Luciferase and Naphthalene (1 $\mu$ M) in 0.2 M PBS (pH 7)

The detection of naphthalene was investigated using the cathodic peak of luciferase at -730 mV (vs. Ag/AgCl) and all analysis was based on this potential. The biosensor system became less conductive, as the cathodic peak decreased with an increase of naphthalene concentration

---

(Figure 61). The decrease in peak current was due to competitive binding of naphthalene with the substrate.

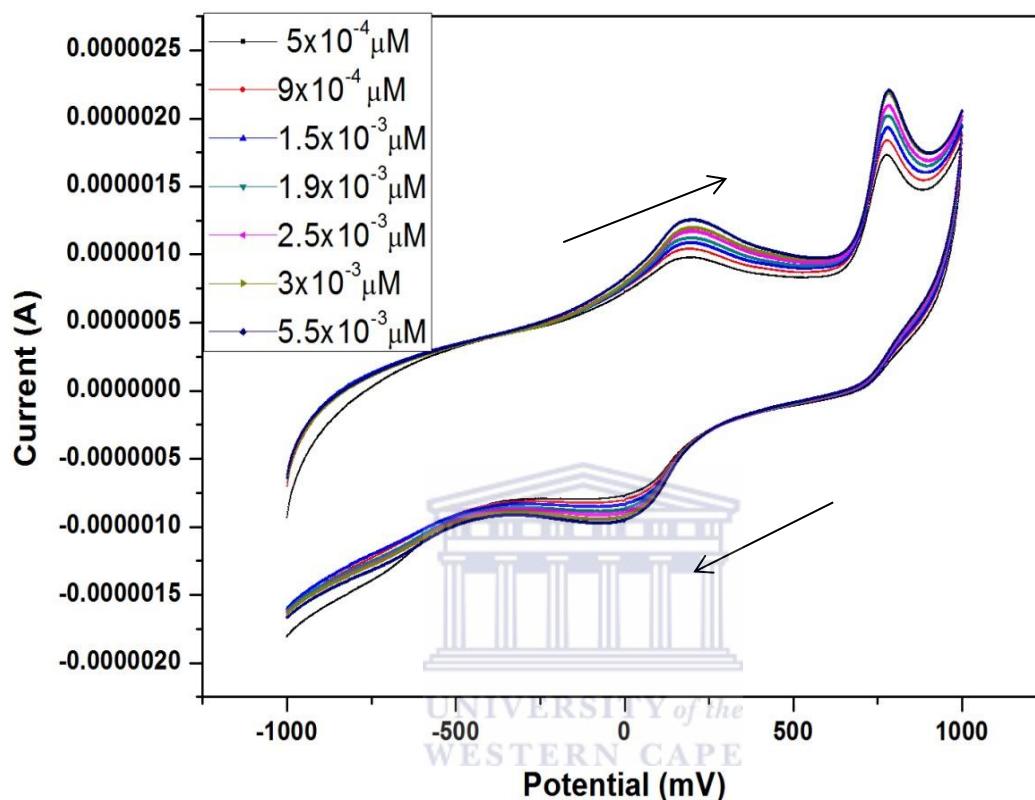


**Figure 61** Cyclic voltammogram of GCE/luciferase with different concentrations of naphthalene in 0.2 M PBS (pH7).

Square wave voltammetry was done to show that when naphthalene was added, the peak around -730 mV (vs. Ag/AgCl) decreased almost completely (Figure 62). Figure 63 shows the calibration curve of  $I_p$  vs concentration of GCE/LUC with increasing concentration of naphthalene. From the linear region of the calibration curve (Figure 64), the sensitivity of enzyme (luciferase) towards naphthalene was  $4 \times 10^{-5}$  M. The limit of detection was

---

calculated to be 0.022  $\mu\text{M}$ . Compared to the bare GCE for the detection of naphthalene; the luciferase biosensor was more sensitive

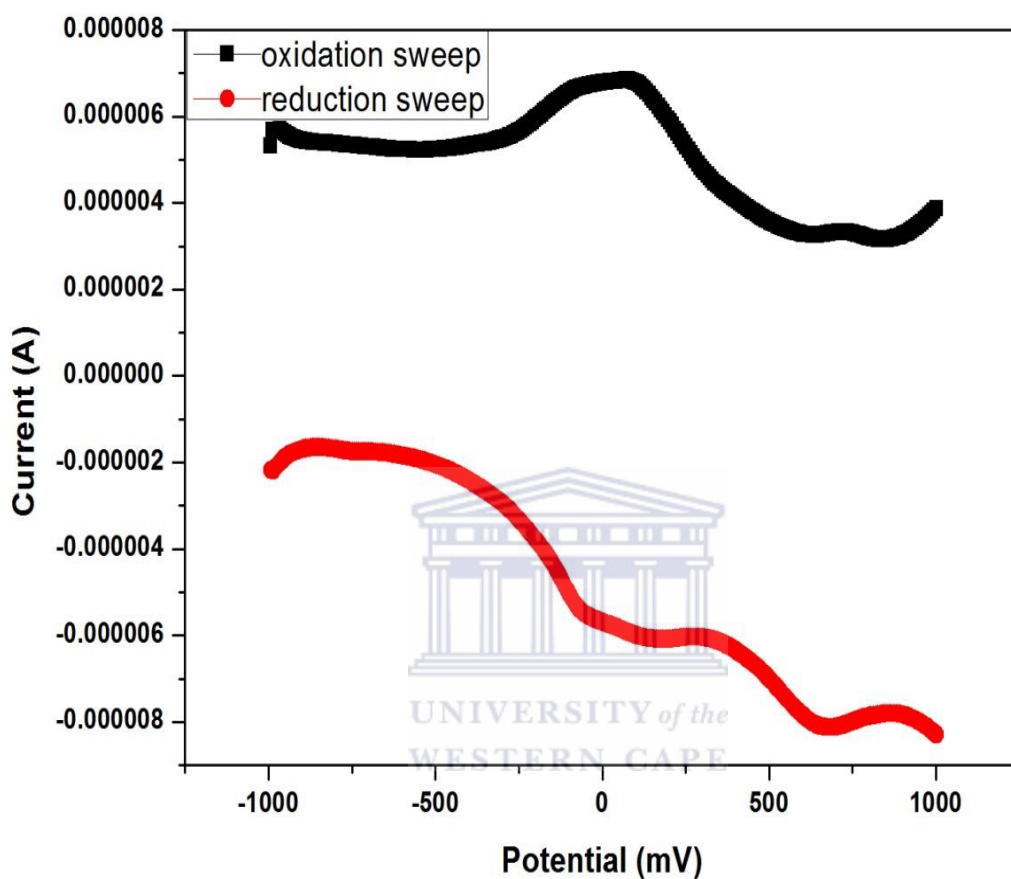


**Figure 62** Square wave voltammogram of GCE/luciferase with  $5.5 \times 10^{-3} \mu\text{M}$  naphthalene in 0.2 M PBS (pH 7), showing the cathodic peak at -730 mV decreased.

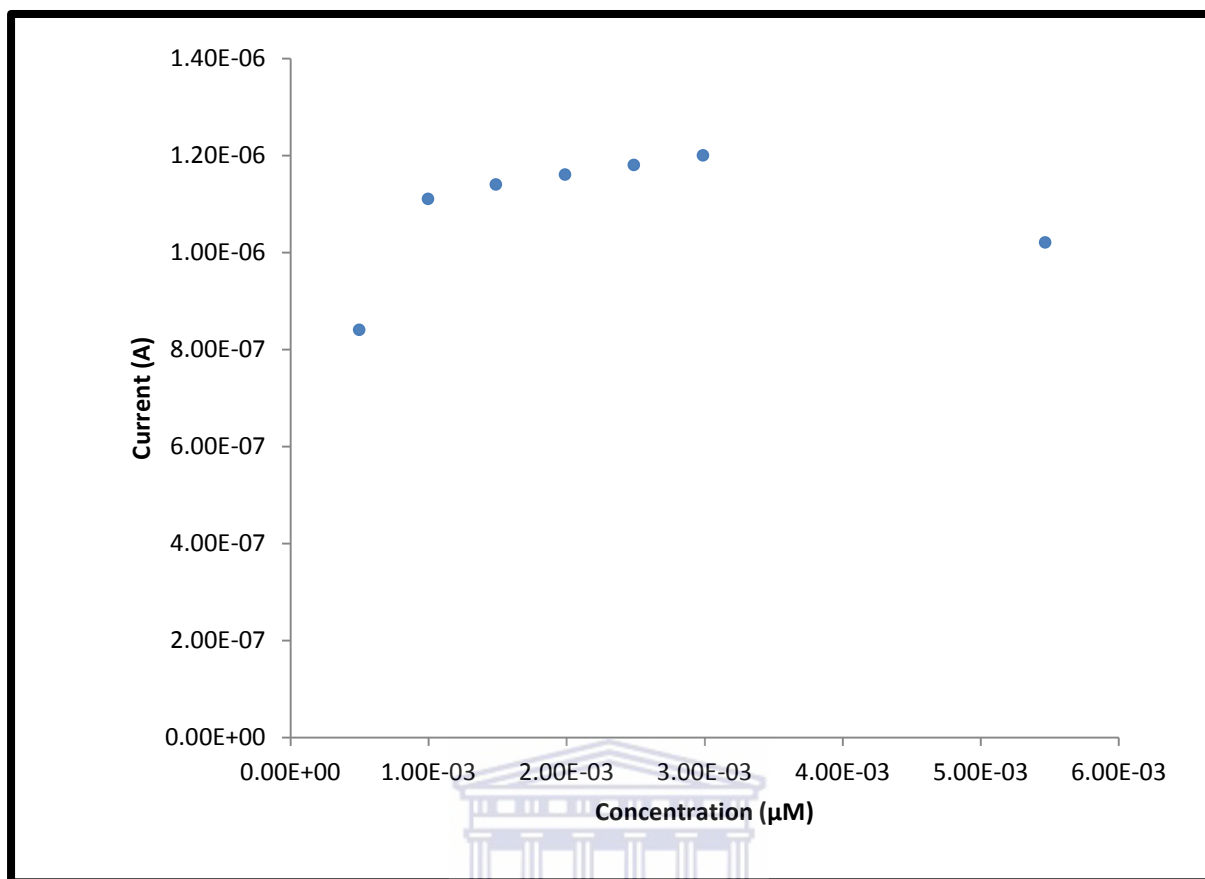


**Figure 63**  $I_p$  vs concentration calibration curve of GCE/luciferase with increasing concentrations of naphthalene in 0.2 M PBS (pH 7).

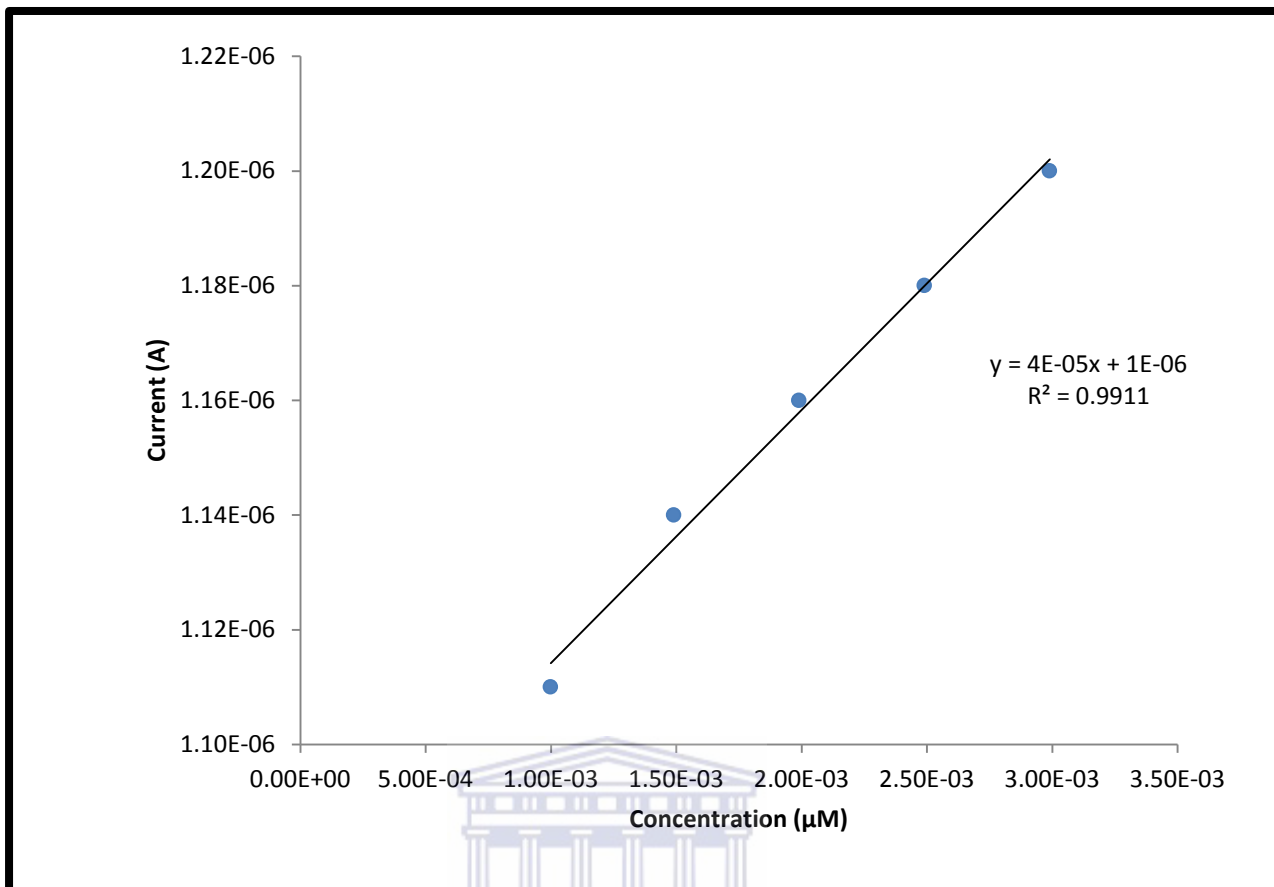


**Figure 64** The linear range of the  $I_p$  vs concentration calibration curve of the GCE/luciferase with increasing concentration of naphthalene in 0.2 M PBS (pH 7).

---

### 5.3.4 Electrochemistry of Fluoranthene on a bare GCE in 0.2 M PBS (pH 7)

An experiment on the electrochemical behaviour of fluoranthene was investigated using a bare GCE in 0.2 M PBS (pH 7) as the electrolyte. The electrochemical process observed at the bare GCE was only for the reduction of fluoranthene. The following discussion is based on the cyclic voltammetric response to fluoranthene (1 mM) dissolved in acetonitrile/water solution. A cathodic peak ( $E_{pc}$ ) around -750 mV (*vs.* Ag/AgCl) was observed for fluoranthene. This irreversible behaviour suggested that fluoranthene was reduced. The bare GCE had a sensitivity of  $2 \times 10^{-4}$   $\mu\text{M}$  towards the detection of fluoranthene.





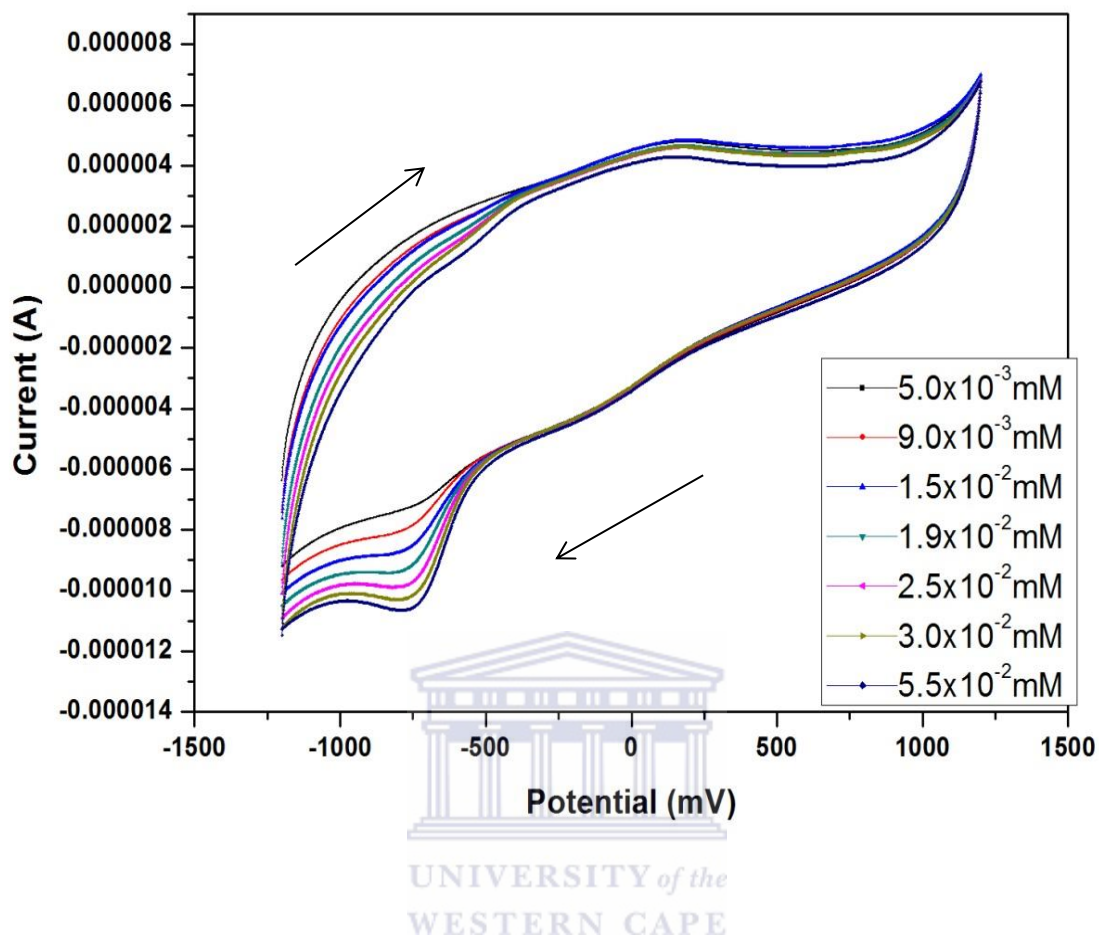


**Figure 65** Cyclic voltammogram of different concentrations ( $5 \times 10^{-3}$  to  $5.5 \times 10^{-3}$  mM) fluoranthene in 0.2 M PBS (pH 7).

From the calibration curve of  $I_p$  vs concentration (Figure 66) the bare GCE had a sensitivity of  $1 \times 10^{-4}$  mM towards the detection of fluoranthene.

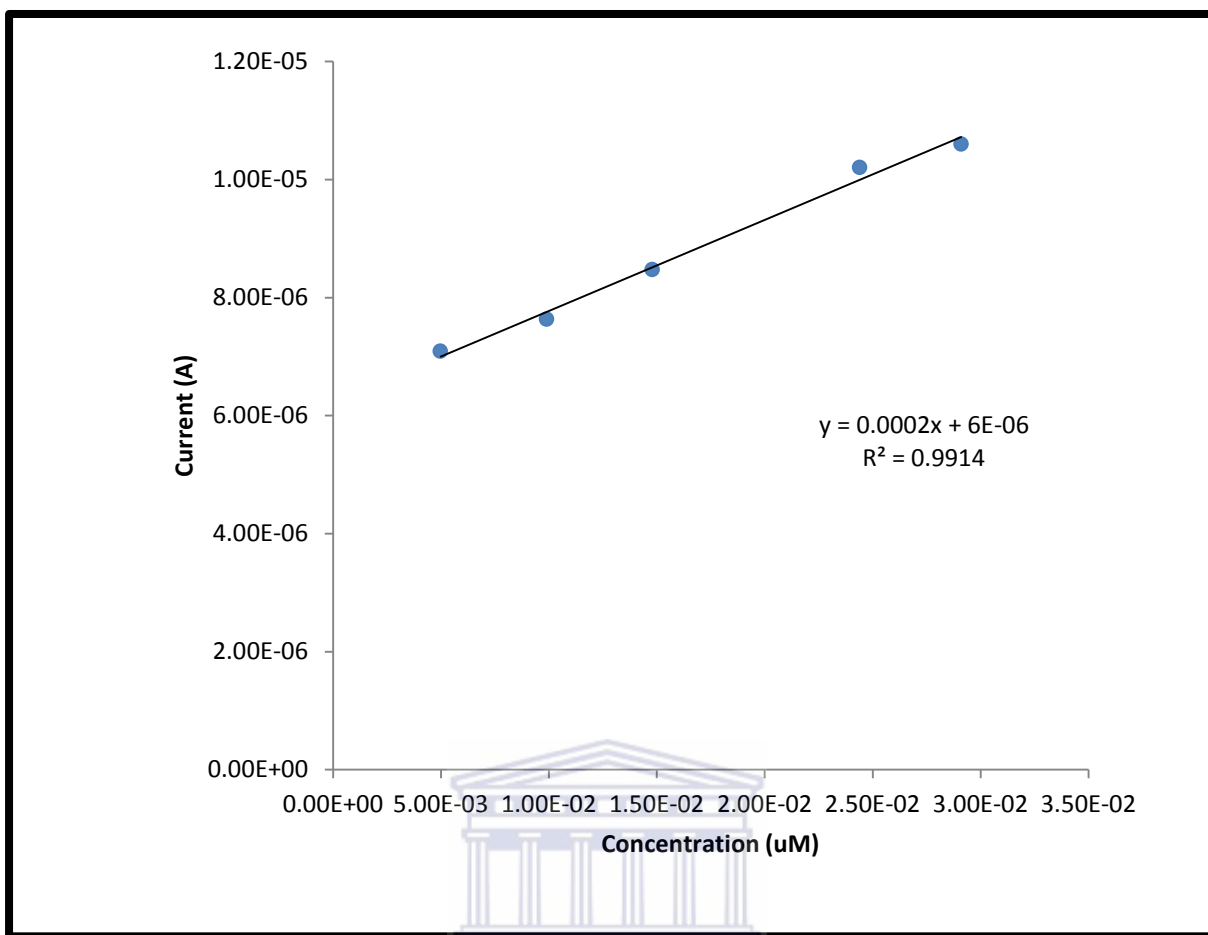


**Figure 66** Calibration curve of different concentrations of fluoranthene at a bare GCE in 0.2 M PBS (pH 7).

---

### 5.3.5 Electrochemistry of GCE/Luciferase with fluoranthene in 0.2 M PBS (pH 7)

The detection of fluoranthene was investigated using the cathodic peak of the enzyme, luciferase at -730 mV (*vs.* Ag/AgCl). As the concentration of fluoranthene increased the cathodic peak of the luciferase decreased. The biosensor system also became less conductive, as the cathodic peak decreased with an increase in fluoranthene concentration (Figure 67). The decrease in peak current was due to competitive binding of fluoranthene with the substrate. Figure 68 shows the SWV of GCE/Luciferase with fluoranthene, and that the peak at -730 mV (*vs.* Ag/AgCl) decreased as a result of adding fluoranthene.



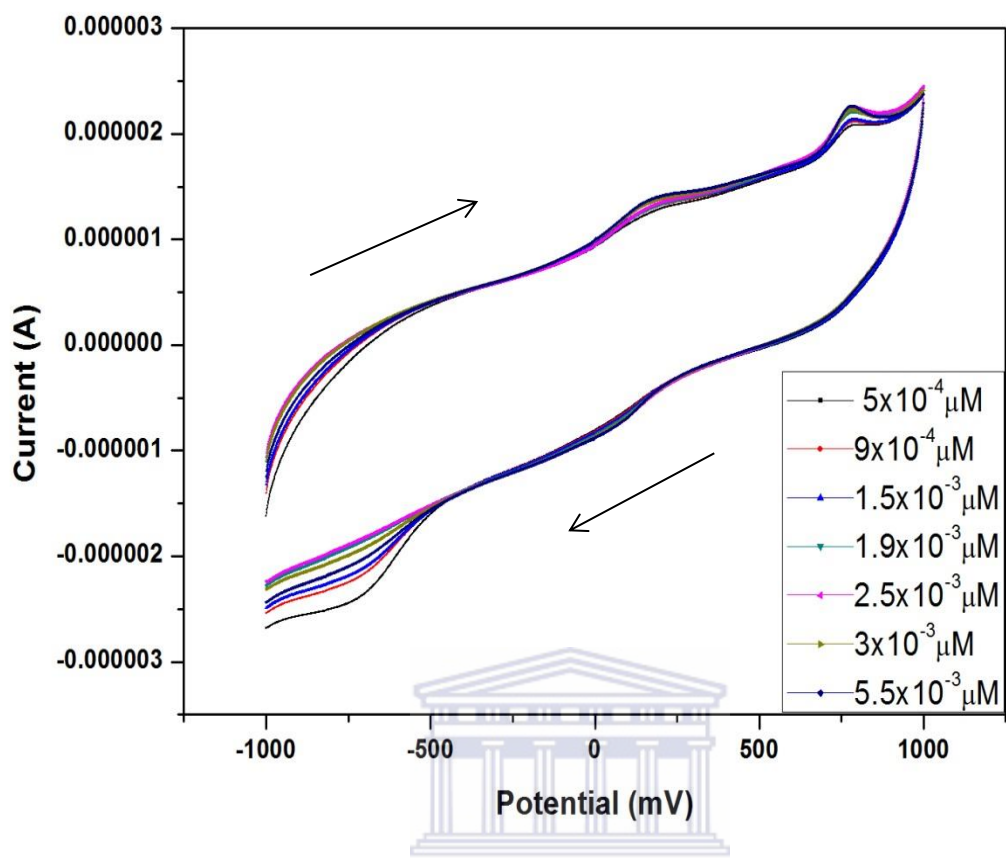


**Figure 67** Cyclic Voltammetry of GCE/luciferase with different concentrations of fluoranthene from  $5 \times 10^{-4}$  to  $5.5 \times 10^{-3}$  in 0.2 M PBS (pH 7).

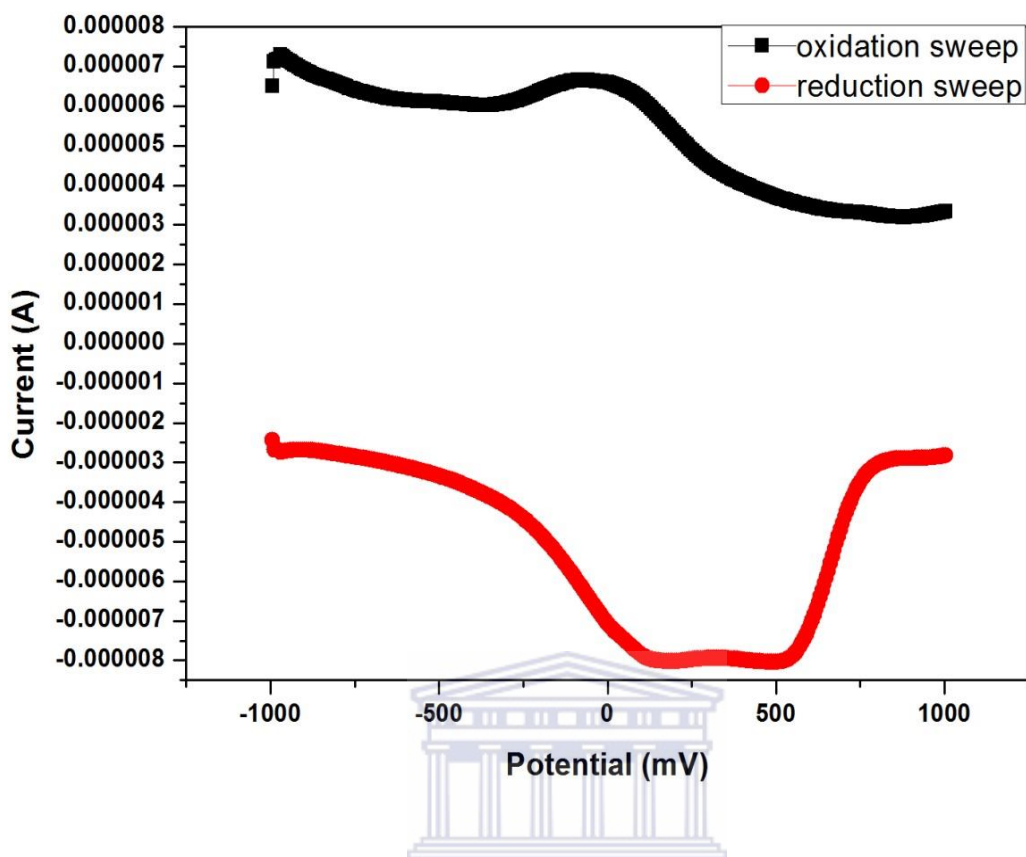


**Figure 68** Square wave voltammetry of GCE/luciferase with fluoranthene in 0.2 M PBS (pH 7).

An  $I_p$  vs concentration profile calibration plot was drawn to show how the  $I_p$  changes with concentration (Figure 69). The GCE/luciferase biosensor had sensitivity (Figure 70) towards fluoranthene of  $2 \times 10^{-4} \mu\text{M}$  and a limit of detection (LOD) of  $4.4 \times 10^{-3}$ . When comparing the luciferase biosensor for the detection of naphthalene and fluoranthene, it was more sensitive for fluoranthene.

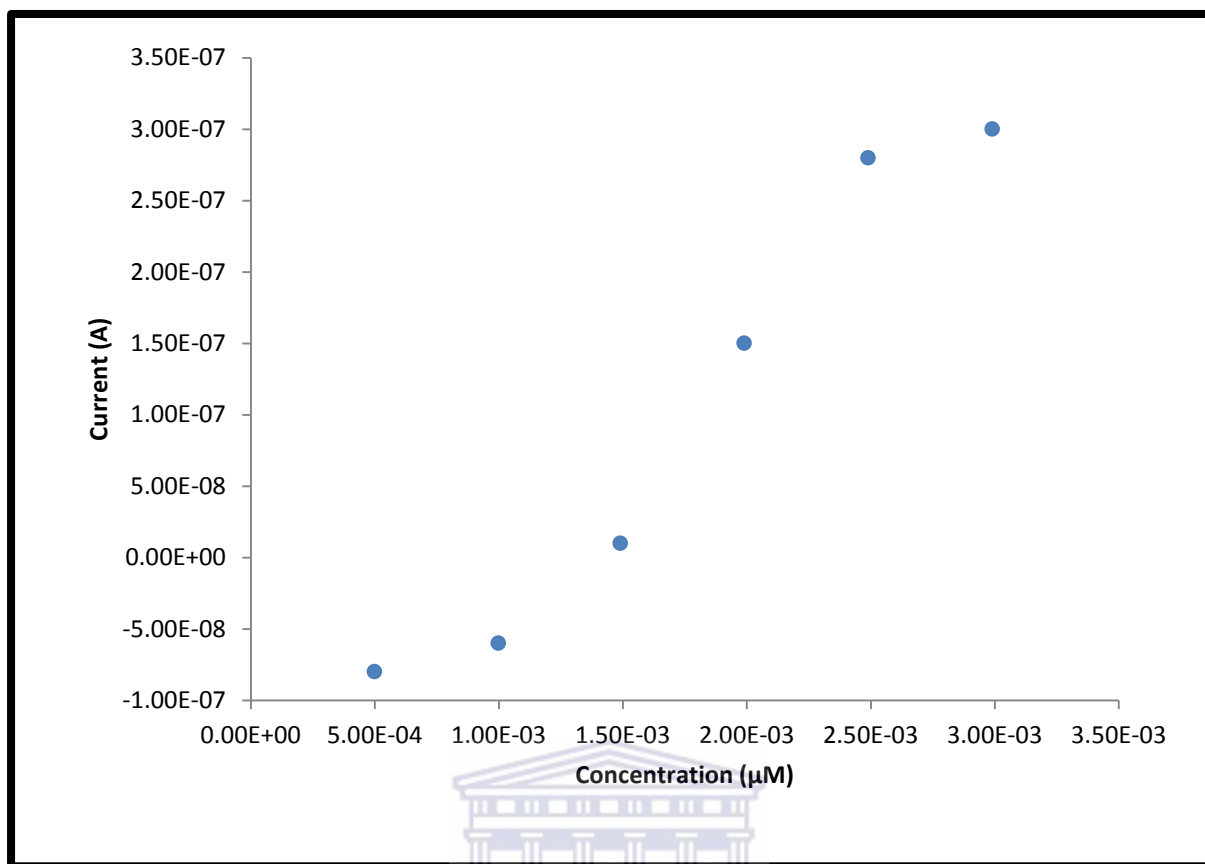


**Figure 69** Calibration curve of GCE/Luciferase with different concentrations of fluoranthene in 0.2 M PBS (pH 7).

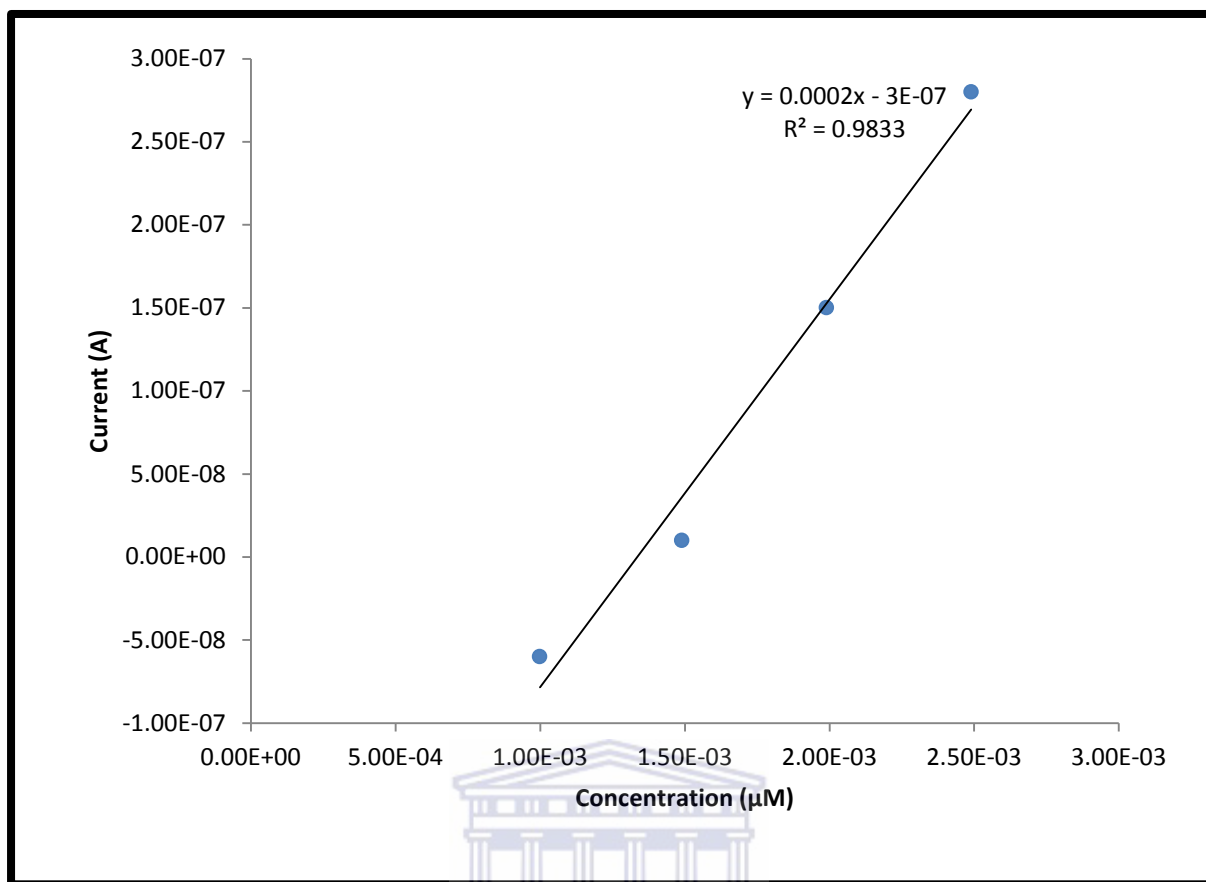


**Figure 70** Linear range of the calibration curve of GCE/Luciferase with different concentrations of fluoranthene in 0.2 M PBS (pH 7).

**Table 7** The analytical response of the biosensor to analytes.

Material	Epa <sub>1</sub> (mV)	Epa <sub>2</sub> (mV)	Epc <sub>1</sub> (mV)	Epc <sub>2</sub> (mV)	E <sup>0'</sup> (mV)	Sensitivity	LOD
GCE/Naphthalene	-	-	-630	-	-630	1 × 10 <sup>-4</sup> A/mM	0.08 mM
GCE/LUC + Naphthalene	175	783	35	-680	-	4 × 10 <sup>-5</sup> A/μM	0.02 μM
GCE/Fluoranthene	-	-	-750	-	-750	2 × 10 <sup>-4</sup> A/mM	0.02 mM
GCE/LUC + Fluoranthene	180	790	55	-705	-	2 × 10 <sup>-4</sup> A/μM	4.4 × 10 <sup>-3</sup> μM

Table 7 shows the anodic peak potentials (Epa<sub>1,2</sub>), cathodic peak potentials (Epc<sub>1,2</sub>), formal potential (E<sup>0'</sup>), sensitivities and the limit of detection (LOD). From the table the biosensor GCE/LUC was most sensitive to fluoranthene with a sensitivity of 2 × 10<sup>-4</sup> A/μM and a LOD of 4.4 × 10<sup>-3</sup> μM. The biosensor GCE/LUC was slightly less sensitive to naphthalene with a sensitivity of 4 × 10<sup>-5</sup> A/μM and a LOD of 0.02 μM. The electrochemistry corroborates what was evaluated in fluorescence spectroscopy, where the solution phase enzyme, luciferase was also most sensitive to fluoranthene then naphthalene.



---

## 5.4 Electrochemical Quartz Microbalance (EQCM) of Luciferase and analytes in 0.2 M PBS (pH 7)

### 5.4.1 EQCM of Luciferase and Naphthalene

Using the EQCM, one determines the ratio of mass deposited at the electrode surface during an electrochemical reaction to the total charge passed through the electrode. The EQCM module is fitted with a 6 MHz crystal oscillator and it can be used to monitor changes in frequency, with a dynamic range of 80 000 Hz. The module is also fitted with a temperature probe, which can be connected to the temperature sensor embedded in the standard electrochemical cell provided with the module. Gold-coated quartz crystal as working electrode was used; a Pt wire as auxiliary electrode and Ag/AgCl as reference electrode was connected for EQCM measurements. The Au-coated quartz crystals (ATcut, 6 MHz) of 0.2 cm<sup>2</sup> geometric area per face were obtained from AutoLab.

The biosensor was prepared by drop coating 50 µL of the stock luciferase solution onto the one side of the Au-coated quartz crystals and leaving it in the fridge for 4 to 5 hours. The effect of luciferase immobilization over the surface of Au-coated quartz crystal microbalance was investigated and how it responded to the addition of PAHs was compared, resulting in a better sensitivity and binding efficiency in the former method. When an inhibition study with the developed sensor was undertaken at the optimized luciferase immobilization with varying concentrations of PAHs (naphthalene and fluoranthene), a sensitive detection for them was possible with the limit of detection (LOD) corresponding to 9.43 µM and 30.6 µM, respectively.

---

Previously studies on the electrochemistry of luciferase onto GCE surface using cyclic voltammetry was investigated and GCE/LUC interactions with PAHs. The study showed that the peak potential at -730 mV gradually decreased to a point where it diminished completely for both analytes; naphthalene and fluoranthene. This was the cause of by the changes in structure of the interface associated with the introduction of PAHs.

Using EQCM, the present studies attempt to shed some light into the mechanism of signal generation involving the luciferase immobilized on the Au-coated quartz microbalance. The mass-potential profiles for PAHs interaction with enzyme were investigated. A change in mass of the quartz crystal following the oxidation/reduction of the attached enzyme can be calculated using Sauerbrey equation (5.3), which relates changes in the resonant frequency of the quartz crystal to the changes in mass of the enzyme:

$$\Delta f = -\frac{2f_0^2}{A\sqrt{\rho_q\mu_q}} \cdot \Delta m$$

**Equation: 5.3**

Where  $\Delta f$  is the change in frequency, in Hz,  $f_0$  is the nominal resonant frequency of the crystal (6 MHz),  $\Delta m$  is the change in mass, in  $\text{g/cm}^2$ ,  $A$  is the area of the crystal in  $\text{cm}^2$ ,  $\rho_q$  is the density of quartz, in  $\text{g/cm}^3$  and  $\mu_q$  is the shear modulus of quartz, in  $\text{g/cm}\cdot\text{s}^2$ . For a 6 MHz crystal, the same equation can be reduced to:

$$-\Delta f = \Delta m \cdot C_f$$

**Equation: 5.4**

Where  $C_f$  is  $0.0815 \text{ Hz/ng/cm}^2$

---

In the liquid phase, QCM data should account for the effect of the piezoelectric movement of the quartz. When a metal part is in contact with solution, the piezoelectric movement is usually hindered, thus resulting in a decrease in frequency (Bruckenstein S., et al., 1985; Monura T., et al., 1982). Such a frequency change may be ignored if the initial and final states are under the same environmental conditions with respect to density, temperature and viscosity of the solution phase. Previous studies on acetylcholinesterase showed inhibition by measuring the precipitation degree of an enzymatic reaction product, 4,4'-diimino-3,3'-diaminobiphenyl which is derived from 3,3'-diaminobenzidine substrate, over the QCM electrode (Kim, N., et al., 2007). This justifies that the validity of the Sauerbrey equation when the crystal electrode is modified. Other several examples have been shown in which Sauerbrey equation is obeyed in the solution phase and when modified (Son, D.; et al., 1994; Ebara, Y. et al., 1993).

The operating principle of the EQCM sensor of this study is based on the measurement of the enzymatic activity of luciferase, immobilized on one side of the QCM and simultaneously exposed to the substrate solution. As the enzymatic reaction product is precipitated over the QCM surface after dimerization (Abad et al., 1998), the degree of sensor response can be traced, in real-time scale, by determining the frequency decrease caused by mass deposit over the QCM surface. After the immobilization of luciferase on Au-coated quartz crystal (Au/LUC), the electrode was rinsed with 0.2 M PBS (pH7) to remove excess luciferase. The  $\Delta m$  vs. potential of Au/LUC is shown in figure 30. The potential was scanned from 1000 mV to -1000 mV, the mass increase until about 0 V and then from  $\sim -0.5$  V it started to decrease towards more negative potentials and then increased on the reversed scan as it went to more positive values. The increase in mass during EQCM experiments correspond to the insertion of ions into the LUC film.

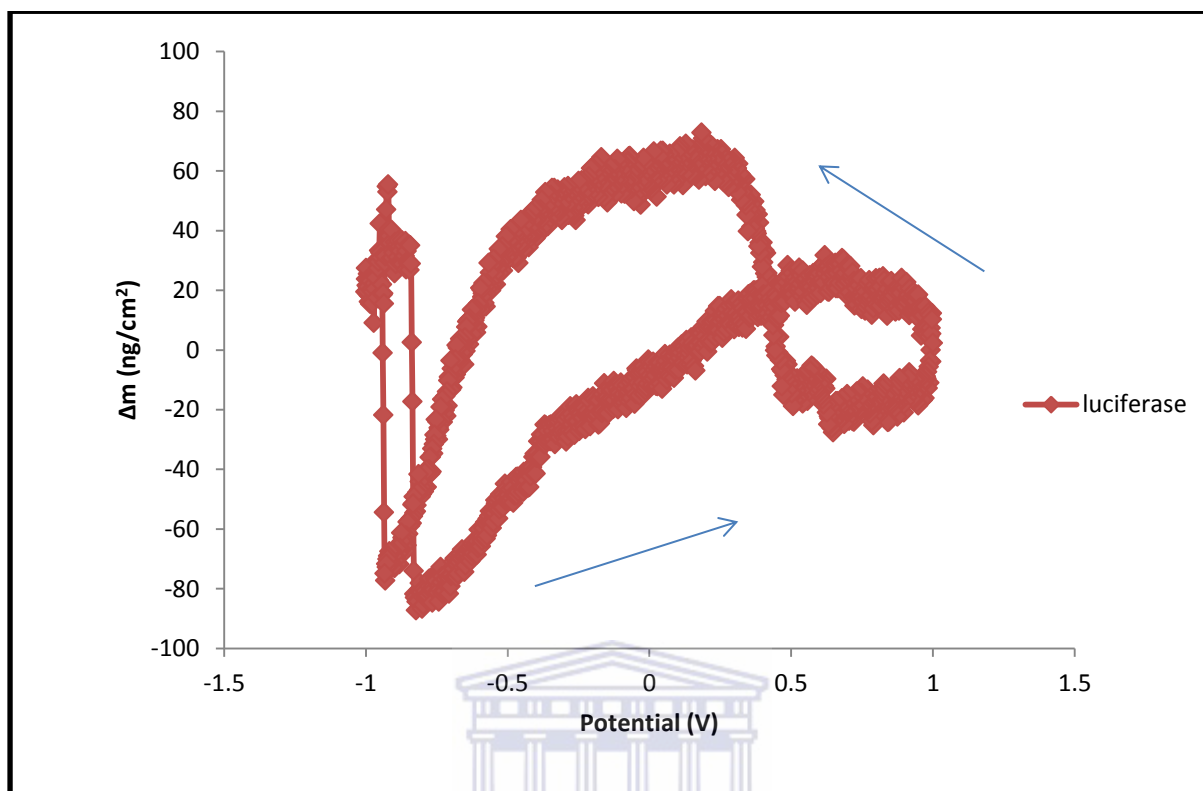


**Figure 71**  $\Delta m$  vs potential profile obtained at Au/LUC coated quartz crystal in 0.2 M PBS (pH 7) at a scan rate of 100 mV.

To the EQCM cell filled with 2 mL 0.2 M PBS (pH 7.0), where the Au/LUC electrode was already inserted, followed by the measurement of resonant frequency of the sensor until a steady-state baseline was obtained. The change in frequency was converted into  $\Delta m$  and  $\Delta m$  was plotted against potential (Figure 71). Then, aliquots of the substrates were injected into the cell, with a simultaneous stirring for 3 min, to induce complete substrate dissolution in the aqueous buffer. The steady-state resonant frequency ( $F_2$ ) was read again to calculate the  $\Delta m$ . An inhibition study on the Au/LUC in the presence of individual model PAHs was conducted. At the potential of - 0.79 V the mass change ( $\Delta m$ ) of luciferase was observed to

---

be  $81.71 \text{ ng/cm}^2$  (Figure 71). The peak at the potential of  $-0.79 \text{ V}$  was used to observe the change in mass as the concentration of naphthalene was increased. The  $\Delta m$  of luciferase was  $81.71 \text{ ng/cm}^2$  and the mass increased to a  $\Delta \text{mass}$  of  $273 \text{ ng/cm}^2$  when naphthalene was added (Figure 72). From the  $\Delta m$  vs concentration calibrations plot a linear regression ( $R^2$ ) of 0.96 and sensitivity of  $2 \times 10^{11} \mu\text{M}$  was observed.



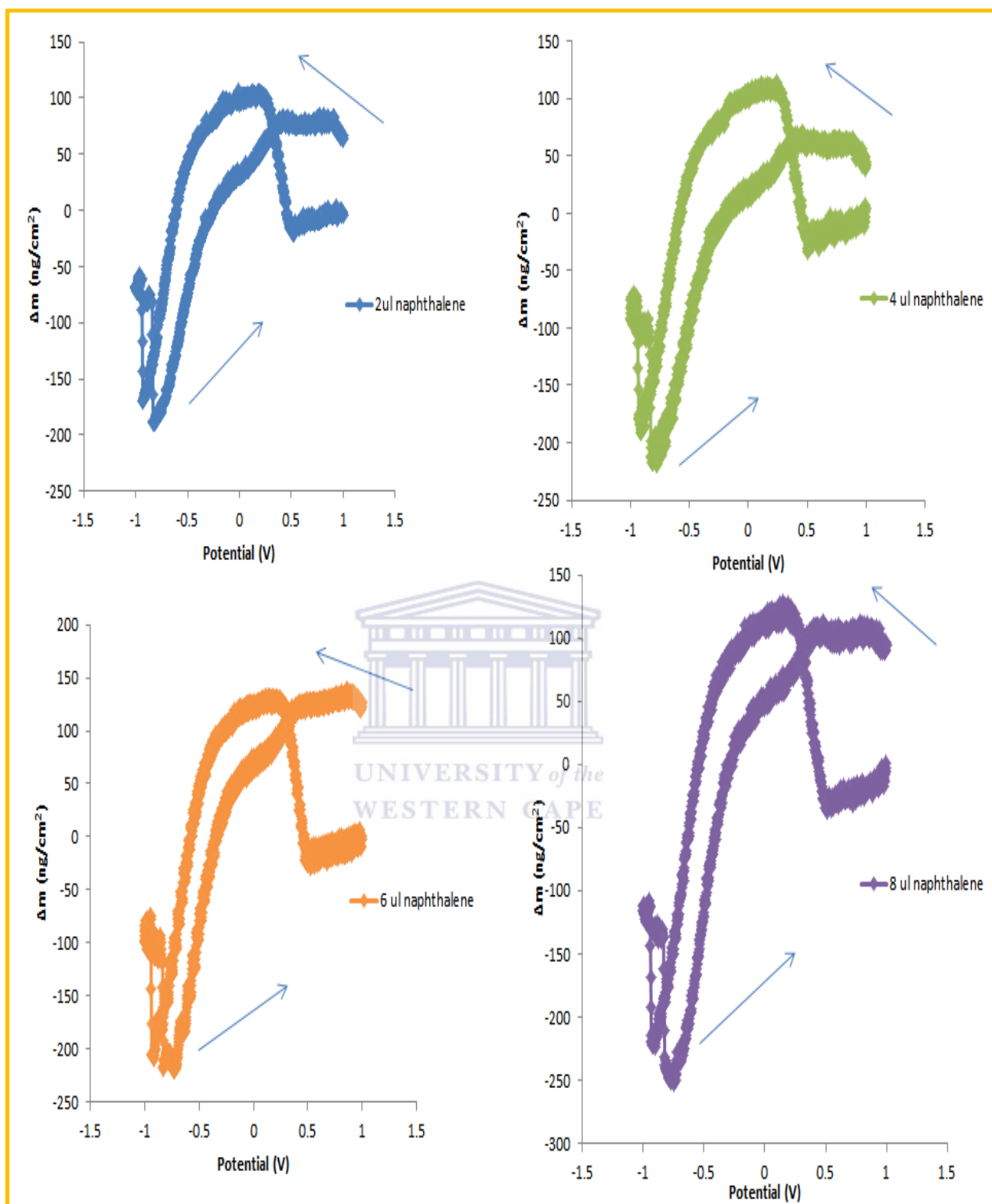


**Figure 72**  $\Delta$ mass vs. potential profiles obtained at an Au/LUC coated quartz microbalance using concentrations of  $9.99 \times 10^{-11}$  M to  $9.99 \times 10^{-10}$   $\mu\text{M}$  of naphthalene in 0.2 M PBS (pH 7) (the concentration profiles up to  $6.99 \times 10^{-10}$   $\mu\text{M}$  were not included in figure).

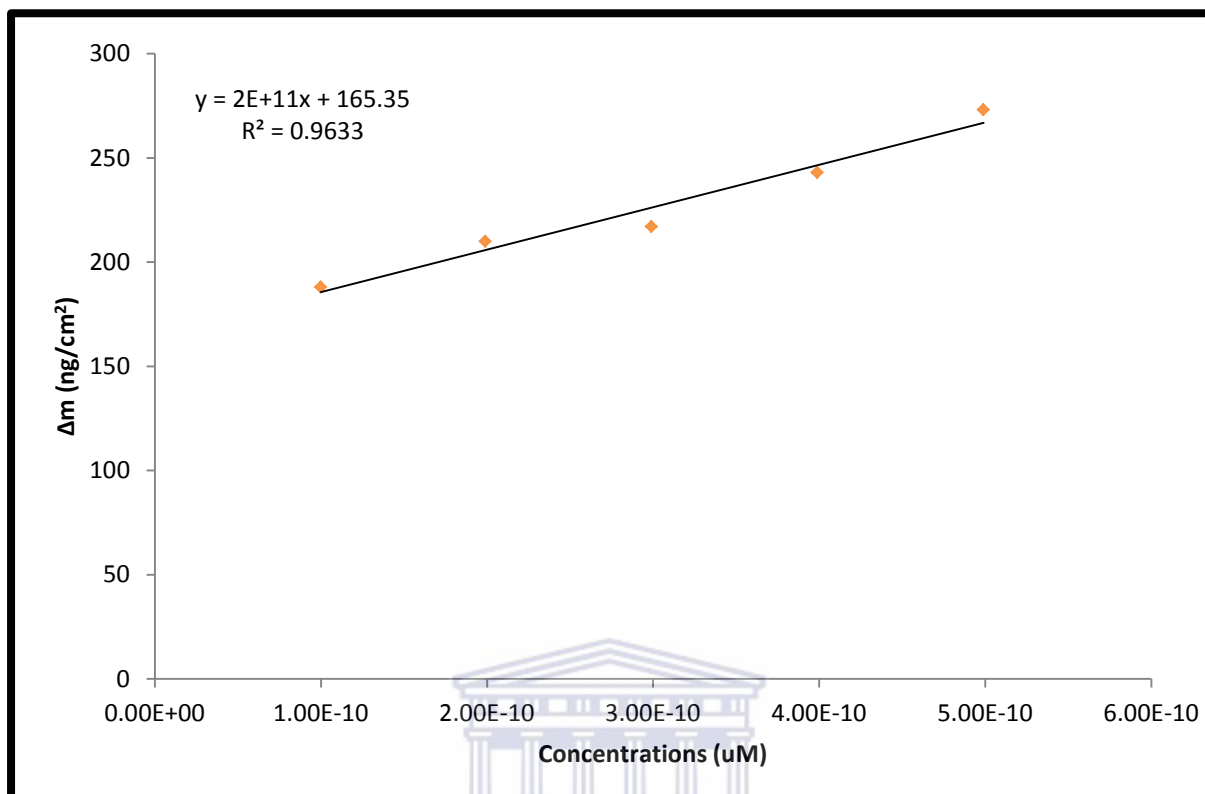


**Figure 73** Concentration-dependent  $\Delta m$  of the Au/LUC sensor with naphthalene plotted calibration curve.

The change in frequency (Hz) *vs.* time (s) was also evaluated (Figure 74), to trace the relationship between naphthalene concentration and the sensor response quantitatively.

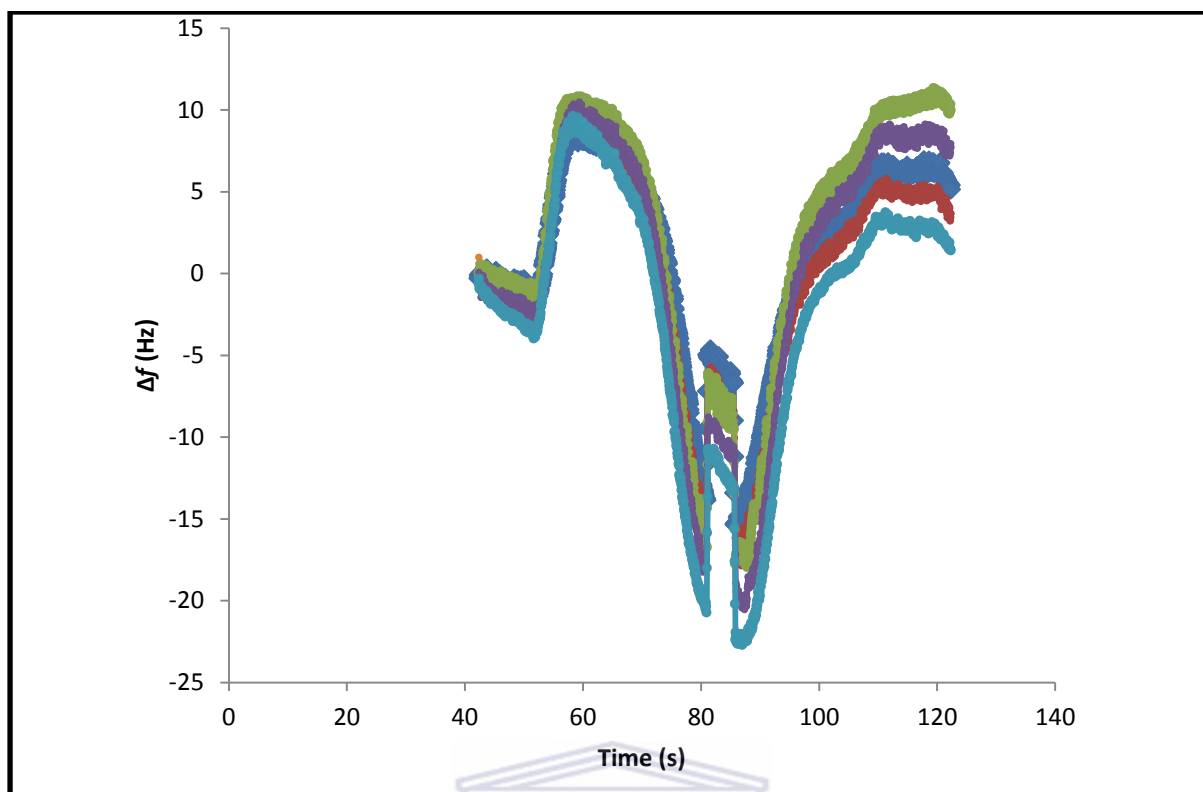
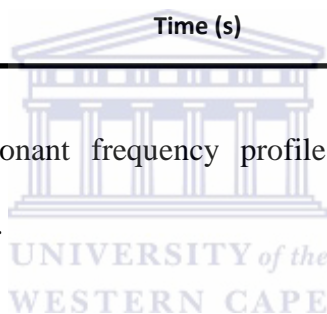


**Figure 74** Time-dependent resonant frequency profiles at different concentrations of naphthalene in 0.2 M PBS (pH 7).



The percent inhibitions were calculated using the following equation:

$$\% I = (\Delta F_0 - \Delta F_p / \Delta F_0) \times 100 \quad \text{Equation 5.5}$$

Where  $\Delta F_0$  is the frequency shift obtained in the absence of analyte and  $\Delta F_p$  is the frequency shift obtained after addition of analyte

The percent inhibitions of the sensor response were plotted against naphthalene concentrations. For this purpose, the concentrations of naphthalene were varied from  $9.09 \times 10^{-11}$  to  $6.99 \times 10^{-10}$   $\mu\text{M}$ , respectively (Figure 75). In the case of naphthalene addition, the increase in concentration was closely related with the increase in frequency shift and a linear



---

relationship was found between analyte concentration and %I, with the linear regression ( $R^2$ ) as 0.94 and sensitivity of  $8 \times 10^{10}$  Hz/ $\mu$ M.

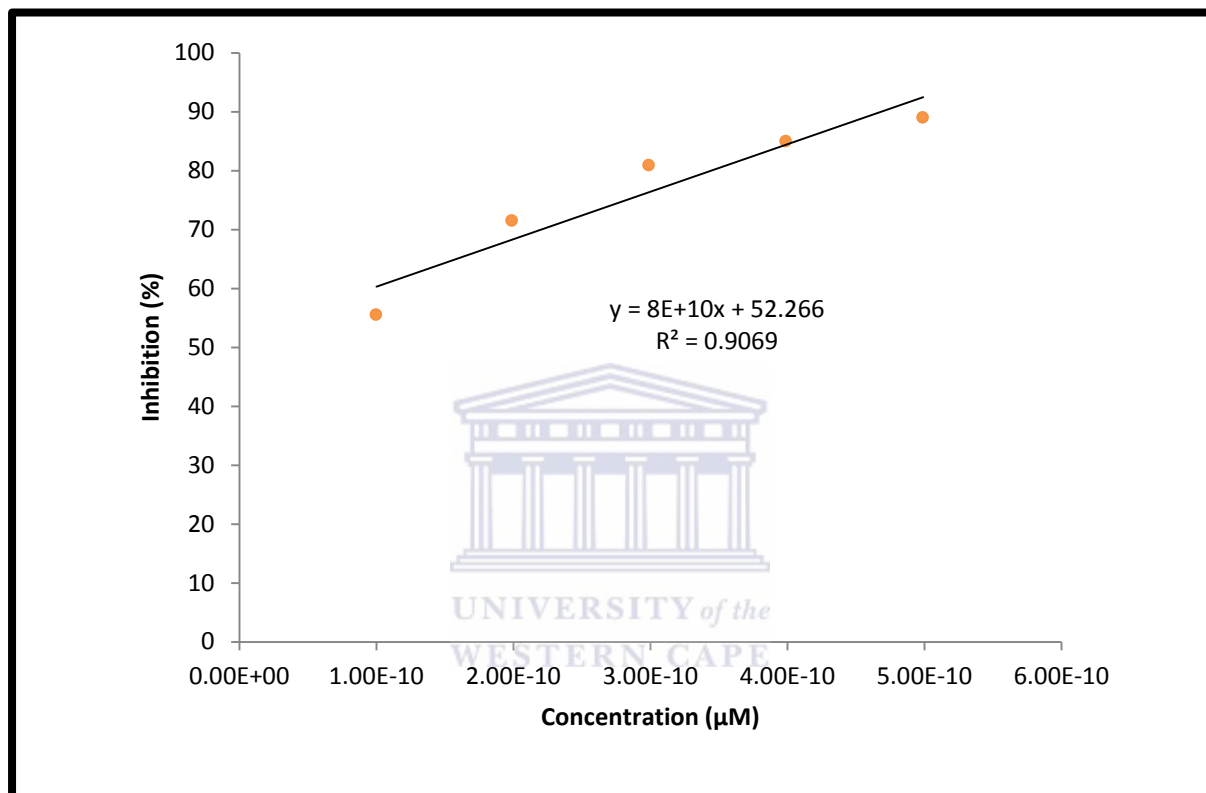


**Figure 75** Concentration-dependent inhibitions of the Au/LUC QCM- sensor with naphthalene concentrations from  $5 \times 10^{-9}$  to  $3.5 \times 10^{-9}$   $\mu$ M.

---

## 5.4.2 EQCM analysis of Luciferase and Fluoranthene

The same procedure as for naphthalene was employed for fluoranthene EQCM analysis. To the EQCM cell filled with 2 mL 0.2 M PBS (pH 7.0), where the Au/LUC electrode was already inserted, followed by the measurement of resonant frequency of the sensor until a steady-state baseline was obtained ( $F_1$ ). Then, aliquots of the fluoranthene were injected into the cell, with a simultaneous stirring for 3 min, to induce complete substrate dissolution in the aqueous buffer. The steady-state resonant frequency ( $F_2$ ) was read again to calculate the frequency shift ( $\Delta F = F_1 - F_2$ ). An inhibition study on the Au/LUC in the presence of individual model PAHs was conducted making use of 0.2M PBS (pH 7.0). The behaviour of the EQCM film containing different concentrations of fluoranthene was studied and mass changes recorded. Results obtained indicate that the interaction of luciferase with different concentrations of fluoranthene at the quartz crystal electrode surface is dependent on the applied potential and the specificity of immobilised enzyme. The peak at  $-0.7$  mV was used as reference for the enzyme and analyte interactions. As the concentration of fluoranthene was increased the  $\Delta m$  increased. The  $\Delta m$  of luciferase was  $16.63 \text{ ng/cm}^2$  and the mass increased to a  $\Delta m$  of  $26 \text{ ng/cm}^2$  when fluoranthene was added (Figure 76). From the  $\Delta m$  vs concentration calibrations plot (Figure 77) a linear regression ( $R^2$ ) of 0.97 and sensitivity of  $6 \times 10^{11} \text{ } \mu\text{M}$  was observed.

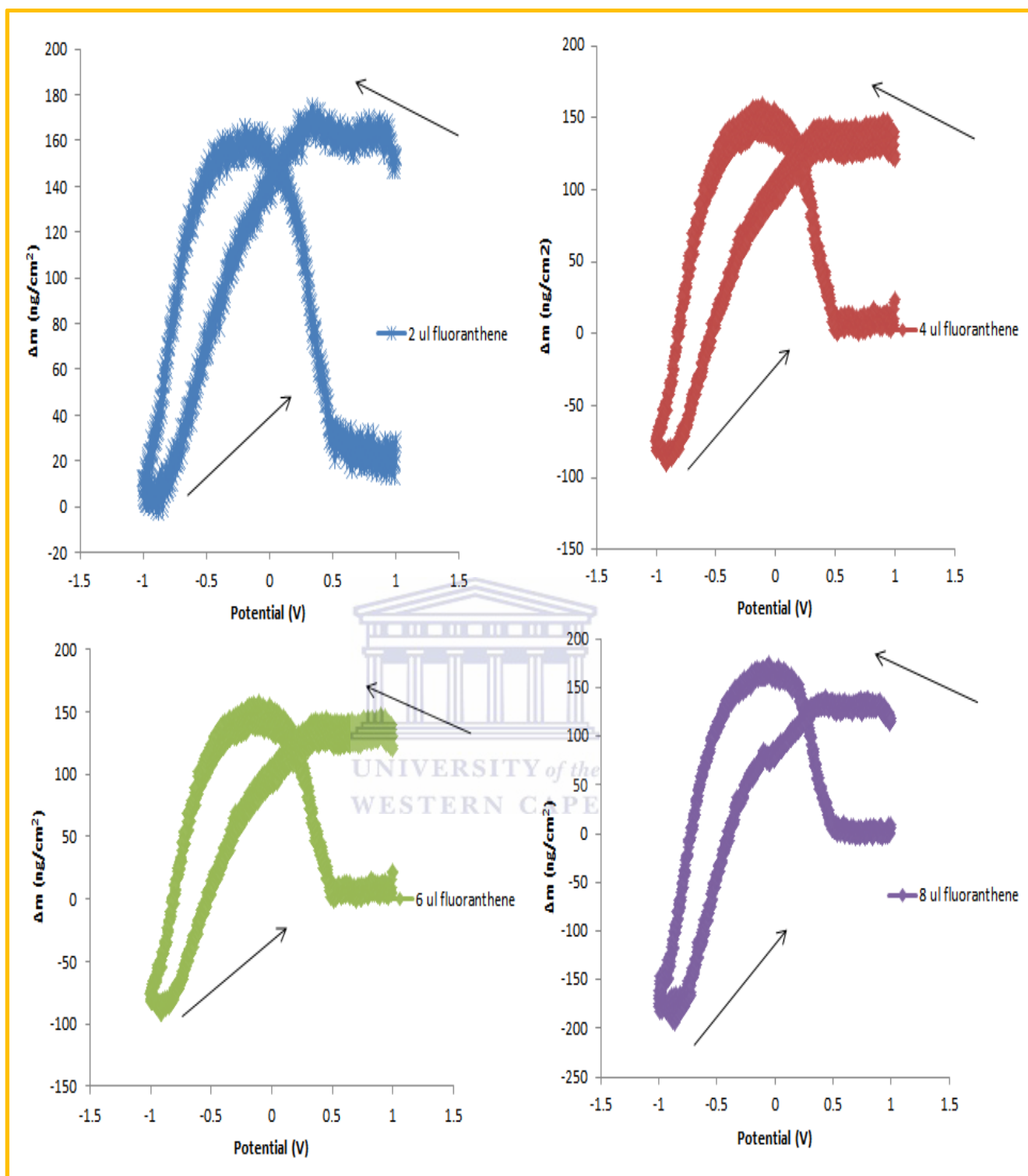


**Figure 76**  $\Delta m$  vs. potential profiles obtained at an Au/LUC coated quartz microbalance using concentrations of  $9.99 \times 10^{-11}$  M to  $9.99 \times 10^{-10}$   $\mu\text{M}$  of fluoranthene in 0.2 M PBS (pH 7) (the concentration profiles up to  $6.99 \times 10^{-10}$   $\mu\text{M}$  were not included in figure).

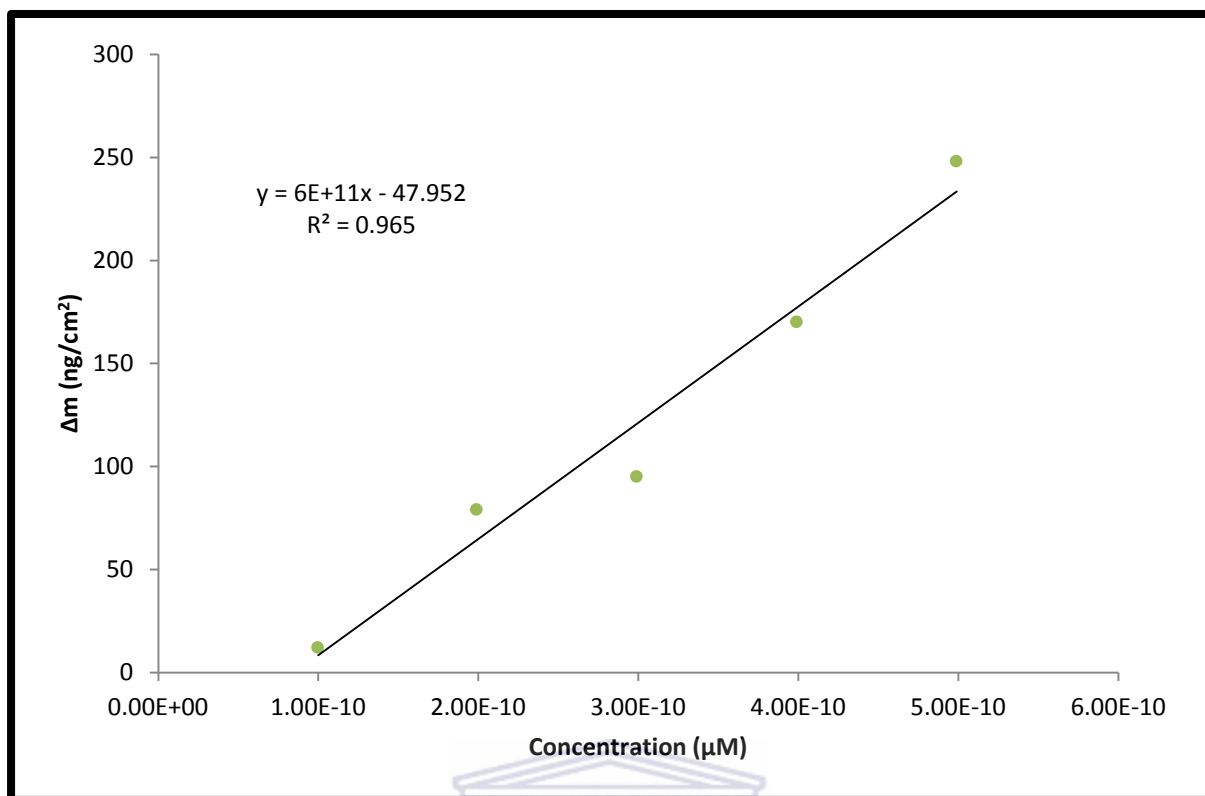
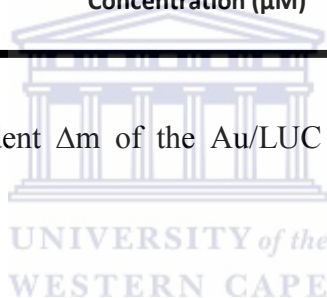


**Figure 77** Concentration-dependent  $\Delta m$  of the Au/LUC sensor with fluoranthene plotted calibration curve.



The percent inhibitions of the sensor response were plotted against fluoranthene concentrations. For this purpose, the concentrations of fluoranthene were varied from  $9.09 \times 10^{-11}$  to  $6.99 \times 10^{-10}$   $\mu\text{M}$ , respectively (Figure 78). In the case of fluoranthene addition, the increase in concentration was closely related with the increase in frequency shift and a linear relationship was found between analyte concentration and %I, with the linear regression ( $R^2$ ) as 0.94 and sensitivity of  $7 \times 10^{10}$  Hz/ $\mu\text{M}$ .

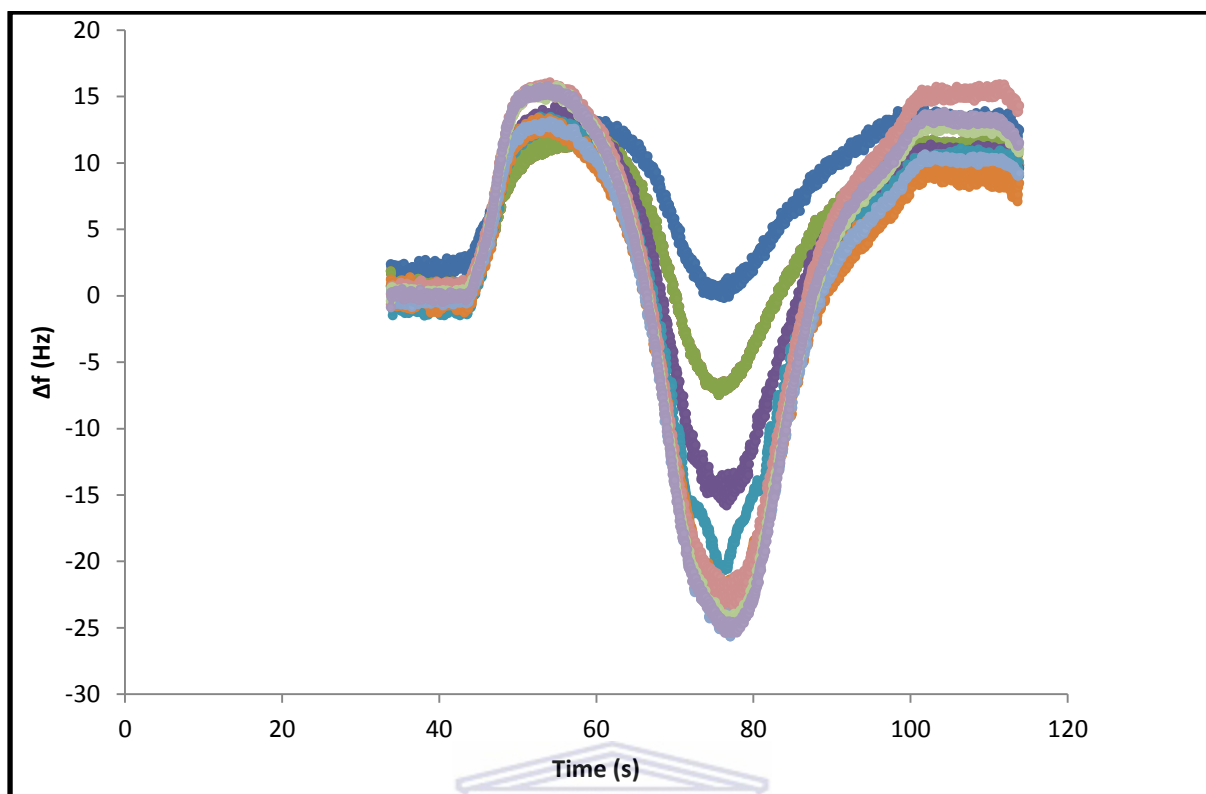


**Figure 78** Time-dependent resonant frequency profiles at different concentrations of fluoranthene in 0.2 M PBS (pH 7).

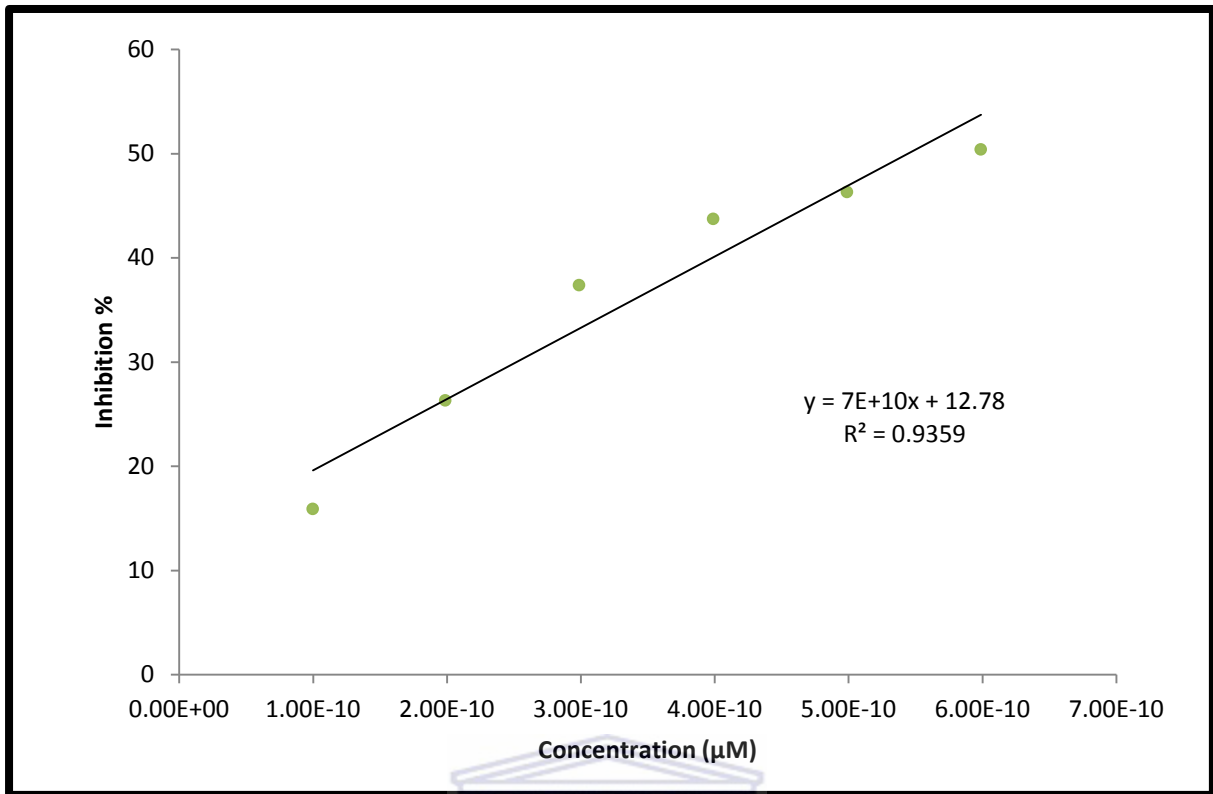


**Figure 79** Concentration-dependent inhibitions of the Au/LUC QCM- sensor with fluoranthene concentrations from  $3 \times 10^{-9}$  to  $3.25 \times 10^{-9}$  µM.

---

## **Part 2: Application of PAA/PPy as a Platform for Luciferase attachment for the Detection of PAHs.**

### **5.5 Evaluation of Electrochemical Impedance Spectroscopy and of the biosensor and Analytes (Naphthalene and Fluoranthene)**

#### **5.5.1 Introduction**

The specificity and simplicity in modern electronics enables electrochemical sensors to rival the most advanced optical protocols (Omowunmi A. Sadik, et al., 2009). Biosensors such as enzyme sensors are primarily based on the immobilization of an enzyme onto an electrode. The development of such enzyme-based sensors for the detection of glucose in blood represents a major area of biosensor research. An important aspect is the material selection for the sensor development, as it allows the response characteristics of a sensor to be altered in a way that minimizes non-specific adsorption by other molecules (Pejcic, B et al., 2006). The application of electrochemical impedance spectroscopy (EIS) in the development of biosensors at conductive and semi-conductive surfaces has been reviewed by a number of investigators (Alfonta, L. et al., 2001; Guan, J. G. et al., 2004; Katz, E. et al., 2003). Electrochemical Impedance Spectroscopy provides important mechanistic information on the adsorption by measuring the changes in the interfacial capacitance and resistance of surfaces (Bordi, F. et al., 2002; Chaki, N. K. et al., 2002). The circuit used to fit the data was the Randle's Circuit (Figure 83).

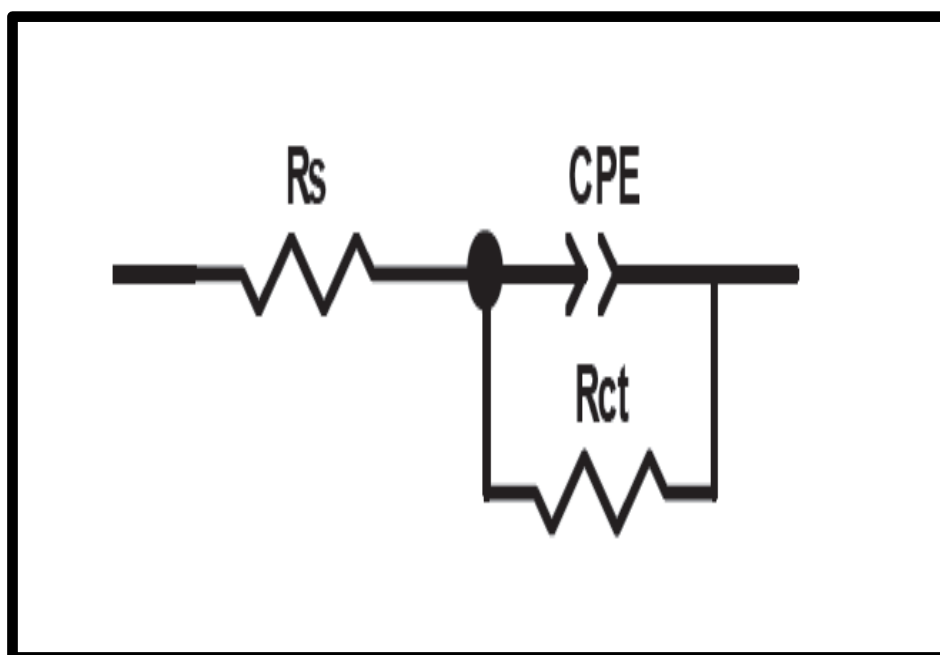


**Figure 80** Randle's Circuit used to fit EIS data.

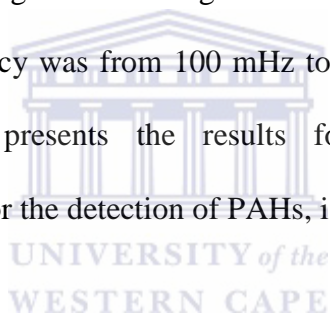
The direct electron transfer between an electrode and a redox enzyme is very crucial for the fundamental studies and the construction of biosensors. Because of the unfavourable orientation of the enzyme on the bare electrode surface or the adsorption of impurities that denature the enzyme, the enzyme often exhibits sluggish electron transfer at electrode surfaces. Modifications of the electrode surface using suitable compatible matrices are known to provide a favourable micro-environment for the protein to exchange its electrons directly with the underlying electrode and thus the study of enzyme electrochemistry can be achieved. Conducting polymers have attracted attention in biological and chemical researches because of their biocompatibility. Nanostructured polymers possess interesting features including high electrical conductivity, stability, improved processability and solubility in a variety of solvents which are superior to those of the parent polymers. They can act as tiny conduction centres to facilitate electron transfer between the enzyme and the electrode surface. They provide a suitable micro-environment for enzyme immobilization during biosensor



---

construction enabling direct communication between the immobilized enzyme and the electrode surface. Luciferase-based biosensors are becoming increasingly used for environmental monitoring. Although there have been studies on luciferase, its direct electrochemistry is relatively difficult to be investigated.

Electrochemical impedance spectroscopy studies of the biosensor were measured with a Voltalab instrument (Radiometer Analytical, France). After the PAA/PPy composite 3 was electrochemically polymerized onto GCE, the enzyme; luciferase was immobilized by the incubation method resulting in an enzyme biosensor. The incubation procedure involved leaving the functionalized GCE/PAA/PPy electrode in a stock solution of luciferase (as prepared in chapter 3) and keeping it in the fridge for 4 to 5 hours. The potential was kept fixed at -730 mV; initial frequency was from 100 mHz to a final frequency of 1 kHz. This part of chapter 5 therefore presents the results for the characterization of the GCE/PAA/PPy/LUC biosensor for the detection of PAHs, i.e. naphthalene and fluoranthene.



### **5.5.2 Electrochemical Impedance Spectroscopy of GCE/PAA/PPy/Luciferase and Naphthalene in 0.2 M PBS (pH 7)**

The potential controlled impedance behaviour of the biosensor with naphthalene at a fixed potential of - 730 mV was measured. The binding of naphthalene to the biosensor was evaluated over a concentration range of 5-20  $\mu$ M. The impedance data was modelled as a Randles Equivalent circuit and the  $R_{ct}$  values were extracted for the fitting of the EIS data. The  $R_{ct}$  values increased (Figure 81) as naphthalene became more concentrated, the system thus became less conductive. The  $R_{ct}$  vs concentration of naphthalene calibration curve was

---

S-shaped in the concentration range evaluated, which is an indication of competitive binding (Yoji K. et. al., 2012). The  $R_{ct}$  values increased until the biosensor was saturated and then started to decrease as a function of naphthalene concentration. This corroborates what was evaluated in Part 1, the electrochemistry (CV) of the luciferase with naphthalene additions. Comparing the sensitivities from CV and sensitivities obtained from EIS the conclusion was made that the GCE/PAA/PPy/LUC biosensor is more sensitive to the detection of naphthalene, than the GCE/LUC biosensor. The biosensor could detect naphthalene with a satisfactory sensitivity of  $1 \times 10^6 \Omega/\mu\text{M}$  (Figure 82) and a limit of detection (LOD) of  $2 \times 10^{-3} \mu\text{M}$  results.

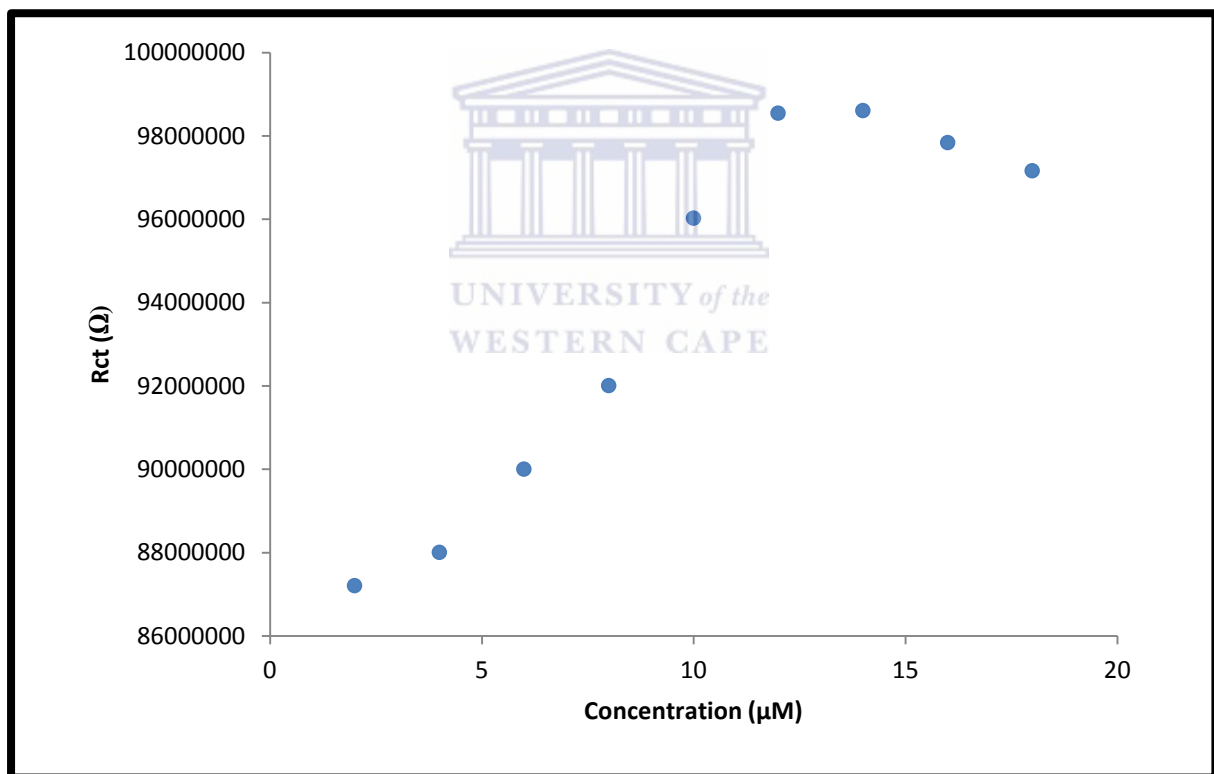


**Figure 81**  $R_{ct}$  vs Concentration calibration plot of the GCE/PAA/PPy/LUC biosensor with different concentrations of naphthalene in 0.2 M PBS (pH 7).

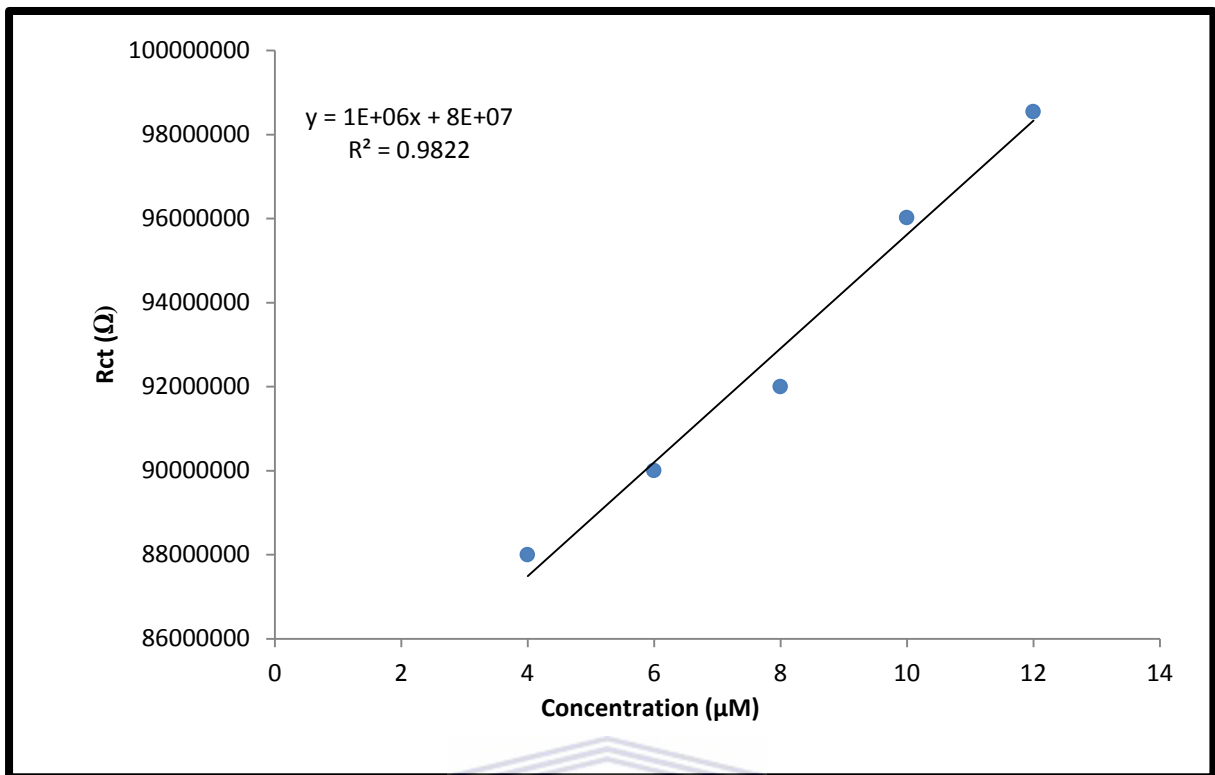


**Figure 82** Linear range of the Rct vs Concentration calibration curve of the GCE/PAA/PPy/LUC biosensor with naphthalene additions.

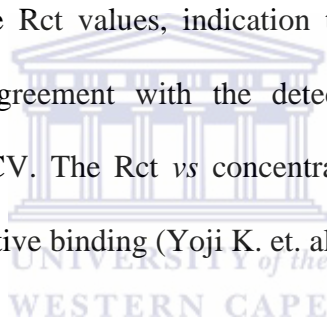
UNIVERSITY of the  
WESTERN CAPE

Rct is a parameter associated with the conductivity of the novel PAA/PPy composite 3. Enzyme binding to naphthalene as well as to fluoranthene would result in the blocking of the conductive surface and hence an increase in Rct.

---

### 5.5.3 Electrochemical Impedance Spectroscopy of GCE/PAA/PPy/Luciferase and Fluoranthene

Electrochemical impedance spectroscopy (EIS) can provide useful information on the impedance changes of the electrode surface during the fabrication process. Figure 83 shows the  $R_{ct}$  vs concentration profile for increasing concentration of fluoranthene in 0.2 M PBS (pH 7). A fix potential of -730 mV was used for analysis binding. It is evident from the  $R_{ct}$  vs concentration profile of the biosensor response to fluoranthene that there is a marked difference in the interfacial electrokinetics after the addition of more than 8  $\mu$ M fluoranthene as there is sharp increase in the  $R_{ct}$  values, indication that the system is becoming less conductive. This is in good agreement with the detection for the biosensor towards fluoranthene as determined by CV. The  $R_{ct}$  vs concentration also showed S-shaped form which is an indication of competitive binding (Yoji K. et. al., 2012).



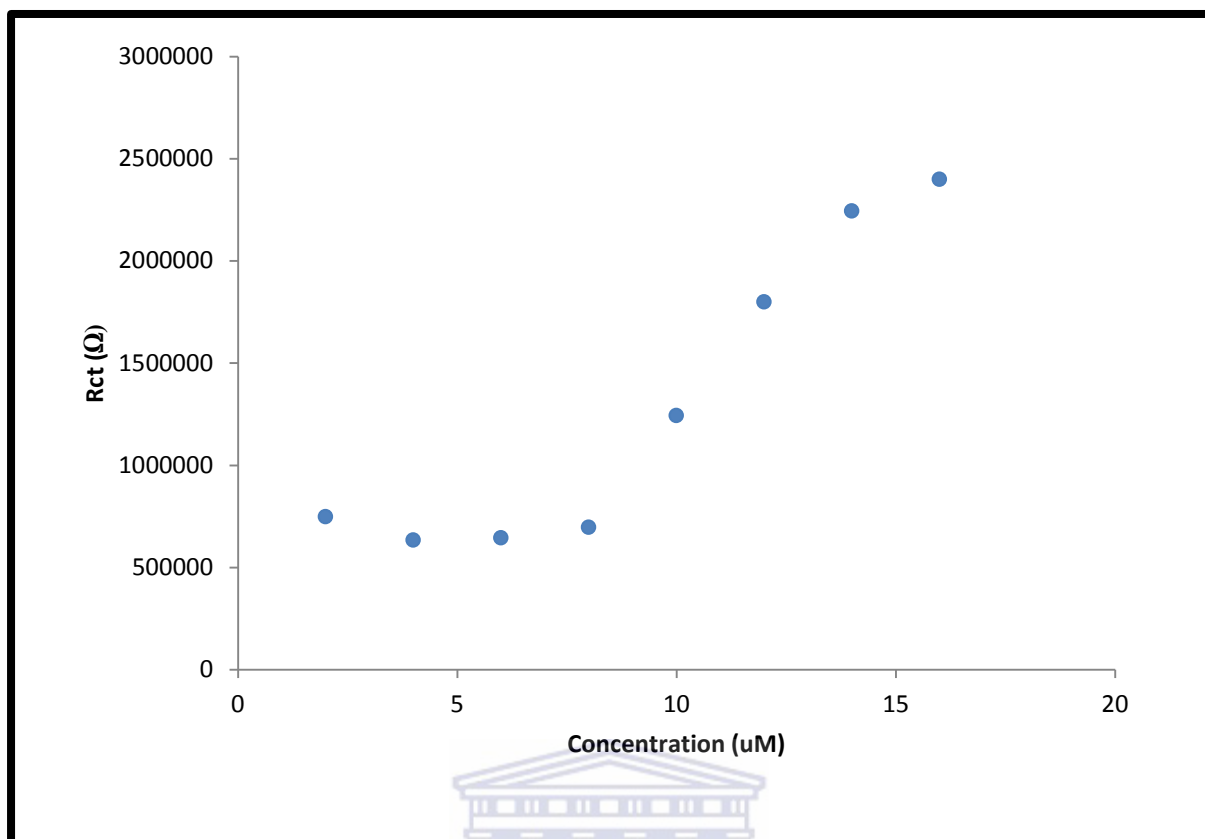


**Figure 83** The Rct vs Concentration calibration curve of the GCE/PAA/PPy/LUC biosensor with increasing concentration of fluoranthene in 0.2 M PBS (pH 7).

The GCE/PAA/PPy/LUC biosensor had sensitivity (Figure 84) for the detection of naphthalene, of  $2.6 \times 10^5$  M and a LOD of  $8 \times 10^{-11}$  μM. Compared to the GCE/LUC biosensor, the GCE/PAA/PPy/LUC biosensor also showed to be more sensitive towards the detection of fluoranthene.

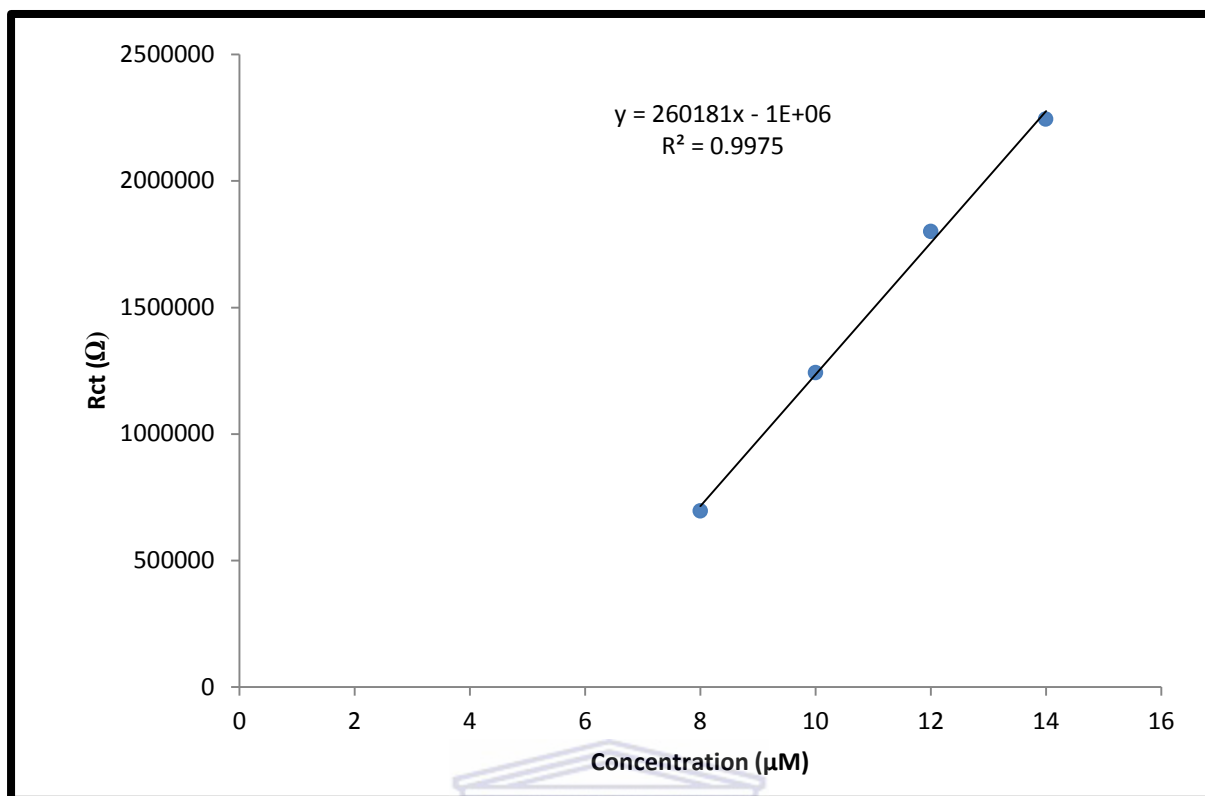
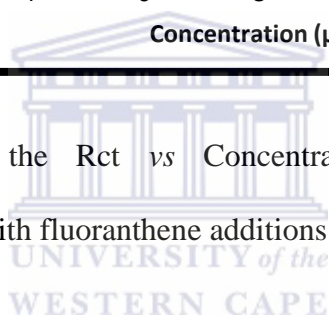


**Figure 84** Linear range of the Rct vs Concentration calibration curve of the GCE/PAA/PPy/LUC biosensor with fluoranthene additions in 0.2 M PBS (pH 7).



---

## Chapter 6

### *Conclusions and recommendations*

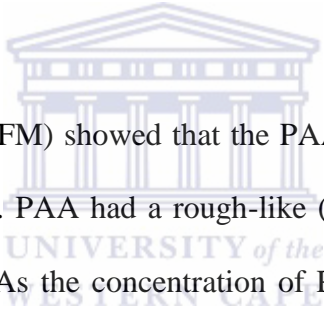
#### 6.1 Conclusions

Polyamic acid was chemically synthesised as a viscous liquid and powder from monomers, ODA and PMDA. The PAA was soluble in PBS (pH 7). Homogeneity played crucial role in composite preparation, thus the viscous PAA was used for composite preparation with PPy. A series of new polyamic acid and polypyrrole (PAA/PPy) composites was electrochemically synthesised *in-situ* and characterized in 0.2 M phosphate buffer solutions at pH of 7. To have some form of control over the PAA/PPy composite preparations, the polyamic acid concentrations was kept constant throughout the *in-situ* synthesis and the PPy concentrations were varied. A total of five PAA/PPy composites were prepared. Electrochemical characterization proved that PAA/PPy composites was formed as a new peak was observed, that was not in observed in the individual polymers (PAA and PPy) characterization. It also proved that PAA ( $E^{02}$ ) was still present in all composites. From the CV parameters i.e. peak potentials and  $D_e$  evaluated, composite 3 was proved to have the best electrochemical properties out of the five composites prepared.

---

The FTIR confirms that the functionalities of both PAA and PPy are present confirming an interaction between the two polymers. The carboxylic and amide moieties from PAA are present in all the composites, confirmation that PAA is still present in the composites as PPy is incorporated into the PAA film.

All the Raman bands characteristic to PAA was present each composite with the difference of intensity of these bands increasing. This shows how PPy affects the Raman spectra of pure PAA film on SPCE. At composite 3 from the Raman shift  $\text{cm}^{-1}$  vs composite calibration plot it is evident that neither the PAA nor the PPy is dominating.

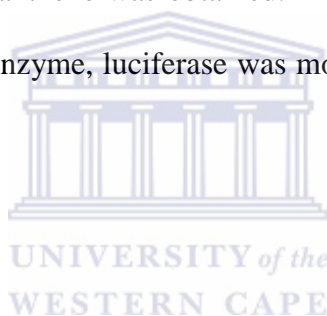


Morphology studies (SEM and AFM) showed that the PAA/PPy composites have structures incorporating both PAA and PPy. PAA had a rough-like (amorphous) film, and PPy film displayed globular-like features. As the concentration of PPy was increased, the composite films became smoother with porous features. The conclusion was that PPy filaments were actually formed and anchored along the PAA matrix. Out of the five composites, composite 3 best described the incorporation of both polymers, because as the concentration of PPy increased the films just became flooded with PPy as to forming homogeneous layers. AFM corroborated what was observed in SEM. The presence of PPy breaks up the large scale like appearance of PAA and introduces a controlled laminar surface. The line roughness ( $R_a$ ) values showed a distribution of roughness associated with PAA and PPy, and the composite films with equal contribution from each polymer were composite 2 and 3.



---

The interaction between the luciferase and naphthalene and fluoranthene in solution was investigated by Fluorescence spectroscopy. To examine the luciferase luminescence system for a study of the effects of naphthalene and fluoranthene on enzyme functions, each analyte was injected into a cuvette containing luciferase mixed in 0.2 M PBS (pH 7), and the corresponding change in the luciferase luminescence intensity was measured. The luciferase luminescence intensity gradually decreased with the increase in concentration of each analyte. The decrease in the luciferase luminescence intensity was caused by competitive binding of the PAHs with the enzyme. From the calibration curves sensitivities of 80  $\mu\text{M}$  and 30  $\mu\text{M}$  for naphthalene and fluoranthene was obtained. From the sensitivities obtained from fluorescence measurements, the enzyme, luciferase was more sensitive towards the detection of fluoranthene.



The electrochemistry of the bare GCE and luciferase on GCE (GCE/LUC) was investigated with addition of each analyte. The GCE/LUC biosensor was more sensitive towards the detection of naphthalene and fluoranthene respectively obtained,  $4 \times 10^{-5}$  A/ $\mu\text{M}$  and  $2 \times 10^{-4}$  A/ $\mu\text{M}$  compared to the bare GCE with sensitivities of  $1 \times 10^{-4}$  A/mM and  $2 \times 10^{-4}$  A/mM. EQCM was also used to investigate the enzyme with analyte interaction in terms of mass changes. The luciferase was immobilised onto the Au-quartz crystal (Au/LUC). The  $\Delta m$  increased as a function of concentration for each analyte.

---

After synthesising the PAA/PPy composites, and investigating the interfacial properties of luciferase with PAHs; the application of PAA/PPy as a platform for luciferase immobilisation as a biosensor for PAHs, the final piece of the puzzle (thesis) was evaluated. The GCE/PAA/PPy/LUC biosensor evaluated using  $R_{ct}$  values obtained from EIS. The biosensor had a sensitivity of  $1 \times 10^6 \mu\text{M}$  for naphthalene and  $2.2 \times 10^5 \mu\text{M}$  for fluoranthene respectively. The detection of both analytes was in good agreement based on other methods of detection HPLC, UV-Vis that's in the  $\mu\text{g/L}$  range.

From the fluorescence measurements, GCE/LUC biosensor, PAA/PPy/LUC biosensor fluoranthene had lower detection limits and was more sensitive than that for naphthalene.



---

## 6.2 Recommendation and Future work:

The results indicate that the PAA/PPy/LUC biosensor is sensitive enough to detect the PAHs at low concentrations. However, in order that the biosensor can be fully applied for the detection of these PAHs in samples containing complex matrices, further optimization and selectivity studies would be required. A follow up procedure should include the studies of interfering species in the analyte solutions.

The application of PAA/PPy/LUC biosensor should be extended to analysis of other PAHs that can inhibit the activity of luciferase. Once optimized, it is clear that this inhibition based biosensor would provide rapid monitoring of environmental occurrence of PAHs. Integration of the PAA/PPy/LUC biosensor into an automated system would be more attractive to provide the detection of many PAHs reducing the time of analysis. Miniaturization is further required for the biosensor to be applied for “on-site” monitoring of these PAHs.

Additional characterization of the GCE/PAA/PPy/LUC biosensor for the detection of PAHs using the different composites is also suggested.

Evaluate the response of the composites with other analytes i.e.  $\text{Fe}(\text{CN})_6^{3+}$ , and study their electro-kinetic behaviour.

---

## References

Adhikari, B.; Majumdar, S., Polymers in sensor applications. *Progress in Polymer Science* **2004**, 29, (7), 699-766.

AFM Theory, Nanosurf easyScan 2 User manual; pg 70-72

Akinyeye, R.O.; Michira, I.; Sekota, M.; Ahmed, A.A; Tito, D.; Baker, P.G.L.; Brett, C.M.A.; Kalaji, M.; Iwuoha, E.I. Electrochemical Synthesis and Characterization of 1,2-Naphthaquinone-4-Sulfonic Acid Doped Polypyrrole. *Electroanalysis* **2007**, 19, 303–309.

Andrade Eiroa, A., E.V.B., López Mahía, P., Muniategui Lorenzo, S., Prada Rodríguez, D. and Fernández Fernández, E., Determination of polycyclic aromatic hydrocarbons (PAHs) in a complex mixture by second-derivative constant-energy synchronous spectrofluorimetry. *Talanta*, **2000**, 51, 677-684.

Andreescu D.; Wanekaya A.K.; Sadik O.A; Wang J.; Nanostructured Polyamic Acid Membranes as Novel Electrode Materials, *Langmuir* 2005, 21, 6891-6899.

Baldwin, T.O; Christopher, J.A; Raushel, F.M; Sinclair, J.F; Ziegler, M.M; Fisher, A.J; Rayment I. Structure of bacterial luciferase. Texas A&M University, College Station and University of Wisconsin, Madison, USA; *Current Opinion in Structural Biology* **1995**, 5, 798-809.

Bartlett, P. N.; Birkin, P. R.; Ghanem, M. A.; Toh, C. S., Electrochemical syntheses of highly ordered macroporous conducting polymers grown around self-assembled colloidal templates. *Journal of Materials Chemistry* **2001**, 11, (3), 849-853.

---

Baumann T.; Haaszio S.; Niessner R. Applications of laser-Induced Fluorescence Spectroscopy Sensor in Aquatic Systems. *Wat. Res.* **2000**, 34(4), 1318-1326.

Beck, J. S.; Vartuli, J. C.; Roth, W. J.; Leonowicz, M. E.; Kresge, C. T.; Schmitt, K. D.; Chu, C. T. W.; Olson, D. H.; Sheppard, E. W.; McCullen, S. B.; Higgins, J. B.; Schlenker, J. L., A new family of mesoporous molecular sieves prepared with liquid crystal templates. *Journal of the American Chemical Society* **1992**, 114, (27), 10834-10843.

Bessonov, M.I.; Koton, M.M.; Kudryavtsev, V.V.; Lais, L.A. Polyimides: Thermally Stable Polymers, 2nd edition, Plenum, New York, **1987**.

Bessonov, M.I.; Zubkov, V.A. editors, Polyamic acids and polyimides: synthesis, transformations, and structure, CRC Press, **1993**.

Blum L. J.; Gautier S. M.; Coulet P. R. Fibre optic biosensors with immobilised bioluminescent enzymes. *Journal of Material Science: Materials in Medicine*, **1991**, 2, 202-204.

Boal, A. K.; Ilhan, F.; Derouchey, J. E.; Thurn-Albrecht, T.; Russell, T. P.; Rotello, V. M., Self-assembly of nanoparticles into structured spherical and network aggregates. *Nature* 2000, 404, (6779), 746-748.

Branchini B.R.; Southworth T.L.; De Angelis J.P.; Roda A.; Michelini E. *Comp. Biochem. Physiol. B* 2006, 145 - 159.

Bredas, J. L.; Street, G. B., Polarons, bipolarons, and solitons in conducting polymers. *Accounts of Chemical Research* **1985**, 18, (10), 309-315.

---

Bruckenstein S., Shay M., *Electrochim. Acta*, 1985, 30, 1295; Monura T., Okumura M., *Anal. Chim. Acta*, **1982**, 142, 281.

Brynda, M.M.; Houska, M.; Schauer, *J. Polymer* **1996**, 37(12), 2577-2579.

Buch, R. M.; Rechnitz, G. A., *Anal. Chem.* **1989**, 61, 533A.

Cai, Z.-Q.; Zhu Y.-X.; Zhang Y.; Simultaneous determination of dissolved anthracene and pyrene in aqueous solution by synchronous fluorimetry. *Spectrochimica Acta Part A: Molecular and Biomolecular Spectroscopy* **2008**, 69(1), 130-133.

Cao, L.; Chen, H. Z.; Zhou, H. B.; Zhu, L.; Sun, J. Z.; Zhang, X. B.; Xu, J. M.; Wang, M. Carbon-nanotube-templated assembly of rare-earth phthalocyanine nanowires. *Advanced Materials* **2003**, 15, (11), 909-913.

Casar, Z.; Leban, I.; Majcen-le Marechal, A.; Piekara-Sady, L.; Lorcy, D., Charge transfer complexes and cation radical salts of azino-diselenadiazafulvalene. *Comptes Rendus Chimie* **2009**, 12, (9), 1057-1065.

Cassagneau, T.; Caruso, F., Semiconducting polymer inverse opals prepared by electropolymerization. *Advanced Materials* **2002**, 14, (1), 34-38.

Chapter 1 POLYIMIDES: chemistry & structure-property relationships.

Chen, Y.; Iroh, J. O. *Polym. Eng. Sci.* **1999**, 39, 699.

Colmsjo A., A.H.N., The handbook of environmental chemistry part 1, PAHs and related compounds. Springer-verlag. **1998**, 3, 55.

Debuigne, A.; Poli, R.; Jérôme, C.; Jérôme, R.; Detrembleur, C., Overview of cobalt-mediated radical polymerization: Roots, state of the art and future prospects. *Progress in Polymer Science* **2009**, 34, (3), 211-239.

---

Demolliens, A.; Muller, C.; Müller, R.; Turquat, C.; Goux, L.; Deleruyelle, D.; Wouters, D. J., Solution growth of metal-organic complex CuTCNQ in small dimension interconnect structures. *Journal of Crystal Growth* **2010**, 312, (22), 3267-3275.

Dhand, C.; Das, M.; Datta, M.; Malhotra, B. D., Recent Advances in Polyaniline Based Biosensors. *Biosensors and Bioelectronics In Press*, Accepted Manuscript.

Di Lena, F.; Matyjaszewski, K., Transition metal catalysts for controlled radical polymerization. *Progress in Polymer Science* **2010**, 35, (8), 959-1021.

Diaz, A.F.; Kanazawa, K.K; Gardini, G.P. *Journal of Chemical Society, Chemical Communications* **1979**, 635.

Ebara, Y.; Okahara, Y.; *Langmuir* **1993**, 9, 574.

Eckenhoff, R.G., J.W. Tanner, P.A. Liebman, Cooperative binding of inhaled anesthetics and ATP to firefly luciferase, *Proteins* **2001**, 42, 436-441.

Endry, A. G. US Patent 3 179 630, "Process for preparing polyimides by treating polyamic acid with lower fatty monocarboxylic acid anhydrides".

Ferrer, R., Guiteras J., and Beltrán J.L., Development of fast-scanning fluorescence spectra as a detection system for high-performance liquid chromatography Determination of polycyclic aromatic hydrocarbons in water samples. *Journal of Chromatography A*, **1997**, 779 (1-2), 123-130.

Fu, G.-D.; Li, G. L.; Neoh, K. G.; Kang, E. T., Hollow polymeric nanostructures-- Synthesis, morphology and function. *Progress in Polymer Science* **2011**, 36, (1),127-167.

Geffard, O., Geffard, A., His, E., Budzinski, H., Assessment of the bioavailability and toxicity of sediment-associated polycyclic aromatic hydrocarbons and heavy metals

---

applied to *Crassostrea gigas* embryos and larvae. *Marine Pollution Bulletin*, 2003, 46(4), 481-490.

Gerard, M.; Chaubey, A.; Malhotra, B. D., Application of conducting polymers to biosensors. *Biosensors and Bioelectronics* **2002**, 17, (5), 345-359.

Gligorich, K. M.; Iwai, Y.; Cummings, S. A.; Sigman, M. S., A new approach to carbon-carbon bond formation: development of aerobic Pd-catalyzed reductive coupling reactions of organometallic reagents and styrenes. *Tetrahedron* **2009**, 65,(26), 5074-5083.

Grant, S.; Davis, F.; Law, K. A.; Barton, A. C.; Collyer, S. D.; Higson, S. P. J.; Gibson, T. D. Label-free and reversible immunosensor based upon an ac impedance interrogation protocol. *Analytica Chimica Acta* **2005**, 537 (1-2), 163-168.

Grennan, K.; Killard, A. J.; Hanson, C. J.; Cafolla, A. A.; Smyth, M. R., Optimisation and characterisation of biosensors based on polyaniline. *Talanta* **2006**, 68, (5), 1591-1600.

Guimard, N. K.; Gomez, N.; Schmidt, C. E., Conducting polymers in biomedical engineering. *Progress in Polymer Science* **2007**, 32, (8-9), 876-921.

(<http://nobelprize.org/chemistry/laureates/2000>)

Hardaker, S.S.; Gregory, R.V.; Mark, J.E. editors, "Polymer Data Handbook", New York, Oxford, **1999**.

Harden, R.A.; Baetjer, A.M. Aplastic anemia following exposure to paradichlorobenzene and naphthalene. *J. Occup. Med.* **1978**, 20(12), 820-822.

Harsányi, G., Polymeric sensing films: new horizons in sensorics? *Materials Chemistry and Physics* 1996, 43, (3), 199-203.



---

Hastings J.W.; Gibson Q.H. Intermediates in the bioluminescent oxidation of reduced flavin mononucleotide. *J. Biol. Chem.* **1963**, 238, 2537–2554.

Hastings J.W.; Potrikus C.J.; Gupta S.C.; Kurfurst M.; Makemson J.C. Biochemistry and physiology of bioluminescent bacteria. *Adv. Microb. Physiol.* **1985**, 26, 235–291.

Hatchett, D. W.; Josowicz, M., Composites of intrinsically conducting polymers as sensing nanomaterials. *Chemical Reviews* **2008**, 108, (2), 746-769.

Haushalter, R.C.; Krause L. J. *Thin Solid Films* **1983**, 102, 161.

Hua M.; Chen H.; Chuang C.; Tsai R.; Jeng J.; Yang H.; Chern Y. The intrinsic redox reactions of polyamic acid derivatives and their application in hydrogen peroxide sensor. *Biomaterials* **2011**, 32, 4885-4895.

Huang, J.; Virji, S.; Weiller, B. H.; Kaner, R. B., Polyaniline nanofibers: Facile synthesis and chemical sensors. *Journal of the American Chemical Society* **2003**, 125, (2), 314-315.

IARC (International Agency for Research on Cancer. 1983. Fluoranthene. In: IARC Monographs on the Evaluation of Carcinogenic Risks to Humans. Polynuclear Aromatic Compounds. Part 1. Chemical, Environmental and Experimental Data, **1983**, Vol. 32. World Health Organization, Lyon, France, pp. 355-364.

Ignowski, J.M.; Schaffer, D.V. Kinetic analysis and modeling of firefly luciferase as a quantitative reporter gene in live mammalian cells, *Biotechnol. Bioeng.* **2004**, 86, 827–834.

Iroh, J.O.; Su, W. *Journal of Applied Polymer Science* 1999, 71, 21, 2075–2086.

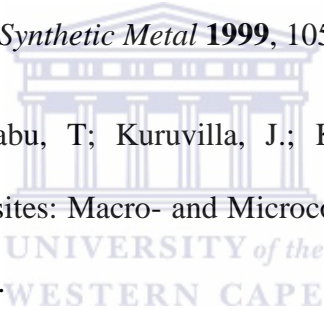
---

Iroh, Jude O.; Levine, Kirill. Invention Disclosure “Novel Method for Producing Polyimide-Polypyrrole Composite with High Electrical Conductivity” filed to the Office of Intellectual Property of the University of Cincinnati in **2000**.

Iwuoha, E.I.; Saenz-de-Villaverde, D.; Garcia, N.P.; Smyth, M.R.; Pingarron, J.M. Reactivities of organic phase biosensors. 2. The amperometric behavior of horseradish peroxidase immobilized on a platinum electrode modified with an electrosynthetic polyaniline film. *Biosensors and Bioelectronics* **1997**, 12, 749-761.

Jia C.; Batterman S. A Critical Review of Naphthalene Sources and Exposures Relevant to Indoor and Outdoor Air. *Int. J. Environ. Res. Public Health* **2010**, 7, 2903-2939.

Jinwey, W.; Srinivasan, M.P. *Synthetic Metal* **1999**, 105, 1-7.

Josmin P.J.; Sant, K.M.; Sabu, T; Kuruvilla, J.; Koichi, G.; Meyyarappallil, S.S. Advances in Polymer Composites: Macro- and Microcomposites – State of the Art, New Challenges, and Opportunities.  UNIVERSITY of the WESTERN CAPE

Kabzinski, A.K.M.; Juszczak, R. Determination of polycyclic aromatic hydrocarbons in water (including drinking water) of Lodz. *Journal of environmental studies*, **2002**, 11(6), 695-706.

Kanally R. A.; Harayama S. Biodegradation of High-Molecular-Weight Polycyclic Aromatic Hydrocarbons by Bacteria. *Journal of Bacteriology* **2000**, 182 (8), 2059–2067.

Kang, E.T.; Li, Z.F.; Neoh, K.G. *Synthetic Metals*, **1997**, 87, 45.

Kanungo, M.; Deepa, P. N.; Collinson, M. M., Template-Directed Formation of Hemispherical Cavities of Varying Depth and Diameter in a Silicate Matrix Prepared by the Sol-Gel Process. *Chemistry of Materials* **2004**, 16, (25), 5535- 5541.

---

Kaynak, A. *Mat. Res. Bulletin*, **1996**, 31, 7, 845-860.

Kazimierska, E.; Muchindu, M.; Morrin, A.; Iwuoha, E.; Smyth, M. R.; Killard, A. J.,  
The fabrication of structurally multiorordered polyaniline films and their application in  
electrochemical sensing and biosensing. *Electroanalysis* **2009**, 21, (3-5), 595-603.

Kelley, I.; Cerniglia C.E. The metabolism of fluoranthene by a species of  
*Mycobacterium*. *J. Ind. Microbiol.* **1991**, 7, 19–26.

Killard, A.J.; Zhang, S.; Zhao, H.; John, R.; Iwuoha, E.I.; Smyth, M.R. Development of  
an electrochemical flow injection immunoassay (FIIA) for the real-time monitoring of  
biospecific interactions. *Anal. Chim. Acta* **1999**, 400 (2), 109-/1190.

Kim, N., Park, I.; Kim, D., High-sensitivity detection for model organophosphorus and  
carbamate pesticide with quartz crystal microbalance-precipitation sensor. *Biosensors and  
Bioelectronics* **2007**, 22, 1593–1599.

Klink, M.J.; Iwuoha, E.I.; Ebenso, E.E; Electrochemical Properties of Nanotubes and  
Nanomicelles from Novel Polyaniline and Derivative. *Int. J. Electrochem. Sci.* **2012**, 7  
3031– 3046.

Kobayashi, Y.; Yoshioka, M.; Saigo, K.; Hashizume, D.; Ogura, T., Hydrogenbonding  
tetrathiafulvalene (TTF) conductors: Carrier generation by self-doping. *Physica B:  
Condensed Matter* **2010**, 405, (11, Supplement 1), S23-S26.

Kohlman, R.S.; Epstein, A.J; Scothorn, T.A; Elsenbaumer, R.L.; Reynolds, J.R. editors,  
“Handbook of Conducting Polymers, 2nd edition, Marcel Dekker, New York, **1998**, 92.

Koton, M.M.; Kudryavtsev, V.V.; Zubkov, V.A.; Yakimansky, A.V; Meleshko, T.K.;  
Bogorad, N. N. *Polymer Science A* **1984**, 26, 2584.

---

Kozlov, A.G.; Levine, K.L.; Eliashevich, G.K., 9th International conference of undergraduate and graduate students "Synthesis, research, modification and processing of macromolecular compounds", Kazan (Russia), **1998**, 19-21, 195.

Kulikov, V.; Mirsky, V. M., Equipment for combinatorial electrochemical polymerization and high-throughput investigation of electrical properties of the synthesized polymers. *Measurement Science and Technology* **2004**, 15, (1), 49-54.

Kulikov, V.; Mirsky, V. M.; Delaney, T. L.; Donoval, D.; Koch, A. W.; Wolfbeis, O. S., High-throughput analysis of bulk and contact conductance of polymer layers on electrodes. *Measurement Science and Technology* **2005**, 16 (1), 95-99.

Kumar, D.; Sharma, R. C., Advances in conductive polymers. *European Polymer Journal* **1998**, 34, (8), 1053-1060.

Lange, U.; Roznyatovskaya, N. V.; Mirsky, V. M., Conducting polymers in chemical sensors and arrays. *Analytica Chimica Acta* **2008**, 614, (1), 1-26.

Lee, J.Y.; Kim, D.Y.; Kim, C.Y. Synthesis of soluble polypyrrole of the doped state in organic solvents, *Synthetic Metals* **1995**, 74, 103-106.

Levin K. L.; Pshchelko N. S.; Electrochemical Properties of a Polypyrrole–Polyimide Composite. Revised Manuscript Received January **2011**, 24.

Levin, K.L.; Borisova, T.I.; Zgonnik, V.N.; Frolov V.I.; Ushakova, I.L. *Polymer Science B*, **2000**, 42(2), 357-360.

Levine, K.L.; Frolov, V.I.; Boyartchuck, Yu.M.; Borisova, T.I. Investigation of Electric conductivity and IR Spectra of composites: electrochemical preparation of conductive Metallic Silver Layers in Polyimide Films. *Polymer Science B* **1999**, 41, 30-33.

---

Levine, K.L.; Zgonnik V.N.; Frolov, V.I. *Polymer Science B*, 35, N10, (1993).

Lu, W.; Meng, X.S; Wang, Z.Y. *Journal of Polymer Science: Part A: Pol. Chem.* 1999, 37, 4295-4301.

Luo, X.; Killard, A. J.; Smyth, M. R., Nanocomposite and Nanoporous Polyaniline Conducting Polymers Exhibit Enhanced Catalysis of Nitrite Reduction. *Chemistry - A European Journal* **2007**, 13, 2138-2143.

Luo, X.; Vidal, G.; Killard, A.; Morrin, A.; Smyth, M., Nanocauliflowers: A Nanostructured Polyaniline-Modified Screen-Printed Electrode with a Self-Assembled Polystyrene Template and Its Application in an Amperometric Enzyme Biosensor. *Electroanalysis* **2007**, 19, (7-8), 876-883.

Macdonald, D.D. Reflections on the history of electrochemical impedance spectroscopy. *Electrochimica Acta* **2006**, 51, 1376-1388.

Macdonald, D.D. Review of mechanistic analysis by electrochemical impedance spectroscopy. *Electrochimica Acta* **1990**, 35, 1509-1525.

Malinauskas, A., Electrocatalysis at conducting polymers. *Synthetic Metals* **1999**, 107, (2), 75-83.

Martin, C. R.; Parthasarathy, R.; Menon, V., Template synthesis of electronically conductive polymers - a new route for achieving higher electronic conductivities. *Synthetic Metals* **1993**, 55, (2 -3 pt 2), 1165-1170.

Mathebe, N. G. R.; Morrin, A.; Iwuoha, E. I., Electrochemistry and scanning electron microscopy of polyaniline/peroxidase-based biosensor. *Talanta* **2004**, 64, (1), 115-120.

Mayer, C.; Wang, X.; Neitzel, M. *Composites Part A*, **1998**, 29, 783-793.

---

Meador, M.B.; Green, D.H.; Auping, J.V.; Gaizer, J.A. *Journal of Applied Polymer Science* **1997**, 63, 821.

Michira, R. Akinyeye, V. Somerset, M. J. Klink, M. Sekota, A. Al-Ahmed, P. G. L. Baker, E. Iwuoha Synthesis, Characterisation of Novel Polyaniline Nanomaterials and Application in Amperometric Biosensors. *Macromol. Symp.* **2007**, 255, 57–69.

Monk, P. M. (2001). *Fundamentals of electroanalytical chemistry*. New York, USA: John Wiley & Sons.

Moreda-Piñeiro, J.; Alonso-Rodríguez, E.; López-Mahía, P.; Muniategui-Lorenzo, S.; Prada-Rodríguez, D.; López-Mahía, P.; Prada-Rodríguez, D.; Romarís-Hortas, V.; Míguez-Framil, M.; Moreda-Piñeiro, A.; Bermejo-Barrera, P., Matrix solid-phase dispersion of organic compounds and its feasibility for extracting inorganic and organometallic compounds. *TrAC Trends in Analytical Chemistry* **2009**, 28, (1), 110-116.

Mott, N.F.; Davis, E.A. *Electronic properties in non-crystalline materials*, Clarendon press, Oxford, 1971.

Muchindu, M.; Waryo, T.; Arotiba, O.; Kazimierska, E.; Morrin, A.; Killard, A.J.; Smyth, M. R.; Jahed, N.; Kgarebe, B.; Baker, P. G. L.; Iwuoha, E. I., Electrochemical nitrite nanosensor developed with amine- and sulphatefunctionalised polystyrene latex beads self-assembled on polyaniline. *Electrochimica Acta* **2010**, 55, (14), 4274-4280.

Murray, P.; Wallace, G.G.; Spinks, G.M.; Burford, R.P. *Synthetic Metals*, **1997**, 84, 847.

Myler, S.; Collyer, S. D.; Davis, F.; Gornall, D. D.; Higson, S. P. J., Sonochemically fabricated microelectrode arrays for biosensors: Part III. AC impedimetric study of aerobic and anaerobic response of alcohol oxidase within polyaniline. *Biosensors and Bioelectronics* **2005**, 21, (4), 666-671.

---

Nakai, H.; Isobe, K., Photochromism of organometallic compounds with structural rearrangement. *Coordination Chemistry Reviews* **2010**, 254, (21-22), 2652-2662.

Nambiar, S.; Yeow, J. T. W., Conductive polymer-based sensors for biomedical applications. *Biosensors and Bioelectronics* **2011**, 26, (5), 1825-1832.

Nishizawa, M.; Matsue, T.; Uchida, I., Penicillin sensor based on a microarray electrode coated with pH-responsive polypyrrole. *Analytical Chemistry* **1992**, 64, (21), 2642-2644.

Noah N.M.; Omole M.; Stern S.; Zhang S.; Sadik O.A; Hess E.H; Martinovic L.; Baker P.G.L.; Iwuoha E.I. Conducting polyamic acid membranes for sensing and site-directed immobilization of proteins. *Analytical Biochemistry* **2012**, 428, 54–63.

Nunes-Halldorson, V.; Duran, N.L. Bioluminescent bacteria: Lux genes as environmental biosensors. *Brazilian Journal of Microbiology* **2003**, 34, 91-96.

Omole M.A; Okello V.A.; Lee V.; Zhou L.; Sadik O.A. Catalytic Reduction of Hexavalent Chromium Using Flexible Nanostructured Poly(amic acids). *ACS Catal.* **2011**, 1, 139–146.

Osteryoung, J.; O’Dea, J.J. Square-wave Voltammetry. In *Electroanalytical Chemistry: A Series of Advances*; A.J. Bard, Ed.; Marcel Dekker: New York, 1986; Vol. 14, 209-308.

Otero, T.F.; Cantero, I. *Journal of power sources* **1999**, 81, 838-841.

Ozin, G. A., Nanochemistry: Synthesis in diminishing dimensions. *Advanced Materials* **1992**, 4, (10), 612-649.

Parthasarathy, R. V.; Martin, C. R., Synthesis of polymeric microcapsule arrays and their use for enzyme immobilization. *Nature* **1994**, 369, (6478), 298-301.

---

Parthasarathy, R. V.; Martin, C. R., Template-synthesized polyaniline microtubules. *Chemistry of Materials* **1994**, 6, (10), 1627-1632.

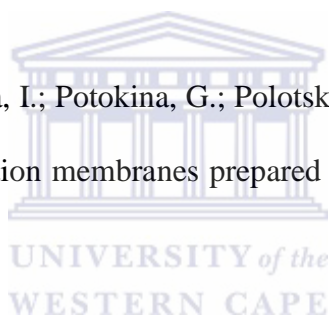
Partridge, A. C.; Harris, P.; Andrews, M. K., High sensitivity conducting polymer sensors. *Analyst* **1996**, 121, (9), 1349-1353.

Pejcic, B.; De Marco, R. Impedance spectroscopy: Over 35 years of electrochemical sensor optimization. *Electrochimica Acta* **2006**, 51, 6217-6229.

Peo, M.; Forster, H.; Mence, K. *Molecular Crystals Liquid Crystals* **1981**, 77, 103.

Polotskaya, G.A.; Kostereva, T.A.; Elyashevich, G.K. Separation and Purification Technology **1998**, 14, 13-18.

Polotskaya A, V.; Cherkasovaa, I.; Potokina, G.; Polotskayab T. Chemically and thermally resistant polyimide ultrafiltration membranes prepared from polyamic acid. *Desalination* **2006**, 200 341–342.



Prasad, K.R.; Munichandraiah, N. Electrocatalytic efficiency of polyaniline by cyclic voltammetry and electrochemical impedance spectroscopy studies. *Synthetic Metals* **2002**, 126, 61-68.

Preuss, R.; Angerer, J.; Drexler, H. Naphthalene—an environmental and occupational toxicant. *Int. Arch. Occup. Environ. Health* **2003**, 76, 556-576.

Rane, S.; Beacauge, G.; Mark, J. E. editors, “Polymer Data Handbook”, New York, Oxford, **1999**.

Rapid analysis of 17 polycyclic aromatic hydrocarbons with UV- and FL-detection according to DIN EN 17993:2002.



---

Ren, A.M.; Goddard, J.D. Predictions of the electronic absorption and emission spectra of luciferin and oxyluciferins including solvation effects. *Journal of Photochemistry and Photobiology B: Biology* **2005**, 81, 163–170.

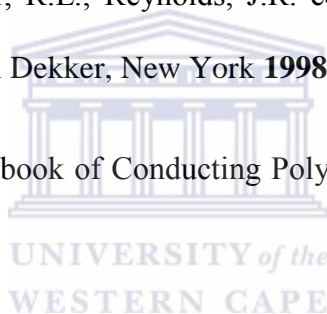
Roda, A.; Guardigli, M.; Michelini, E.; Mirasoli, M. Bioluminescence in analytical chemistry and in vivo imaging. *Trends in Analytical Chemistry* **2009**, 28 (3).

Sadik O.A; Mwilu S.K; Aluoch A. Smart electrochemical biosensors: From advanced materials to ultrasensitive devices. *Electrochimica Acta* **2010**, 55, 4287–4295.

Schlapfer, P.; Mindt, W.; Racine, P., *Clin. Chim. Acta* **57**, 283 (1974).

Scotheim, T.A.; Elsenbaumer, R.L.; Reynolds, J.R. editors, “Handbook of Conducting Polymers, 2nd edition, Marcel Dekker, New York **1998**.

Scotheim, T.A; editor, “Handbook of Conducting Polymers, 1st edition, Marcel Dekker, New York, **1983**.



Selampinar, F.; Akbulut, U.; Toppare, L. *Synthetic Metals* **1997**, 84, 185.

Shah, B.R.; Santucci, K. Naphthalene induced acute hemolytic-anemia in children with glucose-6-phosphate-dehydrogenase (G-6-PD) deficiency - naphthalene has no legitimate place on the market as a moth repellent. *Pediatr. Res.* **1995**, 37 (4), A144.

Shao C. Y.; Howe C. J.; Porter A. J. R.; Glover L. A. Novel Cyanobacterial Biosensor for Detection of Herbicides. *Appl. Environ. Microbiol.* **2002**, 68(10), 5026.

Shimomura O. Bioluminescence: Chemical Principles and Methods, World Scientific Publishing Co. Pte. Ltd., Singapore, **2006**.

Shirakava, H; Louis, E.J; MacDiarmid, A.G; Chiang, C.K; Heeger, A.J. *J. Chem. Soc., Chem. Commun.* **1977**, 578.

---

Shirakawa, H.; Louis, E. J.; MacDiarmid, A. G.; Chiang, C. K.; Heeger, A. J. Synthesis of electrically conducting organic polymers: halogen derivatives of polyacetylene, CH<sub>x</sub>. *J. Chem. Soc. Chem. Commun.* **1977**, 16, 578–580.

Snook, G. A.; Kao, P.; Best, A. S., Conducting-polymer-based supercapacitor devices and electrodes. *Journal of Power Sources* **2011**, 196, (1), 1-12.

Son, D.; Lee, Y.; Kim, K., *J. Phys. Chem.* **1994**, 98, 8488;

Srinivasan, M.P.; Jing, V. *Thin Solid Films* **1998**, 327-329.

Sroog C.E.; Endrey A.L.; Abramo S.V.; Berr C.E.; Edward W.M.; Olivier K.L. *J. Polym. Sci., Part A*, **1965**, 3, 1373.

Storer, J.S.; DeLeon, L.E. Human absorption of crude coal tar products. *Arch. Dermatol.* **1984**, 120, 874-877.

Su, M.; Ball, I.; Conklin, J.; Huang, S.; Larson, R.; Nguen, S.; Lew, B.; Kaner, B. *Synthetic Metals* **1997**, 84, 801-802.

Su, T.M.; Ball, I.J.; Huang, S.; Larson, V.; Nguyen, S.L.; Lew, B.M.; Kaner R.B.; Conklin, J.A. *Synthetic Metals* **1997**, 84, 801-802.

Sumida, T.; Wada, Y.; Kitamura, T.; Yanagida, S., Electrochemical preparation of macroporous polypyrrole films with regular arrays of interconnected spherical voids. *Chemical Communications* **2000**, (17), 1613-1614.

Sun, H.; Hu, N., Electroactive layer-by-layer films of heme protein-coated polystyrene latex beads with poly(styrene sulfonate). *Analyst* **2005**, 130, (1),76-84.

Szolar, O.H.J., Separation of PAHs by capillary electrophoresis (CE) equipped with laser-induced fluorescence. *Journal of molecular Rec.*, **1996**. 9, 515.

---

Takekoshi, T., Polyimides- Fundamentals and Applications, Ed. Ghosh, M.K. and Mittal, K.L., Marcel Dekker, New York, **1996**, Chapter 2.

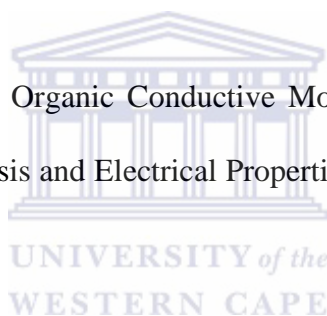
Tan, L.S.; J. E. Mark, editors, "Polymer Data Handbook", NY, Oxford, 1999.

Thomas, P.; Budiantara, L. Reproductive life history stages sensitive to oil and naphthalene in Atlantic croaker. *Mar. Environ. Res.* **1995**, 39, 147-150.

Tieke, B.; Gabriel, W. *Polymer* **1990**, 31, 20

Trivedi, D. C., Handbook of Organic Conductive Molecules and Polymers: Volume 2 Conductive Polymers: Synthesis and Electrical Properties. John Wiley and Sons Ltd: New York, 1996; 506–572.

Trivedi, D. C.; Handbook of Organic Conductive Molecules and Polymers: Volume 2 Conductive Polymers: Synthesis and Electrical Properties. *John Wiley and Sons Ltd: New York, 1996*; 506–572.



Turcu, R.; Graupner, W.; Filip, C.; Bot, A.; Brie, M.; Grecu, R. *Advanced materials for optics and electronics* **1999**, 9, 157-165.

U.S. Environmental Protection Agency, 1988

U.S. EPA (U.S. Environmental Protection Agency). 1988. 13-Week Mouse Oral Subchronic Toxicity Study. Prepared by Toxicity Research Laboratories, Ltd., Muskegon, MI, for the Office of Solid Waste, Washington, DC.

Valaes, T.; Doxiadis, S.A.; Fessas, P. Acute hemolysis due to naphthalene inhalation. *J. Pediatr.* **1963**, 63, 904-915.

Valenciano, G.R.; Job, A.E.; Mattoso, L.H. *Polymer*, **2000**, 41, 4757- 4788

---

Von Schickfus, M.; Stanzel, R.; Kammereck, T.; Weiskat, D.; Dittrich, W.; Fuchs, H., Improving the SAW gas sensor: device, electronics and sensor layer. *Sensors and Actuators B: Chemical* **1994**, 19, (1-3), 443-447.

Vyas, R.N.; Wang B. Electrochemical Analysis of Conducting Polymer Thin Films. *Int. J. Mol. Sci.* **2010**, 11, 1956-1972.

Wallace, G. G., Conductive electroactive polymers: intelligent polymer systems. *CRC Press: Boca Raton*, **2009**, 10-27.

Wallace, G. G.; Spinks, G. M.; Kane-Maguire, L. A.; Teasdale, P. R. Conductive electroactive polymers: Intelligent materials systems (2nd ed.). United States of America: Taylor & Francis Group, 2003.

Wang S.; Xu P.; Mark, J. E. editors, "Polymer Data Handbook", New York, Oxford, 1999.

Wang, J., Nanomaterial-based electrochemical biosensors. *Analyst* **2005**, 130, (4), 421-426.

Wang, J.; Rivas,G.; Luo,D; Cai, X.; Dontha,N.; Farias, P.; Shirashi, H., *Anal. Chem.* **1996**, 68, 4365.

WHO, Guidelines of drinking-water Quality Geneva, 1998. vol. 1 (2nd edition)

Woodward K.L.A.; Determination of polyaromatic hydrocarbon using immunoassays. *Science Total Environment* **1984**, 32, 103.

Wu, C. G.; Bein, T., Conducting polyaniline filaments in a mesoporous channel host. *Science* **1994**, 264, (5166), 1757-1759.

---

Xia, L.; Wei, Z.; Wan, M., Conducting polymer nanostructures and their application in biosensors. *Journal of Colloid and Interface Science* **2010**, 341, (1), 1-11.

Yamasaki S.; Nakashima S.; Yamada S.; Takehara K. Steady-state bioluminescence of bacterial luciferase using electrochemical regeneration of flavin substrate and its application to inhibitory analysis. *Bioelectrochemistry*, **2009**, 75, 67–70.

Yanagisita, H., Kitamoto, D., Haraya, K., Nakane, T., Tsuchiya, T.; Koura N. *Journal of Membrane Science* **1997**, 136, 121-126.

Yoji Kawanami, Shinya Yamasaki, Shuto Yamad, Kô Takehara, Immobilization of Bacterial Luciferase into Poly(N-isopropylacrylamide) Film for Electrochemical Control of a Bioluminescence Reaction. *Analytical Sciences* **2012**, 28, 1013-1015.

Yoon, C.O.; Sung, H.K; Kim, J.H. *Synthetic Metals* **1999**, 99, 201-212.

Zhang, Z.; Wan, M. Composite films of nanostructured polyaniline with poly(vinyl alcohol), *Synthetic Metals* **2002**, 128, 83–89.

Zheng, W.; Min, Y.; MacDiarmid, A. G.; Angelopoulos, M.; Liao, Y. H.; Epstein, A. J., Effect of organic vapors on the molecular conformation of non-doped polyaniline. *Synthetic Metals* **1997**, 84(1-3), 63-64.



UNIVERSITY *of the*  
WESTERN CAPE